PROCEEDINGS
of the
OKLAHOMA ACADEMY OF SCIENCE
Volume 105
2025

EDITOR: Mostafa Elshahed

Production Editor: Lisa Whitworth

Business Manager: Adam Ryburn

The Official Organ of
the
OKLAHOMA ACADEMY OF SCIENCE

Which was established in 1909 for the purpose of stimulating scientific research;
to promote fraternal relationships among those engaged in scientific work in Oklahoma;
to diffuse among the citizens of the State a knowledge of the various departments of science;
and to investigate and make known the material, educational, and other resources of the State.

Affiliated with the American Association for the Advancement of Science.

Publication Date: February 2026

POLICIES OF THE *PROCEEDINGS*

The *Proceedings of the Oklahoma Academy of Science* contains papers on topics of interest to scientists. The goal is to publish clear communications of scientific findings and of matters of general concern for scientists in Oklahoma, and to serve as a creative outlet for other scientific contributions by scientists. ©*2024 Oklahoma Academy of Science*

The *Proceedings of the Oklahoma Academy of Science* contains reports that describe the results of original scientific investigation (including social science). Papers are received with the understanding that they have not been published previously or submitted for publication elsewhere. The papers should be of significant scientific quality, intelligible to a broad scientific audience, and should represent research conducted in accordance with accepted procedures and scientific ethics (proper subject treatment and honesty).

The Editor of the *Proceedings* expects that the author(s) will honor the following principles of the scientific community, which are also policies of the *Proceedings*.

1. Each author shall have contributed substantially to major aspects of the planning, execution, and /or interpretation of the study and to the preparation of the manuscript. It is assumed that all listed authors concur in the submission, that final copy of the manuscript has been seen and approved by all authors, and that all authors share responsibility for the paper.

2. Submission of manuscripts based on unique material (e.g. cloned DNAs; antibodies; bacterial, animal, or plant cells; hybridomas; viruses; and computer programs) implies that these materials will be available for noncommercial purposes to all qualified investigators.

3. Authors of manuscripts reporting nucleic acid sequence(s) must be prepared to submit relevant data to GenBank. Authors of manuscripts reporting crystallographic studies must be prepared to submit the relevant structural data to the Protein Data Base and/or other appropriate repository. Information necessary for retrieval of the data from the repository will be specified in a reference in the paper.

4. Manuscripts that report research involving human subjects or the use of materials from human organs must be supported by a copy of the document authorizing the research and signed by the appropriate official(s) of the institution where the work was conducted. Research involving humans and animals must have been performed in accordance with the recommendations from the Declaration of Helsinki and the appropriate guidelines of the National Institutes of Health.

5. Submission of manuscripts that report research on/with recombinant DNA implies that the relevant physical and biological containment levels conformed to the guidelines of the National Institutes of Health; the Editor may request proof to substantiate this implication.

6. The *Proceedings* does not publish statements of priority or novelty, or mere descriptions of work in progress or planned. The dates of manuscript receipt, revision, and acceptance will be published.

7. A primary research report must contain sufficient details and reference to public sources of information to permit other scientists to repeat the work.

8. Any unusual hazard encountered or anticipated in using chemicals, equipment, or procedures in the investigation should be clearly identified in the manuscript.

PROCEEDINGS OF THE OKLAHOMA ACADEMY OF SCIENCE

Volume 105

CONTENTS

REPORTS

A. Botany

B. Applied Ecology & Conservation

THE QUERCUS UNDULATA TORREY COMPLEX IN OKLAHOMA

Paul M Thomson
Herbarium Research Associate, Department of Biology, Oklahoma State University

Abstract: A reexamination of voucher specimens used for the Flora of Oklahoma project revealed those of *Quercus gambelii* Nuttall, are hybrids likely between it and four other species, *Q. grisea, Q. macrocarpa, Q. muehlenbergii, and Q. turbinella*. The specimens are from or near Tesequite Canyon in Cimarron County, Oklahoma, however, none of parent species occur in the region. Evidence from morphological analysis and prior studies supports their hybrid origin, with a proposed case for their presence based on historical events.

Introduction

My preliminary study of disjunct populations of *Quercus muehlenbergii* Engelmann, in the Four Canyon Nature Preserve, of Ellis County, Oklahoma, (2024), suggested they were of hybrid origin but, at that point, of uncertain parentage. While examining herbarium specimens for the potential source, I found a putative hybrid of *Q. gambelii* × *muehlenbergii* on deposit in the Oklahoma State University herbarium (OKLA) from Woodward County, about 60km northeast of the study site,

In examining the specimen, I found two distinct types of trichomes occurring on the abaxial leaf surface: fasciculate with 1-4 rays and stellate appressed with 6-12 rays. A study of foliar trichomes of species of White Oaks, Thomson and Mohlenbrock (1979) showed this combination to be indicative of *Q. gambelii* × *muehlenbergii.*

This hybridization was first proposed by John Tucker in his seminal work on western white oak hybridization between *Q. gambelii* and six other white oaks, *Q. arizonica* Sargent, *Q. grisea* Liebmann, *Q. havardii* Rydberg, *Q. mohriana* Buckley, *Q. muehlenbergii* Engelmann and *Q. turbinella* Greene, he titled *The Quercus Undulata Complex* (1961). In subsequent studies (1961a,b,1963, 1970, 1971) he provided evidence that *Q. undulata* Torrey was not a species but the hybrid intermediates of species of the Complex where they are or have been sympatric. His preliminary report (1961) contained range maps of the Complex in which its eastern-most extent reached into northeast New Mexico and southeast Colorado. He cited no evidence of the Complex reaching Oklahoma

While Tucker did not provide evidence of the cross in any of his following studies, adding trichome types to the evidence, I was able to report putative populations of *Q. muehlenbergii* introgressed by *Q. gambelii* in the Capitan Mountains of New Mexico, Thomson (2022). Finding the same evidence on the Woodward County specimen was the first indication to me that the Complex may have made its way into the State. Consequently, I decided to conduct a SEINet search (2023) for other records of *Q. gambelii* in Oklahoma. The search returned 17 specimens on deposit in four herbaria. All were collected in or near a place known as Tesequite Canyon about 241 km west of the Preserve in the Panhandle

*Corresponding author: paul.thomson@okstate.edu

County of Cimarron.

Two of the specimens from the search were on deposit in the herbariums of the University of Oklahoma (OKL) and Oklahoma State University (OKLA). I examined them on site and determined them to be *Q. gambelii* × *muehlenbergii* and Q. *mohriana* respectively. Both are members of the Complex.

The Woodward specimen, collected by E. J. Little, Jr (36016: OKLA), is a reference specimen for the Flora of Oklahoma project. With this finding I decided to examine the other specimens and obtained loans for their study. After an initial review, I found five to be duplicates, or erroneously reported for Oklahoma. The 12 specimens in the initial study are listed by herbarium in Table 1.

Members of The Complex, except for *Q. arizonica*, *Q. grisea* and *Q. turbinella*, are included in the Flora of Oklahoma (2023), but the Complex, as such, has not been reported for the State. Because of my previous work with the members of the Complex (2022) I decided to suspend my search for the source of the Preserve hybrids and look further into the oaks of the Tesequite Canyon area. This study purports to show the *Quercus Undulata Complex* in Oklahoma and its influence on the white oak flora.

Methods

As noted above, the specimens of this study were located in the herbaria of the University of Oklahoma and the Oklahoma State University and by searching on-line for records of *Q. gambelii* in Oklahoma on deposit in the herbaria of the Southwest Biodiversity Organization, SEINet (2023), and The Texas and Oklahoma Consortium of Herbaria, TORCH (2023).

Since the specimens all had the determination of *Q. gambelii*, I examined them for three features known to be characteristic for the species: contour of the leaf margin (lobed), twig markings (transverse fissures) and trichome types (fasciculate with 1-4 rays). The features are described further below and pictured in Figs. 1, 2, and 3.

Table 1. Specimens of the study by herbarium
*reference specimen for the Flora of Oklahoma Project

Herbarium	Barcode Number	Collector	Collector Number
BRIT	568108	D. Demaree	13389
BRIT	567802	J & C Taylor	25159
BRIT	567803	P. Nighswonger	1518
BRIT	567804	J & C Taylor	14179-A
BRIT	567805	J & C Taylor	14179-D
BRIT	567806	U.T. Waterfall	7951*
BRIT	567807	U.T. Waterfall	7950
BRIT	745842	P. Nighswonger	1624
MOR	0061510	P. Nighswonger	1669
MOR	0061511	J. Taylor	25197
OKL	52095	E. Little Jr	36016*
OKLA	00573	J & C Taylor	6895

Figure 1. Specimen of *Quercus gambelii* on deposit at the Baylor University Herbarium (BAYLU) depicting lobed contour margins. The specimen was collected and determined by John Tucker. Image from SEINet.

Leaf margin contour. The distinctly lobed leaf margins of *Q. gambelii* are depicted in Fig. 1. Lobes vary from 4-8 with sinuses often extending to the midpoint of the leaf or deeper, Nixon and Mueller (1997).

Twig markings. Transverse fissures are openings in the periderm developing at right angles to the long axis of twigs. This feature was used by Tucker and Mueller (1958) to distinguish *Q. gambelii* from *Q. margaretta* in a reexamination of the origin of *Q. margaretta* and *Q. drummondii*. A photo of a specimen collected by John Tucker (2775-6: DAV) with transverse fissures is shown in Fig. 2.

Figure 2. Twig of *Q. gambelii* showing transverse fissures. Photo by Dan Potter, University of California, Davis. Used with permission.

Trichome type(s). As cited above, fasciculate trichomes with 1-4 rays, are definitive for Gambel's Oak, Fig. 3, plate 20.

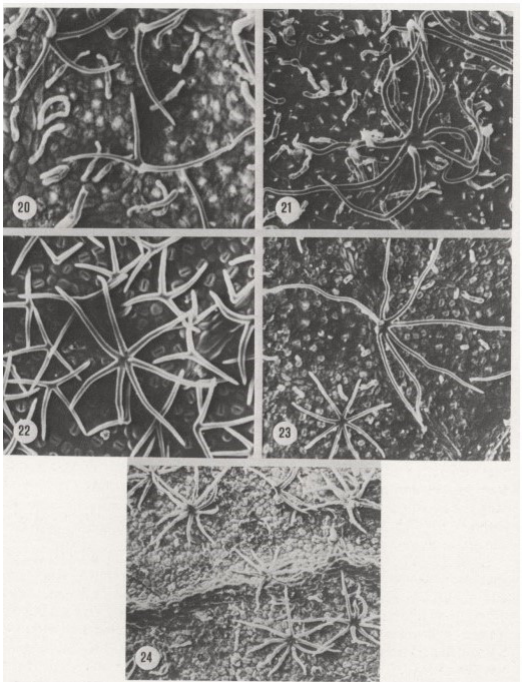

Figure 3. SEMs of *Q. gambelii* trichomes, plate 20, 220x, *Q. grisea* trichomes plate 21, 130x, *Q. gambelii* × *muehlenbergii* plate 22, 220x and *Q. muehlenbergii* plate 24, 130x. Thomson and Mohlenbrock 1979. Used with permission.

Each of the specimens was examined for the definitive characteristics. Margin contour was determined and recorded, twigs were examined for transverse fissures and recorded on a presence/absence basis and the abaxial leaf surface was examined for trichome types. The types were observed using a compound light microscope at 120x and recorded with nomenclature following Hardin (1979).

Study Site

The specimens of this study were collected in an area of Cimarron County, Oklahoma known as Tesequite Canyon (36.9050N -102.8890W) situated at an elevation of 1281ft (930.4m). The Canyon, under private ownership, is near the Black Mesa region about 6 miles (9.7 km) south of Kenton, Oklahoma (36. 5411N -102.5748W). The Mesa, featuring the highest point in Oklahoma at an elevation of 4973 ft. (1516 m), is part of the Western High Plains, a geological feature that begins in Colorado, extends southeasterly into New Mexico and ends in the Oklahoma Panhandle County of Cimarron. To the east the physiography grades into prairie grassland, Johnson and Luza (2008). The climate is semiarid with annual precipitation averaging 17.26 in. (43.84 cm) Oklahoma Climatological Survey (2010).

Results

My initial review revealed forms of the characteristics inconsistent with those of *Q. gambelii.* Some had one or two of the characters but then in combination with characters of other species e.g., lobed leaf margins of *Q. gambelii* with stellate trichomes typical of *Q.muehlenbergii*. Several had none of the *Q. gambelii* features and none displayed all three diagnostic characters. Table 2 shows the characters observed and the species associated with them. The species except for *Q. macrocarpa* are members of the Complex.

Leaf contours were of various forms; entire, undulate, dentate, spiny toothed, lobed and deeply lobed. I found trichomes of the *Q. gambelii* type on five of the specimens, but no fissures on any of them. One specimen, had markings on twigs where one would expect fissures. Whether these are undeveloped fissures or something else I did not pursue. The following are descriptions of the findings by herbarium barcode below and summarized in Table 3.

On five of the specimens I found no features of *Q.gambelii.* Their features were, however, consistent with those of known species. BRIT 568108 and 567802, OKLA 00573 with entire margins and stellate erect trichomes with 6-10 wavy rays that, I believe, are typical of *Q. mohriana.* Leaves of BRIT 567803 and 567804 have undulate and dentate margins respectively and bear stellate erect trichomes with 8-10 straight

Table 2. Trichomes types, Leaf Margin Contour and Presence/Absence of Transverse Fissures displayed by of Species in this study.

Trichome type (s)	Fasciculate with 1-4 rays	Stellate With 8-10 straight rays	Fasciculate erect; stellate appressed; bulbous	Stellate with 6-8 whitish rays	Stellate appressed with 6-12 (16) rays	Minute stellate; Reddish or yellowish glandular	Fasciculate with 6-8 wavy rays
Leaf Margin Contour	Lobed with 4-6 sinuses reaching up to ½ distance to midrib	Undulate with 2-3 rounded teeth per side	Lobed, deepest sinuses below mid-leaf	Entire or 1-3 teeth per side	Dentate, 6-14 mucronate teeth per side	Undulate with 3-5 spinose teeth per side	Entire or Dentate with mucronate teeth
Transverse Fissures	Present	Absent	Absent	Absent	Absent	Absent	Absent

Table 3. Specimen features with annotation. *Presence of transverse markings.

Specimen	Original Determination	Trichome Type(s)	Leaf Contour	Presence/Absence Of Transverse Fissures	Annotation
BRIT 568108	Q. gambelii	Stellate, erect with 6-10 wavy rays	Entire	Absent	Q. mohriana
BRIT 567802	Q. gambelii	Stellate, erect with 6-10 wavy rays	Entire	Absent	Q. mohriana
BRIT 567803	Q. gambelii	Stellate, Stipitate with 6-8 straight rays	Undulate	Absent	Q. havardii
BRIT 567804	Q. gambelii	Stellate, Stipitate with 6-8 straight rays	Five Shallow Lobes	Absent	Q. havardii
BRIT 567805	Q. gambelii	Fasciculate with 6-10 wavy rays; Reddish, Simple	Four Spinose Teeth	Absent	Q. turbinella × grisea
BRIT 567806	Q. gambelii	Fasciculate; rays 1- 4 and stellate-appressed; rays 6-12	Dentate	Transverse Markings*	Q. gambelii × muehlenbergii
BRIT 567807	Q. gambelii	Stellate erect; Fasciculate; 6-8 rays; bulbous; Uniserrate; pigmented	Lobed	Absent	Q. gambelii × macrocarpa
BRIT 745842	Q. gambelii	Fasciculate, rays 1-4; minute; stellate	Six Spinose Teeth	Absent	Q. gambelii × turbinella
MOR 00061510	Q. gambelii	Fasciculate, rays 1-4; Stellate-appressed; rays 6-12	Dentate	Absent	Q. gambelii × muehlenbergii
MOR 00061511	Q. gambelii	Fasciculate, rays 1-4; minute stellate	Five Spinose Teeth	Absent	Q. gambelii × turbinella
OKL 52095	Q. gambelii	Fasciculate; 1-4 rays; Stellate-appressed; 6-12 rays	Dentate	Absent	Q. gambelii × muehlenbergii
OKLA 00573	Q. gambelii	Stellate, non-appressed with 6-10 wavy rays	Entire	Absent	Q. mohriana

rays associated with *Q. havardii*.

The remaining specimens displayed characters of two species. Leaves of MOR 0061510, OKL 52095 and BRIT 56806 have dentate margins and trichomes of two types, 1-4 rayed fasciculate and stellate appressed with 6-12 rays suggesting the combination of *Q. gambelii* × *muehlenbergii*. Leaves of BRIT 745842 and MOR 005111 have margins with spinose teeth and trichomes that are fasciculate with 1-4 rays as well as minute, stellate appressed which I believe are of indicitive of *Q. gambelii* × *turbinella*. The combination is also referred to as Quercus × pauciloba Rydb. (pro sp.), (Bull. N.Y. Bot. Gard. 2:215.1901.).

The leaves of BRIT 57807 produced a combination of trichomes typical of Bur Oak; stellate, fasciculate with 6-8 rays and bulbous, Thomson and Mohlenbrock (1979). The specimen has distinctly lobed leaves with sinuses extending more than half way to the midrib. It is also the specimen bearing the transverse markings noted above. Trichomes typical of *Q. gambelii* were not found. The trichome combination together with features of leaf and twig suggested *Q. gambelii* × *macrocarpa*.

Eleven of the twelve Tesequite Canyon specimens of Table 3 have characteristics of the Undulata Complex: five are species, three of *Q. mohriana* and two of *Q. havardii;* six are putative hybrids, three of *Q. gambelii* × *Q. muehlengbergii,* two of *Q. gambelii* × *Q. turbinella* and one of *Q. turbinella* × *grisea.* The 12th specimen, a suspected hybrid between *Q. gambelii* and *Q. macrocarpa,* is not a member of the Undulate Complex per Tucker. I found no suspected hybrids involving *Q. mohriana* or *Q. havardii.*

I initially annotated BRIT 567805 as *Q. turbinella* but based on further review believe it to be a hybrid of *Q. turbinella* and *Q. grisea* as it bears spinose teeth and fasciculate trichomes of the type produced by *Q. grisea* leaves as shown in Fig. 3, plate 21 and Fig. 4. Present also are reddish pigmented, simple hairs found on *Q. turbinella* which may become yellowish or amber upon drying. Leaves of *Q. turbinella* typically produce minute stellate hairs as well, but these were not present on the specimen.

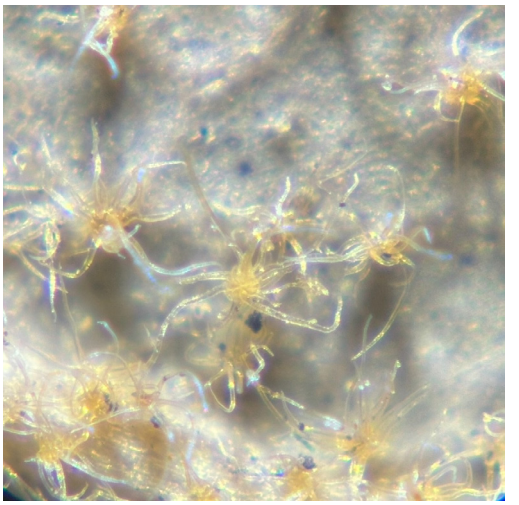

Figure 4. Photo through a compound light microscope of Q. grisea trichomes from a Tesequite Canyon Specimen at 120x

Because seven of the twelve Tesequite Canyon records were putative hybrids, I made a further search for records of the presumed parental species in Oklahoma. For *Q. turbinella* and *Q. grisea,* the search returned three records of *Q. turbinella*, J&C Taylor (14179D: BRIT), and Lowry (4000, 4001: OKLA) and two of *Q. grisea,* Demaree (13395: NYBG) and McGrath (10317: OKLA) all from Tesequite Canyon. All but the Demaree specimen were on site or on loan and were examined. The *Q. turbinella* records I believe are *Q. turbinella* × *grisea.* The specimens bear spinose teeth typical of *Q. turbinella* but trichomes of *Q. grisea*. Fig. 3 plate 21 shows *Q. grisea* trichomes from the 1979 paper. Fig. 4 is a photo of trichomes of *Q. turbinella* × *grisea* from Lowry (4001: OKLA). In both figures the trichomes are fasciculate with 6-10 wavy rays. Trichomes of *Q. turbinella* are of two types, minute stellate, and simple, Nixon and Mueller in the Flora of North America (1997). The stellate type of *Q. turbinella* were not observed in these specimens but the simple hairs were.

The McGrath specimen was examined and found to possess features typical of *Q. mohri-*

ana, however, the Demaree specimen was not examined on site, but from its observable features, via SEINet, I believe them to be of *Q. mohriana* also.

I widened the search for *Q. grisea,* and *Q. turbinella* to the counties of Colorado, New Mexico and Texas bordering Cimarron County. For *Q. grisea,* six records were returned from Union County New Mexico, two of Q. *gambelii* × *grisea*, Tucker (3249-9, 3254-4: UTEP) and four of *Q. grisea,* Demarcee (13396: NYBG), Zimmerman, Jr (1987-09-17: NMC), Castetter (1940-09-26: UNM) and Schiebot (2005-06-09: GREE: GREE). Twelve of *Q. grisea* were recorded in Baca County, Colorado, including one nearest Oklahoma by Tucker (2848-10: BYU). All Colorado records are about 19 km north of the study site. None was found in Dallam County, Texas.

Tucker (1961b) did not indicate the presence of *Q. turbinella* in Oklahoma. His records show occurrence as far east as central Colorado and New Mexico, but none in eastern New Mexico or Oklahoma. However, as noted above, its *Q. gambelii* hybrid, *Q.* × pauciloba, Tucker (2847-18: FLD), was collected in Baca County, CO and Union County, NM, Stevens (17310: KANU). The specimens from BRIT (745842) and MOR (0061511) from the study area bear characters of *Q.* × *pauciloba.* Together with the two specimens of Lowry (4000, 4001: OKLA), *Q. turbinella* × *Q. grisea,* these add further to the evidence of past influence of *Q. turbinella* near and in the State. Although the Flora of Oklahoma includes *Q. gambelii*, I could not confirm it in species form

Table 4. The species and putative hybrids of the Undulata Complex, in Oklahoma. Proposed in this study*.

Specimen	Original Determination	Trichome Type(s)	Leaf Contour	Presence/Absence Of Transverse Fissures	Annotation
BRIT 568108	Q. gambelii	Stellate, erect with 6-10 wavy rays	Entire	Absent	Q. mohriana
BRIT 567802	Q. gambelii	Stellate, erect with 6-10 wavy rays	Entire	Absent	Q. mohriana
BRIT 567803	Q. gambelii	Stellate, Stipitate with 6-8 straight rays	Undulate	Absent	Q. havardii
BRIT 567804	Q. gambelii	Stellate, Stipitate with 6-8 straight rays	Five Shallow Lobes	Absent	Q. havardii
BRIT 567805	Q. gambelii	Fasciculate with 6-10 wavy rays; Reddish, Simple	Four Spinose Teeth	Absent	Q. turbinella × grisea
BRIT 567806	Q. gambelii	Fasciculate; rays 1- 4 and stellate-appressed; rays 6-12	Dentate	Transverse Markings*	Q. gambelii × muehlenbergii
BRIT 567807	Q. gambelii	Stellate erect; Fasciculate; 6-8 rays; bulbous; Uniserrate; pigmented	Lobed	Absent	Q. gambelii × macrocarpa

from the specimens examined in this study.

Characteristics of two species of the Complex not included in the Flora, *Q. grisea* and *Q. turbinella*, were found on two of the specimens; BRIT 567805 (*Q. turbinella* × *grisea)* and BRIT 745842 (*Q. turbinella* × *gambelii)* have leaves with spinose teeth typical of *Q. turbinella* and BRIT 567805 the fasciculate trichomes of *Q. grisea. Quercus macrocarpa* appears to have contributed to the Complex as *Q. gambelii* × *macrocarpa.* No evidence of the seventh member of the Complex per Tucker, *Q. arizonica,* was found. The Oklahoma species and putative hybrids of the Complex with their Oklahoma locations are listed in Table 4. Except for *Q. gambelii* × *macrocarpa* the presumed hybrids are intermediates of the Complex.

Discussion

None of the potential parents of the hybrids occur in Cimarron County. *Quercus macrocarpa* and *Q. muehlenbergii* do occur in Oklahoma, but their nearest records, (Ertreeb 1570 and 1557: OKLA respectively), are in Ellis County 241 km east of the study site. *Quercus gambelii* is noted as occurring in Cimarron County in The Flora of Oklahoma (2024) and by Little in Forest Trees of Oklahoma (2010), but as evidenced above, believed to be in hybrid form only. The search for *Q. turbinella* returned no records from Baca County, or Dallam County, but a record was found (Stevens 17310: KANU) in Union County near the town of Moses, located about 5 km west of the Oklahoma border. While no records of either species were recorded from Cimarron County, their presence in putative hybrid form, *Q. turbinella* × *Q. grisea* and *Q. turbinella* × *gambelii* and the proximity of present day records, suggests their occurrence at some time.

In the absence of co-occurrence, how then to account for the combination of characters possessed by the putative hybrids of Table 4?

Tucker found this situation in his study of The *Quercus Undulata* Complex. To explain, he postulated that migrations occurring during pluvial periods of the Pleistocene allowed for range expansion and sympatry. He further posited that during this time of co-occurrence hybridization and introgression occurred between Gambel's Oak, the six other members of the Complex, and to a more limited extent, some of them with one another where they co-occurred. As the climate became cooler and dryer, traits obtained through the interactions allowed for some to adapt. Today, he believed, we find descendants of those ancient plants bearing signs of their hybrid ancestry and often in areas where the parent species no longer grow.

Similarly, in a study of introgressed populations of *Q. macrocarpa* by *Q. gambelii* in South Dakota, Wyoming and Union County New Mexico, Tucker and Maze (1966) concluded that at one time Bur Oak grew considerably west of its present-day range. To account for hybrids where parent species are not extant, Maze (1968) also posited that the migration occurred during pluvial periods of the Pleistocene. This, he believed, allowed for sympatry and hybridization. Subsequently, as the climate became cooler and drier, conditions favored the hybrids but not the parents.

Finding a putative cross of *Q. macrocarpa* with *Q. gambelii,* in Tesequite Canyon where Bur Oak is not extant, adds to Maze's assertion of an ancient migration. Furthermore, the soils of the Tesequite Canyon area date to the Pleistocene, Johnson and Luza (2008); a supporting element if *Q. macrocarpa* were to occur in the study area during its westward expansion as Tucker and Maze proposed. Because this is a second documented occurrence of *Q. macrocarpa* interacting with a member of the Complex, I believe it should be considered part of it albeit one of local influence. As cited above, Thomson (2022) introgressed populations of *Q. muehlenbergii* by *Q. gambelii* and *Q. muehlenbergii* by *Q. grisea* in disjunct populations of the Capitan Mountains of New Mexico also suggest an ancient range expansion for the Complex.

Tucker found *Q. mohriana* third most active in hybridization, after *Q. gambelii* and *Q. grisea*. As reported above I found three records of the species among the study specimens but with no evidence of hybridization. A SEINet search

(2023) returned 32 records of *Q. mohriana* from Cimarron County, all near to or in Tesequite Canyon. I have examined 20 of those on deposit at OKL and OKLA and again found no indication of hybridization. With a member of the Complex as active in hybridization as Tucker found, I think it surprising. I have not pursued any cause for the absence of interaction in this study, but Tucker reported this situation also with *Q. mohriana* in the Colorado and New Mexico populations (1961).

Quercus havardii is well known in western Oklahoma as a shinnery oak. In a study of shinnery in Oklahoma, Wiedeman and Penfound (1960) mapped the species by county. Their records do not cite any occurrences of *Q. havardii* from Cimarron County, however, a SEIN search for the species (2024) returned eight occurrences from the county including the two from BRIT cited above. None of the other six specimens displayed observable features to suggest they are hybrids of the Complex.

The obvious outlier among the 12 records is *Q. gambelii* × *macrocarpa.* While not a component of the Complex as described by Tucker, finding the putative hybrid in Cimarron County suggests *Q. macrocarpa* once occurred here and appears to have contributed locally to the Complex via *Q. gambelii* as Maze posited it had with *Q. gambelii* in Union County, New Mexico and South Dakota.

From the specimens of this study, I was not able to determine *Q. gambelii* as the source for the aberrant features of the Preserve Oaks, Thomson (2024). Neither was I able to confirm its occurrence in typical species form in Oklahoma. However, it and other members of the Complex in their introgressed forms can be confirmed as occurring in Oklahoma and have left their indelible mark. Lacking extant parental species to account for the hybrids, I am left to assume that these hybrids occurring in Oklahoma today, are also descendants of an ancient time of sympatry. Today they stand as a testiment to resilence in a time of climate change.

What began as a search for features of a putative parent of the Preserve hybrids resulted in evidence for the presence of the Undulata Complex in Oklahoma. The findings not only build upon Tucker's work but change our understanding of the composition of the White Oak Flora in western Oklahoma.

Acknowledgments

I offer my appreciation to Mark Fishbein Associate Department Head of the department of Biology and Curator of the Oklahoma State University herbarium for opening the herbarium to me during my many visits. I also thank him for arranging the loan of material from Morton Arboretum and The Botanical Research Institute of Texas.

To Any Buthod, Collections Manager and Abby Moore, Curator of the University of Oklahoma Bebb Herbarium my special thanks for supporting my study of specimens of this study on deposit and obtaining a loan from BRIT.

Thanks also to Dan Potter, Collections Manager of the John Tucker Herbarium (DAV) at the University of California, Davis for the photo showing transverse fissures.

I appreciate the photo of *Quercus gambelii* for this study from Curator of the Baylor University Herbarium, Joseph White.

A special thank you to the reviewers of this study for their helpful suggestions.

References

Gleason, H. A. (1963). Fagaceae, p. 43 In: The New Britton and Brown Illustrated Flora of the Northeastern United States and Adjacent Canada, vol. 2, revised ed. Hafner Publishing Company, New York, NY.

Hardin, J. W. (1979). Atlas of Foliar Surface Features in Woody Plants, I. Vestiture and Trichome Types in Eastern North American Quercus. Bulletin of The Torrey Botanical Club, Oct.-Dec. 1979. Vol.106, No.4 (Oct-Dec. 1979), pp. 313-

325.

Johnson, H. L. (2010). "Oklahoma Climatological Survey", The Encyclopedia of Oklahoma History and Culture, © Oklahoma Historical Society.

Johnson, K. and Luza, K. (2008). Earth Sciences and Mineral Resources of Oklahoma. Oklahoma Geological Survey. Educational Publication p. 10

Little, Jr, E. L. (1981). Oklahoma Forestry Services, State Department of Agriculture, Food and Forestry. Publication 1, Revised Edition 17. 2010.

Maze, J. "Past hybridization between *Quercus macrocarpa* and *Quercus gambelii*." *Brittonia* 20 (1968): 321-333.

Nixon, K. C. and Muller, C.H. (1997). *Quercus* sect. *Quercus*, pp. 471-506. *In*: Flora of North America Editorial Committee, eds. Flora of North America, North of Mexico, vol.3. Oxford University Press, New York, NY.

Southwest Environmental Information Network. (2023). SEINet data portal. Website (https://swbiodiversity.org/seinet/). Accessed Mar 2023.

Southwest Environmental Information Network. (2024). SEINet data portal. Website (https://swbiodiversity.org/seinet/). Accessed June 2024.

Thomson, P. M. *Quercus prinoides* hybrids in the Capitan Mountains of New Mexico. Rhodora Vol. 123, Issue 995, (Dec 2022) pgs. 335-344.

Thomson, P. M. The Chinquapin Oaks, *Q. muehlenbergii,* of the Four Canyon Nature Preserve, Ellis, County Oklahoma. 2024 Unpublished Study.

Thomson, P. M. and Mohlenbrock, R.H. (1979). Foliar Trichomes of Quercus, Subgenus , Quercus in the Eastern United States. Vol.60 no.3, pp. 350-366.

Tucker, J. M., and Maze, J. R. (1966). Bur Oak (Quercus Macrocarpa) in New Mexico? The Southwestern Naturalist. 11(3): 402-405.

TORCH Portal. 2024. http//:portal.torcherbaria.org/portal/index.php. Accessed on April 3.

Tucker, J. M., and Muller, C.H. "A reevaluation of the derivation of *Quercus margaretta* from *Quercus gambelii*." *Evolution* 12.1 (1958): 1- 17.

Tucker, J. M. "Studies in the *Quercus undulata* Complex I. A preliminary statement." *American Journal of Botany* 48.3 (1961): 202-208.

Tucker, J. M., et al. "Studies in the Quercus Undulata Complex. II. The Contribution of Quercus Turbinella." *American Journal of Botany*, vol. 48, no. 4, 1961, pp. 329–39.

Tucker, J. M. "Studies in the Quercus Undulata Complex. III. The Contribution of Q. Arizonica." *American Journal of Botany*, vol. 50, no. 7, 1963, pp. 699–708.

Tucker, J. M. "Studies in the Quercus Undulata Complex. IV. The Contribution of Quercus Havardii." American Journal of Botany, vol. 57, no. 1, 1970, pp. 71–84.

Tucker, J. M. Studies in the *Quercus undulata* Complex V. The Type of Quercus undulata. 1971. *American Journal of Botany*. Vol. 58. No 4. pp. 329-341.

Wiedeman, V. E. and Wm. T. Penfound. "A Preliminary Study of the Shinnery in Oklahoma". The Southwestern Naturalist 5 (3). 1960. pp. 117-122.

Aberrant characters in Chinquapin Oak populations, *Quercus muehlenbergii* Engelmann, of the Four Canyon Nature Preserve, Ellis County, Oklahoma suggest a time of ancient introgression by Bur Oak, *Quercus macrocarpa* Michaux

Paul M Thomson
Herbarium Research Associate, Department of Biology, Oklahoma State University

Abstract: In canyons of Ellis County, Oklahoma opening to the South Canadian River below, disjunct populations of *Quercus muehlenbergii Engelmann* predominate. In 2022 and 2023 trees of two canyons within the Four Canyon Nature Preserve were sampled. Morphological analysis of the specimens revealed features not associated with the species including, terminal bud stipules, divergent venation, fasciculate trichomes, lobed leaf margins and pubescent twigs. The characters are consistent with those of Bur Oak, *Quercus macrocarpa* Michaux, suggesting hybridization, however, Bur Oak does not co-occur in the canyons. The supposition is the Chinquapin populations are descendants of an ancient time of sympatry with Bur Oak.

Introduction

Disjunct populations of *Quercus muehlenbergii* Engelmann predominate in the canyons above the South Canadian River in Ellis County, Oklahoma. However, this species is not typically dominant in Oklahoma Forest Associations, Hoagland (2000). Throughout its contiguous range in the U.S., from Vermont to west Texas, it occurs occasionally in mature forests or frequent on limestone outcroppings, Sander (1990).

The Canyons' populations represent the western limit of the species' range in Oklahoma, as a SEINet search (2022) of the Panhandle Counties returned no occurrence. Isolated populations of the Chinquapins, however, are also known further west in New Mexico, and Texas and south into northern Mexico, Tucker (1961), Nixon and Muller (1997) and Thomson (2022). The Preserve populations are the eastern-most of these outliers

In Oklahoma, the species is found in the eastern tier of counties as part of the Acer Saccharum Alliance, Hoagland (2000), but typically as a minor component. It is also recorded occasionally throughout Oklahoma but absent from the Panhandle counties. Thus, its dominance in the canyons is remarkable.

*Corresponding author: paul.thomson@okstate.edu

The dry, sub humid conditions of the Canyons are a far different climatic regime from that of the more mesic eastern forests. How, then have they come to predominate in the Canyons?

During a review of specimens of western white oaks in Oklahoma, a voucher specimen, (4C-034), from a biological survey of Ellis County, Oklahoma, Hoagland (2007) was examined. The specimen, on deposit in the Robert Bebb Herbarium at the University of Oklahoma (OKL), was from the Four Canyon Nature Preserve. It appeared unusual in having what seemed to be leafy twigs from two different trees, Fig. 1. The twigs bearing leaves with dentate margins are typical of *Quercus muehlengbergii* Englm. The lobed leaves of the other twig are unlike those of Chinquapin Oaks. While unusual to prepare a record in this way, neither did the specimens seem to be from sun and shade leaves of the same tree.

Figure 1 Leafy Twigs from Four Canyon Nature Preserve Biological Survey. Used with permission.

In the survey, Hoagland described the canyons' vegetation as a *Q. muehlenbergii-Juniperus virginiana* L. association occurring on deep sandstone soil, thus assigning the species dominant status in the association. He states, "Although *Q. muehlenbergii* has been reported from counties immediately south of Ellis, it does not occur as a dominant species." In the canyons it clearly does. What is striking about the trees is that many display a shrub-like habit of producing multiple branches at or near the base. However, on inspection, none of them appeared to be connected by rhizomes or is branching the result of mechanical or fire damage, Figure 2.

Fig. 2. Multi-trunk Chinquapin oak in the Four Canyon Nature Preserve

A request was granted by the Nature Conservancy for permission to sample populations of the trees in two canyons, Cinnamon and Mulberry in 2022 and 2023 respectively. While the stands appear to be those of *Q. muehlenbergii* a detailed examination of specimens showed characters not associated with the Chinquapin Oaks. However, no other species of oaks occur in the canyons. This study provides morphological evidence of their introgression by *Q. macrocarpa* and a timeframe of their sympatry.

Methods

Study Site

The Four Canyon Nature Preserve, managed by the Nature Conservancy, is in Ellis County near Arnett, Oklahoma (36.01.12 N, 99.30.06 W). The Preserve consists of approximately 1620 hectares of rolling hills and deeply eroded hillsides. While the runoff areas are called "Canyons" they are more like deep ravines opening to the Canadian river below. Four of them are named, from west to east: Cinnamon, Horse, Mulberry, and Harsha although there are several smaller unnamed ones. Situated in the Southern Great Plains, the climate of Ellis County is humid, subtropical with average annual precipitation of 60.4 cm (23.78 in.), Oklahoma Climatological Survey (2023).

The area above the canyons is mixed-grass prairie but near the rims woody species are found including, *Q. havardii* Rydberg, Havard Oak, and Eastern Red Cedar, *Juniperus virginiana* L. *Quercus stellata* Wangenheim, Post Oak, is known from the preserve, Buthold (4C-446: OKL), but not the canyons. According to station manager, Chris Hise, "A single Post Oak was located west of Cinnamon Canyon but was destroyed by wildfire in 2008, but Post Oak hybrids (*Q. havardii* × *stellata)* are found in the shinnery west of the Preserve". He further offered, that the previous owner said no fires had reached the canyons from the time he purchased it in 1950 until it was acquired in 2004 by the Nature Conservancy.

While the Canyons' Chinquapins seemed isolated, records of occurrence were searched to determine the nearest reported locations. Records were obtained via SEINet (2023) and from specimens in the herbaria of the University of Oklahoma (OKL) and Oklahoma State University (OKLA). The results confirmed that, notwithstanding an occasional record in counties east and south of the site, the populations are quite isolated.

Disjunct populations of the species are also known from the Capitan Mountains of New Mexico, Thomson (2022) and in the Davis Mountains of west Texas and northern Mexico, Nixon and Muller, (1997). Thus, it seems, Four Canyon Nature Preserve Chinquapins are the eastern-most of the disjunct populations and western-most of its occurrence in Oklahoma.

Cinnamon Canyon

Cinnamon Canyon, western-most of the named canyons, lies in the northeast corner of the Preserve (36.00.11W, -99.28.48 W) and situated along a northwest to southeast orientation. Trees of the canyon have multiple trunks arising at the base (Fig.2). They supported few acorns, but none was accessible for collection. Neither were any found on the canyon floor and no seedling or sapling-sized individuals were observed.

Mulberry Canyon

Mulberry Canyon is the third canyon of the four, west to east and situated northwest to southeast above the Canadian River at 36.00.13 N -99.28.01W. Here, also, many trees are multi-trunked but were found to have acorns accessible for collecting. As with Cinnamon Canyon no seedling or sapling sized trees were observed.

Sample Collection and Preparation

Permission was granted to sample a population from Cinnamon Canyon during September of 2022. The examination revealed five features not associated with Chinquapin Oaks, thus prompting a request to sample a second canyon. Permission was given to sample Mulberry Canyon, in October of 2023. The collections from both canyons were made by Amy Buthod of the Oklahoma Biological Survey and Collections Manager of the Robert Bebb Herbarium (OKL) and Pricilla Crawford of the Oklahoma Biological Survey. In all, twelve individuals of *Q. muehlenbergii* from Cinnamon Canyon in September 2022 and twelve from Mulberry Canyon in October 2023, were identified for collection and two specimens obtained from each. Photos were taken of each tree sampled.

Specimens from two individuals of *Q. havardii* Qh C 1 and 2 occurring above Cinnamon Canyon were also collected and two specimens of *Q. macrocarpa,* Qmc 1 and 2, from Turkey Creek, a site about 8 km northeast of the preserve, and the only recorded site for Bur Oak

in the county. No other species of white oaks were found in the search referred to above or on site in the Preserve.

In collecting specimens care was taken to select twigs of sun leaves, as nearly possible, from the same west-facing aspect of each tree. In cases where leaves of like orientation were not accessible, specimens were taken from twigs closest to west-facing.

For each tree, the height was estimated, and a measurement of the trunk (s) diameter was taken at breast height (dbh). Specimens from Cinnamon Canyon were labeled in order of collection Qm C (Cinnamon) 1 to Qm C 12, for *Q. muehlenbergii.* Specimens from Mulberry Canyon were labeled Qm M (Mulberry) 1 to Qm M 12. For each sample, location and elevation data were recorded, and associated species listed. The specimens were then pressed and returned to University of Oklahoma herbarium for drying and study. While the data for tree height, diameter at breast height and listing of associated species were not germane to this study the data were collected and made part of the record for any future studies.

Morphological Examination

Metrics obtained for this study were based on features of leaves, twigs and terminal buds. Acorns were not included as they were only available from Mulberry Canyon. The limited number were considered insufficient to be useful in the analysis of the status of the plants and were not included. Their metrics, however, are available from the author.

Leaves

Length of leaf blades was measured from base to apex of terminal leaves and width at the midpoint using calipers. Measurements are rounded to the nearest tenth centimeter. The vein pattern was also examined and recorded.

Leaves were examined to determine trichome type(s) by viewing the abaxial surface of terminal leaves at the apex, mid-leaf and base of the blade with a compound light microscope at 60X. The type(s) were determined and recorded.

Leaf contour was determined by constructing an index of indentation. The index was developed from measurements on specimens of *Q. muehlenbergii* in the herbaria of OKL and OKLA and from previous studies, Thomson (2009), Specimens were examined from across its geographic range. Values from sixty-three specimens were used.

The Index was developed using calipers to measure the depth of the second indentation from the apex and the second indentation from the base on the right side of the terminal leaf. An indentation value was obtained by dividing the apex value by the base value. The average was used as the index value representing "typical" *Q. muehlenbergii.* Values for the canyon oaks were compared to this index.

Twigs and *Buds*

Dimensions for twigs and buds were not obtained, but pubescence was noted on a presence/absence basis.

Because *Q. muehlenbergii i*s known to have a tolerance for alkaline soils, a sample from each canyon was collected and sent to the Oklahoma State University Soil, Water and Forage Laboratory (OSU) for analysis.

Results

From the examination of specimens, five features stood out as atypical for *Q. muehlenbergii*: degree of indentation of the leaf margin, pattern of secondary veins, presence of terminal bud stipules, pubescent twigs, and trichome types.

To determine whether the anomalies could be the result of hybridization, the features of four other oak species; *Q. havardii,* and *Q. stellata* because they occur in the Preserve and *Q. macrocarpa* for its presence in the county. The fourth, *Q. gambelii*, while not extant in the county, has been noted in the Panhandle County of Cimarron, Little (2010). Also, a specimen viewed during the study, Little, (36724: OKLA) from Woodward County, determined *Q. gambe-*

lii × *Q. muehlenbergii,* implicated *Q. gambelii.* Because of this finding, and that *Q. gambelii* has been recognized as a participant in hybridizations with *Q. muehlenbergii* in other studies, Tucker (1961) and Thomson (2022), I included it in the study.

The five features are further analyzed below and summarized in Tables 1 and 2.

Margination

The margins of typical *Q. muehlenbergii* are toothed or shallow lobed, often mucronate, with an Index value at or less than 2.1:1. The indentation index procedure was used to obtain a value for each canyon specimen. Eight from Cinnamon and three from Mulberry had values greater than the 2.1:1 ratio for typical *Q. muehlenbergii*.

Venation

The veins of *Q. muehlenbergii* leaves display a distinct pinnate pattern; secondary veins running from midrib to margin. The pattern is shown in Figure 3. The leaf on the left is from Qm M 4 showing a secondary vein dividing into two tertiary veins. The leaf on the right displays pinnate venation typical of *Q. muehlenbergii*.

In three of the Cinnamon Canyon specimens, Qm C 1, 2 and 7, one or more of the secondary veins showed a branch of the same magnitude also reaching the margin, Table 1. This pattern also found in six of the specimens from Mulberry Canyon, Qm M 1, 3, 4, 5, and 12, Table 2. Divergent branching is found in the leaves of oaks with distinct lobes such as *Q. macrocarpa,* and *Q. gambelii* but not the Chinquapins.

Vestiture

Twigs

Twigs of *Q. muehlenbergii* are glabrous or sparingly glabrate. Twigs of *Q. gambelii, Q. macrocarpa* and *Q. stellata* have some degree of persistent pubescence, but those of *Q. havardii* are glabrous or glabrate. Specimens QmC1, C6 and C8 from Cinnamon Canyon displayed pubescent twigs. Those of Mulberry Canyon were glabrous.

Figure 3 divergent veins of suspected hybrid from Mulberry Canyon. Photo by author.

Leaves

Leaves of Chinquapin Oaks are vested with trichomes. Trichome types are considered diagnostic characters for white oaks, Nixon and Muller (1997). Those occurring on *Q. muehlenbergii* and the four potential parents are described here. Nomenclature follows Hardin (1979).

Trichomes of *Q. muehlenbergii* are of a single type, stellate with 6-12 rays appressed to the leaf surface. *Q. gambelii* leaves produce fasciculate trichomes with 1-4 rays, and *Q. havardii* have erect, stellate hairs often with twisted rays. Trichomes of *Q. macrocarpa* are of three types: fasciculate, stellate-appressed and bulbous. Bulbous hairs resemble a drumstick often with the terminal cell pigmented yellow. *Q. stellata* leaves produce stellate-pediculate hairs, and occasionally bulbous ones.

Specimens QmC1, 2 and 12 from the Cinnamon Canyon specimens possessed stellate-appressed, fasciculate and the bulbous type. The others possessed stellate-appressed and fasciculate but not the bulbous type. The trichomes

of Mulberry Canyon Oaks are stellate-appressed, however, three QmM 1, 4 and 12 were found to also have the bulbous type. Their occurrence is shown in Tables 1 and 2.

Terminal Bud Stipules

Stipules were found, subtending and amid, the scales of the terminal buds of several of the specimens. In a study of bud formation in the Pendunulate Oak, *Q. robur* L, they were identified as transitional structures leading to bud scales, Studer-Ehrensberger & Schilperoord, (2016). Why they are present at bud maturity in some but not others was not germane to that study. For purposes of this study, they are consistent in occurrence for the species bearing them and thus of diagnostic value.

The species of this study producing stipules are *gambelii* and *Q. macrocarpa.* Their stipules extend up to or beyond the tip of the bud, are linear and pubescent. Five of the Cinnamon Canyon specimens, Qm C 2 and Qm C 6-9, and one from Mulberry Canyon Qm M 1 produced stipules, Tables 1 and 2. Stipules are not persistent on terminal buds of *Q. muehlenbergii.*

Transverse fissures

This feature of twigs was not observed during the study. However, they are prominent on twigs of *Q. gambelii* and were used in an examination of the origin of *Q. margaretta* and *Q. drummondii* by Tucker and Mueller (1958) to distinguish *Q. gambelii* from *Q. margaretta.* Figure 4 shows transverse fissures on a specimen collected by John Tucker, in the John M. Tucker Herbarium, University of California, Davis Tucker, (2776-6: DAV).

Because fissures were not found on the specimens of this study, they are not included as an anomalous feature, but their absence aided in identifying the possible second parent.

A further search for *Q. gambelii* in Oklahoma via SEINet returned 12 specimens, all in Cimarron County, 241 km northwest of the Preserve. Herbarium loans were obtained from the Botanical Research Institute of Texas (BRIT) and Morten Arboretum (MOR) to examine ten of them. The others were in the herbaria of the University of Oklahoma (OKL) and Oklahoma State University (OKLA) which I viewed on site. I could not confirm *Q. gambelii* in typical form in Oklahoma, Thomson (2025).

The anomalous features possessed by the potential parents are summarized in Table 3. Three occur on *Q. gambelii*, none on *Q. havardii*, five on *Q. macrocarpa* and two on *Q. stellata.*

Figure 4. Photo of Transverse Fissures on a twig of *Q. gambelii,* by Dan Potter, University of California, Davis. Used with permission.

To obtain an overall impression the number of occurrences of the aberrant characters occurring on the specimens from each canyon were combined to determine the total occurrences. The number of occurrences are displayed in, Tables 4 and 5 and described as follows:

Cinnamon Canyon

The Cinnamon Canyon specimens showed 1 to 4 features with a total of 31 occurrences. Qm C 10 is most like *Q. muehlenbergii* in possessing only one of the features. Qm C 2 and Qm C 8 are most aberrant with 4 features. Qm C1, Qm C6, and Qm C9 show three features and Qm C3, Qm C4, Qm C5, Qm C11 and Qm C12 each had two features. Trichome type was the most frequent. All twelve specimens had stellate and fasciculate trichomes and three Qm C1, Qm

C2 and Qm C12 had the bulbous as well. Stipules were next frequent with five terminal buds subtended by them. Pubescent twigs were least frequent with three occurrences. In all the twelve specimens had 31 occurrences of the features.

Mulberry Canyon

The Chinquapins of Mulberry Canyon possessed fewer of the features. Five of the specimens, Qm M 2, 6, 8, 10 and 11 showed none of the characters. Two of them, Qm M 1 and 12 displayed three each, Qm M 3 and 4 two each and Qm M 7 and 9 one feature. Atypical branching of the veins occurred most frequently with six of the specimens, Qm M 1,3,4,5, 7 and 12 displaying the pattern. None were found to have pubescent twigs. Together, the 12 specimens displayed 13 of the suspected hybrid characteristics.

In all, the 24 specimens of this study bore 44 occurrences of putative hybrid characters.

Soil Conditions

Laboratory reports found the sandstone soils of Cinnamon and Mulberry canyons slightly alkaline at pH 7.6 and 7.8 respectively. The reports also indicated the soils to be nutrient poor with exceptionally low levels of nitrogen and phosphorus, but adequate in potassium, OSU Soil Report 1735 (2022) and OSU Soil Report 195042 (2024). Nutrient availability is known to affect stand quality, Johnson et al. (2019), however, no further assessments of edaphic conditions were made.

Analysis of Potential Parentage

To determine the likely parentage each of the four species, identified above, were examined for the source of the five features. The results are described as follow.

Quercus gambelii

Leaves of typical Gambel's Oak are lobed in the lower and upper half, possess divergent veins extending to lobes, and bear trichomes that are simple and fasciculate with 1-4 rays. Terminal bud stipules are typically present, and twigs are pubescent or become glabrate, the periderm often marked with noticeable transverse fissures.

Quercus havardii

Havard Oak is abundant in the area above the canyons. Also called Shin Oak, it varies from being rhizomatous shrubs to small trees (Nellessen, 2004) and occurs throughout much of Ellis County, Wiedeman and Penfound (1960).

Leaf margins are variable; undulate or with 2-3 teeth, or occasionally lobed in the upper half. Secondary veins are branched but rarely reach the margin. Trichomes are stellate with twisted rays. Terminal bud stipules are absent, and twigs are glabrous or become glabrate.

A record from Woodward County, Little (36,505: OKLA) examined during the study, had been determined by him as a cross between *Q. muehlenbergii* and *Q. havardii*. Upon examination it did appear to be of hybrid origin, but none of the aberrant features, as described above, were found and, therefore, was not considered germane to this study.

Quercus macrocarpa.

Leaves are lobed most pronouncedly in the lower half, and some of the lobes contain a vein diverging from a secondary, ending in a lobe tip. Terminal buds are often subtended by pubescent stipules and trichomes are stellate with 6-12 rays, fasciculate with 6-8 rays, and bulbous. Pubescence is persistent on twigs.

Range maps of Bur Oak do not show it in Ellis County, Little (2010), Tirmenstein (1991), and Nixon and Mueller (1997). However, a single record was located in a SEINet search, (Erteeb 1570 OKLA). With the assistance of Preserve Manager, Chris Hise, the site, about 8 km northwest of the Preserve, was located and the specimen referred to above collected. This is believed to be the only location for *Q. macrocarpa* in the county and western-most in Oklahoma.

Quercus stellata

Post Oak would be an inviting possibility for the source of variation in the Canyon Chinquapins for its known history in the preserve. However, none was collected for this study for the reason stated above. However, to evaluate it for a potential role in hybridization, I used features from herbarium records of specimens from western Oklahoma and my previous research, Thomson, (2009).

Post Oak is well known for leaves with cross-like lobes occurring at right angles to the midrib. Secondary veins are divergent, but the branches do not typically run to a lobe tip. Beneath, the leaves bear both stellate and bulbous trichomes but the stellate hairs are erect and often pedestalate. Terminal buds are not subtended by stipules, but twigs are pubescent.

Table 1. Values For Atypical Characteristics of Cinnamon Canyon Oaks
Legend: Index; =< 2.1= Q. muehlenbergii, >2.1=hybrid; Trichomes Types, s=stellate, appressed, f=fasciculate, b=bulbous. Twig Pubescence, g=glabrous, p=pubescent; Stipules, - =feature absent, +=feature present; Vein Pattern, d=divergent, p=pinnate

Specimen	Indentation Index	Trichome Types	Twig Pubescence	Presence/absence Stipules	Vein Pattern
Qm C 1	5.90	s,f,b	g	-	d
Qm C 2	2.00	s,f,b	p	+	d
Qm C 3	2.50	s,f	g	-	p
Qm C 4	3.03	s,f	g	-	p
Qm C 5	3.33	s,f	g	-	p
Qm C 6	2.00	s,f	p	+	p
Qm C 7	1.00	s,f	g	+	d
Qm C 8	3.45	s,f	p	+	p
Qm C 9	4.00	s,f	g	+	P
Qm C 10	2.00	s,f	g	-	p
Qm C 11	5.90	s,f	g	-	p
Qm C 12	5.00	s,f,b	g	-	p

Table 2. Values for atypical characteristics of Mulberry Canyon Oaks
Legend: Index; 2.1 =< Q. muehlenbergii; < 2.1 = hybrid; Trichome Types: s=stellate, f=fasciculate, b=bulbous; Pubescence: p=pubescent; g=glabrous; Stipules: +=present; - = absent; Vein Pattern d = divergent, p = pinnate

Specimen	Indentation Index	Trichome Type(s)	Twig Pubescence	Stipules Present/Absent	Vein Pattern
Qm M 1	3:1	s,b	g	+	d
Qm M 2	2:1	s	g	-	p
Qm M 3	2:1	s	g	-	d
Qm M 4	2:1	s,b	g	-	d
Qm M 5	2:1	s	g	-	d
Qm M 6	2:1	s	g	-	p
Qm M 7	2:1	s	g	-	d
Qm M 8	2:1	s	g	-	p
Qm M 9	2.5:1	s	g	-	p
Qm M 10	2:1	s	g	-	p
Qm M 11	2:1	s	g	-	p
Qm M 12	2.5:1	s,b	g	-	d

Table 3. Anomalous features of Canyon Oaks Occurring on Suspected Parent Species

Species	Q. gambelii	Q. havardii	Q. macrocarpa	Q. stellata
Anomalous feature	Lobing; Stipules; Pubescence	None	Lobing; Stipules; Trichomes; Vena-tion; Pubescence	Pubescence; Trichomes
Number	3	0	5	2

Table 4. Aberrant Feature Occurrence on Cinnamon Canyon Oaks.
Legend: X=presence of feature, - = absence of feature

			Aberrant Features			
Specimen	Lobing	Stipules	Trichomes	Venation	Pubescence	Number of Features
Qm C 1	X	-	X	X	-	3
Qm C 2	-	X	X	X	X	4
Qm C 3	X	-	X	-	-	2
Qm C 4	X	-	X	-	-	2
Qm C 5	X	-	X	-		2
Qm C 6	-	X	X	-	X	3
Qm C 7	-	X	X	X	-	3
Qm C 8	X	X	X	-	X	4
Qm C 9	X	X	X	-	-	3
Qm C 10	-	-	X	-	-	1
Qm C 11	X	-	X	-	-	2
Qm C 12	X	-	X	-	-	2
Total Occurrences	8	5	12	3	3	31

Table 5. Occurrence per Specimen and Totals for Aberrant Features on Mulberry Canyon Oaks.
Legend: X = Presence of Feature - = Absence of Feature; B = bulbous trichomes

			Aberrant Features			
Specimen	Lobing	Stipules	Trichomes	Venation	Pubescence	Number of Features
Qm M 1	-	X	X	X	-	3
Qm M 2	-	-	-	-	-	0
Qm M 3	X	-	-	X	-	2
Qm M 4	-	-	X	X	-	2
Qm M 5	-	-	-	X	-	1
Qm M 6	-	-	-	-	-	0
Qm M 7	-	-	-	X	-	1
Qm M 8	-	-	-	-	-	0
Qm M 9	-	-	-	-	-	1
Qm M 10	X	-	-	-	-	0
Qm M 11	-	-	-	-	-	0
Qm M 12	X	-	X	X	-	3
					-	
					-	
					-	
Total Occurrences	3	1	3	6	0	13

Table 6. Occurrences per specimen and totals of aberrant features of Cinnamon Canyon Oaks

Specimen		Aberrant Features				
	Lobing	Stipules	Trichomes	Venation	Pubescence	Number of Features
Qm 1	X	-	X B	X	-	3
Qm 2	-	X	X B	X	X	4
Qm 3	X	-	X	-	-	2
Qm 4	X	-	X	-	-	2
Qm 5	X	-	X	-		2
Qm 6	-	X	X	-	X	3
Qm 7	-	X	X	X	-	3
Qm 8	X	X	X	-	X	4
Qm 9	X	X	X	-	-	3
Qm 10	-	-	X	-	-	1
Qm 11	X	-	X	-	-	2
Qm 12	X	-	X B	-	-	2
Total Occurrences	8	5	12	3	3	31

Discussion

Of the species considered as the possible source of the features, only Bur Oak has the constellation of characters found among the Canyon Oaks. Especially convincing is the occurrence of *Q. macrocarpa*-like fasciculate trichomes on many of the specimens. However, with respect to trichome types and their occurrence on *Q. muehlenbergii*, my interpretation differs from that of Hardin (1979). His Atlas includes the fasciculate type for *Q. muehlenbergii* whereas I believe they are atypical. Both from field and herbarium studies, I have found when leaves of *Q. muehlenbergii* produce fasciculate hairs there is a correspondence in range and average for quantitative features, i.e., number of rays and spread, to those of *Q. macrocarpa.* A wide leaf form of *Q. muehlenbergii*, *f. alexanderi* Britton, frequently has only the fasciculate trichomes, a condition also sometimes observed in *Q. macrocarpa* Thomson (1979). For this study I have taken the position that fasciculate trichomes are not typical for *Q. muehlenbergii* and their presence adds to the evidence of hybridization.

Taking this position does increase the number of characters and occurrences used to support hybridization. However, if occurrence of fasciculate trichomes is excluded from the analysis, there is still strong support for the plants' hybrid origin as 13 specimens displayed an indentation index above 2.1:1, nine showed the divergent venation pattern, six possessed terminal bud stipules, six produced bulbous trichomes and three had persistent pubescence, Tables 1 and 2.

Of the others, Post oak and Havard Oak are known to occur in the preserve but not Gambel's Oak or Bur Oak. Havard Oak was rejected as a possible second parent as its characteristics are not consistent with it being a partner in introgression.

Post Oak does have twigs that remain pubescent and its trichomes include the bulbous type, but it was also rejected as the parent because its terminal buds do not bear stipules, and its leaves do not have a vein pattern found in some of the suspected hybrids. Also, its stellate trichomes are non-appressed, often attached to pedestals, and its largest lobes are most often found in the mid or upper half of the leaf.

None of the suspected hybrids displayed the diagnostic features of *Q. gambelii,* twigs with transverse fissures and fasciculate trichomes with 1-4 rays, it was rejected as a possible second parent,

If Bur Oak, *Q. macrocarpa,* is the second parent, then this leaves the matter of how and when the pollination may have occurred. In Oklahoma, Bur Oak is widespread but is at the limit of its range in Ellis County. The single record from Turkey Creek is northeast and downwind of the Canyons making them the unlikely pollinators.

For populations of supposed hybrids of *Q. gambelii* and *Q. macrocarpa* occurring in New Mexico and South Dakota, Maze (1968) postulated a more western and northern distribution for Bur Oak during the Pleistocene. This, he posited, allowed them to become sympatric with Gambel's Oak and hybridization and introgression to occur. But the Pliocene precedes the Pleistocene, a time of separation for what would become the modern forests east and west of the Great Plains. Maze further posited that hybrids bearing features of *Q. gambelii* and *Q. macrocarpa* in areas where neither is extant, and geology dating to the Pleistocene, were likely the result of secondary contact during pluvial periods. As the climate became drier again, the hybrids survived but not the parents.

A specimen collected by Waterfall (7950 BRIT) from Cimarron County, which I believe is *Q. gambelii* × *Q. macrocarpa,* was examined during a study of *Q. gambelii* in Oklahoma, Thomson (2025), and offers further evidence of his position. Also, the soils of the site date to the Pleistocene, Johnson and Luza (2008).

Can Maze's supposition of hybridization during Pleistocene sympatry also account for the populations of introgressants in the Four Canyon Preserve? Is it plausible for Bur Oak also to have been sympatric with the Chinquapins and the fea-

tures acquired then? If so, are the Chinquapins of the Four Canyon Preserve also descendants of this time? To be sure this is speculative unless corroborated with additional evidence, but absent co-occurrence, the proposition may account for the condition of the Canyon Chinquapin Oaks.

Are all disjunct populations of *Q. muehlenbergii* Introgressants? In the 2022 study of a Chinquapin population in the Capitan Mountains, elevation 6250ft (1905m), of New Mexico, evidence of introgression by *Q. gambelii* was presented. Chinquapin oaks are not normally found in montane environments, but *Q. gambelii* is. Has the introgression allowed for adaptation to the higher elevations?

In this study I have presented evidence of introgression by Q. macrocarpa which I believe has contributed to the Chinquapins ability to persist in western Oklahoma. Whether all such populations are introgressants I cannot say, but it seems to be so in the ones I have studied. Perhaps further research of disjunct populations, especially with genomic testing, will add to our understanding.

The disjunct populations suggest a once more extensive range for the species, but more so to the white oak clade's capacity for adapting to changing climatic regimes, Kremer and Hipp (2019). The Chinquapins of Ellis County stand with their counterparts from the mountains of New Mexico to the arroyos of west Texas as testaments to this capability.

SPECIMEN AND DATA AVAILIBILTY

A set of each of the specimens used in this study were contributed to the Robert Bebb Herbarium (OKL) and the Oklahoma State University herbarium (OKLA) respectively. For information about them please contact Amy Buthod, Collections Manager (OKL) amybuthod@ou.ed and Mark Fishbein, Curator mark.fishbein@okstate.edu (OKLA).

Acknowledgments

I thank the Nature Conservancy for permission to enter the preserve and make collections for this study and especially to the Preserve Manager, Chris Hise, for his important time saving knowledge of the area.

The author is indebted to Amy Buthod, Collections Manager and Abby Moore, Curator of the Robert Bebb Herbarium for their assistance during the herbarium phase of this study. And, to Amy and her colleague Pricilla Crawford of the Oklahoma Biological Survey for traveling to the preserve and collecting and preparing the specimens, and data sheets and for taking photos in the canyon.

I thank Mark Fishbein, Curator of the Oklahoma State University Herbarium and Chairman of the Department of Plant biology, for supporting my herbarium study of white oak specimens.

My thanks also to Ashley Bales, Collections Manager, of the Botanical Research Institute of Texas herbarium, for preparing a loan for my review of important collections from the panhandles of Texas and Oklahoma. To Jenna Messick Curator of the herbarium at the University of Central Oklahoma for assisting with my study of *Quercus* species in Oklahoma and for introducing me to Amy Buthod at the University of Oklahoma. And to Dan Potter, University of California, Davis, John Tucker Herbarium, for photos of *Q. gambelii* showing transverse features and permission to use them in this study.

I am grateful to the reviewers of this study for their helpful suggestions.

References

Denig, Bryan R., et al. "Screening oak hybrids for tolerance to alkaline soils." *Journal of Environmental Horticulture* 32.2 (2014): 71-76

Gleason, H.A. 1963. Fagaceae, p 43. In: The New Britton and Brown Illustrated Flora of the Northeastern United States and Adjacent Canada, Vol. 2. Revised ed. Hafner Publishing Company, New York, N.Y.

Hardin, James W. 1979. Atlas of Foliar Surface Features in Woody Plants, I. Vestiture and Trichome Types in Eastern North American Quercus. Bulletin of The Torrey Botanical Club, Oct.-Dec. 1979. Vol.106, No.4 (Oct-Dec. 1979), pp. 313-325.

Hise, Chris. 2022. Station Manager, Four Canyon Nature Preserve. Personal Communication.

Hoagland, B. 2000. The Vegetation of Oklahoma: A Classification for Landscape Mapping and Conservation Planning. The Southwestern Naturalist. Vol. 45. No.4. pp 385-420.

Hoagland, B. and A. Buthod. 2007. The Vascular Flora of the Four Canyons Nature Preserve, Ellis County, Oklahoma. J. Bot. Res. Inst. Texas 1 (1): 655-664.

Kremer, Antoine and Hipp, Andrew L. 2019, New Phytologist. Volume 226. Issue 4

Johnson, Kenneth and Luza, K. 2008. Earth Sciences and Mineral Resources of Oklahoma. Oklahoma Geological Survey. Educational Publication p. 10

Johnson, Paul S., Stephen R. Shifley, Robert Rogers, Daniel C. Dey, and John M. Kabrick. The Ecology and Silviculture of Oaks. Cabi, 2019.

Kremer, Antoine and A. Hipp. 2020. Oaks: An Evolutionary Success Story. New Phytologist, No.226, Vol. 4, pp. 987-1011.

Little, Jr, E.L 1981. Oklahoma Forestry Services, State Department of Agriculture, Food and Forestry. Publication 1, Revised Edition 17. 2010.

Maze, Jack. "Past hybridization between *Quercus macrocarpa* and *Quercus gambelii*." Brittonia 20 (1968): 321-333.

Mohlenbrock, Robert H., and Paul M. Thomson. Flowering Plants: Smartweeds to Hazelnuts. SIU Press, 2009.

Nellessen, James E. "*Quercus havardii* Rydb. Havard shin oak." Wildland Shrubs of the United States and Its Territories: Thamnic Descriptions 1 (2004): 613.

Nixon, K.C. and C.H. Muller. 1997. Quercus sect. Quercus, pp. 471-506. In: Flora of North America Editorial Committee, eds. Flora of North America, North of Mexico, vol.3. Oxford University Press, New York, NY.

Oklahoma Climatological Survey. 2022. Website (https://ocs.ou.edu) Accessed Mar 2023.

Oklahoma State Extension Service, Soil, Water and Forage Analytical Laboratory. 2022. Report 1735. Dated Nov. 4 2022.

Oklahoma State Extension Service, Soil, Water and Forage Analytical Laboratory. 2024. Report 195048. Dated Feb. 9 2024.

Sander, I.L. 1990. *Quercus muehlenbergii* Engelm. Chinkapin oak. In: Burns, R.M.; Honkala, B.H., tech. coords. Silvics of North America, Vol. 2: Hardwoods. Agric. Handb. 654. Washington, DC: U.S. Department ofAgriculture, Forest Service. https://research.fs.usda.gov/silvics/chinkapin-oak

Southwest Environmental Information Network. 2023. SEINet data portal. Website (https://swbiodiversity.org/seinet/). Accessed Mar 2023.

Stransky, John J. 1990. Quercus stellata Wangenh. Post Oak. In: Burns, R.M.; Hinkala, B. H., tech. coords. Silvics of North America Vol. 2: Hardwoods. Agric. Handb. 654. Washington DC: U. S. Department of Agriculture, Forest Service. https://research.fs.usda.gov/silvics/post-oak

Studer-Ehrensberger, Kathrin & Schilperoord, Peer. (2016). The Blossom-similarity of the Vegetative Annual Shoot of the Pedunculate Oak (*Quercus robur* L.). 10.13140/RG.2.1.5082.1209.

Thomson, Paul M. 2022. *Quercus prinoides* hybrids in the Capitan Mountains of New Mexico. Rhodora. 123. 335-344.

_____2025. The Quercus undulata Complex in Oklahoma. In Press.

Thomson, Paul M and R. H. Mohlenbrock 1979. "Foliar trichomes of Quercus subgenus Quercus in the eastern United States." Journal of the Arnold Arboretum 60.3 (1979): 350-366.

Tirmenstein, D. A. 1991. *Quercus muehlenbergii*. USDA Forest Service, Rocky Mountain Research Station, Fire Sciences Laboratory.

New County Records of Mammals from Oklahoma

Lynda Samanie Loucks*, J.T. Warr, Nadiya Cavallo, Lillian R. Gunelson, Damon Corvelo, and Michelle L. Haynie

Department of Biology, University of Central Oklahoma, Edmond, OK 73034

Abstract: Since the publication of *Mammals of Oklahoma*, second edition, the number of mammal specimens deposited in natural history collections continues to increase, and county distributions of mammal species in the state continue to change. In this study, we report 31 additional county records, plus one record along a county line, for 12 species representing 5 mammalian orders. These records were verified through 65 voucher specimens deposited in two institutions, as well as 7 new observational records. This study expands the understanding of the distribution of mammals in Oklahoma.

Introduction

Twelve EPA level III ecoregions (High Plains, Southwestern Tablelands, Central Great Plains, Flint Hills, Cross Timbers, East Central Texas Plains, South Central Plains, Ouachita Mountains, Arkansas Valley, Boston Mountains, Ozark Highlands, and Central Irregular Plains) occur in the state of Oklahoma (Caire et al. 2024). The ecoregion diversity makes this region of North America biologically significant and ideal for examining distribution patterns and impacts from land modification, including the influence of global climate change, agricultural conversion, urbanization, mining, oil and gas extraction, and wind-energy facility construction. Blair (1939) published the first comprehensive list of mammal diversity in the state. The second comprehensive compilation for mammal records was the first edition of Mammals of Oklahoma (Caire et al. 1989), followed by the second edition of Mammals of Oklahoma (Caire et al. 2024) published 35 years later. In this study, we report additional county records for 11 mammal species that have vouchered specimens deposited in natural history collections. Additional observational records for mountain lions have also been reported by the Oklahoma Department of Wildlife Conservation (ODWC) and are included here.

*Corresponding author: lloucks@uco.edu

Methods and Materials

Mammalian orders are arranged according to Wilson and Reeder (2005). Taxonomy and common name usage follows Bradley et al. (2014), Caire et al. (2019), and Caire et al. (2024). All specimens represent the first record(s) of the species for the counties reported. The specimens are listed alphabetically within taxonomic groups. Locality data have been modified from the original tag and formatted for consistency with regards to abbreviations and GPS coordinates. Scientific voucher specimens herein reported are deposited in the following institutions: Sam Noble Oklahoma Museum of Natural History, Norman, Oklahoma (OMNH) and University of Central Oklahoma Natural History Museum, Collection of Vertebrates, Edmond, Oklahoma (UCOCV). Specimens were prepared as skins, skulls, skeletons, or fluid specimens fixed in 10% formalin and stored in 70% ethanol. Tissue samples were taken unless specimens were in a deteriorated state, as is the case with many bat specimens submitted to Oklahoma Animal Diagnostic Disease Laboratory (OADDL).

Results and Discussion

Thirty-one new county records are reported for 12 species of mammals represented by 65 museum vouchered specimens and 7 observations from 23 of Oklahoma's 77 counties. An additional vouchered specimen was collected on a county line and not assigned as a specific county record but is an important location record because no specimen had been previously vouchered for either county. These new records include 1 armadillo, 4 bats, 2 carnivores, 2 cervids, and 3 rodents. The addition of this data expands our understanding of mammals in Oklahoma and enhances our knowledge of their diversity and distribution, which is imperative for future research in ecology, evolutionary biology, behavior, and the impact of climate change on natural communities and ecosystems. Some records may be indicative of shifts in distribution; however, some records may be more reflective of the actual distribution patterns of the species that were incomplete due to a lack of voucher specimens. The ODWC utilizes distribution data and species abundance and richness evaluation to aid in important conservation and management plans (ODWC 2016). Maps (Figure 1) are provided for each species denoting new county records as stars based on distribution maps included in Caire et al. (2024).

ORDER CINGULATA
Family Dasypodidae
Dasypus novemcinctus
Nine-banded Armadillo

The Nine-banded Armadillo has been reported in a variety of habitats throughout much of Oklahoma, but few specimen records exist for most parts of the state. Loucks et al. (2023) reported records for 42 counties, with 7 observational county records reported in Caire et al (2024). New records are reported for Kay and Murray counties, and one record is reported on the county line of Osage and Tulsa counties in the town of Skiatook. Logan County, previously reported as an observational record, is updated to hold a specimen record for the county.

Specimen records (4)—Kay County: Interstate 35 south of the Kansas border near mile marker 225, Blackwell Tourism Center, 1 (UCOCV-MAM 7756). Logan County: 10774 Coyote Circle, Arcadia, 1 (UCOCV-MAM 7791). Murray County: Sulphur, Nelson Rd and Williams Dr, 34.5208561, -97.0024663, 1 (OMNH 68657). Osage/Tulsa County line: Skiatook, Osage Ave and W 4th St, 36.3664598, -96.0012868, 1 (OMNH catalogue pending).

ORDER CHIROPTERA
Family Vespertilionidae
Eptesicus fuscus
Big Brown Bat

Big Brown bats have been reported across the state in a disjunct pattern historically. More bats (51%) of this species are turned in for rabies virus testing to OADDL in Oklahoma than any other bat species (Loucks et al. 2024), which has increased the number of known county records. Loucks et al. (2023) reported records from 23 Oklahoma counties in disjunct distribution pattern across the state. Although Oklahoma County was previously listed as observation only for this species (Caire et al. 2024), two recent museum specimens have been documented for this county. New records are reported for Comanche, Muskogee, Nowata, Oklahoma, Okmulgee, Pittsburg, Pontotoc, and Rogers counties, providing additional information regarding statewide distribution.

Specimen records (9)—Comanche: no specific locality, 1 (UCOCV-MAM 7757). Muskogee: no specific locality, 1 (UCOCV-MAM 7744). Nowata: no specific location, 1 (UCOCV-MAM 7728). Oklahoma: UCO campus, 1 (UCOCV-MAM 7695), no specific locality, 1 (UCOCV-MAM 7725). Okmulgee: no specific location, 1 (UCOCV-MAM 7758). Pittsburg: no specific location, 1 (UCOCV-MAM 7730). Pontotoc: no specific location, 1 (UCOCV-MAM 7717). Rogers: no specific location, 1 (UCOCV-MAM 7723).

Lasiurus borealis
Eastern Red Bat

The Eastern Red Bat is associated with eastern deciduous forests throughout North America, although it is widespread across Okla-

homa. Loucks et al. (2023) reported records of this species in most of Oklahoma's 77 counties. These bats were historically the most common species submitted for rabies virus testing in Oklahoma (Caire et al. 2014); however, in recent years *Eptesicus fuscus* has become the most frequently submitted species to OADDL (Loucks et al. 2024). A new record is reported for McIntosh County.

Specimen record (1)—McIntosh: no specific locality, 1 (UCOCV-MAM 7759).

Myotis velifer
Cave Myotis

Cave Myotis are found primarily in the western one-third of the state, reported in 24 counties in Oklahoma (Loucks et al. 2023). This specimen record is not only a new county record for Tulsa County but represents the easternmost record of Cave Myotis in Oklahoma to date. This bat species is cavernicolous, hibernating during winter months in hibernacula and transitioning to maternity roosts for summer periods (Caire et al 2024). It is interesting to note this specimen was not located in a cave environment in February.

Specimen record (1)—Tulsa: 2.5 mi NW Lotsee, 1 (OMNH 68306).

Nycticeius humeralis
Evening Bat

The Evening Bat, typically found in the eastern United States, reaches its westernmost distribution in Oklahoma. Loucks et al. (2023) reported 93 records in 22 counties as discussed in Caire et al. (2024). Evening bats are the third most common bat species (15%) turned in for rabies virus testing to OADDL, although in much lower numbers than the two most common species submitted (Loucks et al. 2024). New records are reported for Lincoln, Pittsburg, Pontotoc, Rogers, and Washington counties.

Specimen records (6)—Lincoln: no specific location, 1 (UCOCV-MAM 7726). Pittsburg: no specific location, 1 (UCOCV-MAM 7760). Pontotoc: no specific location, 1 (UCOCV-MAM 7790). Rogers: no specific location, 1 (UCOCV-MAM 7585). Washington: no specific location, 2 (UCOCV-MAM 7747, 7761).

ORDER CARNIVORA
Family Felidae
Puma concolor
Mountain Lion

Mountain lions have been reported in Oklahoma for many years but were believed to be transient occurrences, observed in 24 counties with museum records for 3 counties (Caire et al. 2024). The ODWC began documenting and verifying reports across the state beginning in 2002 and have confirmed 85 sight records of the species in 31 counties through 2024 (ODWC 2024). Although the records reported indicate widespread distribution in Oklahoma, museum specimen records remain limited. The first reports of offspring with female mountain lions were in Osage and Cimarron counties where kittens were observed on game cameras with the mothers, indicating perhaps the species should be considered a more permanent resident of the state going forward (ODWC 2025). Seven observational records are reported for 6 counties resulting in 33 counties with at least one observational record or vouchered museum specimen.

Observational county records (7) — Creek (2), Dewey, Greer, Payne, Washington, and Woods counties.

Family Mustelidae
Lontra candensis
Northern River Otter

The Northern River Otter has a widespread distribution in the eastern half of Oklahoma, although museum specimen records are limited. Loucks et al. (2023) reported 38 otter records in 21 counties. A new specimen record is reported for Carter County, changing an observational occurrence (Caire et al. 2024) to a vouchered museum county record.

Specimen record (1)—Carter: Ardmore, 0.36 mi E of intersection of P St and Sam Noble Pkwy, 1 (OMNH 6865).

ORDER ARTIODACTYLA
Family Cervidae
Cervus canadensis
Elk

Elk have a limited distribution in Oklahoma and few records of museum specimens exist. Loucks et al. (2023) reported 13 records in two counties, with observational records in an additional 8 counties in Oklahoma reported by Caire et al. (2024). A new specimen record is reported for one county.

Specimen record (1)—Garfield: Drummond Flats Wildlife Management Area on Turkey Creek, 1 (UCOCV-MAM 7700).

Odocoileus virginianus
White-tailed Deer

White-tailed Deer have a widespread distribution in Oklahoma (Caire et al. 2024); however, museum specimen records are limited and reported in 42 counties (Loucks et al. 2023). A new specimen record is reported for one county.

Specimen record (1)—Garfield: Drummond Flats Wildlife Management Area on Turkey Creek, 1 (UCOCV-MAM 7699).

ORDER RODENTIA
Family Cricetidae
Peromyscus attwateri
Texas Deermouse

The Texas Deermouse was reported from 36 counties primarily in southern and eastern parts of Oklahoma (Loucks et al. 2023). The distribution of the Texas Deermouse is discontinuous in Oklahoma and adjacent states due to its preference for rocky habitats (Caire et al. 2024). Two new county records are reported for Creek and Payne counties, represented by multiple specimens in both counties.

Specimen records (33)—Creek: 16.5 km WNW of Sapulpa, Pearl Jackson Crosstimbers Preserve, 1 (OMNH 68437), 15.5 km WNW of Sapulpa, Pearl Jackson Crosstimbers Preserve, 4 (OMNH 68574, 68577, 68580, 68590). Payne: Cushing, Intersection of 9th St and N Norfolk Rd, 28 (UCOCV-MAM 7762–7789).

Reithrodontomys humilis
Eastern Harvest Mouse

Museum records of the Eastern Harvest Mouse were reported from 13 counties in eastern Oklahoma by Loucks et al. (2023) and one observational county record was reported by Caire et al. (2024). A new county record is reported for Creek County.

Specimen records (3)—Creek: 16.5 km WNW of Sapulpa, Pearl Jackson Crosstimbers Preserve, 2 (OMNH 68434, 68459), 15.5 km WNW of Sapulpa, Pearl Jackson Crosstimbers Preserve, 1 (OMNH 68594).

Family Sciuridae
Sciurus carolinensis
Eastern Gray Squirrel

Common in the eastern half of Oklahoma in association with wooded areas (Caire et al. 2024), the Eastern Gray Squirrel was reported from 34 counties by Loucks et al. (2023). These records from Cleveland County extend the range to the west.

Specimen records (5)—Cleveland: Norman, Lexington Wildlife Management Area, 5 (OMNH 68412, 68415–68418).

Acknowledgments

The authors thank the Mammalogy Department of OMNH, especially Rebecca Hawkins and Hayley Lanier, for providing data and access to their collections. We thank Shannon Caseltine and others at OADDL for retention of bat specimens for identification. We thank the following contributors of specimens to advance the understanding of mammal diversity in the state: Phillip Crawford of Oklahoma Biological Survey, William Caire and Matt Parks of UCO, the Nature Conservancy in Oklahoma, Noble Research Institute, WildCare Oklahoma, and UCO student volunteers for assisting in surveys. We also thank Jerrod Davis (ODWC) for providing data and ODWC for collecting permits. We are grateful to our cartographer Brad Watkins for generating species maps.

Figure 1. Updated county maps for *Dasypus novemcinctus, Eptesicus fuscus, Lasiurus borealis, Myotis velifer, Nycticeius humeralis, Puma concolor, Lontra canadensis, Cervus canadensis, Odocoileus virginianus, Peromyscus attwateri, Reithrodontomys humilis*, and *Sciurus carolinensis*. The map of Oklahoma has filled circles with museum records for each county and open circles for observational published records as indicated in Caire et al. 2024. Additional records in this study are denoted by stars in each new county, filled in for museum records and open stars for observational records.

Figure 1 cont. Updated county maps for *Dasypus novemcinctus*, *Eptesicus fuscus*, *Lasiurus borealis*, *Myotis velifer*, *Nycticeius humeralis*, *Puma concolor*, *Lontra canadensis*, *Cervus canadensis*, *Odocoileus virginianus*, *Peromyscus attwateri*, *Reithrodontomys humilis*, and *Sciurus carolinensis*. The map of Oklahoma has filled circles with museum records for each county and open circles for observational published records as indicated in Caire et al. 2024. Additional records in this study are denoted by stars in each new county, filled in for museum records and open stars for observational records.

References

Blair WF. 1939. Faunal relationships and geographic distribution of mammals in Oklahoma. American Midland Naturalist 22:85–133.

Bradley RD, Ammerman LK, Baker RJ, Bradley LC, Cook JA, Dowler RC, Jones C, Schmidly DJ, Stangl Jr FB, Van Den Bussche RA, Würsig B. 2014. Revised checklist of North American mammals north of Mexico. Occasional Papers, Museum of Texas Tech University 327:1–27.

Caire W, Loucks LS, Brown, PL. 2014. Bat rabies in Oklahoma. The Southwestern Naturalist 59:550–555.

Caire W, Loucks LS, Haynie ML, Coyner BS, Braun JK. 2019. Updated and revised checklist of the mammals of Oklahoma, 2019. Proceedings of the Oklahoma Academy of Science 99:1–6.

Caire W, Loucks LS, Haynie ML. 2024. Mammals of Oklahoma, second edition. Norman (OK):University of Oklahoma Press. 672 p.

Caire W, Tyler JD, Glass BP, Mares MA. 1989. Mammals of Oklahoma. Norman (OK): University of Oklahoma Press. 567 p.

Loucks LS, Haynie ML, Caire W, Watkins B. 2023. Mammals of Oklahoma records of occurrence: A companion to Mammals of Oklahoma, second edition. Special Publications, Museum of Texas Tech University 79:1–151.

Loucks LS, Shaw JB, Caire W. 2024. Bat rabies in Oklahoma. The Southwestern Naturalist 68:121–126.

Oklahoma Department of Wildlife Conservation (ODWC). 2016. Oklahoma Comprehensive Wildlife Conservation Strategy: A Strategic Plan for Oklahoma's Rare and Declining Wildlife. Oklahoma Department of Wildlife Conservation, Oklahoma City, Oklahoma.

Oklahoma Department of Wildlife Conservation (ODWC). 2024. Mountain lion sightings in Oklahoma. Available online at https://www.wildlifedepartment.com/wildlife/field-guide/mammals/mountain-lion/confirmed-sightings. Accessed 15 May 2025.

Oklahoma Department of Wildlife Conservation (ODWC). 2025. Mountain lion kittens confirmed in Oklahoma. Available online at https://www.wildlifedepartment.com/outdoor-news/mountain-lion-kittens-confirmed-oklahoma. Accessed 15 May 2025.

Wilson DE, Reeder DM, eds. 2005. Mammal species of the world: A taxonomic and geographic reference, 3rd ed. Baltimore (MD): Johns Hopkins University Press. 2142 p.

Trapping Turtles or Trapping Errors? A case study in Alligator Snapping Turtles

Kameron C. Voves
Department of Biology, Missouri State University, Springfield, Missouri 65897
U.S. Fish and Wildlife Service, Florida Ecological Services Field Office, Gainesville, Florida 32653

Samantha L. Hannabass
Department of Biology, Missouri State University, Springfield, Missouri 65897
Kleinschmidt Associates, Strasburg, Pennsylvania 17579

Day B. Ligon
Department of Biology, Missouri State University, Springfield, Missouri 65897

Abstract: When surveying for a species with a potentially fragmented distribution of variably sized populations, such as the Alligator Snapping Turtle, it is important to use effective sampling methods. While numerous surveys have been conducted to assess the current distribution of Alligator Snapping Turtles, detection probability and risk of falsely concluding absence from limited trapping efforts are seldom addressed. We conducted surveys at four sites in Oklahoma where previous surveys had failed to detect the species. We then used permutation analysis on real and theoretical trapping data to assess the robustness of previous surveys and to determine a baseline level of effort needed to detect populations with different relative abundances. We detected Alligator Snapping Turtles at two of our four sample sites where the species was not detected in previous lower-effort surveys, highlighting the importance of increased sampling effort and multiple sampling bouts through time. Our findings suggest that some surveys conducted near the periphery of the species' geographic range may have been insufficient to detect low-density populations. Based on our permutation analyses, we provided guidelines for minimum sampling effort necessary to effectively detect populations above a predetermined density threshold.

Introduction

Effective species conservation relies on accurate assessments of the distribution, abundance, and demographic structure of populations, often requiring considerable effort to evaluate even small portions of a species' range. With finite resources and time, researchers must balance the breadth of site coverage with the intensity of effort at each site. While surveying more locations may seem efficient, doing so with minimal effort risks falsely concluding absence—especially for rare or elusive species. A priori planning that aligns survey goals with realistic detection probabilities is critical for optimizing efforts that are invariably limited by time and funding.

The secretive Alligator Snapping Turtle (*Macrochelys temminckii*) exemplifies the challenge of detecting low-density populations. Historically widespread across Gulf of Mexico drainages, this species has declined due to habitat loss and overharvesting, leading to range contractions, particularly at the northern periphery (US-

*Corresponding author: kameron_voves@fws.gov

Proc. Okla. Acad. Sci. 105: pp 32-39 (2025)

FWS 2021). Numerous surveys have attempted to document the species' current distribution after a petition to list the Alligator Snapping Turtle under the Endangered Species Act was denied in 1983 due to insufficient information regarding the species' status (Heck 1998). Yet many surveys failed to account for detection probability in their survey design, increasing the risk of erroneous conclusions regarding extirpation.

Detection of turtles varies with environmental conditions, trapping methods, population density, and effort (Buchanan et al. 2019, Rosenbaum et al. 2023). Previous studies suggest that small populations may go undetected without adequate sampling intensity (Tyre et al. 2003). Here, we highlight the importance of sufficient sampling effort by re-examining sites in Oklahoma where past surveys failed to detect Alligator Snapping Turtles (Riedle et al. 2001). Using permutation analyses, we assessed the adequacy of previous survey efforts throughout the species range, offering recommendations for future sampling protocols to ensure accurate population assessments.

Methods

Turtle surveys. We conducted surveys in June–July 2018 at four sites in eastern Oklahoma where Alligator Snapping Turtles historically occurred and past studies reported absence (Riedle 2001). All survey sites were located within the Arkansas River drainage and were upstream of reservoirs or were tributaries of dammed rivers. Sites were navigable by motorboat and typified by high turbidity, muddy stream beds, and tall banks (Voves 2020). We selected these sites because Alligator Snapping Turtles were presumed to be absent, yet habitat appeared to meet the species' life history requirements, making these sites promising candidates for future reintroduction efforts.

We surveyed each site for seven consecutive days, with a minimum of 15 baited hoop nets deployed daily, totaling 100–120 net nights (NN) per site. We used single-throat 0.9-m diameter and double-throat 1.2-m diameter hoop nets with 2.5-cm mesh and baited with fresh or frozen fish. We positioned nets in optimal habitat—near submerged cover such as downed trees and undercut banks. We divided each survey reach into an upper portion and lower portion, and we moved rebaited traps from one section to the other each night (Hollender et al. 2022). In the case of one site, the seven-day trapping effort was split between a small tributary (Chouteau Creek) serving as the upper portion and the main-stem Neosho River as the lower portion. These rivers were not spatially independent, but their habitat differed in such a way that detection could be affected—Chouteau Creek was characterized by greater abundance of submerged structure and canopy cover and less current than the main-stem Neosho River (Voves et al. 2023). Thus, we report the effort separately for this site. We set traps such that a portion remained partially above water with a floatation device placed inside to safeguard against potential rising water. We measured, sexed, and notched captured turtles of all species with a common scute notch to identify recaptures. Alligator Snapping Turtles received Passive Integrated Transponder (PIT) tags in the right rear leg for permanent marking.

Previous surveys occurred May through August 1997–1999 using very similar methods (Riedle 2001, Riedle et al. 2009). In short, they set 1.05-m diameter hoop nets with 2.5-cm mesh baited with fresh fish upstream from submerged structures. They set 3–18 nets each afternoon and checked them the following morning, typically for fewer than three consecutive nights (Riedle 2001). In this past effort, they marked only Alligator Snapping Turtles with drilled holes in a unique sequence along the marginal scutes. Effort per site was reported in Riedle (2001), but specific site coordinates were not attainable. To the best of our knowledge, with correspondence from D. Riedle, past trapping effort included 25 total NN in Big Cabin Creek May 1997 and 1999 (Craig Co.), 10 NN in the Neosho River July 1998 (Mayes Co.), 20 NN each in two stretches of the Deep Fork River July 1997 (Okmulgee Co), and 57 total NN among at least three stretches of the Poteau River August 1998 (LeFlore Co.) with effort ranging from 10–22 nets per site. Riedle (2001) did not trap in the Chouteau Creek. We

recognize the possibility that we did not sample the precise locations and turtle populations as sampled previously (Riedle 2001).

Permutation analyses. To estimate false negative probabilities, we resampled our trapping data from sites with confirmed captures across 10,000 iterations for varying effort levels, calculating the proportion of iterations that resulted in zero captures—leading to a conclusion of false absence. We used these probability curves to evaluate the likelihood that the absences of Alligator Snapping Turtles reported from previous survey efforts (Shipman et al. 1995; Riedle et al. 2009; Bluett et al. 2011; Baxley et al. 2014) were false negatives, assuming surveyed sites supported populations that were comparable to those we surveyed in Oklahoma.

We also generated theoretical catch-per-unit-effort (CPUE) scenarios to determine the minimum NN required to detect populations at different abundance levels with 95% confidence. When Alligator Snapping Turtles occur in greater abundance, more individuals are expected to be captured assuming trapping effort remains constant, resulting in a higher CPUE, defined as the number of captures divided by the total number of traps set. We simulated trapping results for 51 theoretical surveys of 200 NN each, each defined by a different CPUE. For each trap, we assigned a value of 1 if an Alligator Snapping Turtle was detected and 0 otherwise. The simulated CPUEs ranged from 0.005 (1 detection in 200 NN) to 0.500 (100 detections), increasing by 0.010 (2 detections) with each new simulation. For each CPUE level, we conducted permutation analyses across varying effort levels to determine the minimum effort required to reduce the probability of a false negative to below 5%. All analyses were implemented in R version 3.5.0 "Joy in Playing" (R Core Team 2022).

Results

Turtle surveys. We sampled turtles at four sites in Oklahoma over 475 NN and captured 20 individual Alligator Snapping Turtles at two locations—Big Cabin Creek and the Poteau River (Table 1). The capture rate was much higher in the Poteau River (0.130 CPUE) than in Big Cabin Creek (0.024 CPUE). In the Poteau River, we captured 17 turtles (14 juveniles, 2 females, and 1 male) in 127 NN. In Big Cabin Creek, we captured 3 turtles (2 juveniles and 1 female) in 124 NN. All turtles combined, juveniles measured 164–331 mm in carapace length, while adults measured 411–457 mm.

Table 1. Survey sites, counties, length of river surveyed, dates surveyed, net nights (NN), and number of Alligator Snapping Turtles captured in Oklahoma in 2018 (with recaptures in parentheses). Also included are dates and effort (NN) of previous sampling efforts at these locations that occurred in 1997–99 (Riedle 2001). Note that no *M. temminckii* were detected at any of these locations in 1997–99.

River	County	Length surveyed (km)	Dates Surveyed		Effort		*M. temminckii* trapped (2018)
			This Survey (2018)	Riedle (2001)	This Survey (2018)	Riedle (2001)	
Big Cabin Creek	Craig	6.83	2–8 June	May 1997, 1999	124	25	3 (0)
Chouteau Creek	Mayes	2.57	14–16 July	--	55	0	0
Neosho River	Mayes	3.58	17–18 July	Jul 1998	49	10	0
Deep Fork River	Okmulgee	11.99	12–18 June	Jul 1997	120	20–40	0
Poteau River	Le Flore	10.96	24 Jun–1 Jul	Aug 1998	127	10–22	17 (1)

Permutation analyses. We used trapping data from the Poteau River (18 captures in 127 NN, including one recapture) and Big Cabin Creek (3 captures in 124 NN) to conduct permutation analyses. The probability of a false negative declined more rapidly in the Poteau River, where 19 NN sufficed to reduce the probability of a false negative below 5%, compared to 78 NN in Big Cabin Creek. Riedle (2001) failed to detect Alligator Snapping Turtles at these sites in 1997. Assuming detection probabilities in those earlier surveys were comparable to this study, Riedle had a 3–20% chance of falsely concluding absence in the Poteau River (10–22 NN) but a 51% chance in Big Cabin Creek (25 NN). We compared nine additional Oklahoma surveys (Riedle et al. 2009) to our results. Using Big Cabin Creek as a model, one river showed a >50% false negative probability, three rivers exceeded 20%, and two fell below 5% (Fig. 1). Using Poteau River data, only one river exceeded a 5% false negative probability.

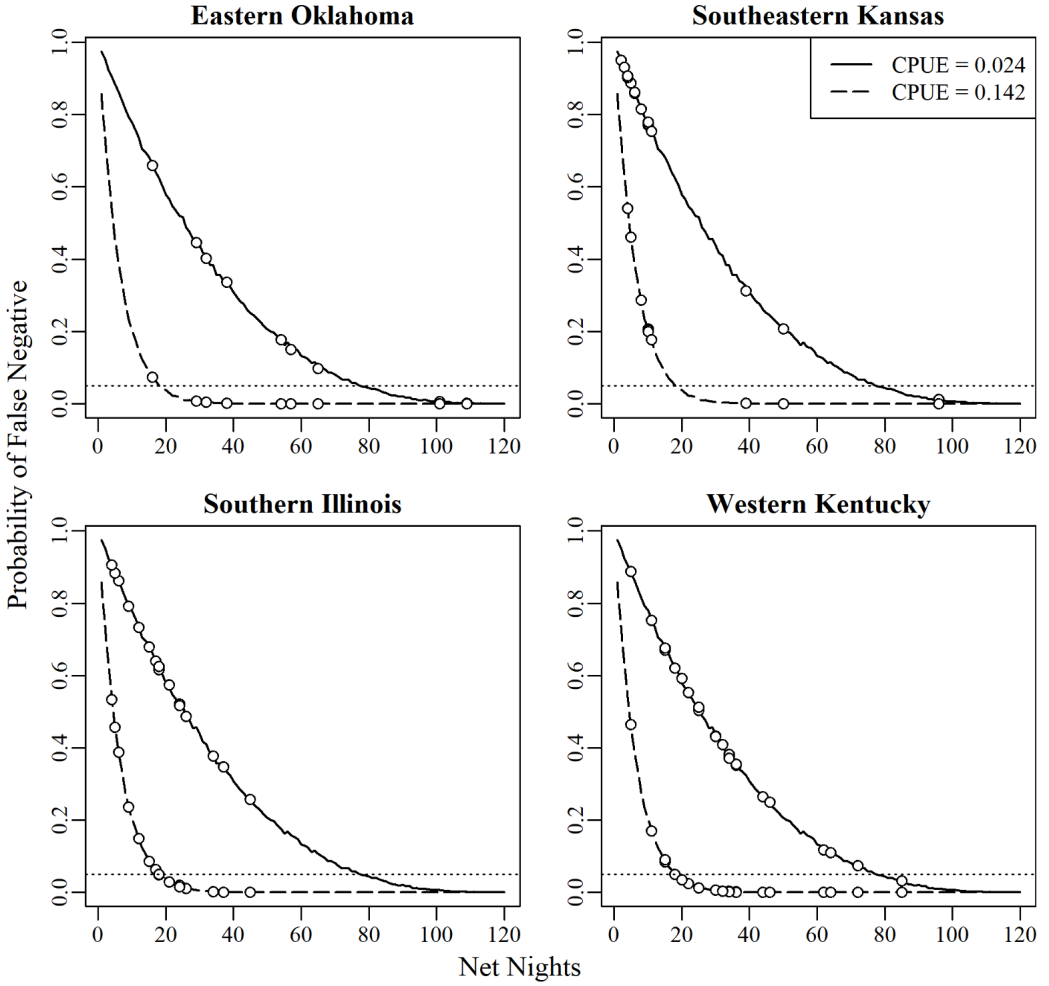

Figure 1. Probabilities of false negatives given reported effort expended at sites during previous surveys where Alligator Snapping Turtles were not detected. Curves are based upon permutations generated from populations in Big Cabin Creek (CPUE = 0.024) and Poteau River (CPUE = 0.142—includes 1 recapture). Each point corresponds to effort invested at one site. The dotted line denotes a probability of 0.05. Data included in the analysis are: Riedle et al. (2009) [Oklahoma], Shipman et al. (1995) [Kansas], Bluett et al. (2011) [Illinois], and Baxley et al. (2014) [Kentucky].

When we extended the analysis to surveys outside of Oklahoma, we found that surveys in Kansas (Shipman et al. 1995) had the highest likelihood of producing false absences. If turtle abundance matched that of our low-density site, 84% of 19 sampled sites in Kansas produced false negative probabilities above 0.75. In Illinois (Bluett et al. 2011), 76% of 17 sites exceeded 0.50, and in Kentucky (Baxley et al. 2014), 38% of 24 sites exceeded 0.50. When we modeled higher abundances like those in the Poteau River, the proportion of sites with false negative probabilities above 0.50 dropped to 37% in Kansas, 6% in Illinois, and 0% in Kentucky.

In simulations of theoretical surveys, we found that high turtle abundance (CPUE $\geq$ 0.26) required fewer than 10 NN to achieve a false negative probability below 5% (Fig. 2). When CPUE exceeded 0.44, just 5 NN were sufficient for detection. In contrast, populations with very low detection rates (CPUE $\leq$ 0.05) required more than 50 NN and detecting turtles at a CPUE of 0.005 required 190 NN.

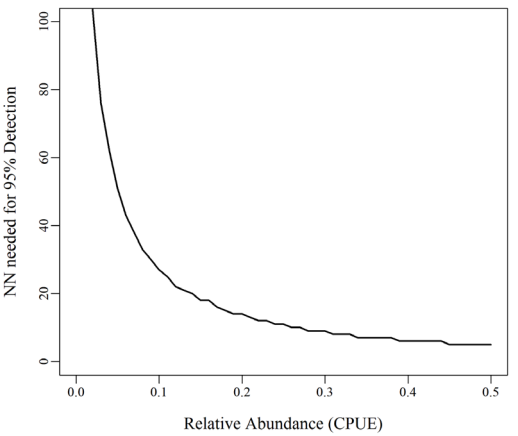

Figure 2. The minimum number of net nights needed with zero captures to conclude absence of *Macrochelys temminckii* with 95% confidence given different relative abundances. Abundance was estimated with increasing catch-per-unit-effort (CPUE) in theoretical capture data consisting of 200 net nights. Permutations were performed under these different CPUE scenarios to estimate minimum effort requirements.

Discussion

Our detection of Alligator Snapping turtles in rivers where they were previously believed to be extirpated highlights the importance of sufficient sampling effort when surveying species with fragmented, variably sized populations. Although Riedle (2001) employed methods similar to ours, the high probability they had of falsely concluding absence at Big Cabin Creek suggests that too little effort was invested to reliably detect low-density populations. In contrast, the low probability they had of concluding false absence at the Poteau River implies other factors reduced detectability. Past surveys in the Poteau River were conducted in August, when elevated water temperatures may have suppressed activity (Thompson 2023) or turtles exhibited seasonal movements into deep, cooler water (Riedle et al. 2006), leading to lowered detection probability. Detection probability between the two sampling periods could also have been affected by air temperature, lunar phase, or water flow velocity (Dreslik et al. 2017, Rosenbaum et al. 2023). Alternatively, the population in the Poteau River may have been smaller in 1997, with the juveniles we captured representing recent recruitment. With 20 years separating the two studies, it is difficult to know what additional factors could be at play to affect detection and occupancy of Alligator Snapping Turtles at these sites.

Permutation analysis proved to be a useful tool for evaluating previous efforts to detect Alligator Snapping Turtles. Catch-per-unit-effort is often used as a proxy for abundance because so few surveys have been sufficient to generate robust population estimates. Our results indicate that past surveys in Kansas, Illinois, and Kentucky likely lacked sufficient effort to confidently conclude species absence. Instead, we recommend that surveys resulting in non-detection report a minimum detectable density based on effort. For example, the average effort expended during surveys conducted in Kansas, Illinois, and Kentucky was 24 NN, which, according to our analysis, would only detect a population with a CPUE greater than 0.12 turtles per NN with 95% confidence. Baxley et al. (2014) similarly inferred that survey efforts in Kentucky were only

sufficient to detect relatively abundant populations that would result in a CPUE of 0.06 given an average effort of 34.5 NN—an effort that corresponded to a CPUE of 0.07 in our analysis. We encourage investigators conducting future surveys to interpret non-detections in this context and clearly relate sampling effort to minimum detectable CPUE thresholds.

Surveyors must also carefully report and interpret trapping effort. Some prior studies, such as Riedle et al. (2009), appeared to expend enough cumulative effort to infer absence, but pooling across nearby tributaries obscured local abundances and detection probabilities of sites with potentially variable habitat suitability (Riedle 2001). Future studies must report effort at the site level, not as aggregated totals, to accurately reflect habitat suitability and turtle abundance. Other surveys have faced similar challenges. Some reported trapping effort inconsistently (Folt and Godwin 2013; Huntzinger et al. 2019), pooled sites into large summaries (Wagner et al. 1996; Jensen and Birkhead 2003; Garig et al. 2021; Pearson et al. 2023) or failed to report site-specific effort altogether (Boundy and Kennedy 2006; Shipman and Riedle 2008). If pooling among sites is necessary, it is helpful to report the number of sites included in the summary, as done in Pearson et al. (2023). To facilitate comparison between studies, it may also be advantageous to report inter-trap distances, as trap saturation also affects detection of Alligator Snapping Turtles (Rosenbaum et al. 2023). Thus, we urge future researchers to prioritize transparent, site-specific reporting of trapping effort and results because misinterpreting absences can complicate efforts to synthesize regional distribution patterns.

In light of our findings, we call for more robust survey design standards for Alligator Snapping Turtles. Although detecting relatively dense populations requires modest effort, detecting sparse or fragmented populations demands greater investment. To minimize the risk of falsely declaring a species absence, we recommend a minimum survey effort of 100 NN per site, which corresponds to a 95% probability of detecting a small population with a CPUE of 0.02 turtles per NN or greater. Our recommended minimum survey effort is greater than the 80 NN recommended by the U.S. Fish and Wildlife Service for rapid assessments of low-density sites (Pearson 2025), which would correspond to detecting a population with a CPUE of 0.025 turtles per NN or greater. These recommended baselines must be viewed as a starting point—not a guarantee. Researchers should adjust effort upward when environmental conditions, such as extreme heat, cold, or flooding, reduce detectability (Rosenbaum et al. 2023). Survey planners should explicitly account for detection probability in study design, report effort and results transparently, and carefully interpret non-detections with respect to sampling intensity. The consequences of inadequate survey design can delay conservation interventions, misinform species assessments, and impair recovery planning. By adopting more rigorous, transparent, and data-driven survey practices, we can ensure that future assessments of Alligator Snapping Turtles—and other elusive species—better reflect biological reality and advance conservation goals.

Acknowledgments

We thank Ashley Gagnon, Krissy Sardina, Teddy Pashia, Parker Golliglee, Anthony Grate, and Stephen Brown for field assistance. All efforts were conducted with approval from the Missouri State University Animal Care and Use Committee (protocol 17-028.0). Funding was provided by Oklahoma Department of Wildlife Conservation (State Wildlife Grant F17AF01213 [T- 101]).

References

Baxley DL, Barnard JO, Venter H. 2014. A survey for the Alligator Snapping Turtle (*Macrochelys temminckii*) in western Kentucky. Southeast. Nat. 13:337–346.

Bluett RD, Woolard DA, Palis JG, Kath JA. 2011a. Survey for *Macrochelys temminckii* in southern Illinois: implications for recovery actions. Trans. Ill. State. Acad. Sci. 104:1–8.

Boundy J, Kennedy C. 2006. Trapping survey results for the Alligator Snapping Turtle (*Macrochelys temminckii*) in south-

eastern Louisiana, with comments on exploitation. Chelonian Conserve Bi 5:3–9.

Buchanan SW, Buffum B, Puggioni G, Karraker NE. 2019. Occupancy of freshwater turtles across a gradient of altered landscapes. J of Wildl Manage 83:435–445

Dreslik, MJ, Carr JL, Ligon DB, Kessler EJ. 2017. Recovery of the Alligator Snapping Turtle (*Macrochelys temminckii*) in the Mississippi River Valley Drainages of Southern Illinois, Oklahoma, and Louisiana. [Technical Report]. Champaign [IL]: Illinois Natural History Survey. 61 p.

Folt B, Godwin JC. 2013. Status of the Alligator Snapping Turtle (*Macrochelys temminckii*) in south Alabama with comments on its distribution. Chelonian Conserve Bi 12:211–217.

Garig D, Ennen JR, Hyder SJ, Simmonds T, Feltmann AJ, Colvin R, Dennison J, Pearson L, Kreiser BR, Sweat SC, Davenport JM. 2021. Status of the Alligator Snapping Turtle, *Macrochelys temminckii*, in west Tennessee. Chelonian Conserve Bi 20:35–42.

Heck BA 1998. The Alligator Snapping Turtle (*Macroclemys temminckii*) in southeast Oklahoma. Proc Okla Acad 78:53–58.

Hollender EC, Ligon DB, McKnight DT. 2022. Learned trap avoidance in freshwater turtles. Wildlife Res https://doi.org/10.1071/WR21061.

Huntzinger CC, Louque Jr I, Selman W, Lindeman PB, Lyons EK. 2019. Distribution and abundance of the Alligator Snapping Turtle (*Macrochelys temminckii*) in southwestern Louisiana. Southeast Nat 18:65–75.

Jensen JB, Birkhead WS. 2003. Distribution and status of the Alligator Snapping Turtle (*Macrochelys temminckii*) in Georgia. Southeast Nat 2:25–34.

Pearson, L. 2025. Recommended Survey Protocol for the Alligator Snapping Turtle (*Macrochelys temminckii*) and Suwannee Alligator Snapping Turtle (*Macrochelys suwanniensis*). United States Fish and Wildlife Service [online]. Available from: https://www.fws.gov/sites/default/files/documents/2025-02/trapping-and-handling-protocol-for-the-alligator-snapping-turtle.pdf.) Accessed September 23, 2023.

Pearson, L, Haralson L, Berry G, Brown GJ, Qualls C. 2023. Distribution patterns and factor influencing relative abundance of the alligator snapping turtle (*Macrochelys temminckii*) in Mississippi. Southeast Nat 22:138–156.

R Core Team. 2022. R: A language and environment for statistical computing. R Foundation for Statistical Computing, Vienna, Austria. Available from: https://www.R-project.org/.

Riedle JD. 2001. The ecology of the Alligator Snapping Turtle, *Macrochelys temminckii*, in Oklahoma [MSc thesis]. Stillwater (OK): Oklahoma State University. 130 p.

Riedle JD, Shipman PA, Fox SF, Leslie Jr DM. 2006. Microhabitat use, home range, and movements of the Alligator Snapping Turtle, *Macrochelys temminckii*, in Oklahoma. Southwest Nat 51:35–40.

Riedle JD, Shipman PA, Fox SF, Leslie Jr DM. 2009. Habitat associations of aquatic turtle communities in eastern Oklahoma. Proc Okla Acad Sci 89:11–22.

Rosenbaum D, Saenz D, Montaña CG, Zhang Y, Schalk CM. 2023. Detection, occupancy, and abundance of the Alligator Snapping Turtle in Texas. J Wildl Manage 87:e22409.

Shipman PA, Edds DR, Shipman LE. 1995. Distribution of the Alligator Snapping Turtle (*Macroclemys temminckii*) in Kansas. Trans Kans Acad Sci 98:83–91.

Shipman PA, Riedle JD. 2008. Status and distribution of the Alligator Snapping Turtle (*Macrochelys temminckii*) in southeastern Missouri. Southeast Nat 7:331–338.

Thompson DM. 2023. Reproductive cycles, activity patterns, and distribution of the Alligator Snapping Turtle (*Macrochelys temminckii*) [PhD dissertation]. Sillwater (OK): Oklahoma State University. 104 p.Available from: OSU Library.

Tyre AJ, Tenhumberg B, Field SA, Niejalke DN,

Parris K, Possingham HP. 2003. Improving precision and reducing bias in biological surveys: estimating false-negative error rates. Ecol App 13:1790–1801.

United States Fish and Wildlife Service (USFWS). 2021. Species Status Assessment for Alligator Snapping Turtle (Macrochelys temminckii). Species Status Assessment Reports. Louisiana Ecological Services Field Office. 218 p.

Voves, KC. 2020. Methods to identify and assess suitability of reintroduction sites for the Alligator Snapping Turtle (*Macrochelys temminckii)* [MSc thesis]. Springfield (MO): Missouri State University. 168 p.

Voves, KC, Hannabass SL, Thompson DM, Ligon DB. 2023. A standardized field method and habitat suitability model to assess reintroduction sites for Alligator Snapping Turtles. Southeast Nat 22:56–77.

Wagner BK, Urbston D, Leek D. 1996. Status and distribution of Alligator Snapping Turtles in Arkansas. Proc Annu Conf Southeast Assoc Fish and Wildl Agencies 50:264–270.

Mechanistic Insight into Gape Limitation and Growth-mediated Competition Among Moronid

Douglas L. Zentner, Oklahoma Department of Wildlife Conservation, Oklahoma Fishery Research Laboratory, 500 East Constellation, Norman, Oklahoma 73072

Austin D. Griffin, Oklahoma Department of Wildlife Conservation, Oklahoma Fishery Research Laboratory, 500 East Constellation, Norman, Oklahoma 73072

Jory B. Bartnicki, Oklahoma Department of Wildlife Conservation, Oklahoma Fishery Research Laboratory, 500 East Constellation, Norman, Oklahoma 73072

Michael J. Porta, Pennsylvania Fish and Boat Commission, Area 6 Fisheries Management Office, 448 Haycock Run Road, Bucksville, PA 18953

Richard A. Snow*, Oklahoma Department of Wildlife Conservation, ODWC HQ, 1801 N. Lincoln, Oklahoma City, Oklahoma 73105

Abstract: Gape limitation is a key mechanism controlling the size of prey a predator can consume, as a fishes gape is intrinsically linked to its body size and changes with growth. Previous studies have shown that gape limitation influences competition among game fishes and helps estimate prey availability. High utilization of shad (*Dorosoma* spp.) by the Moronidae family provides an opportunity to examine gape-limitation theory. Moronids are widely pursued across the United States, with five species present in Oklahoma. This study aimed to determine potential diet overlap among these species using gape-limitation theory and a common forage species, Gizzard Shad (*Dorosoma cepedianum*). Objectives were to: (1) develop equations estimating the proportion of Gizzard Shad vulnerable by size and age to each Moronid species, (2) compare vulnerability among similar-sized Moronids to identify competitive advantages, and (3) assess whether advantages exist when accounting for prey and predator growth trajectories. Results indicate that growth-mediated exploitation occurs among Moronids, allowing individuals that grow faster to achieve a larger gape and better compete for prey. Thus, growth rates and resulting size structures are critical to mediating resource overlap. Managers can apply gap-based vulnerability to estimate forage availability, competition, and exploitation, guiding decisions on whether to manipulate forage or predator populations to meet management goals.

Introduction

Predation is one of the structuring processes in aquatic ecosystems that regulates energy transfer and ecosystem function (Bax 1998; Baxter et al. 2004). Predation is influenced by food-web complexity and the strength of bottom-up and top-down interactions between producers and consumers (Lindeman 1942, Carpenter et al. 1985, McQueen et al. 1986, Power 1992, Pace et al. 1999). Primary mechanisms (e.g., morphological constraints, Mihalitsis and Bellwood 2017) regulated by abiotic and biotic influences (Coutant 2006) within the environment likely control predation. Understanding mechanistic constraints on predation, such as gape lim-

*Corresponding author: richard.snow@odwc.ok.gov
Proc. Okla. Acad. Sci. 105: pp 40-57 (2025)

itation, likely allows for more accurate estimates of consumption and diet overlap and may inform management practices.

Gape limitation is a key mechanism controlling the size of prey a predator can consume (Hill et al. 2004). In theory, the maximum size of prey a predator can consume is based upon the mouth dimensions of said predator (gape width) and the body depth of said prey. Gape limits the breadth of a predator's foraging niche, and therefore influences competition for and consumption of a prey base (Hambright 1991). A fish's gape is intrinsically linked to its size. Therefore, gape-based estimates of prey vulnerability likely vary through time depending on predator and prey growth trajectories (DeVries et al. 1998; Krebs and Turingan 2003). Gape limitation has been shown to be more accurate at predicting consumption relative to other morphometric comparisons between predators and prey (Dennerline and Van Den Avyle 2000). Given its prior use and ecological basis, gape limitation allows for better management of sportfish as it provides insight into potential exploitation and permits the estimation of prey availability.

Gape width has been shown to predict the maximum size of shad (*Dorosoma* spp.) consumed by fishes belonging to the family Moronidae (hereafter Moronids), offering an opportunity for management application of gape-limitation theory (Dennerline and Van Den Avyle 2000). Moronids are some of the most widely pursued sportfish in the United States, and members of this family commonly rank in the top five harvested species within a given state or region (Guy et al. 2002, Bulak et al. 2013). Striped Bass (*Morone saxatillis*), White Bass (*M. chrysops*), and Hybrid Striped Bass (*M. chrysops* × *M. saxatilis*) are sportfish of management interest in Oklahoma (Miller and Robison 2004, Schultz et al. 2013). Competition and resource partitioning among these Moronids have been previously documented, and all three are known to prey upon shad (Gilliland 1978, Rash 2003, Olson 2004).

The amount of food resource exploitation between Moronids of management interest (i.e., Striped Bass, White Bass, and Hybrid Striped Bass) in Oklahoma reservoirs is unknown. However, diet overlap, competition, and resource partitioning among these species has been previously documented (e.g., Rash 2003, Olson 2004). Moronids of management interest in Oklahoma may be further threatened by the invasion of non-native White Perch (*M. americana;* Irons et al. 2002) and possible range expansion of Yellow Bass (*M. mississipiensis)* in the southeastern portion of the state (Snow and Porta 2020). To gain a better understanding of diet overlap, competition, and resource partitioning among these species, the goal of our study was to determine potential diet overlap between Oklahoma Moronids using gape limitation theory and a common forage species (Gizzard Shad; [*Dorosoma cepedianum*]). Given the relation between growth and gape, we compared Gizzard Shad gape vulnerability over similar Moronid size ranges and their potential annual growth trajectories. Specific objectives of our study were to: 1. Develop equations to determine the proportion of Gizzard Shad vulnerable by size and age to five species of Moronids in Oklahoma. 2. Determine potential forage availability overlap among Moronids using gape limitation theory. 3. Determine if advantages exist for a particular species when accounting for prey and predator annual growth trajectories. We then reviewed our findings in the context of managing mixed-Moronid fisheries within the state of Oklahoma.

Methods

Sampling

Fish were collected for this study from nine Oklahoma reservoirs spaced across the state (Table 1). Gizzard Shad were collected in the fall via electrofishing (pulsed DC, high voltage, 7.5 GPP, Smith Root, Vancouver, Washington) from 2018-2021. Moronid species were collected between 2019 and 2022 using experimental gillnets (61 m long x 1.8 m deep and constructed of eight 7.6-m panels [12.7-mm, 15.9-mm, 19.1-mm, 25.4-mm, 38.1-mm, 50.8-mm, 63.5-mm, and 76.2-mm bar mesh]). Gizzard Shad were collected from all nine reservoirs to better estimate variation in fish size and growth across Oklahoma. Striped Bass, White Bass, and Hybrid Striped Bass were collected from 3 of 9 reservoirs (Table

1). Reservoirs for these species were selected based on prior knowledge of growth variability across the state (OFAT 2022). Yellow Bass and White Perch were collected from New Spiro and Sooner reservoirs, respectively (Table 1).

Following collection, fish were euthanized in a 1:1 ice water slurry (Blessing et al. 2010) and returned to the lab where they were measured (TL; mm) and sagittal otoliths were extracted for age estimation. For Moronids, a 150-mm digital caliper (PITTSBURGH 150 mm Digital Caliper, Item #62569, Harbor Freight, Calabasas, CA) was used to measure the horizontal maxillary oral gape (Mihalitsis and Bellwood 2017 and Dennerline and Van Den Avyle 2000) of each individual (0.01 mm).

Estimating Age

Otoliths were cleaned and placed into individually numbered envelopes and allowed to dry for at least 24 h prior to processing (Secor et al. 1992). Sagittal otoliths from Moronid species were broken in the transverse plane and polished using 600-grit wet/dry sandpaper. Clayton and Maceina (1999) suggested that whole otoliths could accurately estimate age of Gizzard Shad under 3 years old. Therefore, sagittal otoliths of Gizzard Shad <3 years old were estimated from whole otoliths and otoliths from older fish were embedded in a 21-cell latex mold (12 mm x 5 mm x 6 mm; Electron Microscopy Sciences, Hatfield, Pennsylvania), immersed in West Systems epoxy (105 resin and 206 harder; Gougeon Brothers Inc., Bay City, Michigan), then cured for more than 12 h. Otoliths were then cut in the sagittal plane using a low-speed Buehler saw (127-mm x 0.4-mm diamond wafering blade; IsoMet®, Buehler, Inc., Lake Bluff, Illinois) and polished using 2000-grit sandpaper (Maceina 1988).

To estimate ages, sectioned otoliths from all species were positioned polished side up in modeling clay and covered with water to reduce glare. Whole otoliths were placed concave side up on the clay. All otoliths were viewed with a variable power stereomicroscope (capable of 130× magnification) using a fiber-optic light and a reflective light source when needed. Annuli were counted to assign an age estimate to each fish. Each otolith was evaluated in random order by two independent readers (Hoff et al. 1997). If there was a disagreement on an estimated age, a concert reading was conducted by both readers and a final age estimate was determined.

Table 1. Reservoirs where Moronid species (Hybrid Striped Bass *Morone saxatilis x M. chrysops* [HSB], Striped Bass *M. saxatilis* [STB], White Bass *M. chrysops* [WHB], White Perch *M. americana* [WHP], Yellow Bass *M. mississippiensis* [YLB]) and Gizzard Shad *Dorosoma cepedianum* (GIS) were collected, including size of reservoirs, sample size (ha), and ranges of TL, weight, gapes, and age estimates. The composition of the Moronid fishery in each reservoir is given in the Moronids column.

				Summary Statistics				
Species	**Reservoir**	**Size (ha)**	**Moronids**	***n***	**TL (mm)**	**Weight (g)**	**Gape (mm)**	**Age (years)**
HSB	Canton	3201	HSB, STB, WHB	161	212-717	120-5445	29-89	1-9
	Sooner	2185	HSB, STB, WHB, WHP	13	408-525	928-2088	46-60	2-7
STB	Canton	3201	HSB, STB, WHB	8	470-659	1180-3220	62-82	3-5
	Texoma	35,612	HSB, STB, WHB	76	194-793	80-6080	23-93	1-7
WHB	Canton	3201	HSB, STB, WHB	114	172-442	13-940	22-57	1-11
	Texoma	35,612	HSB, STB, WHB	24	191-453	80-1170	22-48	1-5
	Sooner	2185	HSB, STB, WHB, WHP	3	306-345	402-600	32-44	2-3
WHP	Sooner	2185	HSB, STB, WHB, WHP	147	191-323	27-496	22-41	2-14
YLB	New Spiro	101	YLB	107	81-302	5-505	10-38	0.5-2.5
GIS	Canton	3201	HSB, STB, WHB	145	65-439	5-810	-	0-8
	Carl Etling	64	HSB	198	45-338	2-280	-	0-12
	Eagle	17	HSB, WHB	34	125-481	10-1450	-	0-7
	Elmer	15	-	110	138-319	10-360	-	1-7
	Guthrie City	83	-	107	81-298	5-270	-	0-6
	New Spiro †	101	YLB	161	108-366	10-530	-	1-6
	Sooner †	2185	HSB, STB, WHB, WHP	76	127-477	10-1210	-	0-12
	Thunderbird	2176	HSB, WHB	127	108-257	10-155	-	0-9
	Texoma †	35,612	HSB, STB, WHB	65	121-471	10-155	-	1-5

†Threadfin shad (*Dorosoma petenense*) also present

Estimating Body Depth or Gape Width from TL

To estimate the mean body depth of each Gizzard Shad present within our samples we used the inverted form of an equation from Lawrence (1957):

$$BD = \frac{(TL - 15.630)}{3.405}$$

where BD and TL represent the estimated mean body depth and observed total length of a Gizzard Shad, respectively. Because this equation is only representative of the mean body-depth to TL relationship, the standard deviation of the regression (SDR = 10.18) reported in Lawrence (1957) was used to estimate the maximum and minimum body-depth of each individual. This was done by adding or subtracting the SDR from the mean estimated body-depth. A small subset (n = 17) of Gizzard Shad were used to graphically validate that the equation from Lawrence (1957) captured the variation in body-size to TL relationship by confirming that our observed values fell within the maximum and minimum body-depth estimates.

Gape width to TL relationships were determined independently for each Moronid species. An information theoretic approach was used to determine which of four common morphometric equations best descripted the relationship between gape-width and TL. We selected linear, second-degree polynomial, exponential, and power functions as the most likely morphometric equations (Hill et al. 2004, Slaughter et al. 2008; Dunic and Baum 2017). Morphometric equations were ranked using Akaike's information criterion adjusted for small sample sizes (AICc; Hurvich and Tsai 1989), where lower values of AICc indicate more likely models (Burnham and Anderson 2002). Both root-mean-square error (RMSE) and mean absolute error (MAE) were used to describe the fit of each morphometric equation relative to the data used to estimate the relationships. Because these equations were used to estimate gape-vulnerability for these fishes and we wanted to capture the full potential range of gapes possible at a given length, we also estimated predictive intervals for each equation ($\alpha = 0.01$).

Comparing Gape Vulnerability by TL

To estimate gape vulnerability by TL, the mean, lower, and upper body-depth estimates for Gizzard Shad were compared to the mean, lower, and upper gape estimates for each Moronid. If Gizzard Shad body depth was less than the gape of the Moronid it was considered vulnerable to that species and assigned a one. If it was greater than the Moronid gape it was considered invulnerable and assigned a zero. This resulted in nine estimates of vulnerability for each mm of TL for both the Moronid and Gizzard Shad. These estimates (i.e., the ones and zeros) were averaged to estimate the average vulnerability as a proportion based on variation in shad body depth and Moronid gape. All estimates were restricted to the TLs observed for the shad population and the specific Moronid.

To compare length-based gape-vulnerability between Moronids, we used a binomially distributed generalized linear model (GLM) with a logit-link function. Our data had three categories (i.e., gape-vulnerability advantage for each species being compared [2 categories], and equal gape-vulnerability); however, a binomial model has two categories, specifically "1" and "0". To facilitate this analysis, we grouped one of the species gape-vulnerability advantages with equal gape-vulnerability (scored "0") and compared it to the other species gape-vulnerability advantage (scored "1"). To decide which Moronid to group with equal gape-vulnerability, we grouped both with equal and looked at the ratio of "1's" and "0's" that resulted from each grouping scheme. The grouping scheme that produced the most even ratio of "1's" and "0's" was used for the analysis. Predictive variables for the binomial GLM were shad TL, Moronid TL, and the interaction between both lengths. This allowed us to determine the relationship between gape advantages for each Moronid species relative to the potential size distribution of forage. All models were restricted to the TLs for which average-vulnerability was estimated in each species (e.g., when Hybrid Striped Bass and Striped Bass were compared, the model was restricted between 212 – 717 mm). McFadden's pseudo R^2 estimates were used to estimate the strength of the relationship, with $\rho^2 = 0.20$ used as the threshold for

"excellent" model fit (McFadden 1974, 1979). A Hosmer-Lemeshow Goodness of Fit test was also used to determine if models appropriately fit the data ($\alpha = 0.05$).

Growth Modeling

The von Bertalanffy growth model (VBGM) was used to estimate growth trajectories for Gizzard Shad and the five Moronids represented. To better estimate the growth trajectory of each species within Oklahoma, the VBGM was fit using TL measurements and age estimates for each individual within our samples regardless of waterbody. Once a baseline equation was established from the nonlinear modeling function, bootstrapping via second-order Taylor expansion (Wang and Iyer 2005) was used to provide final estimates of mean length at age for the species along with 99% prediction intervals. Because predictive intervals incorporate additional uncertainty associated with the data point being estimated they are inherently wider than a confidence interval. In our application, this increased uncertainty produced estimates that were statistically appropriate but biologically impossible (e.g., the lower 99% PI estimate of TL for an age-0 Gizzard Shad was -60mm). Due to this phenomena, post hoc adjustments were made to nonsensical or unlikely estimates based on available literature data (see Growth Modeling results for specific details).

Comparing Gape-Vulnerability by Age

To estimate the influence of growth on gape-vulnerability comparisons, the same comparison process was used (i.e., Gizzard Shad body-depth estimates were compared to Moronid gape estimates). However, for this comparison TL was based on the mean, lower, and upper estimates generated from the VBGM for each age. These three TL estimates were then fed into either the body-depth equation or the gape equation, resulting in nine estimates of either body-depth or gape for each species. This generated 81 estimates of either vulnerable (1) or invulnerable (0) for each Moronid-shad age group. Estimates were averaged to determine vulnerability at each age. For this analysis, ages were restricted from age-0 to the maximum age observed for each species.

Once average vulnerabilities were attained, we compared vulnerability-by-age between species using a Cochran-Mantel-Haenszel Chi-Squared Test (CMH; $\alpha = 0.05$; Cochran 1954, Mantel and Haenszel 1959). This test is an extension of the Chi-Squared test, allowing for comparisons in three dimensions if no three-way interaction is present (Agresti 2002). Because this test requires counts and not proportions, average vulnerabilities were multiplied by 81 (i.e., the number of original comparisons) to attain an estimate of the frequency of vulnerability within each Moronid-by-Moronid age class. Prior to CMH analysis a log-linear model was fit to detect the presence of a three-way interaction ($\alpha = 0.05$). Similar to ANOVA, the CMH test allowed us to determine if there is a significant difference in vulnerability within one dimension of our matrix. Therefore, if the CMH test detected a significant difference with our three-dimensional matrix a groupwise post hoc test was used to test groups two-dimensions at a time using a modified Chi-squared test for independence ($\alpha = 0.05$) with p-values adjusted to minimize the false discovery rate (Benjamini and Hochberg 1995). We first compared vulnerability of shad at each age group among the Moronids. If no significant differences were detected, we determined if the significant CMH test result was due to shad vulnerability significantly varying by age within one of the species. Because statistical significance is often influenced by sample size, an adjusted estimate of Cramer's V (Bergsma 2013) was used to estimate effect size for each comparison. Cramer's V can be interpreted categorically with $V < 0.30$ suggesting "weak" effects, $V \geq 0.30$ being the threshold for "moderate" effects, and $V \geq 0.50$ begin the threshold for "large" effects (Cohen 1988).

Results

Fish collections for this study spanned nine Oklahoma reservoirs ranging in size from 15 to 35,612 ha (Table 1). Hybrid Striped Bass were the most widely distributed among the reservoirs, with TL ranging from 212-717 mm, weights ranging from 120-5,445 g, gape widths from 29-89 mm, and estimated ages up to 9 years old (Table 1). Striped Bass exhibited the largest size

range (194-793 mm TL), weighed up to 6,080 g, and had a gape ranging from 23-93 mm. White Bass were generally smaller (172-453 mm TL) but longer lived (up to 11 years old). White Perch were only sampled from Sooner Lake, ranged 191-323 mm TL, and lived up to 14 years old, making them the longest-lived Moronid observed (Table 1). Yellow Bass collected from New Spiro Lake, were the smallest (81-302 mm TL) and shortest-lived (≤ 2.5 years old). Gizzard Shad were collected from nine reservoirs, with sizes ranging from 45-477 mm TL, and age estimates ranged from 0-12 years old.

Estimating Body-Depth and Gape-Width from TL

The subset of Gizzard Shad used to assess the inverted TL to body-depth equation ranged in TL from 204 to 319 mm and in body depths from 54 to 93 mm. All observed body depths fell within the predicted mean, maximum, and minimum body depths from the inverted Lawrence (1957) equation, suggesting that the equation yielded an appropriate approximation of the variation present in shad body depths.

Gape-TL relationships appeared to vary between species (Figure 1). The relationship between TL and gape for Striped Bass and White Perch was best described by a power equation (Table 2). Hybrid Striped Bass were best described by an exponential equation, Yellow Bass a 2nd-degree polynomial, and White Bass by a linear model (Table 2). Competitive gape-based advantages increased with Moronid size; among species advantages varied based on the size of the individual and variation in the Gape-TL relationship within the species when compared graphically across the size range observed for each species (Figure 2).

Table 2. Mean model parameter estimates, root-mean-square error (RMSE), mean absolute error (MAE), Akaike information criterion adjusted for small sample sizes (AICc), and change in AICc relative to the top ranked model (ΔAICc) for four models predicting the relationship between gape (G) and total length (TL) for each Moronid species (Hybrid Striped Bass *Morone saxatilis x M. chrysops* [HSB], Striped Bass *M. saxatilis* [STB], White Bass *M. chrysops* [WHB], White Perch *M. americana* [WHP], Yellow Bass *M. mississippiensis* [YLB]). The top ranked model used to fit gape-total length relationships has been bolded for interpretability. Mean parameter estimates with values in the hundredths place are presented in reciprocal-power format where "E^{-n}" is equivalent to "$\times 10^{-n}$" for uniformity and conciseness. Note: statistics (e.g., RMSE, AICc) are only comparable within a species and should not be compared across species.

Species	Model	RMSE	MAE	AIC_c	ΔAIC_c
HSB	$\boldsymbol{G = -40.75 + 58.34e^{1.12E^{-3}TL}}$	**2.96**	**2.39**	**879.40**	**0.00**
HSB	$G = 19.10 + 5.43E^{-2}TL + 6.07E^{-5}TL^2$	2.96	2.38	879.48	0.08
HSB	$G = 7.17 + 0.11TL$	3.07	2.44	889.82	10.42
HSB	$G = 0.25TL^{0.88}$	3.13	2.47	896.76	17.36
YLB	$\boldsymbol{G = 3.61 + 7.54E^{-2}TL + 1.27E^{-4}TL^2}$	**1.43**	**1.08**	**389.07**	**0.00**
YLB	$G = -37.33 + 40.50e^{2.06E^{-3}TL}$	1.43	1.08	389.07	<0.01
YLB	$G = 0.12TL^{1.01}$	1.49	1.12	394.53	5.46
WHB	$\boldsymbol{G = 6.93 + 0.10TL}$	**2.73**	**2.12**	**689.58**	**0.00**
WHB	$G = 10.59 + 7.66E^{-2}TL + 4.82E^{-5}TL^2$	2.72	2.11	690.72	1.15
WHB	$G = -80.70 + 90.88e^{8.88E^{-4}TL}$	2.72	2.11	690.75	1.17
WHB	$G = 0.39TL^{0.81}$	2.75	2.14	691.48	1.91
STB	$\boldsymbol{G = 5.07E^{-2}TL^{1.13}}$	**4.11**	**2.97**	**476.44**	**0.00**
STB	$G = -7.09 + 0.13TL$	4.12	3.00	476.85	0.41
STB	$G = -4.09 + 0.12TL + 1.24E^{-5}TL^2$	4.11	2.99	478.87	2.43
STB	$G = -665.50 + 661.00e^{1.78E^{-4}TL}$	4.12	2.99	478.89	2.44
WHP	$\boldsymbol{G = 5.46E^{-2}TL^{1.14}}$	**1.93**	**1.52**	**609.02**	**0.00**
WHP	$G = -3.85 + 0.13TL$	1.94	1.52	609.44	0.42
WHP	$G = -3.21 + 12.02e^{3.90E^{-3}TL}$	1.93	1.51	609.87	0.85
WHP	$G = 13.03 + 1.13E^{-5}TL + 2.50E^{-4}TL^2$	1.93	1.51	609.88	0.85

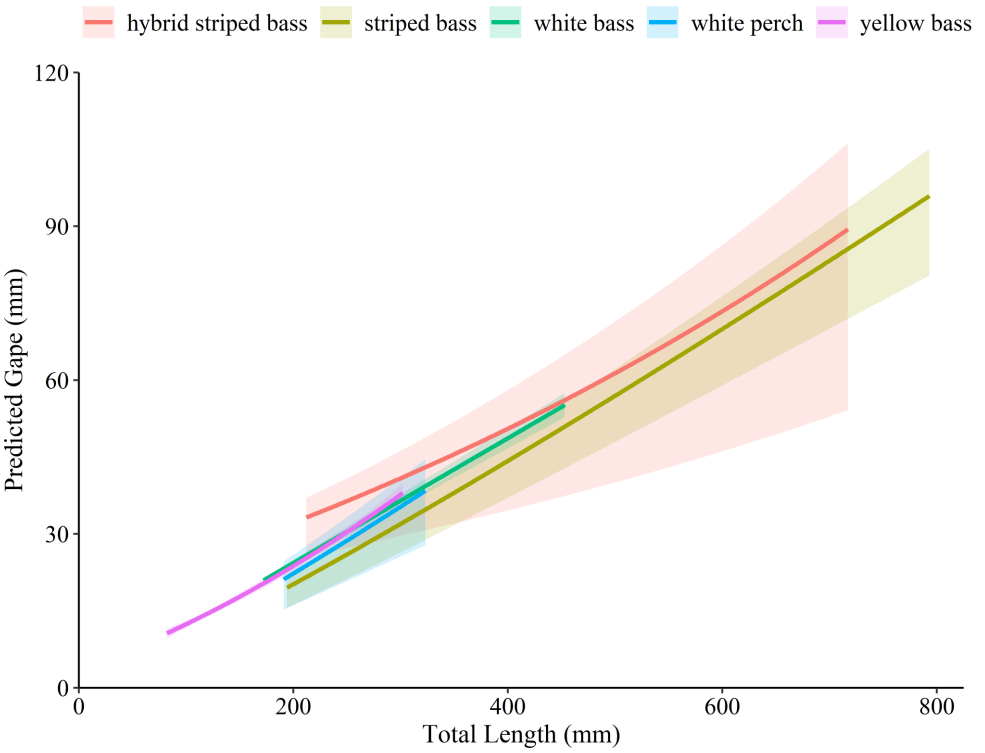

Figure 1. Mean (solid lines) and 99% predictive intervals for the gape-total length relationships observed for Moronids (Hybrid Striped Bass *Morone saxatilis x M. chrysops* [HSB], Striped Bass *M. saxatilis* [STB], White Bass *M. chrysops* [WHB], White Perch *M. americana* [WHP], Yellow Bass *M. mississippiensis* [YLB]) across the sizes observed. Any lines fitted through data points in the figure must be statistically significant and be supported by the mathematical equation and statistical information (P-values and R2 or R values). Keys to the symbols, formulae and regression values can be included in the figure itself or the caption, but not both. The minimum reduction for a figure may be indicated.

Comparing Gape-Vulnerability by TL

This interaction was significant within our binomial models (z range = 5.46-174.40, all $P < 0.05$), therefore only the interaction was interpreted. McFadden's pseudo R^2 estimates for all models were high (ρ^2 range = 0.20-0.64) indicating strong relationships between gape-based vulnerability and the size of Moronids and shad, suggesting all models fit adequately. This was confirmed by results of the Hosmer-Lemeshow Goodness of Fit tests (X^2 range = 8,539-105,397, df range = 23,815-101,559, all $P > 0.05$).

Several relationships were observed within our binomially distributed GLMs (Figure 3). Our results suggest that small Gizzard Shad were more vulnerable to smaller Hybrid Striped Bass than comparably sized Striped Bass, with vulnerability becoming equal to that of mixed as Moronid TL increased. This suggested that larger Gizzard Shad become more vulnerable to Hybrid Striped Bass than Striped Bass as TL increases. However, this is an artifact of the model detecting that Hybrid Striped Bass's gape-advantage increases to larger sized shad as they grow since vulnerability of the largest Gizzard Shad (i.e., 481 mm TL) plotted was equal. Hybrid Striped Bass had a slight competitive advantage for smaller Gizzard Shad at smaller sizes when compared to White Bass, Yellow Bass, and White Perch, although this decreased with increasing TL. White Bass appeared to have a slight gape advantage over Striped Bass and White Perch for the small-

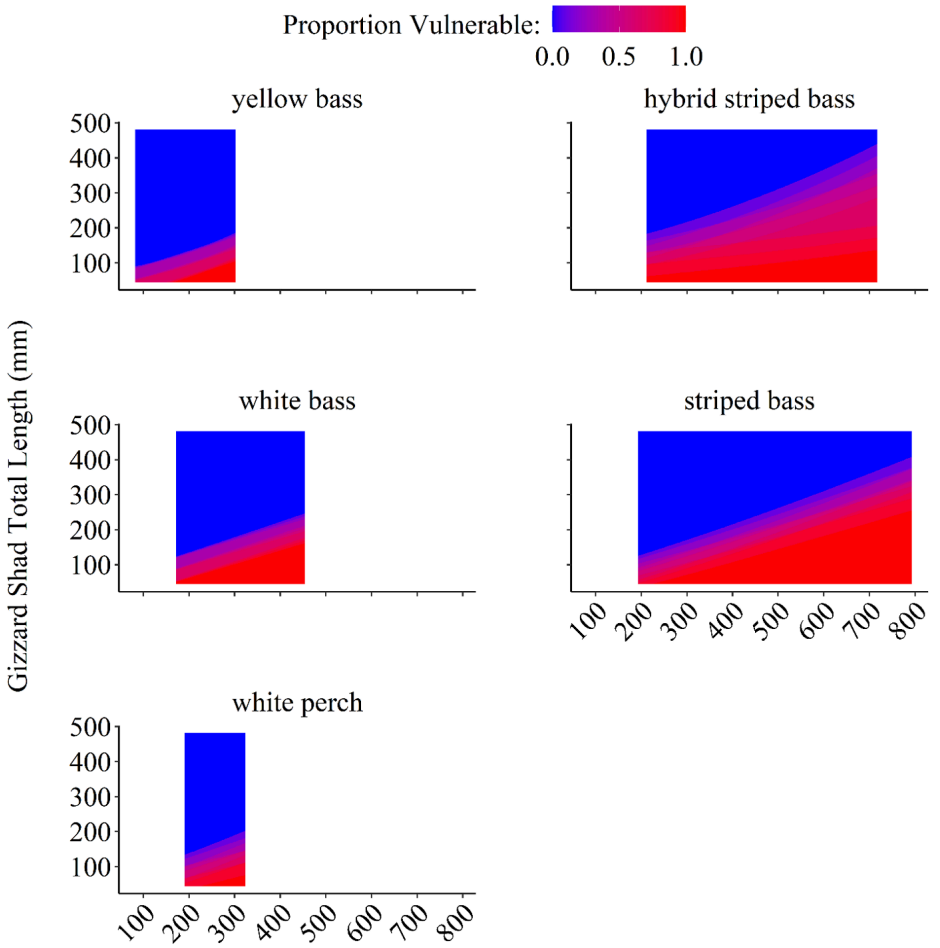

Figure 2. Average gape-based vulnerability of Gizzard Shad (*Dorosoma cepedianum*) to each Moronid (Hybrid Striped Bass *Morone saxatilis x M. chrysops* [HSB], Striped Bass *M. saxatilis* [STB], White Bass *M. chrysops* [WHB], White Perch *M. americana* [WHP], Yellow Bass *M. mississippiensis* [YLB]) predator across the sizes observed.

est Gizzard Shad sizes; however, this advantage decreased with increasing TL. White Bass appeared to have little competitive advantage over Yellow Bass. White Perch had an advantage over Striped Bass of similar size for the smallest sized Gizzard Shad. Small Yellow Bass had a competitive advantage over similarly sized Striped Bass and White Perch when competing for the smallest sized Gizzard Shad. Yellow Bass advantage appears to shift to shad of larger sizes (though still small) as Moronid lengths increased.

Growth Modeling

To make growth trajectories biologically reasonable (i.e., non-negative) the following parameter estimates were adjusted: the lower 0.5% PI for size of an age-0 Yellow Bass was adjusted to 25 mm TL (Burnham 1910), the lower 0.5% PI for size of an age-0 Striped Bass was adjusted to 25 mm TL (Boynton et al. 1981), and the lower 0.5% PI and mean estimated sizes of an age-0 White Bass was adjusted to 46 mm and 51 mm TL, respectively (Bonn 1953). The lower 0.5% PI and mean estimated sizes of an age-0 and age-1 Gizzard Shad were fixed at 25 and 29mm TL (Miller 1960, Michaletz 1997), respectively. Given these estimates were unrealistic, and they impacted a total of 6 observations, we considered this appropriate. To keep growth trajectories feasible, the maximum size a Gizzard Shad

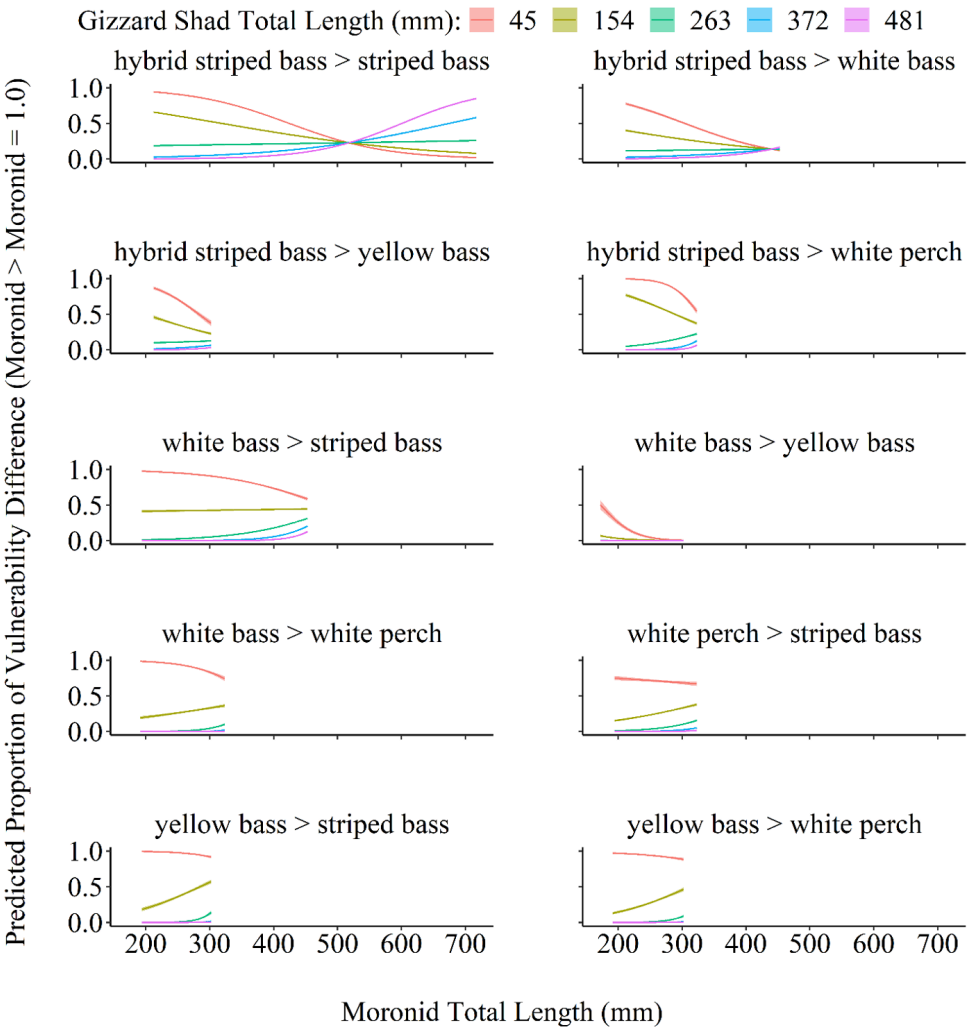

Figure 3. Predictive proportion of vulnerability of Gizzard Shad (*Dorosoma cepedianum*) to each Moronid (Hybrid Striped Bass *Morone saxatilis x M. chrysops* [HSB], Striped Bass *M. saxatilis* [STB], White Bass *M. chrysops* [WHB], White Perch *M. americana* [WHP], Yellow Bass *M. mississippiensis* [YLB]) predator across similar size ranges based on the gape-total length vulnerability relationships. Moronids on the left of the > are scored a "1" and Moronids on the right and equal vulnerability are scored a "0". High estimates can be interpreted as advantages for the Moronid on the left and low estimates can be interpreted as equal or greater advantage for the Moronid on the right.

could attain was set at 521 mm TL (the highest TL ever recorded; Trautman 1981). This affected the upper 99% PI estimates for age-10 to age-13 Gizzard Shad. Given fish of this size are almost completely invulnerable to predation, this did not influence our findings.

Bootstrapped growth trajectories for Gizzard Shad and Moronids appeared to adequately capture the growth trajectories present within our populations, as observed size at age data primarily fell within the estimated 99% PI (Figure 4). Graphical interpretation of bootstrapped growth distributions suggested that Striped Bass had the fastest growth trajectory followed by Hybrid Striped Bass; however, maximum size potential

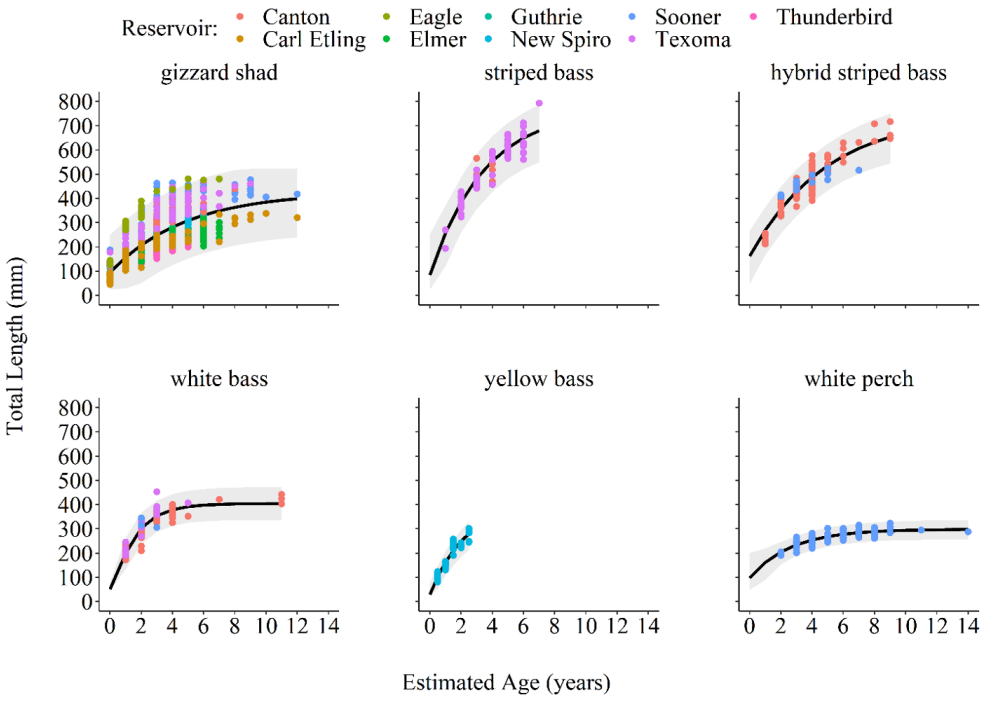

Figure 4. Mean (solid line) and 99% predictive intervals (grey shading) obtained from bootstrapping for Von bertalanffy growth trajectories for each Moronid (Hybrid Striped Bass *Morone saxatilis x M. chrysops* [HSB], Striped Bass *M. saxatilis* [STB], White Bass *M. chrysops* [WHB], White Perch *M. americana* [WHP], Yellow Bass *M. mississippiensis* [YLB]) species. Points indicate individual size at age observations from each population.

of Striped Bass was greater (Figure 2). Likewise, White Bass appeared to have a similar growth trajectory to Yellow Bass; however, they reached a greater theoretical-maximum average length. White Perch exhibited slower early growth and appeared to attain the shortest theoretical maximum lengths of any Moronid.

Gape estimates from growth curve modeling suggest that slow growth results in increased overlap between Moronids, resulting in reduced competitive advantages due to decreased growth (Figure 5). As growth rate increases to the mean rate and above, these estimates deviate from one another. This results in varying competitive advantages for each species based on their growth trajectories. The annular growth of Moronids appeared to allow larger bodied fishes increased access to older and larger shad (Figure 6). For White Perch, and to some degree White Bass, maximum body size appeared to limit access to older and larger shad.

Comparing Gape-Vulnerability by Age

No three-way interactions were detected by log-linear models (all $P > 0.05$). All CMH tests indicated significant variation in the vulnerability estimates of Gizzard Shad across age groups and the age of any two Moronids we compared (M^2 range = 39.2 – 290.7, *df* range = 20 – 132, all $P < 0.05$). Post hoc analyses detected no significant difference in shad vulnerability between ages for Striped Bass, White Bass, and Hybrid Striped Bass (all $P > 0.05$). Likewise, post hoc analyses detected no significant difference in shad vulnerability between ages for Yellow Bass, compared to either White Bass, Striped Bass, or White Perch (all $P > 0.05$). In all the above cases, it was confirmed that the significant result from the CMH test was due to variation in shad vulnerability between ages within one of the species (all $P < 0.05$). Hybrid Striped Bass had a gape-based

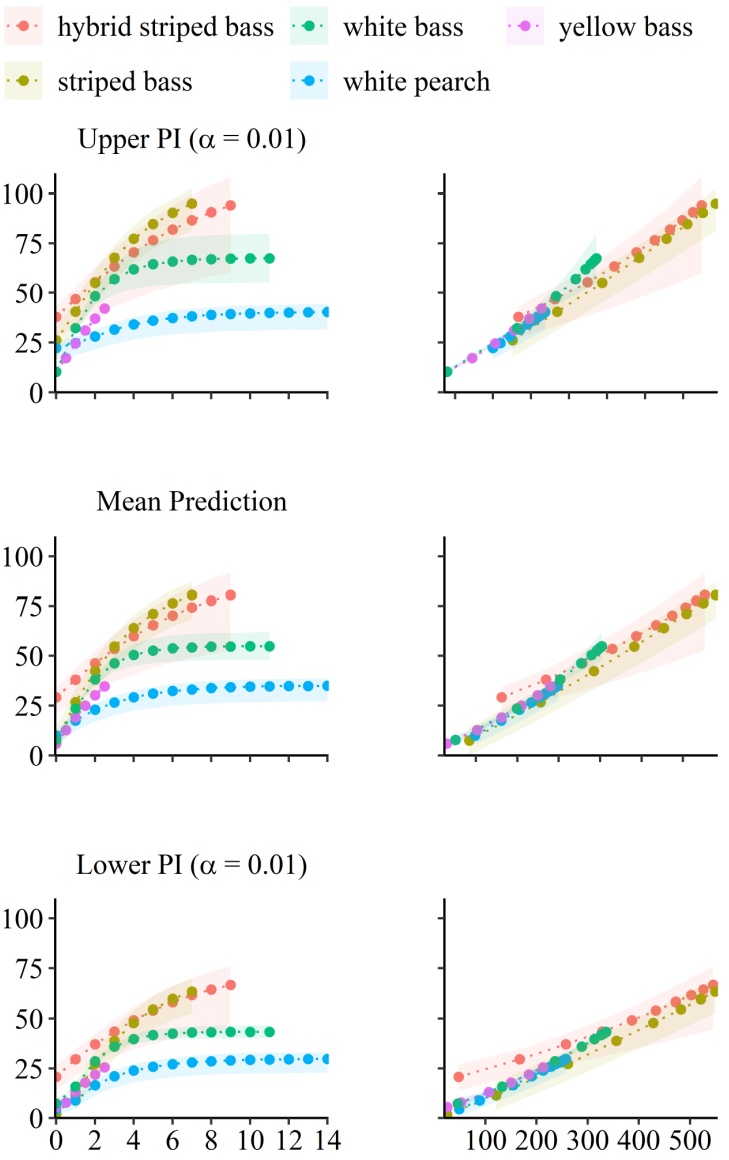

Figure 5. Mean (solid lines) and 99% predictive intervals for the gape-total length relationships observed for Moronids (Hybrid Striped Bass *Morone saxatilis x M. chrysops* [HSB], Striped Bass *M. saxatilis* [STB], White Bass *M. chrysops* [WHB], White Perch *M. americana* [WHP], Yellow Bass *M. mississippiensis* [YLB]) based on the upper, lower, and mean estimates of growth from bootstrapped Von bertalanffy growth trajectories. Comparisons are made based on ages (left) and predicted total lengths (right) for each species to understand how overlap varies relative to growth.

advantage over Yellow Bass across all age ranges compared (all $P < 0.05$); however, this advantage was always weak (V range = 0.18-0.20). We also observed a gape-based advantage for Hybrid Striped Bass over White Perch from age-1 to age-9 (all $P < 0.05$). No advantage was observed at age-0 ($P > 0.05$), a significant but weak advantage was observed from age-1 to age-3 (V = 0.18-

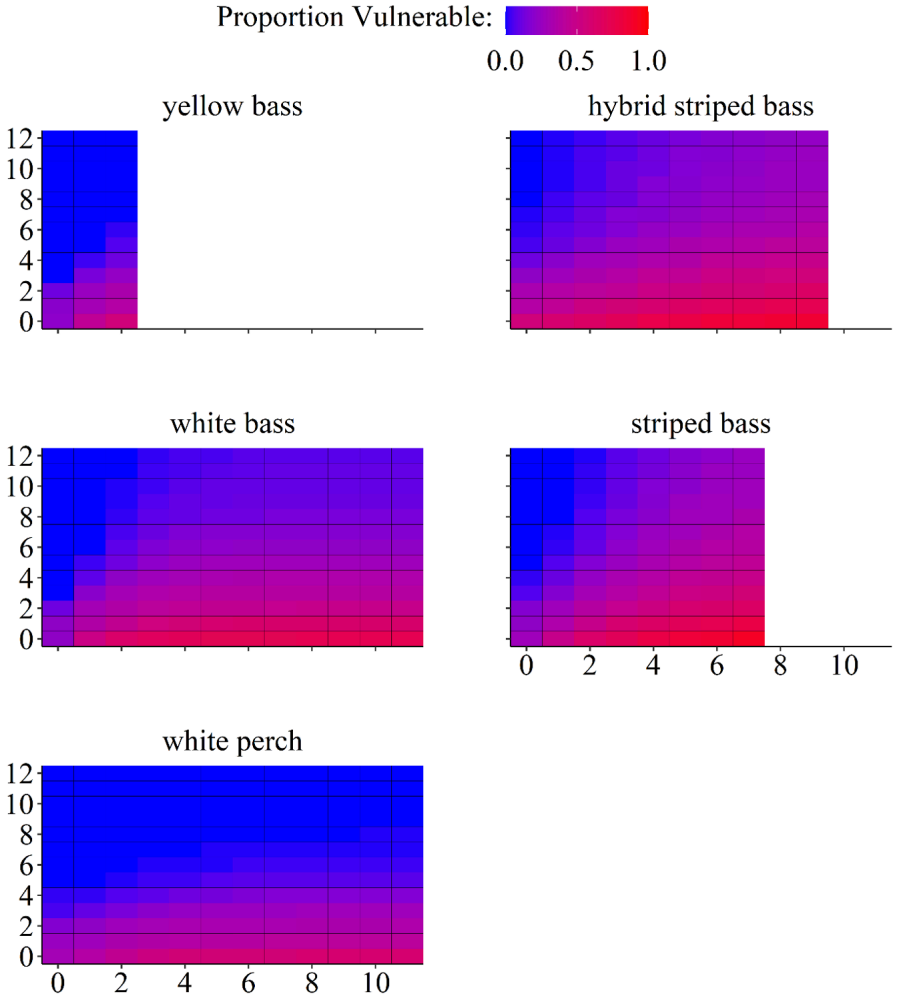

Figure 6. Average gape-based vulnerability of Gizzard Shad (*Dorosoma cepedianum*) to each Moronid (Hybrid Striped Bass *Morone saxatilis x M. chrysops* [HSB], Striped Bass *M. saxatilis* [STB], White Bass *M. chrysops* [WHB], White Perch *M. americana* [WHP], Yellow Bass *M. mississippiensis* [YLB]) predator across the range of age estimates observed.

0.28), and a moderate advantage was observed from age-4 to age-9 (V range = 0.30-0.32), suggesting Hybrid Striped Bass gain increased advantages over White Perch based on their growth trajectories. White Bass also exhibited a varying gape-based competitive advantage over White Perch, with no significant advantage from age-0 to age-2 (all $P > 0.05$) and a weak (V range = 0.23-0.27) significant advantage thereafter to age-11 (all $P < 0.05$). Age-0 and age-1 Striped Bass had no competitive advantage over White Perch (all $P > 0.05$), but a significant advantage from age-3 on (all $P < 0.05$). Their advantage was weak at age-3 and age-4 (V range = 0.21-0.29), then increased to moderate from age-5 on (V ≈ 0.32).

Discussion

Our results collectively demonstrate that gape/TL relationships, vulnerability estimates, and growth trajectories interact to shape competitive foraging advantages among Moronids.

Species differed substantially in their gape/TL allometries, producing size-dependent shifts in the relative vulnerability of Gizzard Shad to each Moronid. GLM analyses showed that these differences translate into variable vulnerability across the size spectrum of both predators and prey, with small-bodied Moronids generally exhibiting greater access to the smallest shad. Growth modeling further revealed that faster-growing species (e.g., Striped Bass, Hybrid Striped Bass) gain increasing gape-based foraging advantages as they age. In contrast, slower-growing or smaller-bodied species (e.g., White Perch, Yellow Bass) are progressively limited to younger, smaller shad. Finally, age-based vulnerability analyses indicated that these competitive hierarchies are reinforced across ontogeny, with some species gaining moderate advantages only after several years of growth. Together, these findings highlight the importance of integrating gape allometry and growth dynamics when evaluating potential diet overlap and forage competition in mixed-Moronid fisheries.

Contrasting results comparing gape-vulnerability suggests accounting for ecological phenomena that confound direct comparisons (e.g., growth trajectories) can better explain diet overlap. Though we were unable to find a similar example of this phenomenon within the Moronid family, size mediated availability for forage has been documented prior in *Lepomis* species, with larger *Lepomis* having reduced niche overlap and likely reduced diet overlap for resources (Mittelbach 1984). Growth-mediated diet overlap appears to be occurring in Moronids, allowing fishes who may not have a competitive advantage at a similar length to reach larger sizes and obtain a larger gape. This allows them to better compete within the conspecifics of their genus. Given the link between gape and forage size (Labropoulou and Eleftheriou 1997, Mihalitsis and Bellwood 2017), these results suggest that growth rates and the resulting size structure of species present within a mixed-Moronid fishery are important in mediating potential overlap in forage availability.

Perhaps most interesting is the advantage of Moronids, which generally reach a smaller maximum size (e.g., Yellow Bass) over those reaching a larger maximum size (e.g., Striped Bass). Though theoretical in nature, the general pattern in TL-gape relationships suggests that smaller bodied Moronids appear to be predisposed to better exploit smaller bodied prey. Apart from Hybrid Striped Bass that appear to inherit the gape-based advantages of White Bass and the growth-based advantages of Striped Bass, smaller bodied Moronids appear to have larger gapes at smaller sizes. This could influence diet overlap, especially in younger Moronids, and impact recruitment, growth, and mortality of gamefish populations (Miller 1960; Michaletz 1997). It is important to note that we investigated the mechanistic potential for diet overlap within these fishes to gain a proper understanding of their ability to exploit the forage base within these systems, and diet studies would be required to measure actual consumption.

Though forage-based competition between Moronids in Oklahoma reservoirs is possible, it can occur only when resources are limited (Polis and Winemiller 1996). By estimating gape-vulnerability, we approximated a theoretical foraging niche (Schoener 2009) for each species. Though this has been documented previously among Moronids (Irons et al. 2002, Olson 2004, Feiner et al. 2013), it may not always occur if species can partition resources among themselves (e.g., Rash 2003). Within the context of our results, the available forage base appears to be a key component of the successful management of Moronids and mixed-Moronid fisheries in particular.

Across the US, *Dorosoma* spp. are an important forage fish and a primary forage source for mature individuals from each of the above mentioned Moronid species (Matthews et al. 1988, Hodson 1989, Bauer 2002, Guy et al. 2002). Large-bodied individuals of the *Dorosoma* genus are associated with negative impacts on sportfish populations (Lyons et al. 2018). Therefore, an inadequate abundance of appropriately sized prey may require manipulation to maintain or enhance Moronid populations and mixed Moronid fisheries. Though shad size structure manipulation may be achieved through predator stocking (Ostrand et al. 2001), abundance ap-

pears to be regulated by abiotic factors (e.g., temperature, precipitation, productivity; DiCenzo et al. 1996, Bremigan and Stein 2001). Therefore, it may be important to monitor alternative prey sources used by Moronids (e.g., insects, Snow and Porta 2020) or introduce new forage (e.g., threadfin shad [*Dorosoma petenense*], Maceina and Sammons 2015) if it appears that diet overlap is limiting growth or production. This is especially true at small sizes where gape overlap appears greatest between Moronids.

Assuming that a proper forage base is maintained, competition between Moronids should be reduced; however, predation-based competition is complex and intragenus predation (i.e., the consumption of one Moronid by another; Polis et al. 1989) may occur. For example, White Perch have been documented to eat eggs of other species, which may influence recruitment (Schaeffer and Margraf 1987). On the eastern coast of the United States Hybrid Striped Bass have been hypothesized to compete with native Striped Bass for food and habitat (Patrick and Moser 2001). Therefore, when applying these results, managers should note that competition for food resources may not be the only axis along which these species compete.

Gape based limitation offers managers another tool for managing Moronids and mixed-Moronid fisheries. For example, our results suggest that further invasion of White Perch and range expansion of Yellow Bass in Oklahoma may induce increased forage overlap between Moronids at smaller sizes. Diet compositions from the literature for White Perch and Yellow Bass suggest that White Perch are likely more detrimental to other Moronids (Schaeffer and Margraf 1987, Snow and Porta 2020).

Within our subset of study reservoirs Sooner Lake and Lake Texoma offer a chance to investigate this hypothesis, focusing on mixed-Moronid relationships between Hybrid Striped Bass, Striped Bass, and White Perch. White Perch are established in Sooner Lake, where growth rates of Hybrid Striped Bass are reduced, and Striped Bass are large but in low abundance. Comparatively, no White Perch are present in Lake Texoma, and both Hybrid Striped Bass and Striped Bass exhibit adequate growth (OFAT 2022). Based on our modeled results, a potential cause of these contrasting scenarios is increased competition at smaller size classes by invasive White Perch. Reduced growth potential in Sooner Hybrid Striped Bass and larger sized but low abundance Striped Bass may result from faster growing individuals from each population having higher survival due to reduced competition with White Perch. This may have allowed faster growing Hybrid Striped Bass to mature early, thus stunting the population through density dependent feedbacks (Ylikarjula et al. 1999). The few Striped Bass that survive through this multi-level competition would then be large, but in lower abundance due to the increased biomass of smaller Hybrid Striped Bass. Though diet information would be needed to prove this hypothesis, the lower productivity of Sooner Lake relative to Lake Texoma makes it probable as productivity is tied to Gizzard Shad abundance (OWRB 2019).

We have shown that gape-vulnerability of forage can be easily estimated and compared between size or age structure for Moronids, allowing fisheries managers another tool to assess diet overlap within a system. We documented gape-based advantages to growth rates, and why they should be considered when managing fisheries. This is important as growth effects on competition, though extensively documented, are poorly understood in the fisheries field (Mittelbach 1984; Reed et al. 2019). Given this strong theoretical basis (Mihalitsis and Bellwood 2017; Dennerline and Van Den Avyle 2000), managers concerned with forage availability for Moronids can use gape-based vulnerability to both estimate forage availability and diet overlap between species as well as gauge how growth mediates these interactions. This being said, and caution against blind application. Suppose forage is hypothesized to be limited and exploitation appears likely, as was the case for our Sooner Lake-Lake Texoma comparison. In that case, managers should first estimate diet overlap, prey abundance, and intragenus predation to determine if manipulation of the forage base or Moronid population is warranted. If this is the case, we recommend following

standardized fisheries methods (e.g., stocking manipulation, Ostrand et al., 2001; forage introduction, Maceina and Sammons, 2015) to determine whether the population can be manipulated to meet management objectives.

Acknowledgements

The authors thank Shelby Jeter, Micah Waters, Graham Montague, and Matthew Lyons for assisting with field and laboratory work. We also thank Dr. Dan Shoup and Graham Montague for reviewing an earlier version of this manuscript. We also want to thank Dr. Mostafa Elshahed and the anonymous reviewers for their edits that improved this manuscript. Financial support for this publication was provided by Sport Fish Restoration Program grants [F-86-D-1] and [F-112-D-1] to the Oklahoma Department of Wildlife Conservation.

References

Agresti, A. 2002. An Introduction to Categorical Data Analysis, 2nd edition. Wiley-Interscience, Hoboken, New Jersey.

Bauer, D. L. 2002. White Bass population differences in Nebraska reservoirs with Gizzard Shad or alewife prey bases. North American Journal of Fisheries Management 22:665-670.

Bax, N. J. 1998. The significance and prediction of predation in marine fisheries. ICES Journal of Marine Science 55:997-1030.

Baxter, C. V., K. D. Fausch, M. Murakami, and P. L. Chapman. 2004. Fish invasion restructures stream and forest food webs by interrupting reciprocal prey subsidies. Ecology 85:2656-2663.

Benjamini, Y., and Y. Hochberg. 1995. Controlling the false discovery rate: a practical and powerful approach to multiple testing. Journal of the Royal Statistical Society Series B 57:289-300.

Bergsma, W. 2013. A bias-correction for Cramer's V and Tschuprow's T. Journal of the Korean Statistical Society 42:323-328.

Blessing, J.J., J.C. Marshall, and S.R. Balcombe. 2010. Humane killing of fish for scientific research: a comparison of two methods. Journal of Fish Biology 76:2571–2577.

Bonn, E. W. 1953. The food and growth rate of young White Bass (*Morone chysops*) in Lake Texoma. Transactions of the American Fisheries Society 82:213-221.

Boynton, W. R., H. Zion, and T. T. Polgar. 1981. Importance of juvenile Striped Bass food habits on the Potomac Estuary. Transactions of the American Fisheries Society 110:56-63.

Bremigan, M. T., and R. A. Stein. 2001. Variable Gizzard Shad recruitment with reservoir productivity: causes and implications for classifying systems. Ecological Applications 11:1425-1437.

Bulak J. S., C. C. Coutant, and J. A. Rice. 2013. Preface. Pages ix-xii *in* J. S. Bulak, C. C. Coutant, J. A. Rice, editors. Biology and management of inland Striped Bass and Hybrid Striped Bass. American Fisheries Society, Bethesda, Maryland.

Burnham, C. W. 1910. Notes on the Yellow Bass. Transactions of the American Fisheries Society 39:103-108.

Burnham, K. P., and D. R. Anderson. 2002. Model selection and inference: A practical information-theoretic approach, 2nd Edition. Springer-Verlag, New York, New York.

Carpenter, S. R., J. F. Kitchell, and J. R. Hodgson 1985. Cascading trophic interactions and lake productivity. Bioscience 35:634-639.

Cochran, W. G. 1954. Some Methods for Strengthening the Common Chi-Squared Tests. Biometrics 10:417–51.

Clayton, D.L., and M.J. Maceina. 1999. Validation of annulus formation in Gizzard Shad otoliths. North American Journal of Fisheries Management. 19:1099-1102.

Cohen, J. 1988. Statistical power analysis for the behavioral sciences. 2nd edition. Routledge. New York, New York.

Coutant, C. C. 2006. Thermal effects on fish ecology. Pages 1146-1151 *in* J. R. Pfafflin JR, and Ziegler EN, editors. Encyclopedia of environmental science and engineering 5th edition. Taylor and Francis

Group, Boca Raton, Florida.

Dennerline, D. E., and M. J. Van Den Avyle. 2000. Sizes of prey consumed by two pelagic predators in US reservoirs: implications for quantifying biomass of available prey. Fisheries Research 45:147-154.

DeVries, D. R., R. A. Stein, and M. T. Bremigan. 1998. Prey selection by larval fishes as influenced by available zooplankton and gape limitation. Transactions of the American Fisheries Society 127:1040-1050.

DiCenzo, V. J., M. J. Maceina, M. R. Stimpert. 1996. Relations between Reservoir tropic state and Gizzard Shad population characteristics in Alabama reservoirs 16:888-895.

Dunic, J. C., and J. K. Baum. 2017. Size structuring and allometric scaling relationships in coral reef fishes. Journal of Animal Ecology 86:577-589.

Feiner Z. S., and J. A. Rice. 2013. Trophic niche and diet overlap between invasive White Perch and resident White Bass in a southeastern reservoir. Transactions of the American Fisheries Society 142:912-919.

Gilliland, E. R. 1978. Food habits of Striped Bass x White Bass hybrids and Largemouth Bass in Sooner Lake, Oklahoma. Master's Thesis, Oklahoma State University, Stillwater, Oklahoma.

Guy, C. S., R. D. Schultz, M. A. Colvin. 2002. Ecology and management of White Bass. North American Journal of Fisheries Management 22:606-608.

Hambright, K. D. 1991. Experimental analysis of prey selection by Largemouth Bass: Role of predator mouth width and prey body depth. Transactions of the American Fisheries Society 120:500-508.

Hill, J. E., L. G. Nico, C. E. Cichra, and C. R. Gilbert. 2004. Prey vulnerability to Peacock Cichlids and Largemouth Bass based on predator gape and prey body depth. Proceedings of the Annual Conference of the Southeastern Association of Fish and Wildlife Agencies 58:47-56.

Hodson, R. G. 1989. Hybrid Striped Bass: biology and life history. Texas Agricultural Extension Service, Southern Regional Aquaculture Center publication no. 300, Texas A&M University, College Station.

Hoff, G.R., D.J. Logen, and M.F. Douglas. 1997. Otolith morphology and increment validation in young Lost River and Shortnose Suckers. Transactions of the American Fisheries Society 126:488-494.

Hurvich, C. M., and C. Tsai. 1989. Regression and time series model selection in small samples. Biometrika 76(2):297-307.

Irons, K. S., T. M. O'Hara, M. A. Mclelland, and M. A. Pegg. 2002. White Perch occurrence, spread, and hybridization in the middle Illinois River, Upper Mississippi River system. Transactions of the Illinois Academy of Science 95:207-214.

Krebs, J. M., and R. G. Turingan. 2003. Intraspecific variation in gape-prey size relationships and feeding success during early ontogeny in Red Drum, Sciaenops ocellatus. Environmental Biology of Fishes 66:75-84.

Labropoulou, M., and A. Eleftheriou. 1997. The foraging ecology of two pairs of congeneric demersal fish species: Importance of morphological characteristics in prey selection. Journal of Fish Biology 50:324-340.

Lawrence, J. M. 1957. Estimated sizes of various forage fishes Largemouth Bass can swallow. Proceedings of the Annual Conference of the Southeastern Association of Fish and Wildlife Agencies 11:220-225.

Lindeman, R. L. 1942. The trophic-dynamic aspect of ecology. Ecology, 23:399–417.

Lyons, M.T., R.A., Snow, and M.J. Porta. 2018. Population characteristics of Gizzard Shad introduced into a small western Oklahoma impoundment. Proceedings of the Oklahoma Academy of Science 98:25-32.

Maceina, M. J., and S. M. Sammons. 2015. Stocking Threadfin Shad to enhance Largemouth Bass population in two Alabama ponds. Proceedings of the Annual Conference of the Southeastern Association of Fish and Wildlife Agencies 2:28-34.

Mantel, N., and W. Haenszel. 1959. Statistical

Aspects of the Analysis of Data from Retrospective Studies of Disease. Journal of the National Cancer Institute 22:719–48.

Matthews W. J., L. G. Hill, D. R. Edds, J. J. Hoover, and T. G. Heger. 1988. Trophic ecology of Striped Bass, Morone saxatilis, in a freshwater reservoir (Lake Texoma, U.S.A.). Journal of Fish Biology 33:273-288.

McFadden, D. 1974. Conditional logit analysis of qualitative choice behavior. Pages 105-142 *in* Zarembka, P, editor. Frontiers in econometrics. New York, New York: Academic Press.

McFadden, D. 1979. Quantitative methods for analyzing travel behaviour of individuals: Some recent developments. Pages 279-318. *in* D. A. Henshe, P. R. Stopher, editors. Behavioural Travel Modeling. Croom Helm, London, United Kingdom.

McQueen, D. J., J. R. Post, E. L., and Mills. 1986. Trophic relationships in freshwater pelagic ecosystems. Canadian Journal of Fisheries and Aquatic Sciences 43:1571–1581.

Michaletz, P. H. 1997. Factors affecting abundance, growth, and survival of Age-0 Gizzard Shad. Transactions of the American Fisheries Society 126:84-100.

Mihalitsis, M., and D. R. Bellwood. 2017. A morphological and functional basis for maximum prey size in piscivorous fishes. PLOS One 12:e0184679

Miller, R. R. 1960. Systematics and biology of the Gizzard Shad (*Dorosoma cepadianum*) and related fishes. Fishery Bulletin 173. United States Department of the Interior. United States Fish and Wildlife Service, Washington, DC.

Miller, R. J. and H. W. Robison. 2004. Fishes of Oklahoma. University of Oklahoma Press, Norman, Oklahoma.

Mittelbach, G. G. 1984. Predation and resource partitioning in two sunfishes (Centrarchidae). Ecology 65:499-513.

OFAT (Oklahoma Fishery Analysis Tool). 2022. Oklahoma fishery analysis tool: an R-based application for analysis of standardized fishery samples. Oklahoma Department of Wildlife Conservation. <https://www.odwcfishdata.shinyapps.io/ssp_app/>. Accessed 29 May 2022.

Oklahoma Water Resources Board. 2019. Oklahoma Lakes Report: Beneficial Use Monitoring Program (Bump). <www.owrb.ok.gov>. Accessed 29 May 2022.

Olson, N. W. 2004. Interactions among Hybrid Striped Bass, White Bass, and Walleye in Harlan County Reservoir. Master's Thesis, Montana State University, Bozeman, Montana.

Ostrand, K. G., H. L. Schramm Jr., J. E. Kraai, B. Braeutigam. 2001. Effects of intensive stocking of Hybrid Striped Bass on the population structure of Gizzard Shad in a West Texas impoundment, a Case Study. Proceedings of the Annual Conference of the Southeastern Association of Fish and Wildlife Agencies 55:324-333.

Pace, M. L., J. J. Cole, S. R. Carpenter, and J. F. Kitchell. 1999. Trophic cascades revealed in diverse ecosystems. Trends in Ecology and Evolution 14:483–488.

Patrick, W. S., and M. L. Moser. 2001. Potential competition between Hybrid Striped Bass (*Morone saxtilis* × *M. americana*) and Striped Bass (*M. saxtilis*) in the Cape Fear River Estuary, North Carolina. Estuaries 24:425-429.

Polis, G. A., C. A. Myers, and R. D. Holt. 1989. The ecology and evolution of intraguild predation: Potential competitors that eat each other. Annual Review of Ecology and Systematics 20:297-330.

Polis, G. A., and K. O. Winemiller. 1996. Food webs: Integration of patterns and dynamics. Springer, New York, New York.

Power, M. E. 1992. Top-down and bottom-up forces in food webs: Do plants have primacy? Ecology 73:733-746.

Rash, J. M. 2003 Comparative ecology of juvenile Striped Bass and juvenile Hybrid Striped Bass in Claytor Lake, Virginia. Master's Thesis, Virginia Polytechnic Institute and State University, Blacksburg, Virginia.

Reed C, R Branconi, J Majoris, C Johnson, and

P Buston. 2019 Competitive growth in a social fish. Biology Letters 15:20180737

Secor, D. H., J. M. Dean, and E. H. Laban. 1992. Otolith removal and preparation for microstructural examination. Pages 19–57 *in* D.K. Stevenson and S.E. Campana, editors. Otolith microstructure examination and analysis. Canadian Special Publication of Fisheries and Aquatic Sciences 117, Ottawa.

Schaeffer, J. S., and F. J. Margraf. 1987. Predation on fish eggs by White Perch, Morone americana, in western Lake Erie. Environmental Biology of Fishes 18:77-80.

Schoener, T. W. 2009. Ecological niche. Pages 3-13 *in* S. A. Levin, S. R. Carpenter, and H. C. Godfray, editors. The Princeton guide to ecology. Princeton University Press, Princeton, New Jersey.

Schultz, R. D., A. L. Fowler, J. M. Goeckler, and M. C. Quist. 2013. Comparisons of growth for Hybrid Striped Bass in North America. Pages 219-227 *in* J. S. Bulak, C. C. Coutant, and J. A. Rice. Editors. Biology and Management of Inland Striped Bass and Hybrid Striped Bass. American Fisheries Society, Symposium 80, Bethesda, Maryland.

Slaughter, J. E., and B. Jacobson. 2008. Gape: Body size relationship of Flathead Catfish. North American Journal of Fisheries Management 28:198-202.

Snow, R. A., and M. J. Porta. 2020. Population dynamics and diets of Yellow Bass in New Spiro Reservoir, Oklahoma. Proceedings of the Oklahoma Academy of Sciences 100:54-61.

Trautman, M. B. 1981. The fishes of Ohio. The Ohio State University Press, Columbus, OH.

Wang, C. J., and H. Iyer. 2005. On higher-order corrections for propagating uncertainties Metrologia 42: 406-410.

Ylikarjula, J., M. Henio, and U. Dieckmann. 1999. Ecology and adaptation of stunted growth in fish. Evolutionary Ecology 13:433-453.

Neoterranova caballaeroi (Nematoda: Anisakidae) from Northern Cottonmouth, *Agkistrodon piscivorus* (Reptilia: Ophidia: Viperidae) in Arkansas

Chris T. McAllister*
Department of Natural Sciences, Northeast Texas Community College, 2886 FM 1735, Chapel Hill Road, Mt. Pleasant, TX 75455

Michelle J. Mejia
Department of Natural Sciences, Northeast Texas Community College, 2886 FM 1735, Chapel Hill Road, Mt. Pleasant, TX 75455

Abstract: Examination of four adult northern cottonmouths, *Agkistrodon piscivorus* collected from western Arkansas for helminth parasites, yielded three, seven, 21, and 70 stomach nematodes, respectively. The nematodes were identified as the anisakid, *Neoterranova caballaeroi*. Although the species has been previously reported from *A. piscivorus*, this is the first time the nematode has been reported from Arkansas. We document a new geographic record for the parasite and the first report of *N. caballaeroi* from west of the Mississippi River.

Introduction

The northern cottonmouth, *Agkistrodon piscivorus* is a moderately large viperid snake that ranges from extreme southern Illinois, western Kentucky, and southeastern Virginia west to through Arkansas to southeastern Oklahoma and southcentral Texas (Powell et al. 2016). In Arkansas, *A. piscivorus* is found statewide in suitable watersheds, including swamps and sloughs to clear upland brooks (Trauth et al. 2004). Trauth and McAllister (1995) reported that in Arkansas, *A. piscivorus* feeds on fish, anurans, small mammals, and snakes.

McAllister et al. (2023) recently summarized reports of helminth parasites of this snake from throughout its range and included data on parasites of eight specimens from Arkansas. Those collected from that study harbored three trematodes, two nematodes, an acanthocephalan, and pentastomid. However, in terms of nematodes, only an unknown ascarid larvae and *Physaloptera abjecta* Leidy, 1856 were found; however, Detterline et al. (1984) reported an unidentified nematode from a northern cottonmouth from Alabama and Davis et al. (2016) documented *Capillaria colubra* Pence, 1970 from *A. piscivorus* from North Carolina. In addition, Scholz et al. (2023) reported on tapeworms (Cestoda) of *A. piscivorus* from Arkansas and Oklahoma, some collected from McAllister et al. (2023), but not reported therein. Here we document an additional nematode from this snake in Arkansas as well as report a new geographic distribution record for the parasite.

*Corresponding author: cmcallister@ntcc.edu
Proc. Okla. Acad. Sci. 105: pp 58-61 (2025)

Materials and Methods

On 20 June 2024, 29 August 2025 (n = 2), and 27 September 2025, four adult *A. piscivorus* (mean ± sd snout-vent length [SVL] = 526.8 ± 88.6, range 402-645 mm) were collected with snake tong from the Ouachita Mountains Biological Station pond, Polk County, Arkansas, and examined for helminth parasites. Snakes were euthanized with a concentrated intraperitoneal injection of tricaine-methanesulfonate solution and a mid-ventral incision was made to expose their gastrointestinal contents. The stomach and intestinal organs were split lengthwise, rinsed with normal saline (0.9% [v/v] NaCl-), placed in a Petri dish with fresh normal saline, and examined under a stereomicroscope. Live nematodes were observed in the stomach, removed, and fixed in hot distilled water. Specimens were transferred to vials containing 90% DNA grade ethanol. They were later examined as temporary mounts in glycerol.

Voucher specimens of hosts were deposited in the Northeast Texas Community College Vertebrate Collection, Mt. Pleasant, Texas. Voucher nematodes were deposited in the Harold W. Manter Laboratory of Parasitology (HWML), University of Nebraska, Lincoln, Nebraska.

Results and Discussion

Numerous anisakid nematodes (Fig. 1A) were found in the stomach of all snakes. Detailed

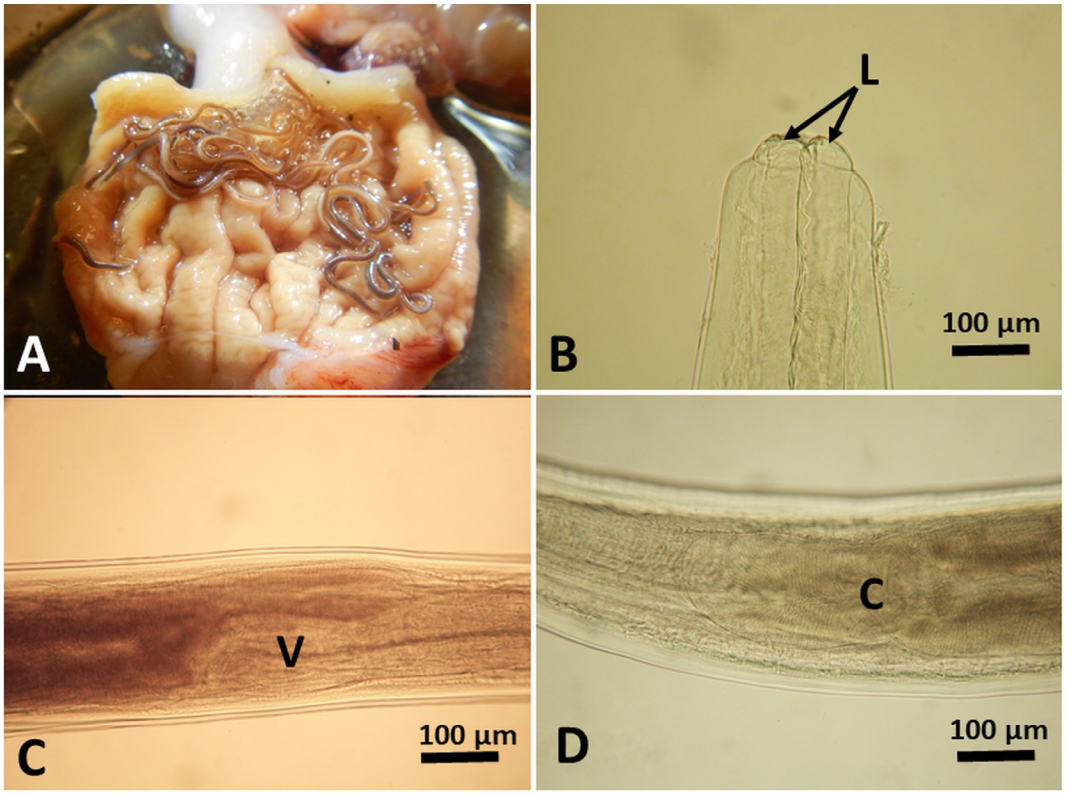

Figure 1. *Neoterranova caballaeroi* from *Agkistrodon piscivorus*. (A) Massive infection showing nematodes in dissected stomach. (B) Cephalic end showing two of three lips (L, arrows) of male specimen. (C) Elongate ventriculus (V). (D) Intestinal caecum (C).

information on this infection is presented below in annotated format.

Nematoda: Rhabditita: Anisakidae
***Neoterranova caballaeroi* Barus and Coy Otero, 1966 (Moravec and Justine, 2020)**
(Figs. 1A-D)

Type host and locality: Cuban racer, *Cubophis canthigerus* (Bibron); Paracoa, Cuba (Barus and Coy Otero 1966)

Host: Northern cottonmouth, *Agkistrodon piscivorus* (Lacépède), four adults, 402, 500, 560, and 645 mm snout-vent length (SVL), collected 20 June 2024, 29 August 2025 (n = 2), and 27 September 2025.

Locality: USA: Arkansas: Polk County, Ouachita Mountains Biological Station pond (34°27'43.4484"N, -93°59'54.3264"W).

Deposited material: HWML 119237.

Prevalence: Three of 3.

Site of infection: Stomach.

Intensity: 25.5 ± 26.5, range 3-70 worms; 3 in 402 mm SVL specimen; 8 in 560 mm SVL specimen; 21 in 500 mm SVL specimen; 70 in 645 mm SVL specimen.

Other reported hosts and localities: North American racer, *Coluber constrictor* L., Florida (Sprent 1979); eastern indigo snake, *Drymarchon couperi* (Holbrook) (Foster et al. 2000); Mississippi green watersnake, *Nerodia cyclopion* (Duméril, Bibron and Duméril), Louisiana (Sprent 1979; Fontenot and Font 1996); eastern hog-nosed snake, *Heterodon platyrhinos* Latreille, broad-banded watersnake, *Nerodia fasciata confluens* (Blanchard), diamond-backed watersnake, *Nerodia rhombifer* (Hallowell), Midland watersnake, *Nerodia sipedon pleuralis* (Cope), brown watersnake, *Nerodia taxispilota* (Holbrook), ***A. piscivorus*****,** Louisiana (Sprent 1979; Fontenot and Font 1996).

Collins (1969) reported a *Neoterranova* (=*Terranova*) sp. from plain-bellied watersnake, *Nerodia erythrogaster* (Forster) from North Carolina that was, in all likehood, N. *caballaeroi*. However, it was not identified to subgenus and specimens were said to be damaged (Camp 1980). In addition, Camp (1980) reported a *Terranova* sp. from *N. taxispilota* from Georgia that also most likely was *N. caballaeroi*.

Geographic range: USA: **Arkansas (this report);** Florida (Sprent 1979; Foster et al. 2000); Georgia? (Camp 1980); Louisiana (Sprent 1979; Fontenot and Font 1996); North Carolina? (Collins 1969); Cuba (Sprent 1979).

Remarks

Barus and Coy Otero (1966) originally described this nematode as *Terranova caballaeroi* and Sprent (1979) followed this classification. However, more recently, Moravec and Justine (2020) assigned this nematode to the newly established genus *Neoterranova*. The most important characters that distinguish the species are the morphologies of the ventriculus and cecum (see Figs. 1C-D).

In conclusion, examination of a small sample of northern cottonmouths from Arkansas yielded new distributional information on a nematode parasite from the stomach. Additional collection of *A. piscivorus* from the state as well as other parts of its range for helminths in the western extreme of its range in Texas (see Dixon 2013), a region where cottonmouths have not yet been examined, may provide additional information on its helminth parasites.

Acknowledgments

The Arkansas Game and Fish Commission issued a Scientific Collecting Permit to CTM. We thank Larry R. Raymond (Ouachita Mountains Biological Station, Big Fork, Arkansas) for providing gratis housing and laboratory space, and J. Mike Kinsella, Missoula, Montana, for providing some literature, photomicrographs, and identifying the nematodes. We also thank NTCC students Xenia Esparza and Estefani Garcia for processing assistance. This study is in partial fulfillment of the requirements of Biol. 2289 at NTCC for MJM.

References

Barus V, Coy Otero A. 1966. Nota sobre la helminthofauna de los ofidios en Cuba. Descripcion de tres especies nuevas de nematódos. Poeyana, ser. A, no. 23. 16 p.

Camp CD. 1980. The helminth parasites of the

brown water snake, *Nerodia taxispilota*, from Kinchafoonee Creek, Georgia. Proc Helminthol Soc Wash 47:276–277.

Collins RF. 1969. The helminths of *Natrix* spp. and *Agkistrodon piscivorus piscivorus* (Reptilia: Ophidia) in eastern North Carolina. J Elisha Mitchell Sci Soc 85:141–144.

Davis E, Beane JC, Flowers JR. 2016. Helminth parasites of pit vipers from North Carolina. Southeast Nat 15:729–741.

Detterline JL, Jacob JJ, Wilhelm WE. 1984. A comparison of helminth endoparasites in the cottonmouth (*Agkistrodon piscivorus*) and three species of water snakes (*Nerodia*). Trans Amer Microsc Soc 103:137–143.

Dixon JR. 2013. Amphibians and reptiles of Texas with keys, taxonomic synopses, bibliography, and distribution maps. Third Edition. College Station (TX): Texas A&M University Press. 437 p.

Fontenot LW, Font, WF. 1996. Helminth parasites of four species of aquatic snakes from two habitats in southeastern Louisiana. J Helminthol Soc Wash 63:66–75.

Foster GW, Moler PE, Kinsella JM, Terrell SP, Forrester DJ. 2000. Parasites of eastern indigo snakes (*Drymarchon corais couperi*) from Florida, U.S.A. Comp Parasitol 67:124–128.

McAllister CT, Bursey CR, Robison HW. 2023. Helminth parasites of northern cottonmouth, *Agkistrodon piscivorus* (Ophidia: Viperidae), from Arkansas. J Ark Acad Sci 77:49–55.

Moravec F, Justine J-L. 2020. Erection of *Euterranova* n. gen. and *Neoterranova* n. gen. n. sp. and new records of two other anisakid nematodes from sharks off New Caledonia. Parasite 27:58. https://doi.org/10/1051/parasites/2020053

Scholz T, de Chambrier A, McAllister CT, Tkach VV, Kuchta R. 2023. Tapeworms (Cestoda, *Ophiotaenia*) from the northern cottonmouth, *Agkistrodon piscivorus*. J Parasitol 109:464–479.

Sprent JFA. 1979. Ascaridoid nematodes of amphibians and reptiles: Terranova. J Helminthol 53:265–282.

Correction: *Kinosternon subrubrum hippocrepis* not *Kinosternon flavescens* from Latimer County, Oklahoma

Chris T. McAllister*
Department of Natural Sciences, Northeast Texas Community College, 2886 FM 1735, Chapel Hill Road, Mt. Pleasant, TX 75455

Abstract: Examination of an originally identified adult yellow mud turtle, *Kinosternon flavescens*, deposited in the Arkansas State University Museum of Zoology as a new county record from Latimer County, Oklahoma, has been found to actually represent a Mississippi mud turtle, *Kinosternon subrubrum hippocrepis*. Here, I document that correction.

The yellow mud turtle, *Kinosternon flavescens* (Agassiz) in a medium-sized aquatic turtle that ranges from Nebraska to southeastern Arizona to the Gulf of México (Powell et al. 2016). In Oklahoma, *K. flavescens* is primarily found in the western part of the state with isolated records from Mayes, Okmulgee, and Rogers counties (Sievert and Sievert 2021). Here, I correct an initial identification of a supposed *K. flavescens* from the state.

An adult specimen of an originally identified *K. flavescens* collected on 19 August 1988 from the vicinity of Gowen off US 270 (34.889171°N, 95.473471°W) in Latimer County by K. Shoemaker and deposited in the Arkansas State University Museum of Zoology (no. ASUMZ 33333) was thought to be a new county record (McAllister 2015). However, it was found to actually represent a Mississippi mud turtle, *Kinosternon subrubrum hippocrepis* Gray based on the fact that it didn't possess the identification character of a ninth marginal scute raised above the margin of the eighth marginal scute as what is present in *K. flavescens* (H, Eichelberger *pers. comm*.). The identification is, therefore, corrected to *K. s. hippocrepis* for this individual.

*Corresponding author: cmcallister@ntcc.edu
Proc. Okla. Acad. Sci. 105: p 62 (2025)

Acknowledgments

I thank Hannah Eichelberger (Collections Manager, Sam Noble Oklahoma Museum) and Drs. Stanley E. Trauth (retired, Arkansas State University-Emeritus) and Stephen J. Mullin (Biological Sciences, Arkansas State University) for bringing this misidentification to my attention.

References

McAllister CT. 2015. Geographic distribution: *Kinosternon flavescens*. Herp Rev 46:214–215.

Powell R, Conant R, Collins JT. 2016. Peterson field guide to reptiles and amphibians. Houghton Mifflin Harcourt: Boston. 492 p.

Sievert G, Sievert L. 2021. A field guide to Oklahoma's amphibians and reptiles. Fourth Ed. Oklahoma City: Oklahoma Department of Wildlife Conservation. 211 p.

Ectoparasites of the Woodchuck, *Marmota monax* (Rodentia: Sciuridae), from Arkansas, with a Summary of Ectoparasite Records from *M. monax*

Chris T. McAllister*
Department of Natural Sciences, Northeast Texas Community College, 2886 FM 1735, Chapel Hill Road, Mt. Pleasant, TX 75455

Lance A. Durden
Department of Biology, Georgia Southern University, Statesboro, GA 30458

Jeffrey G. Pittman
Ouachita Mountains Biological Station, Big Fork, AR 71953

Henry W. Robison
602 Big Creek Drive, Sherwood, AR 72120

Abstract: Examination of the pelage of a dead-on-the-road woodchuck, *Marmota monax*, opportunistically collected from western Arkansas for ectoparasites, yielded two fleas and two ticks. The two ticks were both nymphs of *Amblyomma americanum*. One of the fleas was a female *Ctenocephalides felis* and other was a male *Pulex simulans*. Although all three ectoparasites have been reported from Arkansas hosts, we document *C. felis* from *M. monax* for the first time anywhere. We also provide a summary of previously reported ectoparasites from this host.

Introduction

The woodchuck, *Marmota monax* (L.), also commonly known as the groundhog or marmot, is a large, heavy-bodied member of the order Rodentia, family Sciuridae. In addition to harboring numerous helminth parasites (Twitchell 1939; Fleming et al. 1979), it has been reported as a host of several ectoparasites (Whitaker and Schmelz 1973), including lice (Olsen 1938), mites (Whitaker and Wilson 1974), ticks (Cooley and Kohls 1938; Twichell 1939; Ko 1972a, 1972b), and fleas (Baker 1904; Ewing and Fox 1943). Various studies on fleas, lice, ticks and other mites, or a combination of ectoparasitic arthropods, from mammals, in different localities in North America, have also included records of ectoparasites from *M. monax.*

More recently, McAllister et al. (2016, 2017) provided a summary of the hosts of ticks and fleas of Arkansas, respectively, but *M. monax* was not listed as a host. Here we provide new host records one species of tick and two species of fleas from *M. monax* from western Arkansas. One of the flea records is the first of this species reported from *M. monax* anywhere. In addition, a summary of the ectoparasites of woodchucks

*Corresponding author: cmcallister@ntcc.edu

is provided.

Methods

On 30 August 2025, a single *M. monax* was found freshly dead on the road, apparently hit by an automobile, and salvaged off St. Hwy. 8 at Big Fork, Polk County, Arkansas (34°29'31.0"N, 93°58'21.0"W). The pelage was brushed vigorously over a white enamel tray and ectoparasites were collected and placed in individual vials of 95% (v/v) DNA grade ethanol. Samples were shipped to Durden for processing and identification. Fleas were cleared in 10% potassium hydroxide, dehydrated through an ethanol series, further cleared in xylene, and slide-mounted in Canada balsam (Price et al. 2003); ticks were examined in situ.

The host was deposited as a photovoucher (Fig. 1) in the Northeast Texas Community College Vertebrate Collection, Mt. Pleasant, Texas. Ectoparasites were deposited in the General Ectoparasite Collection in the Department of Biology at Georgia Southern University, Statesboro, Georgia, under accession lot number L3981.

Figure 1. Photovoucher (DOR) host *Marmota monax* from Polk County, Arkansas.

Results and Discussion

Two individual ticks and two individual fleas were collected from *M. monax*. Data are presented below in an annotated format as follows:

Arthropoda: Arachnida: Acari: Ixodida: Ixodidae
***Ambylomma americanum* (L.)**

Host: Woodchuck, *Marmota monax* (L., 1758) adult, salvaged 30 September 2025 off the road.

Locality: USA: Polk County, off St. Hwy. 8, Big Fork (34°29'31.0"N, 93°58'21.0"W).

Deposited material: L-3981.

Prevalence: 1 of 1.

Site of infection: Pelage

Intensity: 2 nymphs.

Other reported hosts in Arkansas of A. americanum: domestic cattle, *Bos taurus*, domestic dog, *Canis lupus familiaris*, domestic horse, *Equus caballus*, domestic cat, *Felis catus*, human, *Homo sapiens*, river otter, *Lontra canadensis*, *M. monax*, eastern woodrat, *Neotoma floridana*, whitetail deer, *Odocoileus virginiana*, domestic sheep, *Ovis aries*, fox squirrel, *Sciurus niger*, and cottontail rabbit, *Sylvilagus floridanus* (Tugwell and Lancaster 1952; McAllister et al. 2016).

Geographic range of A. americanum: USA: Arkansas (Tugwell and Lancaster 1952; this report). Eastern and Central USA (Springer et al. 2014).

Remarks

The Lone Star tick is one of the most abundant tick species in the eastern United States (Cooley and Kohls 1944) and on Arkansas hosts. Tugwell and Lancaster (1962) previously reported this tick from *M. monax* in Arkansas. There are additional records of *A. americanum* (mostly nymphs) from this host in five other eastern states (Table 1) but it does not appear to be common on *M. monax.*

Insecta: Siphonaptera: Pulicidae
***Ctenocephalides felis* (Bouché, 1835)**

Host: Woodchuck, *Marmota monax* (L., 1758) adult, salvaged 30 September 2025 off the road.

Locality: USA: Polk County, off St. Hwy. 8, Big Fork (34°29'31.0"N, 93°58'21.0"W).

Deposited material: L-3981.

Prevalence: 1 of 1.

Site of infection: Pelage

Intensity: 1 ♀.

Other reported hosts in Arkansas of C. felis: C. l. familiaris, Virginia opossum, *Didelphis virginiana*, *F. catus*, striped skunk, *Mephitis mephitis*, Norway rat, *Rattus norvegicus*, spotted skunk, *Spilogale putorius*, and gray fox, *Urocyon cinereoargenteus* (McAllister et al. 2016).

Geographic range of C. felis: Nearly cosmopolitan. USA: **Arkansas (this report).**

Remarks

The common "cat flea" is a nuisance biter of domestic cats and wild felids and is also common on domestic dogs (Durden and Hinkle 2019), wild canids, and other mammals, including, rodents and the Virginia opossum (Hastriter 2023). However, this is the first time it has been reported from *M. monax*.

***Pulex simulans* Baker, 1895**

Host: Woodchuck, *Marmota monax* (L., 1758) adult, salvaged 30 September 2025 off the road.

Locality: USA: Polk County, off St. Hwy. 8, Big Fork (34°29'31.0"N, -93°58'21.0"W).

Deposited material: L-3981.

Prevalence: 1 of 1.

Site of infection: Pelage.

Intensity: 1 ♂.

Other reported hosts in Arkansas of P. simulans: northern raccoon, *Procyon lotor* (Richardson et al. 1994; McAllister et al. 2016).

Geographic range of P. simulans: From Canada to the southern regions of South America (Hopla 1980; Hastriter 2023). USA: **Arkansas (this report).**

Remarks

This flea is distributed widely in the Western Hemisphere and has been confused with the cosmopolitan species, *Pulex irritans* (L.). It is an ectoparasite of carnivores and some other medium-sized and large mammals. Hopla (1980) recorded *P. simulans* from yellow-bellied marmot, *Marmota flaviventris* in a Table of host records from Colorado, Montana, and Wyoming. The only previous records of this flea from *M. monax* are from Alabama and Missouri (Palmer and Wingo 1972; Sanford and Hays 1974).

Based on morphology, only male specimens of *Pulex simulans* and *Pulex irritans* can be reliably separated (Lewis and Eckerlin 2024). In cleared, slide-mounted males, the genitalia of *P. simulans* can be seen to have a broad dorsal aedeagal sclerite (d.a.s.) and a ventral crochet that is narrow throughout, whereas *P. irritans* has a narrow d.a.s. and a crochet that is very broad apically. Baker (1895) described *P. simulans* as a new species but Jordan and Rothschild (1908) synonymyzed it with *P. irritans,* before Smit (1958) reinstated *P. simulans* as a distinct species and illustrated the morphological differences between the male genitalia of these two species. Both species are widespread in North America and have been recorded from a variety of large and medium-sized mammals plus a few species of birds (Hopla 1980).

A summary of the ectoparasites reported from *M. monax* from various Canadian provinces and US states is listed in Table 1. Eight species of ticks have been previously reported from *M. monax* (Table 1); three have been reported from various Arkansas hosts, but only one of them, *A. americanum,* from *M. monax* (Tugwell and Lancaster 1962; McAllister et al. 2016). The most abundant and widespread species of tick parasitizing *M. monax*, especially in northeastern states, and in Canada, is *Ixodes cookei* (Table 1). This tick is sometimes referred to as the groundhog tick but adults also parasitize various carnivores (Keirans and Clifford 1978; Durden and Keirans 1996). Notably, *I. cookei* is the principal vector of Powassan virus and groundhogs are a principal reservoir host (Durden and Keirans 1996). Although *I cookei* rarely attaches to humans (Hall et al. 1991), this zoonotic diseases can cause Powasaan encephalitis in humans which can be fatal (Piantadosi and Solomon 2022).

Other ixodid ticks, including *Dermacentor variabilis* (American dog tick), *A. americanum* and *Ixodes scapularis* (blacklegged tick) have also been recorded from *M. monax* in eastern states (Table 1). All three of these generalist tick species that can transmit medically important pathogens to humans (Cooney and Burgdorfer 1974; Durden and Keirans 1996; Cohen et al.

2010; Kennedy et al. 2025). In addition to these ticks, the non-native invasive Asian longhorned tick, *Haemaphysalis longicornis* has been reported from *M. monax* in some northeastern states and there are one or two records of the rabbit tick *Haemaphysalis leporispalustris* and of *Ixodes texanus* and *Ixodes robbinsi* (previously treated as *Ixodes auritulus*) from *M. monax* (Table 1). Adults of *I. texanus* mainly parasitize carnivores and all active stages of *I. robbinsi* parasitize birds (Keirans and Clifford 1978; Durden and Keirans 1996; Apanaskevich et al. 2022) so these are unusual ectoparasite records from *M. monax*.

With the addition of one species reported in this paper, 10 species of fleas have now been recorded from *M. monax* (Table 1). *Oropsylla arctomys* Baker is the most commonly reported flea on this host especially in northern states and Canada (Hamilton 1935; Fox 1968; Fleming et al. 1979; Holland 1985; Poole and Gentilli 1986; Hastriter 2023; Lewis and Eckerlin 2024). Not surprisingly, *O. arctomys* has not been found on any Arkansas hosts as it is from *M. monax* from British Columbia, Canada, Alaska, Montana, and northeastern and midwestern states (Lewis and Eckerlin 2024) (Table 1). The other nine species of fleas recorded from *M. monax* are typically associated with other mammal species and are accidental parasites on groundhogs. One of these species, *Cediopsylla simplex* (rabbit flea) has been reported from swamp rabbit, *Sylvilagus aquaticus*, *S. floridanus*, black-tailed jackrabbit, *Lepus californicus*, and *U. cineroargenteus* in Arkansas (McAllister et al. 2016). Both species of fleas we recorded on *M. monax* in Arkansas represent unusual host associations and one of them, *C. felis,* has not been reported previously from this host anywhere. However, Lewis and Eckerlin (2024) state that *C. felis* has been recorded from more host species than any other flea. The other species, *P. simulans* has been reported previously from several medium-sized to large mammals in the Americas (Hopla 1980; Lewis and Eckerlin 2024) but only twice previously from *M. monax* (Palmer and Wingo 1972; Sanford and Hays 1974).

One species of sucking louse, *Enderleinellus marmotae* Ferris is a host-specific ectoparasite of *M. monax* (Table 1) (Kim et al. 1986; Durden and Musser 1994). This louse may parasitize *M. monax* throughout its range but it has not been recorded from several states where the host occurs, probably because it is a small ectoparasite (< 1 mm long as an adult) that may be missed during host examinations.

None of the species of three species of mesostigmatan mites or three species of chiggers recorded from *M. monax* (Table 1) are host-specific but several collections of the chigger *Euschoengastia marmotae* Ewing are from this host (Farrell 1956; Whitaker and Schmeltz 1973).

Overall, a variety of ectoparasites has been reported from *M. monax* across its geographical range including one species of sucking louse, 10 fleas, eight ticks, three mesostigmatan mites and three chigger mites (Table 1). Some of these fleas and ticks, especially the cat flea, *C. felis,* and the groundhog tick, *I. cookei*, are known vectors of zoonotic pathogens. In this paper, we have added one species of flea to the list of ectoparasites reported from *M. monax* anywhere, and also documented, for the first time, another species of flea and one species of tick from this host in Arkansas.

Acknowledgments

The Arkansas Game and Fish Commission issued a Scientific Collecting Permit to CTM. We thank Larry R. Raymond (OMBS) for providing gratis housing and laboratory space for CTM, and James T. McAllister, III, Engineering and Honors College Librarian, University of Arkansas, for providing some literature.

Table 1. Ectoparasites reported from *Marmota monax*.

Ectoparasites	Localities	References
SIPHONAPTERA (FLEAS)		
Cediopsylla simplex	Canada, Delaware	MacCreary (1945); Holland (1985); Kennedy et al. (2024)
Ctenocephalides canis	Massachusetts	Fox (1968)
*Ctenocephalides felis**	**Arkansas**	**This report**
Orchopeas howardi	Indiana, Missouri, New York, Rhode Island	Geary (1959); Wilson (1961)†; Mathewson and Hyland (1964); Palmer and Wingo (1973)
Orchopeas leucopus	Iowa, New York	Joyce and Eddy (1944); Geary (1959)
Opisocrostis bruneri	Wisconsin	Amin (1976)
Opisodasys pseudarctomys	Canada, New York	Geary (1959); Holland (1985)
Oropsylla arctomys	Canada, Alaska, Connecticut, Delaware, Illinois, Indiana, Maine, Massachusetts, Michigan, Minnesota, Montana, New Hampshire, New York, North Dakota, Ohio, Pennsylvania, Rhode Island, West Virginia, Wisconsin, Vermont	Hamilton (1934); Hubbard (1935); Jellison (1945); MacCreary (1945); Wilson (1957, 1961†); Geary (1959); Benton and Smiley (1963); Mathewson and Hyland (1964); Humphreys (1967); Holland and Benton (1968); Benton et al. (1969); Main (1970, 1983); Haas and Wilson (1973); Whitaker and Schmeltz (1973); Benton and Kelly (1975); Amin (1976); Fleming et al. (1979); Benton (1980); Scharf and Stewart (1980); Holland (1985); Cohn et al. (1986); Poole and Gentlli (1986); Haas et al. (1989); Farkas and Surgeoner (1990); Scharf et al. (1990); Larson (1997); Eckerlin et al. (2008); Eckerlin (2016); Eckerlin and Gardner (2021); Hastriter (2023); Kennedy et al. (2024); Lewis and Eckerlin (2024)
Pulex simulans	Alabama, **Arkansas,** Missouri	Palmer and Wingo (1972); Sanford and Hays (1974); **This report**
Thrassis spenceri	Canada	Holland (1985)
ANOPLURA (SUCKING LICE)‡		
Enderleinellus marmotae	Indiana, Maine, Maryland, Minnesota, Missouri, New Jersey, New York, North Dakota, Ohio, Rhode Island, South Carolina, Washington (DC)	Wilson (1961)†; Mathewson and Hyland (1962); Whitaker and Schmeltz (1973); Fleming et al. (1979); Kim et al. (1986); Reeves et al. (2004); Nelder and Reeves (2015)
ACARI (MITES OTHER THAN CHIGGERS)		

Androlaelaps fahrenholzi	Canada, Indiana, Minnesota, New York, North Carolina	Whitaker and Schmeltz (1973); Fleming et al. (1979); Cohn et al. (1986); Farkas and Surgeoner (1990); Timm (1975); Reeves et al. (2007)
Macrocheles mesocthonius	Indiana	Krantz and Whitaker (1988); Whitaker (1991)
Eulaelaps stabularis	Canada, Indiana	Banks (1909); Wilson (1961)†; Whitaker and Schmeltz (1973); Whitaker (1982)
TROMBICULIDAE (CHIGGER MITES)		
Euschoengastia marmotae	Indiana, New Jersey, Pennsylvania	Farrell (1956); Manischewitz (1966); Whitaker and Schmeltz (1973)
Euschoengastia peromysci	Indiana	Whitaker and Loomis (1979)
Eutrombicula cinnabaris	Indiana	Whitaker and Schmeltz (1973)
IXODIDA (TICKS)		
Ambylomma americanum	**Arkansas,** Delaware, Kentucky, Oklahoma, Tennessee, Virginia	Bishopp and Trembley (1945); Tugwell and Lancaster (1962); Kokernot et al. (1969); Clymer et al. (1970); Sonenshine et al. (1971); Cooney and Burgdorfer (1974); Zimmerman et al. (1988); White et al. (2020); Kennedy et al. (2025); **This report**
Dermacentor variabilis	Canada, Alabama, **Arkansas,** Connecticut, Delaware, Indiana, Kansas, Kentucky, Massachusetts, New York, North Carolina, Oklahoma, Pennsylvania, Tennessee, Virginia, Wisconsin	Bequaert (1945); Bishopp and Trembley (1945); Wilson (1961)†; Tugwell and Lancaster (1962); Sonenshine et al. (1965); Snetsinger (1968); Clymer et al. (1970); Sonenshine et al. (1971); Cooney and Hays (1972); Conney and Burgdorfer (1974); Fleming et al. (1979); Whitaker and Schmeltz (1973); Sonenshine (1979); Carey et al. (1980); Zimmerman et al. (1988); Fish and Dowler (1989); Brillhart et al. (1994); Reeves et al. (2007); Cohen et al. (2010); Dergousoff et al. (2013); Lee et al. (2019); White et al. (2020); Kennedy et al. (2025)
Haemaphysalis leporispalustris	**Arkansas**	Tugwell and Lancaster (1962)
Haemaphysalis longicornis	Delaware, New Jersey, Virginia	White et al. (2020); Kennedy et al. (2025)
Ixodes cookei	Canada, Alabama, **Arkansas,** Connecticut, Delaware, Illinois, Indiana, Kansas, Kentucky, Maine Maryland, Massachusetts Michigan, Minnesota, Missouri,	Hamilton (1934); Twitchell (1939); Bequaert (1945); Bishopp & Trembley (1945); Wilson (1961)†; Tugwell and Lancaster (1962); Sonenshine et al. (1965); Sonenshine and Stout (1971); Cooney and Kays (1972); Ko (1972a, b); Whitaker and

	New Hampshire, New Jersey, New York, North Carolina, Ohio, Pennsylvania, Rhode Island, Vermont, Virginia, West Virginia, Wisconsin	Schmeltz (1973); Keirans and Clifford (1978); Sonenshine (1979); Fleming et al. (1979); Anderson and Magnarelli (1980); Cohn et al. (1986); Fish and Dowler (1989); Farkas and Surgeoner (1990); Durden and Keirans (1996); Walker et al. (1998); Reeves et al. (2007); Lee et al. (2019); White et al. (2020); Kennedy et al. (2025)
Ixodes robbinsi (listed as *Ixodes auritulus*)	North America (State/Province not listed)§	Bishopp and Trembley (1945)
Ixodes scapularis	Connecticut, New Jersey, New York, Virginia, Wisconsin	Fleming et al. (1979); Main et al. (1982); Fish and Dowler (1989); Lee et al. (2019); White et al. (2020)
Ixodes texanus	Missouri, Wisconsin	Twichell (1939); Lee et al. (2019)

*New host record.

†Unpublished Ph.D. dissertation.

‡Kim et al. (1986) also listed the sucking lice *Linognathoides marmotae* and *Linognathoides laeviusculus* from *M. monax* but did not provide details. Unfortunately, we cannot locate records of these sucking lice from *M. monax*. *Linognathoides marmotae* mainly parasitizes yellow-bellied marmot, *Marmota flaviventris* in western North America whereas *L. laeviusculus* mainly parasitizes ground squirrels (Sciuridae) in the Holarctic region (Durden and Musser, 1994).

§North American ticks previously assigned to *Ixodes auritulus* are currently treated as *Ixodes robbinsi* Apanaskevich and Edgy (Apanaskevich et al. 2022).

References

Amin OM. 1976. Host associations and seasonal occurrence of fleas from southeastern Wisconsin mammals, with observations on morphologic variations, J Med Entomol 13: 179–192.

Anderson JF, Magnarelli LA. 1980. Vertebrate host relationships and distribution of *Ixodes* ticks (Acari: Ixodidae) in Connecticut, USA. J Med Entomol 17:314–323.

Apanaskevich DA, Apanaskevich MA, Klimov PB, Edgy BM, Bermúdez SE, Labruna MB, Korseev AI, Barker SC. 2022. Description of eight new species of *Ixodes* Latreille, 1795 (Acari: Ixodidae) and redescription of *I. auritulus* Neumann, 1904, parasites of birds in the Australasian, Nearctic and Neotropical regions. Zootaxa 5173(1):1–73.

Baker CF. 1895. Preliminary studies in Siphonaptera. I. Canadian Entomol 27:63–67.

Baker CF. 1904. A revision of American Siphonaptera, or fleas, together with a complete list and bibliography of the group. Proc U.S. Natl Mus 27:365–469.

Banks N. 1909. New Canadian mites (Arachnoidea, Acarina). Proc Entomol Soc Wash 11: 133–143.

Benton AH. 1980. An atlas of the fleas of the eastern United States. Fredonia (NY): Marginal Media. 177 p.

Benton AH, Kelly DL. 1975. An annotated list of New York Siphonaptera. J New York Entomol Soc 83:142–156.

Benton AH, Smiley D. 1963. The fleas of Ulster County, N.Y. John Burroughs Nat Hist Soc Bull 6:1–7.

Benton AH, Tucker HH Jr. Kelly DL. 1969. Siphonaptera from northern New York. J New York Entomol Soc 77:193–198.

Bequaert JC. 1945. The ticks, or Ixodoidea, of the northeastern United States and eastern Canada. Entomol Amer (ns) 25:73–232.

Bishopp FC, Trembley HL. 1945. Distribution and hosts of certain North American ticks. J Parasitol 31:1–54.

Brillhart DB, Fox LB, Upton SJ. 1994. Ticks (Acari: Ixodidae) collected from small and medium-sized Kansas mammals. J Med Entomol 31:500–504.

Carey AB, Krinsky WL, Main AJ. 1980. *Ixodes dammini* (Acari: Ixodidae) and associated ixodid ticks in south-central Connecticut, USA. J Med Entomol 17:89–99.

Clymer BC, Howell DE, Hair JA. 1970. Animal hosts of economically important ticks (Acarina) in east-central Oklahoma. Ann Entomol Soc Amer 63:612–614.

Cohen SB, Freye JD, Dunlap BG, Dunn JR, Jones TF, Moncayo AC. 2010. Host associations of *Dermacentor, Amblyomma,* and *Ixodes* (Acari: Ixodidae) ticks in Tennessee. J Med Entomol 47:415–420.

Cohn DL, Erb HN, Georgi JR, Tennant, BC. 1986. Parasites of the laboratory woodchuck (*Marmota monax*). Lab Anim Sci 36:298–302.

Cooney JC, Burgdorfer W. 1974. Zoonotic potential (Rocky Mountain spotted fever and tularemia) in the Tennessee Valley region. I. Ecologic studies of ticks infesting mammals in Land Between the Lakes. Am J Trop Med Hyg 23:99–108.

Cooney JC, Hays KL. The ticks of Alabama (Ixodidae: Acarina). Auburn Univ Agric Exp Stn Bull 426. 40 p.

Cooley RA, Kohls GM. 1944b. The genus *Amblyomma* (Ixodidae) in the United States. J Parasitol 30:77–111.

Dergousoff SJ, Galloway TD, Lindsay R, Curry PS, Chilton NB. 2013. Range expansion of *Dermacentor variabilis* and *Dermacentor andersoni* (Acari: Ixodidae) near their northern distributional limits. J Med Entomol 50:510–520.

Durden LA, Hinkle NC. 2019. Fleas (Siphonaptera). In: Mullen GR, Durden LA, editors. Medical and Veterinary Entomology. Third edition. London: London Academic Press. p 145–169.

Durden LA, Keirans JE. 1996. Nymphs of the genus *Ixodes* (Acari: Ixodidae) of the United States: taxonomy, identification key, distribution, hosts, and medical/veterinary importance. Monogr Thomas Say Publ Entomol Lanham, MD, Entomol Soc Amer. 95 p.

Durden LA, Musser GG. 1994. The sucking lice (Insecta: Anoplura) of the world: a taxonomic checklist with records of mammalian hosts and geographical distributions. Bull Amer Mus Nat Hist 218:1–90.

Eckerlin RP. 2016. The fleas (Siphonaptera) of West Virginia. Ann Carnegie Mus 83:295–310.

Eckerlin RP, Gardner AL. 2021. Records of fleas (Siphonaptera) and other ectoparasites from Maine. Northeastern Nat 28:77–93.

Eckerlin RP, Paul K, Carpenter S. 2008. New records of fleas (Siphonaptera) from Pennsylvania. J Penn Acad Sci 82:74–78.

Ewing HE, Fox I. 1943. The fleas of North America. Washington (DC): USDA Misc Publ No 500. 143 p.

Farkas MJ, Surgeoner GA. 1990. Incidence of *Ixodes cookei* (Acari: Ixodidae) on groundhogs, *Marmota monax,* in southwestern Ontario. Proc Entomol Soc Ontario 121:105–110.

Farrell CE. 1956. Chiggers of the genus *Euschoengastia* (Acarina: Trombiculidae) in North America. Proc US Natl Mus 106:85–251.

Fish D, Dowler RC. 1989. Host associations of ticks (Acari: Ixodidae) parasitizing medium-sized mammals in a Lyme disease endemic area of southern New York. J Med Entomol 26: 200–209.

Fleming WJ, George JR, Caslick JW. 1979. Parasites of the woodchuck (*Marmota monax*) in central New York state. Proc Helminthol Soc Wash 46:115–127.

Fox I. 1968. Fleas of eastern United States. New York (NY): Hafner Publishing Company. 191 p. (facsimile of 1940 edition).

Geary JM. 1959. The fleas of New York. Cornell

Univ Agric Exp Stn Mem 355. 104 p.

Haas GE, Wilson N. 1973. Siphonaptera of Wisconsin. Proc Entomol Soc Wash 75:302–314.

Haas GE, Wilson N, Osborne TO, Zarnke RL, Johnson L, Wolff JO. 1989. Mammal fleas (Siphonaptera) of Alaska and Yukon Territory. Canadian J Zool 67:394–405.

Hall JE, Amrine JW Jr, Gais RD, Kolanko VP, Hagenbuch BE, Gerencser VF, Clark SM. 1991. Parasitization of humans in West Virginia by *Ixodes cookei* (Acari: Ixodidae) a potential vector of Lyme borreliosis. J Med Entomol 28:186–189.

Hamilton WJ, Jr. 1934. The life history of the rufescent woodchuck, *Marmota monax rufescens* Howell. Ann Carnegie Mus 23:85–178.

Hastriter MW. 2023. An assemblage of fleas (Siphonaptera) from Canada, Mexico, and the United States of America, in the Hastriter Collection (Brigham Young University). Ann Carnegie Mus 88:13–90.

Holland GP. 1985. The fleas of Canada, Alaska and Greenland (Siphonaptera). Mem Entomol Soc Canada 117(S130):3–632.

Holland GP, Benton AH. 1968. Siphonaptera from Pennsylvania mammals. Am Midl Nat 80: 252–261.

Hopla CE. 1980. A study of the host associations and zoogeography of *Pulex*. In Traub R, Starcke H, editors. Fleas: Proc Intn Conf Fleas. Rotterdam: (Netherlands). p 185–207.

Humphreys JG. 1967. Records of Ohio fleas (Siphonaptera). Ohio J Sci 67:186–190.

Jellison WL. 1945. Siphonaptera: the genus *Oropsylla* in North America. J Parasitol 31:83–97.

Jordan K, Rothschild NC. 1908. Revision of the non-combed eyed Siphonaptera. Parasitology 1:1–100.

Joyce CR, Eddy GW. 1944. A list of fleas (Siphonaptera) collected at Tama, Iowa. Iowa State Coll J Sci 18:209–215.

Keirans JE, Clifford CM. 1978. The genus *Ixodes* in the United States: a scanning electron microscope study and key to the adults. J Med Entomol Suppl 2:1–149.

Kennedy AC, Redus S, Winter WS, Newcomer JR, Egizi AM, Fonseca DM, Occi JL, Robbins RG. 2025. Ticks of Delaware revisited: an updated checklist of hard ticks (Ixodidae) and first records of soft ticks (Argasidae) in the First State. J Med Entomol 62:851–865.

Kennedy AC, Winter WS, Gardner AL, Woodman N, Shifflett SA, Redus S, Newcomer JR, Eckerlin RP. 2024. Records of fleas (Siphonaptera) from Delaware. J Med Entomol 61:959–964.

Kim KC, Pratt HD, Stojanovich CJ. The sucking lice of North America: An illustrated manual for identification. University Park (PA): The Pennsylvania State University Press. 241 p.

Ko RC. 1972a. Biology of *Ixodes cookei* Packard (Ixodidae) of groundhogs (*Marmota monax* Erxleben). Canadian J Zool 50:433–436.

Ko RC. 1972b. The transmission of *Ackertia marmotae* Webster, 1967 (Nematoda: Onchocercidae) of groundhogs (*Marmota monax*) by *Ixodes cookei*. Canadian J Zool 50:437–450.

Kokernot RH, Callisher CH, Stannard LJ, Hayes J. 1969. Arbovirus studies in the Ohio-Mississippi Basin, 1964-1967. VII. Lone Star virus, a hitherto unknown agent isolated from the tick *Amblyomma americanum* (Linn.). Amer J Trop Med Hyg 18:789–795.

Krantz GW, Whitaker JO Jr. 1988. Mites of the genus *Macrocheles* (Acari: Macrochelidae) associated with small mammals in North America. Acarologia 29:225–259.

Kwiecinski GG. 1998. *Marmota monax*. Mamm Spec 591:1–8.

Larson OR. 1997. North Dakota fleas. X. An atlas of the state's siphonapterans. Univ North Dakota Inst Ecol Studies Res Rept 47. 77 p.

Lee X, Murphy DS, Johnson DH, Paskewitz SM. 2019. Passive animal surveillance to identify ticks in Wisconsin, 2011-2017. Insects 10(9):289. doi:10.3390/insects10090289.

Lewis RL, Eckerlin RP. 2024. The Siphonaptera

of North America north of Mexico, including Greenland. Ann Carnegie Mus 89:1–562.

Main AJ Jr. 1970. Distribution, seasonal abundance and host preferences of fleas in New England. Proc Entomol Soc Wash 72:73–89.

Main AJ. 1983. Fleas (Siphonaptera) on small mammals in Connecticut, USA. J Med Entomol 20:33–39.

Main AJ, Carey AB, Carey MG, Goodwin RH. 1982. Immature *Ixodes dammini* (Acari: Ixodidae) on small animals in Connecticut, USA. J Med Entomol 19:655–664.

Mathewson JA, Hyland KE. 1962. The ectoparasites of Rhode Island mammals. II. A collection of Anoplura from non-domesticated hosts. J New York Entomol Soc 70:167–174.

Mathewson JA, Hyland KE. 1964. The ectoparasites of Rhode Island mammals. III. A collection of fleas from non-domestic hosts. J Kansas Entomol Soc 37:157–163.

McAllister CT, Durden LA, Robison HW. 2016. The ticks (Arachnida: Acari: Ixodida) of Arkansas. J. Ark. Acad. Sci. 70:141–154.

McAllister CT, Durden LA, Robison HW, Connior MB. 2017. The fleas (Arthropoda: Insecta: Siphonaptera) of Arkansas. J. Arkansas Acad. Sci. 71:69–76.

Nelder MP, Reeves WK. 2005. Ectoparasites of road-killed vertebrates in northwestern South Carolina, USA. Vet Parasitol 129:313–322.

Palmer DB Jr, Wingo CW. 1972. Siphonaptera occurring on Missouri mammals. Trans Missouri Acad Sci 6:43–55.

Piantodosi A, Solomon IH. 2022. Powassan virus encephalitis. Infect Dis Clin North Amer 36: 671–688.

Poole RW, Gentili P. (eds.). 1996. Nomina Insecta Nearctica: a checklist of the insects of North America. Volume 3 (Diptera, Lepidoptera, Siphonaptera). Rockville (MD): Entomological Information Services. 1,143 p.

Price RD, Hellenthal RA, Palma RL, Johnson KP, Clayton DH. 2003 The chewing lice: world checklist and biological overview. Ill Nat Hist Surv Spec Publ no. 24. 501 p.

Reeves WK, Durden LA, Ritzi CM, Beckham KR, Super PE, OConnor BM. 2007. Ectoparasites and other ectosymbiotic arthropods of vertebrates in the Great Smoky Mountains National Park, USA. Zootaxa 1392:31–68.

Reeves WK, Durden LA, Wrenn WJ. 2004. Ectoparasitic chiggers (Acari: Trombiculidae, Leeuwenhoekiidae), lice (Phthiraptera), and Hemiptera (Cimicidae and Reduviidae) from South Carolina, U.S.A. Zootaxa 647:1–20.

Robbins RG. 2025. Ticks of Delaware revisited: an updated checklist of hard ticks (Ixodidae) and first records of soft ticks (Argasidae) in the first state. J Med Entomol 62:851–865.

Sanford LG, Hays KL. 1974. Fleas (Siphonaptera) of Alabama and their host relationships. Auburn Univ Agric Exp Stn Bull 458. 42 p.

Scharf WC, Lederle PE, Allan TA. 1990. Siphonaptera records and host associations from the central and eastern Upper Peninsula of Michigan. Great Lakes Entomol 23:201–203.

Scharf WC, Stewart KR. 1980. New records of Siphonaptera from northern Michigan. Great Lakes Entomol 13:165–167.

Smit FGAM. 1958. A preliminary note on the occurrence of *Pulex irritans* L. and *Pulex simulans* Baker in North America. J Parasitol 44:523–526.

Snetsinger R. 1968. Distribution of ticks and tick-borne diseases in Pennsylvania. Pennsylvania State Univ Agric Exp Stn Progress Rept 288. 7 p.

Sonenshine DE. 1979. Ticks of Virginia (Acari: Metastigmata). The Insects of Virginia: No. 13. Research Div. Bull. 139. Blacksburg (VA): Virginia Polytechnic Institute and State University. 42 p.

Sonenshine DE, Lamb JT Jr, Anastos G. 1965. The distribution, hosts and seasonal activity of Virginia ticks.Virginia J Sci 16:26–91.

Sonenshine DE, Stout IJ. 1971. Ticks infesting

medium-sized wild mammals in two forest localities in Virginia (Acarina: Ixodidae). J Med Entomol 8:217–227.

Springer YP, Eisen L, Beati L, James AM, Eisen RJ. 2014. Spatial distribution of counties in the continental United States with records of occurrence of *Amblyomma americanum* (Ixodida: Ixodidae). J Med Entomol 51:342–351.

Timm RM. 1975. Distribution, natural history, and parasites of mammals of Cook County, Minnesota. Occ Pap Bell Mus Nat Hist, Univ Minnesota No. 14. 56 p.

Tugwell P, Lancaster JL Jr. 1962. Results of a tick-host study in northwest Arkansas. J Kansas Entomol Soc 35:202–211.

Twichell AR. 1939. Notes on the southern woodchuck in Missouri. J Mammal 20:71–74.

Walker ED, Stobierski MG, Poplar ML, Smith TW, Murphy AJ, Smith PC, Schmitt SM, Cooley TM, Kramer CM. 1998. Geographic distribution of ticks (Acari: Ixodidae) in Michigan, with emphasis on *Ixodes scapularis* and *Borrelia burgdorferi.* J Med Entomol 35:872–882.

Whitaker JO, Loomis RB. 1979. Chiggers (Acarina: Trombiculidae) from the mammals of Indiana. Proc Indiana Acad Sci 88:426–433.

Whitaker JO Jr. 1991. Additions to the list of ectoparasites of the mammals of Indiana. Proc Indiana Acad Sci 100:91–97.

Whitaker JO, Schmeltz LL. 1973. External parasites of the woodchuck, *Marmota monax*, in Indiana. Entomol News 84:69–72.

White SA, Bevins SN, Ruder MG, Shaw D, Vigil SL, Randall A, Deliberto TJ, Dominguez K, Thompson AT, Mertins JW, Alfred JT, Yabsley MJ. 2020. Surveys for ticks on wildlife hosts and in the environment at Asian longhorned tick (*Haemaphysalis longicornis*)-positive sites in Virginia and New Jersey. Transbound Emerg Dis 68:605–614.

Wilson N. 1957. Some ectoparasites from Indiana mammals. J Mammal 38:281–282.

Wilson NA. 1961. The ectoparasites (Ixodes, Anoplura, and Siphonaptera) of Indiana mammals. [Ph.D. dissertation]. West Lafayette (IN): Purdue University. 527 p.

Zimmerman RH, McWherter GR, Bloemer SR. 1988. Medium-sized mammal hosts of *Amblyomma americanum* and *Dermacentor variabilis* (Acari: Ixodidae) at Land Between the Lakes, Tennessee, and effects of integrated tick management on host infestations. J Med Entomol 25:461–466.

Helminth Parasites (Cestoda: Nematoda) of Baird's Pocket Gopher, *Geomys breviceps* (Rodentia: Geomyidae) from Northeastern Texas

Chris T. McAllister*
Department of Natural Sciences, Northeast Texas Community College, 2886 FM 1735, Chapel Hill Road, Mt. Pleasant, TX 75455

Isabel Tresidder
Department of Natural Sciences, Northeast Texas Community College, 2886 FM 1735, Chapel Hill Road, Mt. Pleasant, TX 75455

Abstract: Little is known about the helminth parasites of Baird's pocket gopher, *Geomys breviceps*, particularly from specimens collected and examined from northeastern Texas. Four adult pocket gophers collected from Lamar (n = 3) and Titus (n = 1) counties yielded a cyclophyllidean tapeworm, *Hymenolepis* sp. in two (50%), and spirurid nematodes, *Mastophorus muris* in one (25%). These tapeworms were the same morphologically but new information suggests significant difference in mitochondrial sequences representative of a new species. The nematode represents a new geographic record and confirms our belief that there may be more than one species of *M. muris* present in the USA.

Introduction

Baird's pocket gopher, *Geomys breviceps* Baird, 1855 is native to eastern Texas, western Louisiana, eastern Oklahoma, and southwestern Arkansas (Sulentich et al. 1991). There are two subspecies: *Geomys breviceps breviceps* Baird, 1855 (in far eastern Louisiana) and *G. b. sagittalis* Merriam, 1895 (in Arkansas, Louisiana, Oklahoma, and Texas). In Texas, *G. breviceps* occurs in the eastern sector of the state (Schmidly and Bradley 1994). This gopher, like others, is a burrower that digs tunnels in sandy to loamy soils and generally lives underground, except during the rainy seasons.

In terms of previously reported endoparasites, *G. breviceps* has been reported with a coccidian, *Eimeria geomydis* Skidmore, 1929, tapeworms, *Monoecocestus anoplocephaloides* (Douthitt, 1915) and *Hymenolepis* spp., and nematodes, *Litomosoides westi* Gardner and Schmidt, 1986, *Protospirura ascaroidea* Hall, 1916, and *Mastophorus muris* (Gmelin, 1790) (Douthitt 1915; English 1932; Upton et al. 1992; Pitts et al. 2000; Connior et al. 2017). The purpose of the current study was to examine *G. breviceps* from northeastern Texas for endoparasites and report any new host and geographic distribution records.

Methods

During December 2024 (n = 3) and January 2025 (n = 1), four adult *G. breviceps* (three from Lamar County and one from Titus County),

*Corresponding author: cmcallister@ntcc.edu
Proc. Okla. Acad. Sci. 105: pp 74-78 (2025)

was collected with Victor® gopher traps and examined for helminth parasites. Four tapeworms was removed from the small intestine and select terminal proglottids were placed in 80% (v/v) DNA grade ethanol for molecular analysis and the remaining strobilae was fixed in hot 4% (v/v) formalin. Specimens from formalin were dehydrated in an increasing series of ethanol, stained in Semichon's acetocarmine, cleared in methyl salicylate, and mounted in Canada balsam. A nematode from the stomach was fixed in hot distilled water and transferred to DNA grade ethanol. It was examined as a temporary mount on a microscopic slide in glycerol.

Voucher specimens of hosts (alcoholics) were deposited in the Northeast Texas Community College Vertebrate Collection, Mt. Pleasant, Texas. Voucher parasites were deposited in the Harold W. Manter Laboratory of Parasitology (HWML), University of Nebraska, Lincoln, Nebraska

Results and Discussion

Four tapeworms (two each) were found in the small intestine of two *G. breviceps*, and a single nematode was in the stomach of one individual. Detailed information on these infections are presented below in annotated format.

Cestoda: Cyclophyllidea: Hymenolepididae
***Hymenolepis* sp. Weinland, 1858**
(Figs. 1A-D, 2)

Hosts: Baird's pocket gopher, *Geomys breviceps* (Baird, 1855), adult (total length 203, tail length 51, hind foot 26, ear 3 mm), collected 3 December 2025; adult (total length 223, tail length 49, hind foot 27, ear 6 mm), collected 5 January 2025.

Localities: USA: Texas: Titus County, Northeast Texas Community College campus (34°27'43.4484"N, 93°59'54.3264"W); Lamar County, northeast of Blossom off US 82 (33°39'55"N, 95°19'12"W).

Deposited material: HWML 218133 (photovoucher).

Prevalence: Two of 4 (50%).

Site of infection: Small intestine.

Intensity: Four worms, two in each host.

Other reported pocket gophers in the Nearctic and northern Neotropical regions with Hymenolepis s.str.: Volcán De Toluca pocket gopher, *Cratogeomys planiceps* Merriam, plains pocket gopher, *Geomys bursarius* (Shaw), Attwater's pocket gopher, *Geomys attwateri* Merriam, Sand Hills pocket gopher, *Geomys lutescens* Merriam, Central Texas pocket gopher, *Geomys texensis* Merriam, Camas pocket gopher, variable pocket gopher, *Heterogeomys heterodus* (Peters), *Thomomys bulbivorus* (Richardson), Botta's pocket gopher, *Thomomys bottae* (Eydoux and Gervais), mountain pocket gopher, *Thomomys monticola* (J.A. Allen), northern pocket gopher, *Thomomys talpoides* (Richardson), southern pocket gopher, *Thomomys umbrinus* (Richardson) (Gardner et al. 2020; also see summary in Dursahinhan et al. 2023).

Geographic range of *Hymenolepis* s.str. *in pocket gophers in the Nearctic and northern Neotropical regions:* USA: California, Colorado, Illinois, Indiana, Minnesota, Nebraska Oklahoma, Oregon, Utah, Washington (Douthitt 1915; English 1932; Gardner and Schmidt 1988; Dursahinhan et al. 2023); **Texas (**English 1932; LaBrasseur 2017 [unpublished]; **this report).** México, State of Mexico, Tuluca (Gardner et al. 2020). Costa Rica, Potrero Cerrado, Cartago (Gardner et al. 2020).

Remarks

These *Hymenolepis* tapeworms from both gophers from different county localities (87 km apart) were morphologically identical (Figs. 1A-D). Interestingly, their mitochondrial DNA sequences did not match anything from GenBank (VV Tkach, *pers. comm.*). It has been suggested (SL Gardner, *pers. comm.*) these specimens are either *Hymenolepis weldensis* Gardner and Schmidt, 1988 or *Hymenolepis geomydis* Gardner and Schmidt, 1988 described from *G. bursarius* from Nebraska (Gardner and Schmidt 1988). The length of the medial hooks of the larvae is the distinguishing morphological characteristic between these two taxa; otherwise, it is difficult to differentiate them from one another. Various multivariate statistics of different measurements is necessary to separate the two.

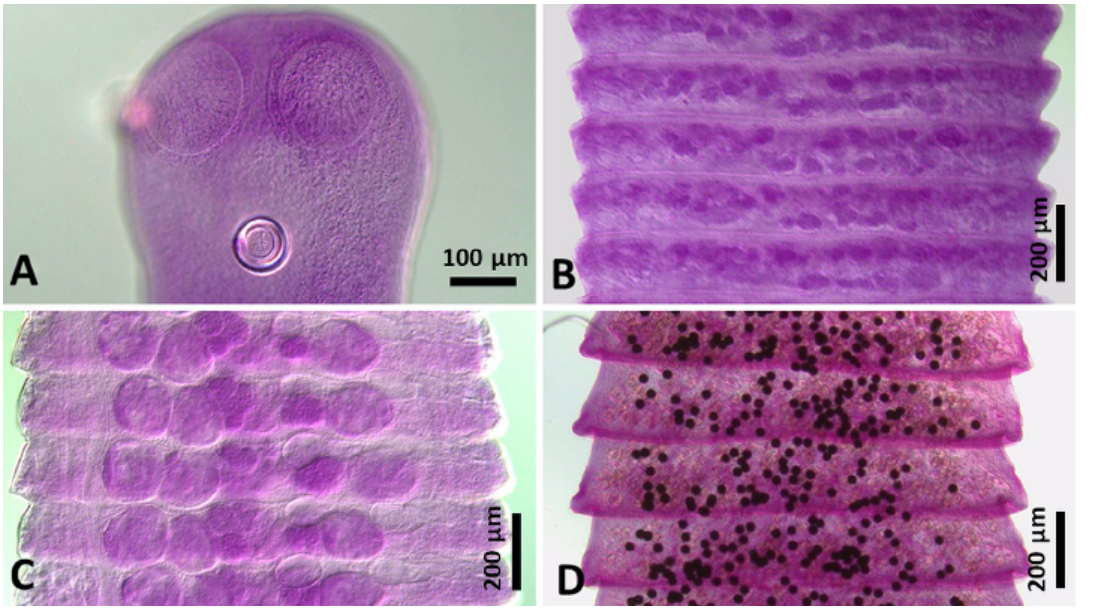

Figure 1. *Hymenolepis* sp. from *Geomys breviceps*. (A) Scolex (with rogue ovum). (B) Immature proglottid. (C) Mature proglottid with numerous large testes and centrally located ovary. (D) Gravid proglottid showing numerous ova (black dots).

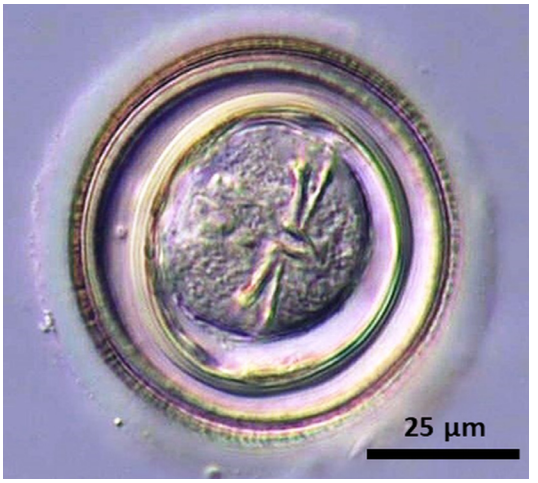

Figure 2. Ovum of *Hymenolepis* sp. showing degree of development of hooks of embryo with typical dimorphic hooks of the lateral pairs and the monomorphic hooks of the central pair in the larval embryophore.

Nematoda: Spiruroidea: Spirocercidae
***Mastophorus muris* (Gmelin, 1790)**

Hosts: Baird's pocket gopher, *Geomys breviceps* (Baird, 1855), adult (total length 220, tail length 65, hind foot 28, ear 5 mm), collected 5 January 2025.

Localities: USA: Texas: Lamar County, northeast of Blossom off US 82 (33°39'55"N, 95°19'12"W).

Deposited material: Retained for molecular analysis.

Prevalence: One of 4 (25%).

Site of infection: Stomach.

Intensity: One worm.

Other reported North American pocket gopher hosts with M. muris: southeastern pocket gopher, *Geomys pinetis* Rafinesque (Hubbell and Goff 1939); *G. breviceps* (Connior et al. 2017).

Geographic range in North American pocket gophers of M. muris: USA: Arkansas (Connior et al. 2017), Florida (Hubball and Goff 1939); **Texas (this report);**

Remarks

Recently, Jost et al. (2024) recognized two groups of *M. muris* without a change in their formal taxonomy: one collection were from specimens infecting house mice, *Mus musculus* (L.) and the second group including various taxa infecting non-*Mus* rodents. However, recovery of the current specimen confirms our belief that there may be more than one species of *M. muris* present in the USA, and mitochondrial DNA se-

quencing is ongoing (VV Tkach, *pers. comm*.).

Various specimens of *M. muris* from western Texas are deposited in the Museum at Texas Tech University Invertebrate Zoology Collection from hispid cotton rats, *Sigmodon hispidis* Say and Ord (https://www.gbif.org/occurrence/2556318850). However, this is the first time, to our knowledge, that *M. muris* has been documented from Texas in *G. breviceps*.

There are 10 species of *Hymenolepis* s.str. known from North America (Rowan et al. 2022). They infect a wide range of rodents, including arvicolines, geomyids, neotomines, and sciurids (Makarikov et al. 2015; Hoberg et al. 2016; Gardner et al. 2020). The life cycle is indirect and transmission occurs by ingestion of infected tissues of various intermediate hosts such as coprophilic arthropods of three insect orders (Coleoptera, Lepidoptera, and Siphonaptera).

Douthitt (1915) reported numerous individuals of eight different species of *Hymenolepis* from various gophers, including *G. breviceps* collected in Oklahoma and Texas; however, he did not indicate what species of tapeworm was involved. Likewise, English (1932) only identified specimens as *Hymenolepis* sp. from Texas *G. bursarius*. Burnham (1953) reported the rat tapeworm, *Hymenolepis diminuta* (Rudolphi, 1819) from supposed Baird's pocket gophers from Marshall County, Oklahoma; however, both *G. bursarius* and *G. breviceps* occur in that county (Caire et al. 2024) so we will never be able to know what species was the true host as vouchers were not mentioned. In an unpublished thesis, LeBrasseur (2017, his Fig. 4) reported *Hymenolepis* spp. from *G. attwateri*, *G. bursarius*, and *G. texensis* from Texas.

The tapeworms from our study were found to be significantly different in mitochondrial sequences (VV Tkach, *pers. comm.,* not shown) from the closest sequenced species, *Hymenolepis ackerti* Rowan, Hope and Jimenéz, 2022, recently described from symbiotype cotton rats, *Sigmodon hispidus* Say and Ord, and also reported in eastern woodrats, *Neotoma floridana* (Ord), and prairie voles, *Microtus ochrogaster* Wagner from Kansas (Rowan et al. 2022). Examination of museum specimens, particularly from those previously described by Gardner and Schmidt (1988) from different species of pocket gophers (*Geomys* and *Thomomys*) in Colorado and Oregon should be completed to help diagnose the current species. However, unfortunately, there are no DNA sequences to compare from those samples. Nevertheless, we believe that our samples represent a novel species to be described in a future separate paper.

The nematode, *Mastophorus muris*, is a cosmopolitan roundworm species primarily infecting wild and urban rodents, from *M. musculus* to rice rats (*Oryzomys* spp.), but also other less frequent mammalian hosts such as marsupials and carnivores, including canines and felines (Baylis 1927; Smales 1995; Torres et al. 1998, 2001; Smith and Kinsella 2011) that uses insects (Orthoptera, Dermaptera, Blattodea, and Siphonaptera) as intermediate hosts in a euryxenous life cycle. In one study, several *M. muris* was found in the stomach of two of eight (25%) *G. breviceps* from Benton County, Arkansas (Connior et al. 2017).

In conclusion, we document some new geographic distributional records for two endoparasites of *G. breviceps* from northeastern Texas. One noteworthy helminth, an unknown species of tapeworm of the genus *Hymenolepis* sp., may be a new species. Additional work is necessary to completely sequence this parasite as well as compare it to previously known *Hymenolepis* spp. from pocket gophers.

Acknowledgments

This study helps fulfill the requirements for Biol. 2389 at NTCC for IT (Independent Study). We thank Drs. Scott L. Gardner and Gábor R. Racz (HWML) for expert curatorial assistance and comments on the tapeworm, Vasyl V. Tkach (University of North Dakota, Grand Forks, North Dakota) for identification, processing the tapeworms, future sequencing, and photomicrographs, and J. Mike Kinsella (Missoula, Montana) for help with the nematode. CTM was issued a Scientific Collecting Permit by the Texas

Parks & Wildlife Department.

References

Baylis HA. 1927. Some new parasitic nematodes from Australia. Ann Mag Nat Hist 20:215–225.

Burnham GL. 1953. A study of the helminth parasites of the pocket gophers of Woods, Alfalfa, Grant, and Marshall counties, Oklahoma. Proc Okla Acad Sci 34:59–61.

Caire W, Loucks LS, Haynie ML. 2024. Mammals of Oklahoma. Second edition. Norman (OK): University of Oklahoma Press. 650 p.

Connior MB, Durden LA, McAllister CT, Seville RS, Bursey CR, Robison HW. 2017. New records of parasites (Apicomplexa, Nematoda, Acari, Anoplura) from rodents in Arkansas. J Ark Acad Sci 71:211–214.

Douthitt H. 1915. Studies on the family Anoplocephalidae. Ill Biol Monogr 1:1–96.

English PF. 1932. Some habits of the pocket gopher *Geomys breviceps*. J Mammal 13:126–132.

Gardner SL, Schmidt GD. 1988. Cestodes of the genus *Hymenolepis* Weinland, 1858 sensustricto from pocket gophers *Geomys* and *Thomomys* spp. (Rodentia: Geomyidae) in Colorado and Oregon, with a discriminant analysis of four species of *Hymenolepis*. Can J Zool 66:896–903.

Gardner SL, Dursahinhan AT, Campbell ML, Rácz SE. 2020. A new genus and two new species of unarmed hymenolepidid cestodes (Cestoda: Hymenolepidiciae) from geomyid rodents in Mexico and Costa Rica. Zootaxa 4766:358–376.

Jost J, Hirzmann J, Ďureje Ľ, Maaz D, Martin P, Stach T, Heitlinger E, Jarquín-Díaz VH. 2024. Dentition patterns and molecular diversity of *Mastophorus muris* (Gmelin, 1790) (Nematoda: Spiruroidea) support a host-associated subdivision. Parasitol Res 123:237. doi: 10.1007/s00436-024-08259-1.

LaBrasseur KM. 2017. Endoparasites of the digestive systems of four species of pocket gophers (Genus: *Geomys*) in Texas. [MSc thesis] San Angelo (TX): Angelo State University. 36 p. Available from: Texas Digital Library.

Pitts RM, Dronen NO, Bickham JW. 2000. Additional occurrence of the filarioid nematode, *Litomosoides westi*, in *Geomys* spp. in Texas. Texas J Sci 52:69–71.

Rowen B, Hope, AG, Jiménez FA. 2023. *Hymenolepis ackerti* n. sp. (Eucestoda: Hymenolepididae) infecting cricetid rodents from the central Great Plains of North America. Rev Mexicana Biodivers 94:3944927. https://doi.org/10.22201/ib.20078706e.2023.94.4927.

Skidmore LV. 1929. Note on a new species of coccidia from the pocket gopher (*Geomys bursarius*) (Shaw). J Parasitol 15:183–184.

Smales LR. 1995. *Mastophorus muris* (Nematoda: Spirocercidae) from the musky rat-kangaroo, *Hypsiprymnodon moschatus*. Trans Roy Soc Sci Aust 119:95–96.

Smith JA, Kinsella JM. 2011. Gastric spiruridiasis caused by *Mastophorus muris* in a captive population of striped possums (*Dactylopsila trivirgata*) J Zoo Wildl Med 42:357–359.

Torres J, Garcia-Perea R, Gisbert J, Feliu C. 1998. Helminth fauna of the Iberian lynx, *Lynx pardinus*. J Helminthol 72:221–226.

Torres J, Miquel J, Motje M. 2001. Helminth parasites of the Eurasian badger (*Meles meles* L.) in Spain: a biogeographic approach. Parasitol Res 87:259–263.

Upton SJ, Pitts RM, McAllister CT, Hollander RR. 1992. New host records for *Eimeria geomydis* Skidmore, 1929, from *Geomys* (Rodentia: Geomyidae) and redescriptions of the oocysts from *Geomys bursarius*. Texas J Sci 44:95–98.

New Host and Distributional Records for Hematozoan and Helminth Parasites of Midland Watersnake, *Nerodia sipedon pleuralis* (Ophidia: Natricidae), from Western Arkansas

Chris T. McAllister*
Department of Natural Sciences, Northeast Texas Community College, 2886 FM 1735, Chapel Hill Road, Mt. Pleasant, TX 75455

Charles R. Bursey
Department of Biology, Pennsylvania State University-Shenango Campus, Sharon, PA 16146

Gracie J. Gray
College of Biomedical and Translational Sciences, University of North Texas Health Science Center, Ft. Worth, TX 76107

Stephanie Hernandez
Division of Natural Sciences, Northeast Texas Community College, 2886 FM 1735, Chapel Hill Road, Mt. Pleasant, TX 75455

Henry W. Robison
602 Big Creek Drive, Sherwood, AR 72120

Abstract: Four Midland watersnakes, *Nerodia sipedon pleuralis*, collected in June 2024 and May and August 2025 from Polk County, Arkansas, were examined for hematozoan and helminth parasites. A single snake was infected with an intraerythrocytic hematozoan, *Hepatozoon* sp., as well as the digenetic trematodes, *Styphlodora magna* Byrd and Denton, 1938, and *Dasymetra conferta* Nicoll, 1911. Another harbored several helminths, including the digenetic trematodes, *Renifer aniarum* (Leidy, 1890) and *Paralechriorchis natricis* (Holl and Allison, 1935), a cestode, *Mesocestoides* sp., and a nematode, *Ophidascaris ashi* Walton, 1927; one other snake was infected with only *R. aniarum* and the other specimen was negative. We document some new host and geographic distributional records for these parasites.

Introduction

The Midland watersnake, *Nerodia sipedon pleuralis* (Cope) ranges from southern Illinois and Indiana south through western Tennessee, western Kentucky, Arkansas, eastern Oklahoma, most of Mississippi and Alabama, and eastward to Georgia and South Carolina (Powell et al. 2016). In Arkansas, this snake occurs throughout the Interior Highlands and West Gulf Coastal Plain with sporadic records from the

*Corresponding author: cmcallister@ntcc.edu

Mississippi Alluvial Plain (Trauth et al. 2004). It feeds mostly on fish but the diet also includes amphibians (Ernst and Barbour 1989; Mount 1975).

Most of the information on hematozoans (Fantham and Porter 1954; Hull and Camin 1960; Smith et al. 1994; Smith and Desser 1997) and helminths (Ernst and Ernst 2006; Walley et al. 2012) of *N. sipedon* is provided on the nominal subspecies, the northern watersnake, *N. sipedon sipedon* (L.) from Ohio, Ontario, and Québec, Canada. However, McAllister et al. (2017) reported a hematozoan, *Hepatozoon* sp. from *N. s. pleuralis* from Missouri, and Detterline et al. (1984) documented helminths of *N. s. pleuralis* from Alabama. Here, we report a hematozoan and several helminths from a small sample of *N. s. pleuralis* from western Arkansas.

Methods

On 21-22 June 2024 ($n = 2$), 27 May 2025 ($n = 1$), and 30 August 2025 ($n = 1$), four adult *N. s. pleuralis* (mean ± sd snout-vent length [SVL] = 550 ± 76.8, range 460-670 mm) were collected from Butcherknife Creek at Big Fork off St. Hwy 8, Polk County, Arkansas (34°28′5.109″N, 93°56′52.1772″W) (Fig. 1) with a snake tong or in a baited minnow trap and examined for helminth parasites. Specimens were euthanized with an intraperitoneal injection of concentrated tricaine methanesulfonate (SIH 2004). We follow McAllister et al. (2017) in processing snakes for hematozoan parasites in the blood. The oral cavity was examined for trematodes, and a mid-ventral incision was made to expose the viscera. The entire gastrointestinal tract was removed and split lengthwise, rinsed in 0.9% (v/v) saline, and examined as well as other organs, including the heart, lungs, liver, and gonads. Trematodes and cestodes were fixed in nearly boiling tap water without coverslip pressure, stained with acetocarmine, dehydrated in a graded ethanol series, cleared in methyl salicylate, and mounted in Canada balsam. Nematodes were fixed in hot tap water and studied as temporary mounts on a microscopic slide in a drop of glycerol. Parasites were either retained for future molecular studies or deposited as vouchers in the Harold W. Manter Laboratory of Parasitology (HWML), University of Nebraska-Lincoln. Host voucher specimens were deposited in the Northeast Texas Community College (NTCCVC) Vertebrate Collection, Mt. Pleasant, Texas. Host common and scientific names follow Nicholson (2025).

Figure 1. Habitat of *Nerodia sipedon pleuralis* at Butcherknife Creek, Polk County, Arkansas. Photo by CTM.

Results and Discussion

Three of four *N. s. pleuralis* harbored parasites. A single *N. s. pleuralis* was infected with an intraerythrocytic hematozoan parasite as well as two trematodes. Two others harbored helminth parasites as follows: one harbored multiple infection of two trematodes, a cestode, and a nematode; another was infected with a trematode; one specimen was negative. Detailed information on each parasite is provided below in an annotated format.

Apicomplexa: Adeleina: Hepatozoidae

***Hepatozoon* sp.** – one specimen, a 670 mm SVL individual collected from a minnow trap on 30 August 2025 from the Butcherknife

Creek site was found to harbor an intraerythrocytic hematozoan of the genus *Hepatozoon*. Intensity (parasitemia) was relatively high as approximately 2-3% of the red blood cells contained elongate-shaped and partially recurved thin banana-shaped gamonts (Fig. 2). Interestingly, McAllister et al. (2017) reported a *Hepatozoon* sp. from *N. s. pleuralis* from Missouri with very similar morphologies (their Figs. 2A-C) but with a much lower parasitemia of less than 0.5%. In addition, Smith et al. (1994) reported *Hepatozoon sipedon* Smith, Desser, and Martin, 1994 from *N. s. sipedon* from Ontario, Canada, with a parasitemia of only 0.2%. All hemogregarines from snakes are members of the genus *Hepatozoon* according to Smith (1996). However, without complete life cycle data including developmental stages from hematophagus invertebrates, specific identification of these hematozoans is difficult (Jacobson 2007; Smith and Desser 1997). Although the Midland watersnake has been previously reported as a host, albeit in Missouri, we document a new distributional record for the parasite.

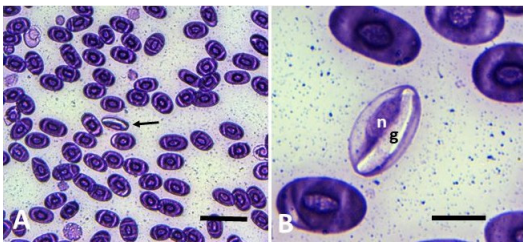

Figure 2. *Hepatozoon* sp. from *Nerodia sipedon pleuralis*. (A) View showing infected red blood cell (rbc, arrow). Scale bar = 25 µm. (B) Closer microscopic view showing nucleus (n) of infected rbc with banana-shaped gamont (g). Scale bar = 10 µm.

Trematoda: Digenea: Plagiorchiida: Reniferidae

***Dasymetra conferta* Nicoll, 1911** – The same specimen above harbored 15 specimens (Fig. 3) in its oral cavity and esophagus/lungs. Nicoll (1911) originally described this trematode from northern diamond-backed watersnake, *Nerodia rhombifer rhombifer* (Hallowell) from an unknown North American locality. This digenean has been previously reported in various natricines, including plain-bellied watersnake *N. e. erythrogaster* (Forster), broad-banded watersnake, *N. fasciata confluens* (Blanchard) *N. r. rhombifer*, and *N. s. pleuralis* from Alabama, Missouri, Oklahoma, and Texas (see Ernst and Ernst 2006; McAllister and Bursey 2012). We document a new geographic record for *D. conferta*.

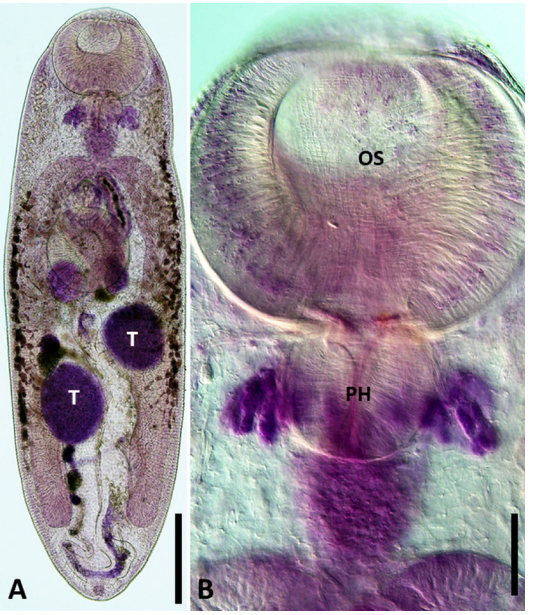

Figure 3. *Dasymetra conferta* from *Nerodia sipedon pleuralis*. (A) Whole mount showing testes (T). Scale bar = 500 µm. (B) Higher magnification of anterior region of same specimen showing oral sucker (OS) and pharynx (PH). Scale bar = 125 µm.

***Renifer aniarum* (Leidy, 1891)** – a 460 mm SVL *N. s. pleuralis* collected on 27 May 2025 was found to harbor two *R. aniarum* (HWML 119232) in its oral cavity. Another *N. s. pleuralis* (660 mm SVL) collected on 21 June 2024 from the same site had four specimens of *R. aniarum* (Fig. 4) in its oral cavity. McAllister et al. (2008) provided a summary of the North American hosts of *R. aniarum* that included 23 species/subspecies of snakes, including 12 species/subspecies of natricines. This digenean has been previously reported from *N. s. pleuralis* from Alabama, Arkansas (Washington County), North Carolina, and Texas (Detterline et al. 1984; McAllister and Bursey 2008; McAllister et al. 2025) and

N. s. sipedon from Michigan and Pennsylvania (McAllister and Bursey 2008). It has been also been reported previously from Lonoke County (Arkansas) in a yellow-bellied watersnake, *Nerodia erythrogaster transverva* (Hallowell) (McAllister and Bursey 2008). Interestingly, introduced *R. aniarum* have been reported from grass snakes, *Natrix natrix* (L.) from southern Italy, which is thought to have originated from translocated American bullfrogs, *Rana catesbeiana* (Santoro et al. 2011). The life cycle involves first intermediate host snails (pulmonates) which possess cercariae that penetrate second intermediate host anuran tadpoles, which then preyed on by snakes (Schell 1985). This is the second time the parasite has been reported from a Midland watersnake from Arkansas, but the first record from Polk County.

***Paralechriorchis natricis* (Holl and Allison, 1935) Byrd and Denton, 1938** – the same 460 mm SVL specimen above harbored three specimens (HWML 119231) of *P. natricis* in its oral cavity. The original name *Zeugorchis natricis*, proposed by Holl and Allison (1935), was for trematodes found in the uterus of a *N. s. sipedon* collected from Wolf Creek, Grove City, Mercer County, Pennsylvania. Byrd and Denton (1938a) later stated *"we found it impossible to distinguish between Z. natricis Holl and Allison, 1935, and Lechriorchis secundus Canavan, 1937. Due to this striking similarity of body plan and almost identical size range for the various internal anatomy we feel justified in considering L. secundus as a synonym of Z. natricis. Since Z. natricis possesses the characters of the genus Paralechriorchis we transfer it to that genus. The species becomes Paralechriorchis natricis (Holl and Allison. 1935)."* In addition, Goodman (1951, 1952), in an unpublished dissertation, reported the parasite with the name *Dasymetra natricis*, but we do not accept it. This parasite has been previously reported from eastern copperhead, *Agkistrodon contortrix* (L.), *N. erythrogaster*, and a *Nerodia* sp. from Illinois and Indiana (Ernst and Ernst 2006). We document *P. natricis* from Arkansas, and from *N. s. pleuralis*, for the first time.

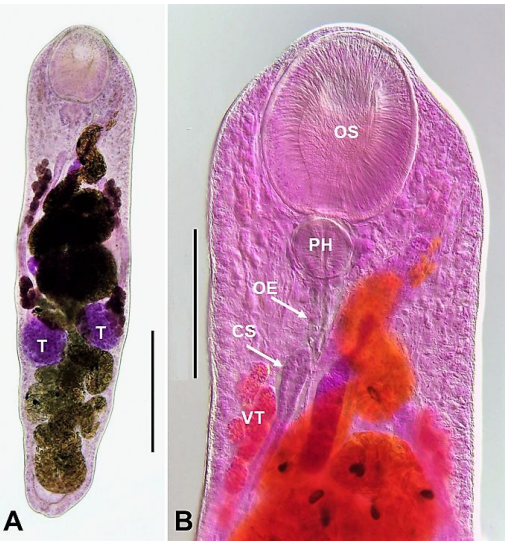

Figure 4. *Renifer aniarum* from *Nerodia sipedon pleuralis*. (A) Whole mount showing testes (T). Scale bar = 500 µm. (B) View of upper region of same specimen showing cirrus sac (CS), oesophagus (OE), oral sucker (OS), pharynx (PH), and vitellaria (VT). Scale bar = 250 µm.

Plagiorchiida: Plagiorchiidae

***Styphlodora magna* Byrd and Denton, 1938** – eight specimens (Fig. 5) were taken from the gallbladder of a single snake (670 mm SVL) collected on 30 August 2025. This species has similar species with their synonymies needing clarification, but fortunately, in the current case, the large difference in egg size was sufficient for differentiation (VV Tkach, *pers. comm.*). In fact, Ernst and Ernst (2006) list it in synonomy as *Ochetosoma magnum*. Byrd and Denton (1938b) originally described this digenean from the gallbladder of *N. s. sipedon* from Georgia and Mississippi. McAllister et al. (2020, 2021, 2023) previously reported *S. magna* from northern cottonmouths, *Agkistrodon piscivorus* (Lacépède) from Arkansas and Oklahoma. In addition, McAllister et al. (2023) provided a summary of the ophidian hosts and localities of *S. magna*, to include several species of North American watersnakes (*Nerodia*), *A. piscivorus*, North American racer, *Coluber constrictor* L., and eastern ratsnake, *Pantherophis alleghaniensis* (Holbrook) from Florida, Louisiana, and North Carolina. We document the first time this digenean has

been reported from *N. s. pleuralis*.

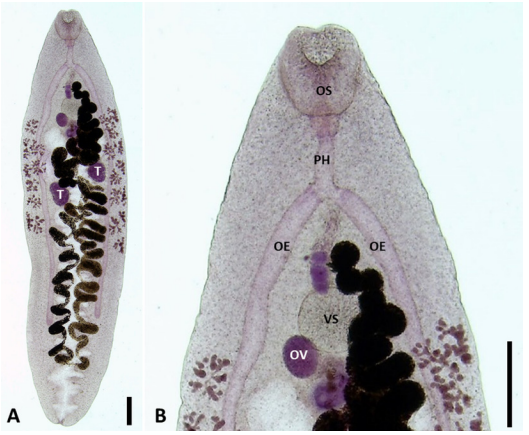

Fig. 5. *Styphlodora magna* from *Nerodia sipedon pleuralis*. (A) Whole mount showing testes. Scale bar = 1.0 mm. (B) Higher magnification of anterior region of same specimen showing oesophagus (OE), oral sucker (OS), ovary (OV), pharynx (PH), and ventral sucker (VS). Scale bar = 500 µm.

Cestoda: Cyclophyllidea: Mesocestoididae

***Mesocestoides* sp.** – the 460 mm SVL host was infected in its intestine with a single tetrathyridial specimen (HWML 119230) of *Mesocestoides* sp. The life cycle is an ongoing enigma, yet to be solved, but may involve at least three hosts, an arthropod first intermediate host, a vertebrate second intermediate host, and a vertebrate definitive host (Rausch 1994). However, McAllister et al. (2018) recently suggested that these tapeworms may develop through a simple two-host life cycle. This tapeworm has been reported from a variety of amphibians and reptiles, including several snakes from the Nearctic realm (Bursey et al. 2012; McAllister et al. 2013). In Arkansas, *Mesocestoides* sp. has been reported from various herpetofauna, including six species of salamanders, five species of frogs and toads, three species of lizards, and three species of snakes (McAllister et al. 2013, 2014a, b). We are unaware of reports of *Mesocestoides* sp. from any species of North American watersnake, although the genus has been documented in three species of *Natrix* watersnakes from Myanmar and Italy (see summary in McAllister et al. 1991).

Nematoda: Ascaridida: Ascarididae

***Ophidascaris ashi* Walton, 1927** – a single *O. ashi* (HWML 119229) was found in the stomach of the same *N. s. pleuralis* above. This nematode (as *O. labiatopapillosa*) has been reported from several amphibians as adult worms and encysted larval stages from Florida, and from at least six species of snakes from Alabama, Florida, Louisiana, and Texas, including *N. s. sipedon* from Michigan (see Baker 1987). Sprent (1988) described *O. ashi* as a new species name for *O. labiatopapillosa* in North American colubrids. The life cycle of *Ophidascaris* spp. is indirect with various snakes as definitive hosts (Sprent 1988). We document *O. ashi* from Arkansas, and from *N. s. pleuralis*, for the first time.

In summary, we provide new records for some helminths from a small sample of *N. s. pleuralis* collected from western Arkansas. Surveys on additional Midland watersnakes from other parts of its range, where they have not yet been examined, will likely yield new host and distributional records for helminths.

Acknowledgments

The Arkansas Game and Fish Commission issued Scientific Collecting Permit No. 032820232 to CTM. Larry R. Raymond (Ouachita Mountains Biological Station, Big Fork, Arkansas) is acknowledged for providing gratis housing and laboratory space to CTM, GJG, and SH. We also thank OMBS Resident Manager, Jeffrey Pittman, for assistance in collecting on one outing. NTCC students GJG and SH partially fulfilled requirements for Biol. 2289 (Independent Study) via this research. Dr. Vasyl V. Tkach (University of North Dakota, Grand Forks, North Dakota) is gratefully acknowledged for providing helminth photomicrographs, verifying the identity of trematodes, and future molecular sequencing on select specimens from these hosts.

References

Baker MR. 1987. Synopsis of the Nematoda parasitic in amphibians and reptiles. Mem Univ Newfoundland Occ Pap Biol No 11. 325 p.

Byrd EE, Denton JF. 1938a. New trematodes of the subfamily Reniferinae, with a discussion of the systematics of the genera and species assigned to the subfamily group. J Parasitol 24:379–401.

Byrd EE, Denton JF. 1938b. Two new trematode parasites of the genus *Styphlodora* (Plagiorchiidae: Styphlodorinae) from the gall bladder of a water-snake. Proc Helminthol Soc Wash 5:42–46.

Detterline JL, Jacob JS, Wilhelm WE. 1984. A comparison of helminth endoparasites in the cottonmouth (*Agkistrodon piscivorus*) and three species of water snakes (*Nerodia*). Trans Amer Microsc Soc 103:137–143.

Ernst CH, Barbour, RW. 1989. Snakes of Eastern North America. Fairfax (VA): George Mason University Press. 282 p.

Ernst CH, Ernst EM. 2006. Synopsis of helminths endoparasitic in snakes of the United States and Canada. Soc Study Amph Rept Herpetol Circ No 34. 86 p.

Fantham HB, Porter A. 1954. The endoparasites of some North American snakes and their effects on the Ophidia. Proc Zool Soc London 123:867–898.

Goodman JD. 1951. Taxonomic studies on the family Ochetosomatiidae Leao, 1944, and the life history of *Stomatrema guberleti* Byrd, 1937, Trematoda. Ph.D. dissertation, University of Michigan, p. 322. Digitized Nov 17, 2022.

Goodman JD. 1952. Taxonomic studies on the family Ochetosomatidae Leao, 1944, and the life history of *Stomatrema guberleti* Byrd, 1937. Diss Abstr 13(12):231.

Holl FJ, Allison LN. 1935. *Zeugorchis natricis* n. sp. a trematode from the water snake. J Parasitol 21:197–199.

Hull RW, Camin JH. 1960. Haemogregarines in snakes: The incidence and identity of the erythrocytic stages. J Parasitol 46:515–523.

Jacobson ER. 2007. Parasites and parasitic diseases of reptiles. In: Jacobson ER (editor): Infectious diseases and pathology of reptiles: Color atlas and text. Boca Raton (FL): CRC Press, p. 571–566.

McAllister CT, Bursey CR. 2008. First report of *Ochetosoma aniarum* (Digenea: Ochetosomatidae) from the Brazos water snake, *Nerodia harteri* (Serpentes: Colubridae), in Texas, with a summary of definitive hosts of this parasite. Texas J Sci 60:63–68.

McAllister CT, Bursey CR. 2012. New host and distributional records for helminth parasites (Trematoda, Cestoidea, Nematoda) of herpetofauna from southeastern Oklahoma. Proc Okla Acad Sci 92:29–35.

McAllister CT, Bursey CR, Koch RW, Trauth SE, Conn DB, Robison HW. 2020. Additional records of hemoparasites (Apicomplexa) and helminth parasites (Trematoda, Cestoda, Nematoda, Acanthocephala) from Oklahoma amphibians (Anura) and reptiles (Testudines: Ophidia). Proc Okla Acad Sci 100:84–94.

McAllister CT, Bursey CR, Fayton TJ, Trauth SE, Robison HW. 2025. New host and distributional records for helminth parasites (Monogenoidea, Trematoda, Cestoda, Nematoda) of Arkansas reptiles (Testudines, Ophidia). J Ark Acad Sci 79:(in press).

McAllister CT, Bursey CR, Robison HW. 2021. Noteworthy records of helminth parasites (Monogenea, Trematoda, Cestoda, Nematoda, Acanthocephala) from select herpetofauna (Anura, Testudines, Ophidia) from McCurtain County, Oklahoma. Proc Okla Acad Sci 101:101–108.

McAllister CT, Bursey CR, Robison HW. 2023. Helminth parasites of northern cottonmouth, *Agkistrodon piscivorus* (Ophidia: Viperidae), from Arkansas. J Ark Acad Sci 77:49–55.

McAllister CT, Conn DB, Freed PS, Burdick DA. 1991. A new host and locality record for *Mesocestoides* sp. tetrathyridia (Cestoidea: Cyclophyllidea), with a summary of the genus from snakes of the world. J Parasitol 77:329–331.

McAllister CT, Connior MB, Trauth SE. 2014a. New host records for *Mesocestoides* sp. tetrathyridia (Cestoidea: Cyclophyllidea) in anurans (Bufonidae, Ranidae) from Arkansas, with a summary of North American amphibian hosts. J Ark

Acad Sci 68:158–162.

McAllister CT, Connior MB, Bursey CR, Trauth SE, Robison HW, Conn DB. 2014b. Six new host records for *Mesocestoides* sp. tetrathyridia (Cestoidea: Cyclophyllidea) from amphibians and reptiles of Arkansas, U.S.A. Comp Parasitol 81:278–283.

McAllister CT, Fayton TJ, Robison HW. 2017. First report of a *Hepatozoon* sp. (Apicomplexa: Adeleina: Hepatozoidae) from Midland water snake, *Nerodia sipedon pleuralis* (Ophidia: Colubridae), from Missouri. Proc Okla Acad Sci 97:79–82.

McAllister CT, Trauth SE, Plummer MV. 2013. A new host record for *Mesocestoides* sp. (Cestoidea: Cyclophyllidea: Mesocestoididae) from a rough green snake *Opheodrys aestivus* (Ophidia: Colubridae) in Arkansas, U.S.A. Comp Parasitol 80:130–133.

McAllister CT, Tkach VV, Conn DB. 2018. Morphological and molecular characterization of post-larval pre-tetrathyridia of *Mesocestoides* sp. (Cestoda: Cyclophyllidea) from ground skink, *Scincella lateralis* (Sauria: Scincidae), from southeastern Oklahoma. J Parasitol 104:246–253.

Mount RH. 1975. The reptiles and amphibians of Alabama. Auburn (AL): Auburn University Experimental Station. 347 p.

Nicoll W. 1911. On three new trematodes from reptile. Proc Zool Soc London 3:677–686.

Nicholson KE (ed.). 2025. Scientific and standard English names of amphibians and reptiles of North America North of Mexico, with comments regarding confidence in our understanding. Ninth edition. Topeka (KS): Society for the Study of Amphibians and Reptiles. 87 p.

Powell R, Conant R, Collins JT. 2016. Peterson field guide to reptiles and amphibians. Boston (MA): Houghton Mifflin Harcourt. 494 p.

Rausch RL. 1994. Family Mesocestoididae Fuhrmann, 1907. In: Keys to the cestode parasites of vertebrates. Khalil LF, Jones A, and Bray RA (eds). Wallingford, Oxon (UK). p. 309–314.

Santoro M, Tkach V, Mattiuchi S, Kinsella M, Nascetti G. 2011. *Renifer aniarum* (Digenea: Reniferidae), an introduced North American parasite in grass snakes *Natrix natrix* in Calabria, southern Italy. Dis Aquat Org 95:233–240.

Schell SC. 1985. Handbook of trematodes of North America north of Mexico. Moscow (ID): University Press of Idaho. 263 p.

Smith TG. 1996. The genus *Hepatozoon* (Apicomplexa: Adeleina). J Parasitol 82:565–585.

Smith TG, Desser SS. 1997. Phylogenetic analysis of the genus *Hepatozoon* Miller, 1908 (Apicomplexa: Adeleorina). Syst Parasitol 36:213–221.

Smith TG, Desser SS, Martin DS. 1994. The development of *Hepatozoon sipedon* sp. nov. (Apicomplexa: Adeleina: Hepatozoidae) in its natural host, the northern water snake (*Nerodia sipedon sipedon*), in the culicine vectors *Culex pipiens* and *C. territans*, and in an intermediate host, the northern leopard frog (*Rana pipiens*). Parasitol Res 80:559–568.

Society of Ichthyologists and Herpetologists (SIH). 2004. Guidelines for use of live amphibians and reptiles in field and laboratory research. Second Edition, Revised by the Herpetological Animal Care and Use Committee (HACC) of the American (Committee Chair: SJ Beaupre, ER Jacobson, HB Lillywhite, and K Zamudio). Available from: https://www.aaalac.org/accreditation/RefResources/SS_Amphib.pdf (Accessed 29 July, 2025).

Sprent. J.F.A. 1988. Ascaridoid nematodes of amphibians and reptiles: *Ophidascaris Baylis*, 1920. Syst Parasitol 11:165–213.

Trauth SE, Robison HW, Plummer MV. 2004. The amphibians and reptiles of Arkansas. Fayetteville (AR): University of Arkansas Press. 421 p.

Walley HD, King RB, Ray JM, Wusterbarth TL. 2012. *Nerodia sipedon*. Cat Amer Amph Rept 899:1–58.

External Morphology of the Tubercles on the Ears of the Brazilian Free-tailed Bat, *Tadarida brasiliensis*

William Caire, Lynda Samanie Loucks*, and Melville B. Vaughan
Department of Biology, University of Central Oklahoma, 100 N. University Drive, Edmond, Oklahoma 73034

Abstract: The Brazilian Free-tailed bat, *Tadarida brasiliensis*, has small tubercles along the dorsal leading edge of the ears. Ear tubercles may serve an aerodynamic function similar to the hydrodynamic function of tubercles on the pectoral flippers of humpback whales. Descriptive morphology of 52 adult bats was examined and the average number of tubercles was nine for both ears, ranging from five to twelve on each ear. Distances between tubercles and mean volumes are variable. Possible physiological functions for tubercles include thermoregulation and thermosensory capability, in addition to increased maneuverability during foraging bouts and enhanced control during cave entry and exit.

Introduction

Small tubercles along the outer anterior edges of the Brazilian Free-tailed bat, *Tadarida brasiliensis*, ears have been referenced in the literature (Wilkins 1989; Caire et al. 2024); however, their external morphology has not been described in detail nor have all the possible functions they serve been examined. We describe the external morphology of the ear tubercles, including the number of tubercles, successive distances apart, tubercle volume, and a scanning electron microscopic (SEM) view of the tubercles. Based on the external anatomy and other studies presented in the literature we suggest possible functions of the tubercles.

Methods and Results

Fifty-two (23 males, 29 females) adult *T. brasiliensis* preserved in 70% ethanol and deposited in the University of Central Oklahoma Museum of Natural History were used for the external morphological descriptions. The general location of the tubercles located across the leading edge of the bat ears is shown in Figure 1.

Figure 1. General location of tubercles along the leading edge of *Tadarida brasiliensis* ear.

Left and right ears of each bat were photographed at 10x magnification with a Moticam 1000 1.3MP Live Resolution Microscope Camera mounted on an Omano Microscope. The number (minimum, maximum, mode, mean) of tubercles on the left and right ears of each specimen were counted through examination of the photographs. For the 52 adult bats examined (sexes combined), the number of tubercles on an ear ranged from 5–12 with a mode of 9 on left ear and 8 on right ear (Table 1). The average was 9 tubercles for both ears.

*Corresponding author: lloucks@uco.edu

Proc. Okla. Acad. Sci. 105: pp 86-95 (2025)

Table 1. Minimum, maximum, mode, and mean number of tubercles on left and right ears of 52 *Tadarida brasiliensis*.

	Minimum	Maximum	Mode	Mean
Left Ear	5	12	9	9
Right Ear	5	11	8	9

Males had a mode and mean of 9 tubercles ranging from 6–12 on the left ear and a mode of 8 and a mean of 9 tubercles ranging from 7–11 on the right ear (Table 2). Females had a mode and mean of 8 tubercles ranging from 5–11 on the left ear and a mode of 8 and a mean of 9 tubercles ranging from 5–11 on the right ear (Table 2).

Table 2. Mode, mean and range of the number of tubercles counted on male (n=23) and female (n=29) *Tadarida brasiliensis* ears.

Gender		Mode	Mean	Range
Male	Left Ear	9	9	6–12
	Right Ear	8	9	7–11
Female	Left Ear	8	8	5–11
	Right Ear	8	9	5–11

All the ears on the bats examined had the first 5 tubercles on the left and right ears (Table 3). However, the number of ears having each of the successive tubercles along the ear varied. On the left ear of 51 bats, tubercle 6 was present; 48 possessed the 7th; 41 possessed the 8th; 28 possessed the 9th; 12 possessed the 10th; 3 possessed the 11th; and 1 bat had a 12th tubercle. On the right ear of 50 bats, tubercles 6 and 7 were present; 44 possessed the 8th; 26 possessed the 9th; 16 possessed the 10th; 4 possessed the 11th; and none of the bats had a 12th tubercle. The number of male and female bats having each tubercle on the left and right ears are in Table 4.

Table 3. Number of bat (males and females combined n = 52) ears having each tubercle.

Tubercle	1	2	3	4	5	6	7	8	9	10	11	12
Left ear	52	52	52	52	52	51	48	41	28	12	3	1
Right ear	52	52	52	52	52	50	50	44	26	16	4	0

Table 4. Number of male (n = 23) and female (n = 29) bats having each tubercle.

	Tubercle	1	2	3	4	5	6	7	8	9	10	11	12
Males	Left ear	23	23	23	23	23	23	22	18	16	8	2	1
	Right ear	23	23	23	23	23	23	23	20	12	7	2	0
Females	Left ear	29	29	29	29	29	28	26	23	12	4	1	0
	Right ear	29	29	29	29	29	27	27	24	14	9	2	0

The Moticam Camera Motic Images Plus 2.0 MS Software was used to measure the distance between successive tubercles on the left and right ears. Measurements rounded to the nearest one-hundredth micrometer (µm) were made starting from the lateral edge of the most medial tubercle to the medial edge of the next tubercle continuing along the ear distally until all distances between each successive pair of tubercles were recorded. The minimum, maximum, and mean distances between each tubercle on the left and right ears for the sexes combined are listed in Table 5 and for males and females separately in Table 6

Table 5. Number (n), minimum (min), maximum (max), and mean ($\bar{x}$) distances (µm) between successive tubercles on left and right ears of *Tadarida brasiliensis* (males and females combined).

	Left Ear				Right Ear			
Tubercles	n	min	max	$\bar{x}$	n	min	max	$\bar{x}$
1 → 2	52	117.6	1458.2	551.1	52	104.7	1137.1	576.8
2 → 3	52	297.7	1176.6	686.4	52	202.4	1367.3	616.3
3 → 4	52	88.7	1016.8	611.1	52	123.4	1434.4	603.9
4 → 5	52	108.9	1527.3	559.2	52	270.5	1051.1	527.8
5 → 6	51	91.5	995.0	438.0	50	83.2	821.7	441.9
6 → 7	48	96.5	775.2	373.6	50	74.4	776.2	331.8
7 → 8	41	88.7	575.0	292.9	44	80.1	493.6	256.6
8 → 9	28	90.6	432.2	271.7	26	80.1	554.5	187.7
9 → 10	12	74.4	422.5	204.6	16	115.8	307.0	190.9
10 → 11	3	137.9	231.2	170.4	4	123.4	213.0	176.7
11 → 12	1	403.9			0			

Table 6. Distances (μm) between successive left and right ear tubercles of male and female *Tadarida brasiliensis*. The mean distance between successive tubercles, (number) of distances measured, and [range] is presented for male and female left and right ears.

	Male		Female	
Tubercles	Left	Right	Left	Right
1–2	541 (23)	516 (23)	605 (29)	579 (29)
	[131–1350]	[178–1140]	[118–1460]	[105–1090]
2–3	620 (23)	554 (23)	739 (29)	665 (29)
	[299–1120]	[202–879]	[298–1180]	[364–1370]
3–4	629 (23)	627 (23)	597 (29)	586 (29)
	[88.7–1020]	[332–997]	[213–886]	[123–1430]
4–5	513 (23)	538 (23)	596 (29)	520 (29)
	[161–869]	[276–765]	[109–1530]	[271–1050]
5–6	418 (23)	420 (23)	455 (28)	461 (27)
	[91.5–995]	[83.2–690]	[178–840]	[122–822]
6–7	352 (22)	329 (23)	392 (26)	334 (27)
	[108–748]	[112–563]	[96.5–775]	[74.4–776]
7–8	316 (18)	212 (20)	275 (23)	293 (24)
	[91.5–575]	[87.9–451]	[88.7–496]	[80.1–494]
8–9	264 (16)	206 (12)	282 (12)	172 (14)
	[112–432]	[136–555]	[90.6–432]	[80.1–494]
9–10	193 (8)	193 (7)	227 (4)	189 (9)
	[74.4–423]	[137–307]	[120–305]	[116–265]
10–11	187 (2)	185 (2)	138 (1)	168 (2)
	[142–231]	[165–205]		[123–213]
11–12	404 (1)			

Using the Motic Images Plus 2.0 MS Software, the height (μm³) and radius (μm³) taken at the base of each tubercle on the left and right ears were used to estimate tubercle volume ($1/3\pi r^2h$) Table 7 contains the mean ($\bar{x}$) of the estimated volumes (μm³) of individual tubercles 1–12 on right and left ears (males and females combined). Males and females are separated in Table 8. Tubercles with the largest volumes were located at the medial edge of the ear closest to the head and the volumes of the subsequent tubercles decreased toward the distal edge of the ear.

Table 7. The number (n) of tubercles examined and the estimated mean volumes ($\bar{x}$ in µm³) of individual tubercles on left and right ears of *Tadarida brasiliensis* (males and females combined).

	Left Ear		Right Ear	
Tubercle	n	$\bar{x}$	n	$\bar{x}$
1	52	1.56E+07	51	1.80E+07
2	52	9.80E+06	51	1.10E+07
3	52	7.80E+06	51	8.20E+06
4	52	7.40E+06	51	6.60E+06
5	52	7.50E+06	51	7.10E+06
6	51	5.80E+06	49	7.80E+06
7	48	5.50E+06	49	7.30E+06
8	41	6.40E+06	42	6.10E+06
9	28	5.40E+06	26	6.20E+06
10	13	4.20E+06	16	8.10E+06
11	4	4.80E+06	4	9.30E+06
12	1	7.00E+06	0	

Table 8. The number (n) of tubercles examined and the estimated mean volume ($\bar{x}$ in µm³) of tubercles of male and female *Tadarida brasiliensis*.

		Estimated mean volume				Estimated mean volume		
		Left Ear		Right Ear		Left Ear		Right Ear
Tubercle	n	$\bar{x}$	n	$\bar{x}$	n	$\bar{x}$	n	$\bar{x}$
1	23	1.21×10^7	23	1.18×10^7	29	1.72×10^7	29	2.24×10^7
2	23	8.29×10^6	23	7.01×10^6	29	1.10×10^7	29	1.42×10^7
3	23	7.25×10^6	23	6.27×10^6	29	8.20×10^6	29	9.69×10^6
4	23	5.86×10^6	23	5.54×10^6	29	8.66×10^6	29	7.28×10^6
5	23	6.48×10^6	23	5.79×10^6	29	8.37×10^6	29	8.06×10^6
6	23	5.66×10^6	23	5.36×10^6	28	5.98×10^6	27	9.78×10^6
7	22	5.88×10^6	23	5.77×10^6	26	5.21×10^6	27	8.42×10^6
8	19	6.57×10^6	20	6.02×10^6	22	6.11×10^6	24	6.34×10^6
9	18	5.49×10^6	13	5.13×10^6	12	5.26×10^6	14	6.88×10^6
10	8	4.32×10^6	8	6.27×10^6	4	4.25×10^6	9	9.14×10^6
11	3	4.91×10^6	3	1.02×10^7	1	4.32×10^6	2	6.02×10^6
12	1	7.00×10^6	0		0		0	0

A Zeiss DSM 960 scanning electron microscope (SEM) was used to provide a three-dimensional high-resolution visualization of the tubercles across the bat ear and the surface of a single tubercle. Figure 2 is a composite SEM photograph of the leading edge of the left bat ear showing the relative position and shape of the ear tubercles. The topography of a single tubercle is shown in SEM photographs in Fig. 3a, and the microtubercles on the tubercle and their arrangement are shown in Fig. 3b.

Figure 2. Scanning electron microscope composite photograph of a *Tadarida brasiliensis* right ear tubercles 1-9.

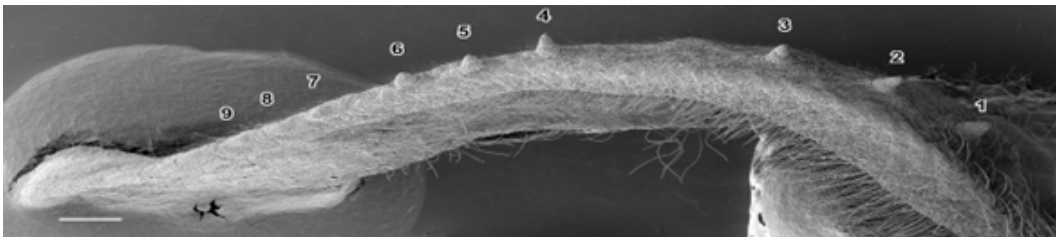

Figure 3. Scanning electron microscope of (a) a single tubercle and (b) the surface of a tubercle showing arrangement of micro-tubercles across the tubercle surface.

a.

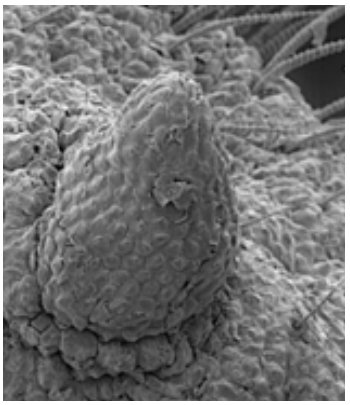

b.

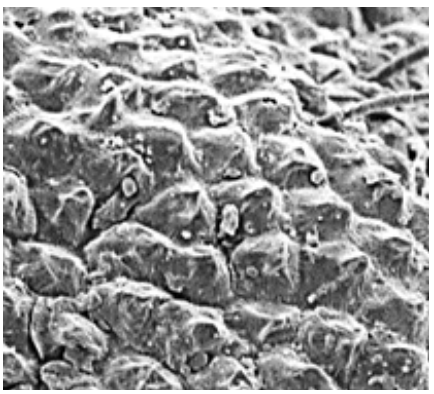

Discussion

Fish and Battle (1995), Fish (2002), Fish et al. (2011) and Miklosovic et al. (2004) describe the leading-edge tubercles on humpback whale (*Megaptera novaeanglia)* flippers. The tubercles help delay the stall angle, decrease drag, and maintain lift of the flippers at high angles of attack, allowing for greater maneuverability. Thus, the humpback whale can make more extreme banking and turning maneuvers during its feeding bouts in comparison to other whale species (Jurasz and Jurasz 1979; Hain et al. 1982). Based on the observed similarity between humpback whale flippers and the Brazilian Free-tailed bat tubercles, we propose that bat ear tubercles may serve an aerodynamic function similar to the hydrodynamic function of tubercles on the pectoral flippers of humpback whales.

The function of the leading-edge tubercles on *Tadarida* ears during exit flights from roosts, while foraging, and during steep returning dives to roosts might increase our understanding of *Tadarida* flight and morphological features. Petrin et al. (2018) used flow visualization studies of the wake behind a model *Tadarida brasiliensis* ear with and without tubercles to demon-

strate that tubercles influence lift and drag during flight and suggested they serve a similar function as tubercles on the leading edge of the pectoral flippers (Fig. 4a.) of the humpback whale. The tubercles seemingly allow bats to delay or stall more gradually at higher angles of attack (Petrin et al. 2018), as is the case with whales (Miklosovic et al. 2004; van Nierop et al. 2008).

Figure 4. Leading edge tubercles (a) on the pectoral flipper of the humpback whale *Megaptera novaeangliae* (*Humpback Stellwagen* by Whit Welles, under a CC-BY 3.0) and (b) the ear of the Brazilian Free-tailed Bat, *Tadarida brasiliensis*.

a.

b.

The fastest flight speed recorded for an animal in horizontal flight (up to 160 km/hr) was documented in *Tadarida brasiliensis* in 2016 (McCracken et al. 2016). The long, narrow wings of *Tadarida* are aerodynamically designed for high wing loading and high aspect ratios, but do not provide enough lift at slower speeds for the bat to take off directly from a surface and fly to foraging areas, sometimes as far as 50 km away (Best and Geluso 2003). To begin flight, they usually drop from a high roosting site and freefall for several meters to build up speed before the wings generate enough lift to pull out of the drop. During these initial slower speeds, the ear tubercles probably help generate lift until the bat gains the speed necessary to produce sufficient lift via the wings. Ground and radar tracking have documented *T. brasiliensis* at altitudes up to 3,000 m and covering 100 km in one night (Williams et al. 1973). Long, narrow wings are obviously important for rapid long-distance travel, but the presence of ear tubercles may also contribute to their high flying, rapid flight adaptation. Martin (2017) reported that *T. brasiliensis* tubercles serve to reduce drag at low angles of attack and increase drag at high angles of attack. Also, airfoil models revealed bat ear tubercles delayed stall, making the ears the likely flow control structure during free fall (Petrin et al. 2018).

Another flight behavior that probably involves the ear tubercles are the tight counterclockwise circling turns (slower in speed in comparison to normal high-altitude flight) inside the cave opening prior to exiting. Although the reason for counterclockwise flight inside caves is not well understood, the loops have a sharp turn radius somewhat analogous to the tight feeding turns and loops made by humpback whales during bubble net feeding (Fish and Battle 1995, Fish 2002, Fish et al. 2011, Miklosovic et al. 2004). After the circling turns, the bats emerge from the roost and usually climb to higher altitudes around 3,000 m (Williams et al. 1973; McCracken et al. 2021).

The ear tubercles likely aid bats aerodynamically during foraging flights for diverse prey including fast-flying moths, beetles, and slower-moving swarms (Easterla and Whitaker 1972; Whitaker 1996; McWilliams 2005). Considerable flight maneuverability which involves changes in lift and drag is required to capture the prey.

In many situations *Tadarida* return from foraging at high altitudes (Williams et al. 1973; Horn and Kunz 2008) and perform steep re-entry flights at close proximity to conspecifics (Wilkins 1989). They often drop perpendicular to the ground from altitude (Pudlo and Kloepper 2019) at speeds in excess of 128–158 km/h (Davis et al. 1962; Pudlo and Kloepper 2019) and make sharp

turns to enter the roost (Kloepper and Kinniry 2018; Williams *et al.* 1973). The leading-edge tubercles are probably associated with positional control and orientation during these returns to the cave. This pattern of free-falling return flights has been described in bats at Carlsbad Caverns, New Mexico (Hill and Smith 1984). The bats approach the cave at an altitude of 300–400 m, fold their wings and plummet to about 2 m off the ground before reopening their wings and entering the cave (Hill and Smith 1984). The bats would need aerodynamic control of flight as they near the roost opening and coordinate a sharp turn to enter the roost while avoiding collision with conspecifics (Theriault et al. 2010; Kloepper and Kinniry 2018; Wilkins 1989). Hubel et al. (2012) examined changes in kinematics and aerodynamics of *Tadarida* over a range of speeds, but future studies focused on the ear tubercles might help understand this complex flight behavior during re-entry or when flying close to conspecifics. Bats can adjust echolocation calls during these high-speed roost reentries (Pudlo and Kloepper 2019).

These various flight maneuvers employed by *Tadarida* are energetically costly. *Tadarida* encounters a variety of thermal environs while transitioning from roost sites to high altitudes and during returns. To help maintain a stable body temperature, the bats regulate some of the heat generated during flight via thermal windows (Reichard et al. 2010; Reichard and Fellows 2010; Reichard et al. 2012). The ear tubercles increase the surface area of the bat and might also aid in thermoregulation. A histological examination of blood circulating to and from the tubercles might reveal possible heat retention and dissipation functions.

The microanatomy of microtubercles and the apparent hexagonal arrangement on the surface of the tubercles, visible in the electron microscopic images (Fig. 3), has not been investigated nor has the possible functional significance. In some vertebrates, skin cells appear to have a packing geometry that has been described as a flattened version of a 14-sided shape called a tetrakaidecahedron (Yokouchi et al. 2016) which allows cells to tightly interlock, providing a strong cohesive barrier. Thus, the apparent geometrical arrangement of the microtubercles (Fig. 3) on the *Tadarida* tubercles might provide dense cell packing with minimal space between them which could provide structural stability, prevent water loss, and protect the bat from germicidal substances.

The microtubercles on the bat ears also have small hairs interspersed among them (Fig. 3) which might serve as sensory hairs. Similar structures referred to as Merkel cell-containing domes and hairs have been described on bat wings which allow bats to sense and detect airflow across the wing surface (Jones 2011; Marshall et al. 2015). These would aid in better maneuverability during flight, in capturing flying prey, and in navigating complex environments. A histological examination of the ear tubercles might help in understanding the function of the hairs and possible other functions.

A survey of natural history museum specimens and examination of closeup images of bats in the Family Molossidae revealed ear tubercles are present on some but not all species of mollosid bats. Wilson and Mittermeier (2019) recognized 22 genera comprised of 126 species in Family Molossidae and of these, more than one species in each of the following genera had ear tubercles present: *Chaerephon*, *Eumops*, *Mops*, *Nyctinomops*, *Otomops*, and *Tadarida*. Ear tubercle functions may be similar among the species having them and comparisons of roosting, foraging, and flight behaviors of the species with and without the tubercles could be insightful.

Acknowledgments

The authors thank Eileen Parks and Kerstin Allison, students from the University of Central Oklahoma, for assistance in making morphological measurements. Brian R. Elbing, Trevor Martin, and Christopher Petrin with the School of Mechanical and Aerospace Engineering at Oklahoma State University conducted the aerodynamic analysis of bat ear tubercles. The Samuel Roberts Noble Microscopy Laboratory at the University of Oklahoma provided SEM photographs of the tubercles. We are grateful to the collaborators that helped with this study.

References

Best TL, Geluso KN. 2003. Summer foraging range of Mexican free-tailed bats (*Tadarida brasiliensis mexicana*) from Carlsbad Cavern, New Mexico. Southwestern Naturalist 48:590-596.

Caire W, Loucks LS, Haynie ML. 2024. Mammals of Oklahoma, second edition. Norman (OK): University of Oklahoma Press. 672 p.

Davis RB, Herreid CF, Short HL. 1962. Mexican free-tailed bats in Texas. Ecological Monographs 32:311–346.

Easterla DA, Whitaker J. 1972. Food habits of some bats from Big Bend National Park, Texas. Journal Mammalogy 53:887–890.

Fish FE. 2002. Balancing requirements for stability and maneuverability in cetaceans. Integrative and Comparative Biology 42:85–93.

Fish FE, Battle JM. 1995. Hydrodynamic design of the humpback whale flipper. Journal of Morphology 225:51–60.

Fish FE, Weber PW, Murray MM, Howle LE. 2011. The tubercles on humpback whales' flippers: application of bio-inspired technology. Integrative and Comparative Biology 51:203–213.

Hain JHW, Carter GR, Kraus SD, Mayo CA, Winni HE. 1982. Feeding behavior of the humpback whale, *Megaptera novaeangliae,* in the western north Atlantic. Fishery Bulletin 80:259–268.

Hill JE, Smith JD. 1984. Bats: a natural history. Austin (TX): University of Texas Press. 243 p.

Horn JW, Kunz TH. 2008. Analyzing NEXRAD doppler radar images to assess nightly dispersal patterns and population trends in Brazilian free-tailed bats (*Tadarida brasiliensis*). Integrative and Comparative Biology 48:24–39.

Hubel TY, Hristov NI, Swartz SM, and Breuer KS. 2012. Changes in kinematics and aerodynamics over a range of speeds in *Tadarida brasiliensis*, the Brazilian free-tailed bat. Journal Royal Society Interface 9:1120–1130.

Jurasz CM, Jurasz VP. 1979. Feeding modes of the humpback whale, *Megaptera novaeangliae*, in southeast Alaska. Scientific Reports of the Whales Research Institute 31:69–83.

Jones G. 2011. Sensory biology: Bats feel the air flow current. Current Biology 21:666–667.

Kloepper LN, Kinniry M. 2018. Recording animal vocalizations from a UAV: bat echolocation during roost re-entry. Scientific Reports 8:7779.

Marshall KL, Chadha M, deSouza LA, Sterbing-D'Angelo SJ, Moss CF, Lumpkin EA. 2015. Somatosensory substrates of flight control in bats. Cell Reports 11:851–858.

Martin T. 2017. Flow modification by tubercles in Brazilian free-tailed bats [MSc thesis]. Stillwater (OK): Oklahoma State University. Available from: OSU Library.

McCracken GF, Safi K, Kunz TH, Dechmann DKN, Swartz SM, and Wikelski M. 2016. Airplane tracking documents the fastest flight speeds recorded for bats. Royal Society Open Science 3:1–10.

McCracken GF, Lee YF, Gillam EH, Frick W, Krauel J. 2021. Bats flying at high altitudes. In: Lim BK, Brock Fenton M, Brigham MR, Mistry S, Kurta A, Gillam EH, Russell A, Ortega J editors. 50 years of bat research. New York: Springer. pp 189–205.

McWilliams LA. 2005. Variation in diet of the Mexican free-tailed bat (*Tadarida brasiliensis mexicana*). Journal of Mammalogy 86:599–605.

Miklosovic DS, Murray MM, Howle LE, Fish FE. 2004. Leading-edge tubercles delay stall on humpback whale (*Megaptera novaeangliae*) flippers. Physics of Fluids 16: 39–42.

Petrin CE, Caire W, Thies M, Elbing BR, Martin T. 2018. Modification of drag on the ear of Brazilian free-tailed bats (*Tadarida brasiliensis*) via leading-edge tubercles. 2018 Fluid Dynamics Conference.

Pudlo A, Kloepper LN. 2019. Echolocation adap-

tations during high-speed roost re-entry for Brazilian free-tailed bats (*Tadarida brasiliensis*). Journal of Acoustical Society of America 145:EL1–EL6.

Reichard JD, Fellows SR. 2010. Thermoregulation during flight: body temperature and sensible heat transfer in free-ranging Brazilian free-tailed bats (*Tadarida brasiliensis*). Physiological and Biochemical Zoology 83:885–897.

Reichard JD, Prajapati SI, Austad SN, Keller C, Kunz. 2010. Thermal windows on Brazilian free-tailed bats facilitate thermoregulation during prolonged flight. Integrative and Comparative Biology 50:358–570.

Reichard JD, T.H. Kunz, C. Keller, and S.I. Prajapati. 2012. Vascular contrast enhanced micro-CT imaging of ‘‘radiators’’ in the Brazilian free-tailed bat (*Tadarida brasiliensis*). The Anatomical Record 295:563–566.

Theriault D, Wu Z, Hristov N, Swartz S, Breuer K, Kunz T, Betke M. 2010. Reconstruction and analysis of 3D trajectories of Brazilian free-tailed bats in flight. CS Department, Boston University.

van Nierop EA, Alben S, Brenner MP. 2008. How bumps on whale flippers delay stall: an aerodynamic model. Physical Review Letters 100:5–8.

Welles W. 2007. *Humpback Stellwagen* [Photograph]. Wikimedia Commons (CC BY 3.0). Available online at: https://commons.wikimedia.org/w/index.php?curid=2803881. Accessed 14 January 2026.

Whitaker Jr JO. 1996. Dietary variation in the Mexican free-tailed Bat (*Tadarida brasiliensis mexicana*). Journal of Mam malogy 77:716.

Wilkins KT. 1989. *Tadarida brasiliensis.* Mammalian Species 331:1–10.

Williams TC, Ireland LC, Williams JM. 1973. High altitude flights of the free-tailed bat, *Tadarida brasiliensis*, observed with radar. Journal of Mammalogy 54:807–821.

Wilson DE, Mittermeier RA (Eds). 2019. Handbook of the Mammals of the World: Vol 9, Bats. Barcelona (Spain): Lynx Edicions. 1008 p.

Yokouchi M, Atsugi T, Logtestijn MV, Tanaka RJ, Kajimura M, Suematsu M, Furuse M, Amagai M, Kubo A. 2016. Epidermal cell turnover across tight junctions based on Kelvin’s tetrakaidecahedron cell shape. Elife, 5, p.e19593.

Writing Scaffolding Introduction and Effectiveness Across Chemistry Curriculum

Stephanie L. Skiles-Jones*
University of Central Oklahoma, Chemistry Department, Edmond, OK 73034

Eric S. Eitrheim
University of Central Oklahoma, Chemistry Department, Edmond, OK 73034

Cheryl Frech
University of Central Oklahoma, Chemistry Department Emeritus, Edmond, OK 73034

Luis D. Montes
Rose State College, Division of STEM, Midwest City, OK 73110

Tracy Morris
University of Central Oklahoma, Mathematics and Statistics Department, Edmond, OK 73034

Dallas G. New
University of Central Oklahoma, Chemistry Department, Edmond, OK 73034

Amanda L. Waters
University of Central Oklahoma, Chemistry Department, Edmond, OK 73034

Abstract: Scientific writing is essential for students' future success in STEM careers, yet many chemistry and other science majors receive little formal instruction in writing. Scientific writing is a critical skill for student success in STEM fields, yet formal instruction in writing remains limited across many chemistry programs. To address this gap, a comprehensive writing support system—referred to here as "writing scaffolding"—was instituted department-wide throughout the entire chemistry curriculum, spanning from students' first year through graduation and aligning with the degree plan as students progress through their coursework. In this context, "writing scaffolding" refers to an integrated, multi-course strategy that introduces, reinforces, and assesses scientific writing through structured support at each curricular level. This initiative includes three key components: an introductory course schedule, a shared departmental writing style guide, and standardized rubrics for major writing sections. The formal rollout began with instructors taking responsibility for introducing different components of scientific writing (such as abstracts, introductions, and discussions) and modeling disciplinary norms for structure and tone. Students receive multiple rounds of feedback on newly introduced sections, while

*Corresponding author: sjones116@uco.edu
Proc. Okla. Acad. Sci. 105: pp 96-103 (2025)

earlier writing skills are reinforced in later courses. This study assessed the effectiveness of the scaffolding effort midway through implementation, focusing on writing outcomes in Quantitative Chemical Analysis. Student work from before and after implementation was blindly reevaluated in triplicate by faculty using the new rubrics. Rubric criteria included clarity of writing, appropriate structure, use of scientific tone, and integration of data. Statistical analysis of the scores was used to determine the impact of the writing scaffolding. Results showed a modest improvement, with average scores increasing from 6.7 ± 1.4 (n=65) to 8.1 ± 1.0 (n=48) on a 10-point scale following implementation. The most notable improvements were in structural organization and clarity of discussion sections.

Introduction

Writing is a fundamental part of scientific literacy, which encompasses the ability to read, write, and speak about scientific concepts in an informed, critical, and communicative way (Howell and Brossard, 2021; Shaffer et al., 2019). In chemistry education, however, writing instruction is often underemphasized in favor of content mastery and theoretical understanding (Durst and Newell, 1989). Developing students' linguistic and rhetorical skills—particularly through reading and writing scientific texts—can support deeper comprehension and critical engagement with scientific material (Glynn and Muth, 1994). Effective strategies to improve student writing in chemistry have included peer instruction (Golde et al., 2006), progressive writing assignments,(van de Pol et al., 2010) and single-course scaffolding with peer review (Weaver et al., 2014). More comprehensive approaches that scaffold writing across the curriculum have shown promise in chemistry and other STEM disciplines (Cohen and Williams, 2019; Klein and Aller, 1998; Whitaker and Reimer, 2019).

Beyond academia, employers consistently rank communication and critical thinking among the top skills they seek in college graduates (Ater Kranov and Khalaf, 2016; Morreale et al., 2017; Stevens, 2005; Stevens et al., 2019). These abilities are closely tied to scientific writing, which requires clarity, logical reasoning, and the ability to synthesize and present information (Paul and Elder, 2020). Yet, instruction in writing and peer review is often unstructured, inconsistently implemented, or overlooked entirely in STEM curriculum (Cho and Schunn, 2007; Kramer et al., 2022; Puntambekar and Hubscher, 2005). Kramer emphasizes the importance of timing and structure in peer review, showing that students' perception of authority and their capacity for critical thinking evolve over time. Structured feedback is more impactful when paired with intentional, developmentally appropriate writing assignments (Kramer et al., 2022).

In response to these needs, the Department of Chemistry at the University of Central Oklahoma (UCO) launched a curriculum-wide scientific writing scaffolding initiative. The program was designed to embed scientific writing instruction consistently and progressively across the chemistry major. Instructors were responsible for introducing, modeling, and assessing different sections of scholarly writing—such as abstracts, methods, results, and discussions—throughout the curriculum. A universal set of rubrics was developed to assess each section, helping to standardize expectations and reduce inconsistencies in grading and feedback across courses (Cockett and Jackson, 2018; Finkenstaedt-Quinn et al., 2019; Weaver et al., 2014).

An introduction timeline to academic writing has been established to align with the most common student path through the chemistry curriculum. This timeline is designed to have students producing full, journal-style reports by their fifth semester in the department. Courses involved in the scaffolding are required for the chemistry major and include both traditional content/lab pairings—such as General Chemistry, Organic Chemistry, and Physical Chemistry—as well as department-specific offerings like Professionalism in Chemistry, Directed Research, and Capstone.

Each course introduces specific sections of scientific writing, with expectations build-

ing as students advance. Early courses focus on writing basic abstracts, tables, and results sections, while upper-division courses emphasize full-length scientific papers, literature searches, and oral/poster presentations. Students receive guided feedback and complete multiple rounds of revision, in line with departmental guidelines. Instructors may structure this as three rounds of feedback on a single assignment or one round of feedback across three separate assignments.

All writing assignments are scored using department-wide rubrics developed collaboratively by faculty and vetted by the curriculum committee. These rubrics have helped standardize instruction, reduce variability across instructors, and minimize student confusion around expectations. Table 1 outlines the scaffolding sequence and identifies the writing components introduced in each course.

Individual chemistry courses are listed along with the writing sections introduced in each. These sections were emphasized throughout the semester with multiple rounds of feedback. Sections from previous semesters were also included, though they may not have undergone the same level of feedback in those courses.

A pilot of this program began the semester before full departmental implementation with two sections of General Chemistry I Laboratory. Full implementation of the writing scaffolding program began in the following semester. After three years, all required courses in the chemistry major were participating in the initiative, and students were consistently producing journal-style writing and oral presentations by their junior year.

While this scaffolding structure was carried through to students' final year—including senior projects such as Capstone and Directed Research—quantitative evaluation of senior-lev-

Table 1. Individual chemistry courses are found within each cell above. Writing sections listed under the course are those which are introduced in the curriculum for that course. Courses continue to practice skills taught in prior semesters in the table.

1st Semester	General Chemistry 1 Lab *Abstract *Calculations/Tables		
2nd Semester	General Chemistry 2 Lab *Results *Procedures		Professionalism in Chemistry 1 *Literature Search
3rd Semester	Quantitative Analysis *Equation Editor *Discussion *Conclusions *Proper Lab Notebook *Oral Presentation	Organic 1 Lab *Methods *Chem Draw/ Biovia *Mechanisms *Discussions *Proper Lab Notebook	
4th Semester	Instrumental Analysis *Introduction *Methods	Organic 2 Lab *Introductions *Conclusions	Professionalism in Chemistry 2 *Citations *Poster Presentations
5th Semester	Experimental Physical Chemistry Lab *Electronic Notebook *Full Reports	Experimental Biochemistry Lab *Full Reports	Inorganic Chemistry Lab *Full Reports
6th Semester	Directed Research *Full Report *Oral Presentations	Capstone *Full Report *Oral Presentation	

el writing has proven difficult due to variability in project formats and the relatively small number of students completing each course in a given year. However, faculty have noted a clear improvement in the overall quality and clarity of student writing in these upper-division experiences. Anecdotally, the department believes that students are graduating with stronger writing skills, better rhetorical awareness, and greater confidence in scientific communication.

This study presents a mid-program assessment of the initiative, focusing on writing outcomes in Quantitative Chemical Analysis (CHEM 2104). The goal was to determine whether the scaffolded writing instruction had a measurable impact on student writing and to identify specific areas of strength or continued need.

Methods

This project evaluated the effectiveness of a department-wide writing scaffolding initiative by analyzing student laboratory reports from the Quantitative Chemical Analysis Laboratory course. While the scaffolding process was already embedded across the curriculum, this study focused specifically on measuring its impact on students' writing performance.

Lab reports submitted prior to the implementation of the scaffolded writing approach were compared with those submitted post-implementation. Because electronic submission of lab reports has been standard for several years, a substantial archive of student work was available for analysis. These archived reports were deidentified and randomly mixed with current reports written under the scaffolding model to eliminate potential reviewer bias. All feedback was scored using department-approved rubrics, and reports were anonymized prior to evaluation. This project was reviewed and approved by the University of Central Oklahoma Institutional Review Board (IRB) as IRB Exempt, ensuring compliance with ethical standards for research involving student work.

A total of 136 lab reports were included in the study. Each report was scored independently by either three (n = 74) or four (n = 62) randomly selected reviewers. Reviewers consisted of UCO Chemistry Department faculty members trained in using the department's universal rubrics.

Each report was evaluated using a detailed rubric that included ten subscores, each rated on a 1–5 scale, with 5 being the highest. The rubric grouped scoring criteria into three primary sections:

- Abstract: including Purpose, General Methodology, and Major Results;
- Results and Discussion: including Results Presentation, Data Tables, Discussion of Logic Behind Calculations, and Discussion of Data Quality/Error Analysis;
- Formatting: including Appropriate Length, Formatting, and Spelling and Grammar.

In addition to the ten section scores, each report also received one overall score rated on a 1–10 scale, with 10 being the highest.

Each report received quadruplicate scoring wherever possible, aligning with best practices in multi-rater reliability (Rosenthal and Rosnow, 2008). Scores for each section were averaged, and both subsection scores and overall scores were analyzed statistically. Independent samples t-tests assuming unequal variances were used to compare mean scores before and after implementation of the writing scaffolding. Cohen's d was calculated to determine effect sizes, with p-values < 0.05 considered statistically significant and $d > 0.8$ considered a large effect. All statistical analysis was conducted using R version 4.2.0.

Results and Discussion

To assess the effectiveness of the department-wide scientific writing scaffolding initiative, student lab reports from the Quantitative Chemical Analysis course were evaluated using

a standardized rubric. These reports, collected before (n = 62) and after (n = 74) the implementation of the scaffolding program, were assessed across ten rubric categories and an overall score. Summary statistics are presented in Table 2, and boxplots for subscores and overall scores are shown in Figures 1 and 2.

Table 2. Comparison of mean lab report scores before and after implementation of the department-wide writing scaffolding program. Scores represent averages across ten rubric categories (each rated on a 1–5 scale) and one overall score (rated on a 1–10 scale). Statistically significant improvements were observed in all categories post-implementation, with large effect sizes in most cases (Cohen's d > 0.8).

	Before	After			
	(*n* = 62)	(*n* = 74)			
Category	mean (sd)	mean (sd)	*t*	*p*-value	effect size
Purpose	3.76 (0.62)	4.25 (0.40)	5.38	<0.001	0.94
General Methodology	3.53 (0.75)	4.05 (0.50)	4.66	<0.001	0.82
Major Results	3.63 (0.76)	4.10 (0.45)	4.28	<0.001	0.75
Results	3.37 (0.64)	4.14 (0.43)	8.12	<0.001	1.42
Data Tables	3.63 (0.64)	4.33 (0.37)	7.50	<0.001	1.32
Discussion of Logic	3.14 (0.72)	4.19 (0.46)	9.88	<0.001	1.73
Discussion of Data Quality	3.04 (0.76)	3.94 (0.51)	7.85	<0.001	1.37
Appropriate Length	3.36 (0.70)	4.48 (0.28)	11.83	<0.001	2.10
Appropriate Formatting	3.54 (0.55)	4.30 (0.36)	9.27	<0.001	1.62
Spelling & Grammar	3.69 (0.47)	4.09 (0.43)	5.14	<0.001	0.89
Overall Score	6.74 (1.07)	8.02 (0.74)	7.96	<0.001	1.39

b. ACS scores

	Before	After			
	(*n* = 103)	(*n* = 82)			
	mean (sd)	mean (sd)	*t*	*p*-value	effect size
ACS Scores	23.8 (5.85)	24.4 (6.72)	0.61	0.543	0.09

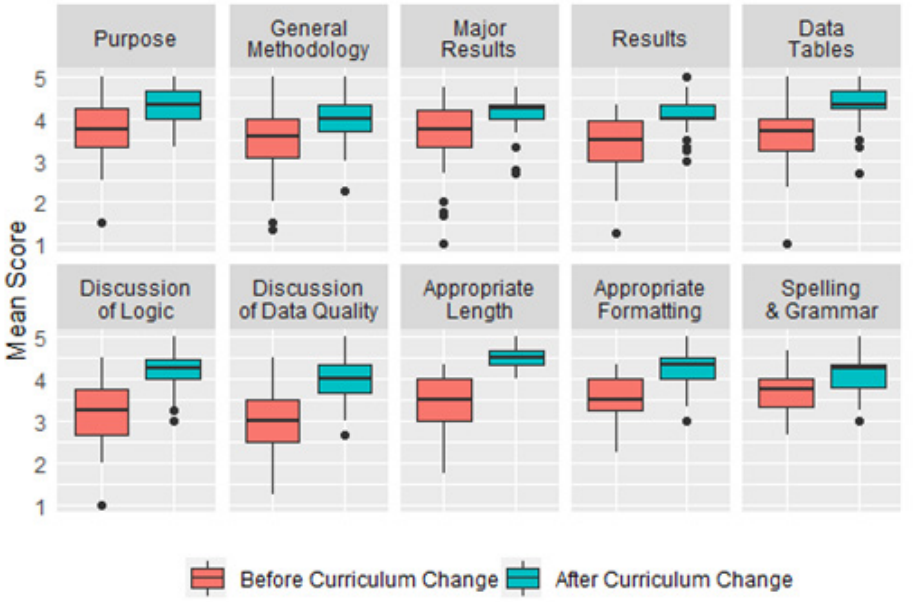

Figure 1. Boxplots of sub scores for each of the categories scored on a 1-5 scale with 5 being the highest.

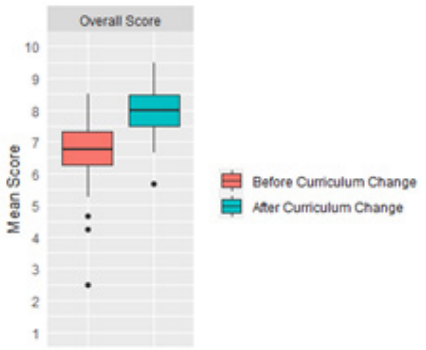

Figure 2. Boxplots of overall scores

The analysis revealed statistically significant improvements across all rubric categories. Post-scaffolding reports scored significantly higher in all ten subscores and in the overall score ($p < 0.001$ for all comparisons). Effect sizes (Cohen's d) were large for all but one category, suggesting the improvements were not only statistically significant but also educationally meaningful.

One of the most striking trends was the marked improvement in writing elements requiring higher-order cognitive skills. The Discussion of Logic (effect size d = 1.73), Appropriate Formatting (d = 1.62), and Discussion of Data Quality (d = 1.37) categories all showed large gains. These areas are often the most challenging for students and typically benefit the most from repeated exposure, guided practice, and targeted feedback—all key features of the scaffolding model. Students seemed to gain a better grasp of how to explain their reasoning and address sources of error, indicating a deeper understanding of experimental context and implications.

The Appropriate Length category showed the single largest effect size (d = 2.10), suggesting students became much more adept at adhering to structural expectations. This likely reflects the influence of department-wide formatting norms and clear expectations reinforced consistently across courses. Similarly, improvements in Spelling and Grammar (d = 0.89) and Major Results (d = 0.75), though less dramatic, still point to improved clarity and communication over time.

The overall score increased from a mean

of 6.74 (±1.07) before the curriculum change to 8.02 (±0.74) after implementation, with a large effect size (d = 1.39). These findings suggest that the writing scaffolding program has had a broad and positive impact on student writing competency, particularly in their ability to structure and articulate scientific arguments.

In contrast, the analysis of ACS Analytical Exam scores did not show a statistically significant difference between the pre- and post-scaffolding groups (Table 2b; Figure 3). The average scores rose slightly from 23.8 (±5.85) to 24.4 (±6.72), but the effect size was negligible (d = 0.09, p = 0.543). This outcome is not unexpected, as the ACS exam emphasizes chemistry content knowledge rather than communication skills. The lack of change in ACS performance reinforces that gains observed in writing were likely due to the scaffolding initiative rather than a broader shift in overall academic performance.

Although formal data collection in senior-level courses was limited, anecdotal feedback from faculty indicates that writing quality in capstone and research-based courses has improved. In Capstone for Chemistry and Directed Research courses, faculty have noted that students enter with stronger foundational skills, are better prepared to articulate their work in writing, and require less remedial instruction in basic formatting and structure. The variability of senior projects—ranging from experimental reports to community outreach projects to literature reviews—made systematic rubric scoring difficult. However, the department's collective impression is that the scaffolding program has led to greater consistency and confidence in student writing at the senior level.

These anecdotal observations align well with broader research on disciplinary writing development. Studies have shown that peer review and structured writing interventions benefit students differently depending on their academic maturity (Kramer et al., 2022). Lower-division students tend to show the greatest gains in writing mechanics, while upper-division students develop more advanced skills such as synthesis and critical evaluation. Our results from the Quantitative Chemical Analysis course reflect this pattern, with middle-stage students showing significant growth in both foundational and analytical writing dimensions

Overall, this project supports the value of a consistent, department-wide writing scaffold. By explicitly introducing different sections of scientific writing across multiple courses, using shared rubrics, and requiring multiple rounds of revision, students are better equipped to engage in scientific communication. Importantly, this approach appears to be effective without negatively impacting other learning goals, such as content knowledge.

Looking forward, the department plans to continue refining rubric language, encouraging faculty development around writing instruction, and exploring ways to extend more structured peer review into upper-division courses. With time and consistent application, the scaffolding initiative is expected to further close the gap between novice and expert writers, ultimately producing graduates who can communicate their scientific knowledge with clarity and professionalism.

References

Ater Kranov, A., Khalaf, K., 2016. Investigating the employment gap: What employers want from engineering graduates. https://doi.org/10.1109/EDUCON.2016.7474708

Cho, K., Schunn, C.D., 2007. Scaffolded writing and rewriting in the discipline: A web-based reciprocal peer review system. Comput. Educ. 48, 409–426. https://doi.org/10.1016/j.compedu.2005.02.004

Cockett, A., Jackson, C., 2018. The use of assessment rubrics to enhance feedback in higher education: An integrative literature review. Nurse Educ. Today 69, 8–13. https://doi.org/10.1016/j.nedt.2018.06.022

Cohen, A.J., Williams, A.L., 2019. Scalable, scaffolded writing assignments with online peer review in a large introductory economics course. J. Econ. Educ. 50,

371–387.

Durst, R., Newell, G., 1989. The Uses of Function: James Britton's Category System and Research on Writing. Rev. Educ. Res. - REV EDUC RES 59. https://doi.org/10.2307/1170204

Finkenstaedt-Quinn, S., Snyder-White, E., Connor, M., Gere, A., Shultz, G., 2019. Characterizing Peer Review Comments and Revision from a Writing-to-Learn Assignment Focused on Lewis Structures. J. Chem. Educ. 96. https://doi.org/10.1021/acs.jchemed.8b00711

Glynn, S.M., Muth, K.D., 1994. Reading and writing to learn science: Achieving scientific literacy. J. Res. Sci. Teach. 31, 1057–1073. https://doi.org/10.1002/tea.3660310915

Golde, M.F., McCreary, C.L., Koeske, R., 2006. Peer Instruction in the General Chemistry Laboratory: Assessment of Student Learning. J. Chem. Educ. 83, 804. https://doi.org/10.1021/ed083p804

Howell, E.L., Brossard, D., 2021. (Mis)informed about what? What it means to be a science-literate citizen in a digital world. Proc. Natl. Acad. Sci. 118, e1912436117. https://doi.org/10.1073/pnas.1912436117

Klein, B., Aller, B.M., 1998. Writing Across the Curriculum in College Chemistry: A Practical Bibliography. Lang. Learn. Discip. 2, 25–35. https://doi.org/10.37514/LLD-J.1998.2.3.03

Kramer, T.J., Zeccardi, J., Emhoff, C.-A., Williams, C., Dunn, R., Rose, J., 2022. How Timing and Authority in Peer Review Impact STEM Students: A Comparative Assessment of Writing and Critical Thinking in Kinesiology Courses. Discip. 18, 305–319. https://doi.org/10.37514/ATD-J.2022.18.3-4.06

Morreale, S.P., Valenzano, J.M., Bauer, J.A., 2017. Why communication education is important: a third study on the centrality of the discipline's content and pedagogy. Commun. Educ. 66, 402–422. https://doi.org/10.1080/03634523.2016.1265136

Paul, R., Elder, L., 2020. The miniature guide to critical thinking: concepts and tools, Eighth edition. ed, Thinker's guide library. Rowman & Littlefield, Lanham Boulder New York London.

Puntambekar, S., Hubscher, R., 2005. Tools for Scaffolding Students in a Complex Learning Environment: What Have We Gained and What Have We Missed? Educ. Psychol. 40, 1–12. https://doi.org/10.1207/s15326985ep4001_1

Rosenthal, R., Rosnow, R.L., 2008. Essentials of behavioral research: methods and data analysis, 3. ed. ed, McGraw-Hill higher education. McGraw-Hill, Boston.

Shaffer, J.F., Ferguson, J., Denaro, K., 2019. Use of the Test of Scientific Literacy Skills Reveals That Fundamental Literacy Is an Important Contributor to Scientific Literacy. CBE—Life Sci. Educ. 18, ar31. https://doi.org/10.1187/cbe.18-12-0238

Stevens, B., 2005. What Communication Skills Do Employers Want? Silicon Valley Recruiters Respond. J. Employ. Couns. 42. https://doi.org/10.1002/j.2161-1920.2005.tb00893.x

Stevens, S., Mills, R., Kuchel, L., 2019. Teaching communication in general science degrees: highly valued but missing the mark. Assess. Eval. High. Educ. 44, 1163–1176. https://doi.org/10.1080/02602938.2019.1578861

van de Pol, J., Volman, M., Beishuizen, J., 2010. Scaffolding in Teacher–Student Interaction: A Decade of Research. Educ. Psychol. Rev. 22, 271–296. https://doi.org/10.1007/s10648-010-9127-6

Weaver, C., Duran, E., Nikles, J., 2014. An Integrated Approach for Development of Scientific Writing Skills in Undergraduate Organic Lab, in: ACS Symposium Series. pp. 105–123. https://doi.org/10.1021/bk-2014-1180.ch008

Whitaker, L., Reimer, E., 2019. Scaffolding critical reflection across the curricula of a social welfare degree. Soc. Work Educ. 40, 1–13. https://doi.org/10.1080/02615479.2019.1687665

Analytical and Numerical Solutions of the Relativistic Schrödinger Differential Wave Equation

James H. McNeill, Natural Sciences Department, Middle Georgia State University, Macon, GA 31206, USA

James E. Bidlack*, Department of Biology, University of Central Oklahoma, Edmond, OK 73034, USA

Abstract: This paper discusses the relativistic Schrödinger differential wave equation for the hydrogen atom and hydrogen-like cations, which have measured ionization energies from hydrogen to the Cu^{28+} hydrogen-like cation. The analytical solution to the relativistic Schrödinger differential wave equation correlates with experimental data if the angular momentum quantum number $l > 0$. For quantum levels with $l = 0$, the analytical solutions predict ionization energy values larger than that measured for the hydrogen atom and hydrogen-like cations. Also, beyond the element erbium, $Z > 68$ for $l=0$ quantum states, the analytical solution yields energy values that are complex numbers. This is similar for the Dirac relativistic differential wave equation which fails for nuclei that have an atomic number larger than 137. Using measured 1*s* ionization energy values of hydrogen-like cations, a numerical solution to the relativistic Schrödinger differential wave equation is possible since an analytical one is not when the measured ionization energy is different from the analytical result. In addition, since the analytical solutions to the radial part of the relativistic Schrödinger differential wave equation are complicated, normalized numerical solutions are less difficult to obtain using Microsoft Excel. Most differential equations do not have analytical solutions, and, therefore, only numerical solutions are possible utilizing boundary or initial conditions.

Classical Schrödinger Differential Wave Equation and Wave-Particle Duality in Quantum Mechanics

The authors are a nuclear chemist and a plant physiologist, interested in the chemical physics of our natural world, with previous publications in this journal about similar topics (McNeill and Bidlack, 2018; McNeill et al., 2021). This paper focuses on the subtle effects of the *Special Theory of Relativity* (Einstein, 1905a; 1905b; 1905c; 1905d) upon atomic structure. As such, the larger the atomic number, Z, the greater the relativistic effect may be on how atoms exist.

The classical Hamiltonian for any particle in motion bound by a negative potential $-U$, such as the negative gravitational potential between a planet orbiting the sun, has a constant mechanical energy value E_m less than zero (Kleppner and Kolenkow, 2014). In classical Newtonian physics for a planet orbiting the sun, the total mechanical energy E_m is the kinetic energy $KE = \frac{1}{2}m_p v^2$, where m_p is the rest mass of the moving planet in kilograms and v is the speed or magnitude in units of meters per second of the planet's velocity vector $\mathbf{v}$ orbiting the sun, plus the energy value of the negative gravitational potential energy $-U$.

*Corresponding author: jbidlack@uco.edu

$$KE + (-U) = \frac{1}{2}m_p v^2 + \left(-\frac{GM_S m_p}{r}\right) = \frac{m_p^2 v^2}{2m_p} - \frac{GM_S m_p}{r} = \frac{p_p^2}{2m_p} - \frac{GM_S m_p}{r} = E_m < 0 \quad (1)$$

In Equation 1, the p_p^2 is the squared magnitude of the planet's momentum vector $\mathbf{p}_p = m_p\mathbf{v}$, M_s is the rest mass of the sun in kilograms, r is the separation distance in meters from the center-of-mass of the planet to that of the sun, and G is the gravitational constant which can only be measured to four significant figures.

$$G = 6.673 \times 10^{-11} \frac{\text{m}^3}{\text{kg s}^2} \text{ (Kleppner and Kolenkow, 2014)} \quad (2)$$

If the value of the mechanical energy E_m is equal to or greater than zero ($E_m \geq 0$), the planet is unbound and can escape from the negative potential of the sun's gravitational force due to sufficient kinetic energy of motion.

For the electron in the hydrogen atom, or hydrogen-like cations that have only one electron and more than one proton in the atomic nucleus, the negative gravitational potential is replaced in Equation 1 by the negative Coulomb potential between the negatively charged electron and the positively charged atomic nucleus.

$$\frac{p^2}{2m_e} - \frac{1}{4\pi\varepsilon_0}\frac{Zq^2}{r} = E_m \text{ where the negative potential } -U \text{ is } -U = -\frac{1}{4\pi\varepsilon_0}\frac{Zq^2}{r} \quad (3)$$

In the above equation, m_e is the measured mass of an electron at rest in kilograms

$$m_e = 9.10938 \times 10^{-31} \text{ kilogram (Tipler and Llewellyn, 2012)} \quad (4)$$

And ε_0 is the electrostatic permittivity of a vacuum which in MKS units is measured to be the numerical value shown below.

$$\varepsilon_0 = 8.854187817 \times 10^{-12} \frac{\text{Coulomb}^2\,\text{second}^2}{\text{kilogram meter}^3} \text{ (Tipler and Llewellyn, 2012)} \quad (5)$$

Z is the atomic number or number of protons in the atomic nucleus, and q is the measured magnitude of charge for both the electron and proton expressed in units of the Coulomb.

$$q = 1.602177 \times 10^{-19} \text{ Coulomb (Tipler and Llewellyn, 2012)} \quad (6)$$

In addition, r is the distance between the centers-of-mass of the electron and atomic nucleus in meters, analogous to the orbiting planet and sun in the gravitational potential.

In quantum mechanics, subatomic particles have wave-particle duality as photons of light (Tipler and Llewellyn, 2012). The wavelength λ, is directly proportional to the reciprocal of the magnitude $p = mv$ of the momentum vector $\mathbf{p} = m\mathbf{v}$ for any subatomic particle or a photon of light with Planck's constant h as the measured proportionality constant (numerical value from Tipler and

Llewellyn, 2012).

$$\lambda = \frac{h}{p} = \frac{h}{mv} \text{ and } h = 6.62607 \times 10^{-34} \text{ Joule seconds or } \frac{\text{kg m}^2}{\text{sec}} \text{ in meters, kilograms and seconds (MKS)units} \quad (7)$$

For the above equation, mass is in kilograms, speed in meters per second, and wavelength in meters. The time-independent wave function ψ for a freely moving subatomic particle or a photon of light is the real part of the next equation.

$$\psi = \psi(r) = e^{ikr} \text{ where } k = \frac{2\pi}{\lambda} = \frac{2\pi}{h}mv = \frac{p}{\hbar} \text{ and } \hbar = \frac{h}{2\pi} = 1.05457 \times 10^{-34} \frac{\text{kg m}^2}{\text{sec}} \text{ (Walker et al., 2014)} \quad (8)$$

Therefore, the second derivative of the wave function yields the following equation for the vector dot product of the momentum vector $\mathbf{p} \bullet \mathbf{p} = p^2$ of such a moving particle displaying wave-particle duality.

$$\frac{d^2\psi}{dr^2} = -\frac{p^2}{\hbar^2}\psi \quad \text{So } p^2\psi = -\hbar^2\frac{d^2\psi}{dr^2} \quad (9)$$

Thus, using the expression ψ for the wave function of an electron in a hydrogen atom or a hydrogen-like cation by the substitution of Equation 9 for the classical kinetic energy in Equation 3, one arrives at the classical Schrödinger differential wave equation for the single electron in a hydrogen atom or hydrogen-like cation.

$$-\frac{\hbar^2}{2m_e}\nabla^2\psi - \frac{1}{4\pi\varepsilon_0}\frac{Zq^2}{r}\psi = E_m\psi \quad (10)$$

In addition, the electron motion is a three-dimensional wave encircling the atomic nucleus, resulting in taking the double derivative of the wave function ψ with respect to each of the three rectangular coordinates *x, y,* and *z*. In Equation 10, ∇^2 is the following dot product of the vector operator $\boldsymbol{\nabla}$.

$$\nabla^2\psi = \boldsymbol{\nabla}\cdot\boldsymbol{\nabla}\psi = \left[\frac{\partial}{\partial x}\hat{\mathbf{x}} + \frac{\partial}{\partial y}\hat{\mathbf{y}} + \frac{\partial}{\partial z}\hat{\boldsymbol{z}}\right]\cdot\left[\frac{\partial}{\partial x}\hat{\mathbf{x}} + \frac{\partial}{\partial y}\hat{\mathbf{y}} + \frac{\partial}{\partial z}\hat{\boldsymbol{z}}\right]\psi = \frac{\partial^2\psi}{\partial x^2} + \frac{\partial^2\psi}{\partial y^2} + \frac{\partial^2\psi}{\partial z^2} \text{ (Walker et al., 2014)} \quad (11)$$

In the rectangular coordinate system with the center of the nucleus being at the origin, the magnitude for the distance between centers-of-mass of the electron and the atomic nucleus can be expressed as

$$r = (x^2 + y^2 + z^2)^{1/2} = \sqrt{x^2 + y^2 + z^2} \quad (12)$$

It is necessary to transform the ∇^2 operator into spherical-polar coordinates r, θ, and ϕ to obtain an analytical solution. First, there is the position vector **r**, with a magnitude equal to the separation distance from the center-of-mass of the atomic nucleus to the electron's center-of-mass, given in the next expression (Wangsness, 1986).

$$\mathbf{r} = r\hat{\mathbf{r}} = r[\cos\phi \sin\theta\, \hat{\mathbf{x}} + \sin\phi \sin\theta\, \hat{\mathbf{y}} + \cos\theta\, \hat{\mathbf{z}}] = r\cos\phi \sin\theta\, \hat{\mathbf{x}} + r\sin\phi \sin\theta\, \hat{\mathbf{y}} + r\cos\theta\, \hat{\mathbf{z}} \quad (13)$$

In Equation 13, $\hat{\mathbf{r}}$ is a unit vector like the orthonormal unit vectors $\hat{\mathbf{x}}$, $\hat{\mathbf{y}}$, and $\hat{\mathbf{z}}$ in rectangular coordinates. The angle between the z-axis and vector $\mathbf{r}$ is the spherical-polar coordinate θ. The angle between the projection of vector $\mathbf{r}$ ($r\sin\theta$) onto the xy-plane, at z=0, and the x-axis is ϕ.

Using the chain rule in differential calculus, $\nabla\psi$ is the following expression.

$$\nabla\psi = \left[\frac{\partial\psi}{\partial r}\frac{\partial r}{\partial x} + \frac{\partial\psi}{\partial\theta}\frac{\partial\theta}{\partial x} + \frac{\partial\psi}{\partial\phi}\frac{\partial\phi}{\partial x}\right]\hat{\mathbf{x}} + \left[\frac{\partial\psi}{\partial r}\frac{\partial r}{\partial y} + \frac{\partial\psi}{\partial\theta}\frac{\partial\theta}{\partial y} + \frac{\partial\psi}{\partial\phi}\frac{\partial\phi}{\partial y}\right]\hat{\mathbf{y}} + \left[\frac{\partial\psi}{\partial r}\frac{\partial r}{\partial z} + \frac{\partial\psi}{\partial\theta}\frac{\partial\theta}{\partial z} + \frac{\partial\psi}{\partial\phi}\frac{\partial\phi}{\partial z}\right]\hat{\mathbf{z}} \quad (14)$$

Table I displays the partial derivatives of each of the three spherical-polar coordinates with respect to each of the three rectangular coordinates. In addition to unit vector $\hat{\mathbf{r}}$, there are two additional unit vectors $\hat{\boldsymbol{\theta}}$ and $\hat{\boldsymbol{\phi}}$ in spherical-polar coordinates, and all three are likewise orthonormal as $\hat{\mathbf{x}}$, $\hat{\mathbf{y}}$, and $\hat{\mathbf{z}}$ in rectangular coordinates.

$$\hat{\boldsymbol{\theta}} = \frac{\partial\hat{\mathbf{r}}}{\partial\theta} = \cos\phi\cos\theta\, \hat{\mathbf{x}} + \sin\phi\cos\theta\, \hat{\mathbf{y}} - \sin\theta\, \hat{\mathbf{z}} \qquad \hat{\boldsymbol{\phi}} = \frac{1}{\sin\theta}\frac{\partial\hat{\mathbf{r}}}{\partial\phi} = -\sin\phi\, \hat{\mathbf{x}} + \cos\phi\, \hat{\mathbf{y}} \text{ (Wangsness, 1986)} \quad (15)$$

Table I Partial Derivatives of Spherical-Polar Coordinates with Respect to Rectangular Coordinates

$$\frac{\partial r}{\partial x} = \frac{\partial}{\partial x}\left[(x^2 + y^2 + z^2)^{1/2}\right] = \cos\phi \sin\theta$$

$$\frac{\partial r}{\partial y} = \frac{\partial}{\partial y}\left[(x^2 + y^2 + z^2)^{1/2}\right] = \sin\phi \sin\theta$$

$$\frac{\partial r}{\partial z} = \frac{\partial}{\partial z}\left[(x^2 + y^2 + z^2)^{1/2}\right] = \cos\theta$$

$$\frac{\partial\theta}{\partial x} = \frac{\partial}{\partial x}\text{arccosine}\left[\frac{z}{(x^2 + y^2 + z^2)^{1/2}}\right] = \frac{1}{r}\cos\phi\cos\theta$$

$$\frac{\partial\theta}{\partial y} = \frac{\partial}{\partial y}\text{arccosine}\left[\frac{z}{(x^2 + y^2 + z^2)^{1/2}}\right] = \frac{1}{r}\sin\phi\cos\theta$$

$$\frac{\partial\theta}{\partial z} = \frac{\partial}{\partial z}\text{arccosine}\left[\frac{z}{(x^2 + y^2 + z^2)^{1/2}}\right] = -\frac{1}{r}\sin\theta$$

$$\frac{\partial\phi}{\partial x} = \frac{\partial}{\partial x}\text{arccosine}\left[\frac{x}{(x^2 + y^2)^{1/2}}\right] = -\frac{1}{r}\frac{\sin\phi}{\sin\theta}$$

$$\frac{\partial\phi}{\partial y} = \frac{\partial}{\partial y}\text{arcsine}\left[\frac{y}{(x^2 + y^2)^{1/2}}\right] = \frac{1}{r}\frac{\cos\phi}{\sin\theta}$$

$$\frac{\partial\phi}{\partial z} = \frac{\partial}{\partial z}\text{arcsine}\left[\frac{y}{(x^2 + y^2)^{1/2}}\right] = 0$$

Using the chain rule with the partial derivatives displayed in Table I for Equation 14, $\boldsymbol{\nabla}\psi$ is the next expression in spherical-polar coordinates, transformed from rectangular coordinate unit vectors into spherical-polar coordinate unit vectors, after collection of terms that have rectangular coordinate unit vectors comprising the spherical-polar coordinate unit vectors.

$$\boldsymbol{\nabla}\psi = \left[\frac{\partial}{\partial x}\hat{\mathbf{x}} + \frac{\partial}{\partial y}\hat{\mathbf{y}} + \frac{\partial}{\partial z}\hat{\mathbf{z}}\right]\psi = \left[\hat{\mathbf{r}}\frac{\partial}{\partial r} + \hat{\boldsymbol{\theta}}\frac{1}{r}\frac{\partial}{\partial \theta} + \hat{\boldsymbol{\phi}}\frac{1}{r\sin\theta}\frac{\partial}{\partial \phi}\right]\psi \tag{16}$$

The following vector dot product can then be used to transform Equation 11 from rectangular coordinates to spherical-polar coordinates.

$$\nabla^2\psi = \boldsymbol{\nabla}\cdot\boldsymbol{\nabla}\psi = \left[\hat{\mathbf{r}}\frac{\partial}{\partial r} + \hat{\boldsymbol{\theta}}\frac{1}{r}\frac{\partial}{\partial \theta} + \hat{\boldsymbol{\phi}}\frac{1}{r\sin\theta}\frac{\partial}{\partial \phi}\right]\cdot\left[\hat{\mathbf{r}}\frac{\partial}{\partial r} + \hat{\boldsymbol{\theta}}\frac{1}{r}\frac{\partial}{\partial \theta} + \hat{\boldsymbol{\phi}}\frac{1}{r\sin\theta}\frac{\partial}{\partial \phi}\right]\psi \tag{17}$$

In Equation 17, it is important to note that unit vectors $\hat{\mathbf{r}}$ and $\hat{\boldsymbol{\theta}}$ are functions of θ and ϕ, as unit vector $\hat{\boldsymbol{\phi}}$ is a function of ϕ when performing the dot product of $\boldsymbol{\nabla}\cdot\boldsymbol{\nabla}\psi$ (see Table II). It is necessary to take the partial derivatives of these three spherical polar coordinate unit vectors while conducting this vector dot product. After performing the vector dot-product in Equation 17 and algebraic rearrangement, one has $\nabla^2\psi$ transformed into spherical polar coordinates.

$$\nabla^2\psi = \left[\frac{\partial^2}{\partial x^2} + \frac{\partial^2}{\partial y^2} + \frac{\partial^2}{\partial z^2}\right]\psi = \left[\frac{1}{r^2}\frac{\partial}{\partial r}\left(r^2\frac{\partial}{\partial r}\right) + \frac{1}{r^2\sin\theta}\frac{\partial}{\partial \theta}\left(\sin\theta\frac{\partial}{\partial \theta}\right) + \frac{1}{r^2\sin^2\theta}\frac{\partial^2}{\partial \phi^2}\right]\psi \tag{18}$$

Table II Partial Derivatives in Equation 17 not Equal to Zero

$$\frac{\partial\hat{\mathbf{r}}}{\partial\theta} = \cos\phi\cos\theta\,\hat{\mathbf{x}} + \sin\phi\cos\theta\,\hat{\mathbf{y}} - \sin\theta\,\hat{\mathbf{z}} = \hat{\boldsymbol{\theta}}$$

$$\frac{\partial\hat{\boldsymbol{\theta}}}{\partial\theta} = -\cos\phi\sin\theta\,\hat{\mathbf{x}} - \sin\phi\sin\theta\,\hat{\mathbf{y}} - \cos\theta\,\hat{\mathbf{z}} = -\hat{\mathbf{r}}$$

$$\frac{\partial\hat{\mathbf{r}}}{\partial\phi} = -\sin\phi\sin\theta\,\hat{\mathbf{x}} + \cos\phi\sin\theta\,\hat{\mathbf{y}} = (-\sin\phi\,\hat{\boldsymbol{x}} + \cos\phi\,\hat{\boldsymbol{y}})\sin\theta = \sin\theta\,\hat{\boldsymbol{\phi}}$$

$$\frac{\partial\hat{\boldsymbol{\theta}}}{\partial\phi} = -\sin\phi\cos\theta\,\hat{\mathbf{x}} + \cos\phi\cos\theta\,\hat{\mathbf{y}} = (-\sin\phi\,\hat{\mathbf{x}} + \cos\phi\,\hat{\mathbf{y}})\cos\theta = \cos\theta\,\hat{\boldsymbol{\phi}}$$

$$\frac{\partial\hat{\boldsymbol{\phi}}}{\partial\phi} = -\cos\phi\,\hat{\mathbf{x}} - \sin\phi\,\hat{\mathbf{y}}$$

The classical Schrödinger differential wave equation is appropriate when the electron in an atom never approaches the speed of light. However, for large nuclei, such as lead (Pb) with an atomic number of 82 or 82 protons, the electrons with the angular momentum quantum number l=0 approach the speed of light as they come into close contact with the nucleus. Theoretically, electrons that have angular momentum quantum number equal to zero, in classical physics, have linear oscillatory motion (Walker et al., 2014) and penetrate through the atomic nucleus twice during each oscillation. Thus, it is necessary to evaluate the relativistic Schrödinger differential wave equation for such large nuclei.

Einstein's Special Theory of Relativity and the Relativistic Schrödinger Differential Wave Equation

By Einstein's Special Theory of Relativity, kinetic energy, KE, is equal to the difference between the relativistic mass m_{re} of an electron multiplied by the speed-of-light squared c^2 and the electron rest mass m_e times the speed-of-light squared.

$$KE = m_{re}c^2 - m_e c^2 \text{ (Tipler and Llewellyn, 2012)} \tag{19}$$

Concisely, the speed of light in units of meters per second is the following large integer number.

$$c = 299{,}792{,}458 \frac{\text{meters}}{\text{second}} \text{ (Tipler and Llewellyn, 2012)} \tag{20}$$

And the relativistic mass m_{re} of the electron is equal to the electron rest mass m_e divided by the square-root of the quantity $1-v^2/c^2$, where v is the speed of the electron and c is the speed of light.

$$m_{re} = \frac{m_e}{\sqrt{1 - v^2/c^2}} = \frac{m_e}{(1 - v^2/c^2)^{1/2}} \text{ (Tipler and Llewellyn, 2012)} \tag{21}$$

Therefore, the Hamiltonian, kinetic energy plus negative potential energy, for the electron in a hydrogen atom or hydrogen-like cation becomes the following expression when using Equation 19 to express the kinetic energy of the electron.

$$(m_{re}c^2 - m_e c^2) - \frac{1}{4\pi\varepsilon_0}\frac{Zq^2}{r} = E_m \tag{22}$$

And Equation 22 can be rearranged into the following more convenient expression.

$$m_{re}c^2 - \frac{1}{4\pi\varepsilon_0}\frac{Zq^2}{r} = E_m + m_e c^2 = E_s \tag{23}$$

E_s is the energy sum or sum of the electron rest mass energy $m_e c^2$ and the mechanical energy E_m. $E_s$can only be a positive number and greater than zero (E_s>0) when including angular momentum. If the sum energy E_s=0, then E_m=$-m_e c^2$, and the relativistic energy of the orbiting electron becomes equal to the magnitude of the negative Coulomb potential.

$$m_{re}c^2 = \frac{1}{4\pi\varepsilon_0}\frac{Zq^2}{r} \tag{24}$$

In classical physics, if an electron in a hydrogen-like cation has a perfectly circular orbit, the centrifugal force for the relativistic electron in motion equals the magnitude of the Coulomb force of attraction.

$$m_{re}\frac{v^2}{r} = \frac{1}{4\pi\varepsilon_0}\frac{Zq^2}{r^2} \tag{25}$$

Next, multiply both sides of Equation 25 with distance r

$$m_{re}v^2 = \frac{1}{4\pi\varepsilon_0}\frac{Zq^2}{r} (= m_{re}c^2 \text{ because } v = c \text{ when } E_s = 0) \tag{26}$$

Hence, when E_s=0 and the centrifugal force equals the magnitude of the attractive Coulomb force, the relativistic electron moves at the speed-of-light with a relativistic mass equal to infinity, which would only be possible if the electron and atomic nucleus were both point masses and separation distance r=0. This is one explanation of why the sum energy E_s is greater than zero, and the mechanical energy E_m is greater than the negative electron rest mass energy ($E_m > -m_e c^2$). In addition, if one squares the result in Equation 24

$$\frac{m_e^2 c^4}{1 - v^2/c^2} = \left(\frac{1}{4\pi\varepsilon_0}\frac{Zq^2}{r}\right)^2 \tag{27}$$

Then Equation 27 can be rearranged into the next expression.

$$\left(\frac{1}{4\pi\varepsilon_0}\frac{Zq^2}{r}\right)^2 \frac{v^2}{c^2} = \left(\frac{1}{4\pi\varepsilon_0}\frac{Zq^2}{r}\right)^2 - m_e^2 c^4 \tag{28}$$

Afterwards, substitute the result of Equation 24 into Equation 28 to arrive at

$$m_{re}^2 v^2 c^2 = p_{re}^2 c^2 = m_{re}^2 c^4 - m_e^2 c^4 \tag{29}$$

Where in Equation 29, p_{re} is the magnitude of the relativistic momentum $\mathbf{p}_{re}$=$m_{re}\mathbf{v}$ of the electron in motion such that

$$\mathbf{p}_{re} = \frac{m_e}{\sqrt{1 - v^2/c^2}}\mathbf{v} \text{ (Tipler and Llewellyn, 2012)} \tag{30}$$

The expression in Equation 29 is derived from the following famous equation in Einstein's Special Theory of Relativity.

$$E = m_{re}c^2 = \frac{m_e c^2}{\sqrt{1 - v^2/c^2}} = \frac{m_e c^2}{(1 - v^2/c^2)^{1/2}} \text{ (Tipler and Llewellyn, 2012)} \tag{31}$$

For energy levels with angular momentum, this is another explanation why the sum energy E_s can only be a positive number greater than zero and the mechanical energy E_m must be larger than the negative electron rest mass energy.

If one adds the electron rest mass energy squared $m_e^2 c^4$ on both sides of Equation 29, and then takes the square-root of both sides, the next expression is the result.

$$m_{re}c^2 = \sqrt{p_{re}^2 c^2 + m_e^2 c^4} = (p_{re}^2 c^2 + m_e^2 c^4)^{1/2} \tag{32}$$

This result of Equation 32 is then substituted in Equation 23 for the electron's relativistic mass energy $m_{re}c^2$.

$$\sqrt{p_{re}^2 c^2 + m_e^2 c^4} - \frac{1}{4\pi\varepsilon_0}\frac{Zq^2}{r} = E_s \tag{33}$$

To use the squared momentum operator in Equation 33 above, the Coulomb potential is added to both sides of the equation, and then squaring both sides of the equation to obtain the next relation.

$$p_{re}^2 c^2 + m_e^2 c^4 = \left(E_s + \frac{1}{4\pi\varepsilon_0}\frac{Zq^2}{r}\right)^2 = E_s^2 + 2E_s\frac{1}{4\pi\varepsilon_0}\frac{Zq^2}{r} + \left(\frac{1}{4\pi\varepsilon_0}\frac{Zq^2}{r}\right)^2 \tag{34}$$

Then, subtract the square of the rest mass energy $m_e^2c^4$ of the electron from both sides of Equation 34 and square the Coulomb potential to arrive at the next expression.

$$p_{re}^2c^2 = (E_s^2 - m_e^2c^4) + 2E_s\frac{1}{4\pi\varepsilon_0}\frac{Zq^2}{r} + \frac{1}{(4\pi\varepsilon_0)^2}\frac{Z^2q^4}{r^2} \tag{35}$$

Now when using the dot product of the momentum operator ∇^2, the relativistic version of the Schrödinger differential wave equation becomes the next differential expression.

$$-\hbar^2c^2\nabla^2\psi = \left[(E_s^2 - m_e^2c^4) + 2E_s\frac{1}{4\pi\varepsilon_0}\frac{Zq^2}{r} + \frac{1}{(4\pi\varepsilon_0)^2}\frac{Z^2q^4}{r^2}\right]\psi \tag{36}$$

After dividing Equation 36 by squared product $\hbar^2c^2$ and rearranging this equation to equal zero

$$-\nabla^2\psi - \left[\frac{E_s^2 - m_e^2c^4}{\hbar^2c^2} + \frac{2E_s}{\hbar^2c^2}\frac{1}{4\pi\varepsilon_0}\frac{Zq^2}{r} + \frac{1}{\hbar^2c^2(4\pi\varepsilon_0)^2}\frac{Z^2q^4}{r^2}\right]\psi = 0 \tag{37}$$

The expression in Equation 37 can be further simplified by substitution of the following unitless term α such that

$$\alpha = \frac{q^2}{\hbar c 4\pi\varepsilon_0} = \frac{(1.602177\times10^{-19}\ \text{Coulomb})^2}{\left(1.05457\times10^{-34}\frac{\text{kg m}^2}{\text{sec}}\right)\left(299{,}792{,}458\frac{\text{m}}{\text{sec}}\right)4\pi\left(8.854187817\times10^{-12}\frac{\text{Coul}^2\text{sec}^2}{\text{kg m}^3}\right)} = \frac{1}{137.036} \tag{38}$$

to obtain the next expression.

$$-\nabla^2\psi - \left[\frac{E_s^2 - m_e^2c^4}{\hbar^2c^2} + \frac{2E_s}{\hbar c}\frac{Z\alpha}{r} + \frac{Z^2\alpha^2}{r^2}\right]\psi = 0 \tag{39}$$

The unitless numerical reciprocal of 137.036 in Equation 38 is calculated using the numerical values with units given in Equations 2, 8, 9 and 20. The relativistic version of the Schrödinger differential wave equation is now the following expression in terms of spherical-polar coordinates.

$$-\frac{1}{r^2}\frac{\partial}{\partial r}\left(r^2\frac{\partial\psi}{\partial r}\right) - \frac{1}{r^2\sin\theta}\frac{\partial}{\partial\theta}\left(\sin\theta\frac{\partial\psi}{\partial\theta}\right) - \frac{1}{r^2\sin^2\theta}\frac{\partial^2\psi}{\partial\phi^2} - \left[\frac{E_s^2 - m_e^2c^4}{\hbar^2c^2} + \frac{2E_s}{\hbar c}\frac{Z\alpha}{r} + \frac{Z^2\alpha^2}{r^2}\right]\psi = 0 \tag{40}$$

Equation 40 is a linear, nonhomogeneous partial differential equation that may have an analytical solution (Walker et al., 2014) by separation of variables r, θ, and ϕ when setting $\psi(r,\theta,\phi)=R(r)\Theta(\theta)\Phi(\phi)$, the product of three separate different functions of the spherical-polar coordinates. It is obvious that the analytical solution for the differential expression of θ and ϕ are the same as in the classical Schrödinger differential wave equation (Walker et al., 2014). The analytical solution for angle ϕ is the following simple exponential function.

$$\Phi(\phi) = e^{\pm im_l\phi} \tag{41}$$

In Equation 41, m_l is the magnetic quantum number whose values range from $-l$ to $+l$. The analytical solution for angle θ is the following polynomial.

$$\Theta(z) = (1-z^2)^{\frac{|m_l|}{2}}\frac{d^{|m_l|}}{dz}P_l(z) \text{ and } z = \cos\theta \tag{42}$$

In Equation 42, P_l(z=cosθ) are solutions to the homogeneous Legendre differential equation given below.

$$\frac{d}{dz}\left[(1-z^2)\frac{dP_l}{dz}\right] + l(l+1)P_l = 0 \text{ (Arfken and Weber, 2005)} \tag{43}$$

Equation 42 instead is the analytical solution to the homogeneous associate Legendre differential equation.

$$\frac{d}{dz}\left[(1-z^2)\frac{d\Theta}{dz}\right]+\left[l(l+1)-\frac{m_l^2}{1-z^2}\right]\Theta=0 \text{ (Arfken and Weber, 2005)} \tag{44}$$

In Equations 43 and 44, $dz{=}-\sin\theta d\theta$ when $z{=}\cos\theta$ involving the angular momentum quantum number l. Empirically, the squared quantized angular momentum is observed (Walker et al., 2014) to be proportional to $l(l{+}1)$ instead of l^2 and this is in correlation with the Heisenbug uncertainty principle of linear momentum.

The major difference between the relativistic Schrödinger differential wave equation and the classical one is in the radial wave function $R(r)$ when taking relativistic effects into account. With reference to the analytical solutions of θ and ϕ (Walker et al., 2014), equation 40 becomes the following differential function of R.

$$-\frac{1}{r^2}\frac{d}{dr}\left(r^2\frac{dR}{dr}\right)+\frac{1}{r^2}l(l+1)R-\left[\frac{E_s^2-m_e^2c^4}{\hbar^2c^2}+\frac{2E_s}{\hbar c}\frac{Z\alpha}{r}+\frac{Z^2\alpha^2}{r^2}\right]R=0 \tag{45}$$

Multiply -1 through Equation 45, take the derivatives with respect to r on the left-hand-side of Equation 45, and substitute $+\left[(E_s^2-m_e^2c^4)/(\hbar^2c^2)\right]$ with equivalent expression $-\left\{-\left[(E_s^2-m_e^2c^4)/(\hbar^2c^2)\right]\right\}$, Equation 45 becomes

$$\frac{2}{r}\frac{dR}{dr}+\frac{d^2R}{dr^2}+\frac{2E_s}{\hbar c}\frac{Z\alpha}{r}R-\left[-\frac{(E_s^2-m_e^2c^4)}{\hbar^2c^2}\right]R+\frac{Z^2\alpha^2-l(l+1)}{r^2}R=0 \tag{46}$$

Then use the following same relationship as in the classical Schrödinger differential wave equation for the unitless parameter ρ (Walker et al., 2014) to have a dimensionless distance variable instead of r.

$$\rho=2\beta r \tag{47}$$

Where β^2 is set equal to next expression for E_s values greater than zero and less than the electron rest mass energy, since the mechanical energy E_m is a negative number greater than the negative rest mass energy value of the electron.

$$\beta^2=-\frac{(E_s^2-m_e^2c^4)}{\hbar^2c^2}=\frac{1}{\hbar^2c^2}(m_e^2c^4-E_s^2)>0 \qquad \text{If } 0<E_s<m_ec^2 \text{ and } -m_ec^2<E_m<0 \tag{48}$$

Note that the units of β is 1/meter. Equation 46 is now transformed into units of ρ since $r=\frac{\rho}{2\beta}$ with the substitution of $\beta^2=-\left[(E_s^2-m_e^2c^4)/(\hbar^2c^2)\right]$ into Equation 46

$$(2\beta)^2\frac{2}{\rho}\frac{dR}{d\rho}+(2\beta)^2\frac{d^2R}{d\rho^2}+(2\beta)^2\frac{1}{\beta}\frac{E_s}{\hbar c}\frac{Z\alpha}{\rho}R-\beta^2R+(2\beta)^2\frac{Z^2\alpha^2-l(l+1)}{\rho^2}R=0 \tag{49}$$

When one applies the following expression for deriving Equation 49.

$$2\beta\frac{2E_s}{\hbar c}=4\beta\frac{\beta}{\beta}\frac{E_s}{\hbar c}=(2\beta)^2\frac{1}{\beta}\frac{E_s}{\hbar c} \tag{50}$$

Again, unitless parameter γ is used to obtain a nonhomogeneous associate Laguerre differential equation as in the case of the classical Schrödinger differential wave equation (Walker et al., 2014), and this time

$$\gamma = \frac{E_s Z\alpha}{\beta\hbar c} = \frac{E_s Z\alpha}{\frac{\sqrt{m_e^2c^4 - E_s^2}\hbar c}{\hbar c}} = \frac{E_s Z\alpha}{\sqrt{m_e^2c^4 - E_s^2}} = \frac{E_s Z\alpha}{m_e c^2\sqrt{1 - E_e^2}} = \frac{E_e Z\alpha}{\sqrt{1 - E_e^2}} \qquad 0 < E_s < m_e c^2 \qquad E_e = \frac{E_s}{m_e c^2} \tag{51}$$

In Equation 51, E_e is in units of the electron rest mass energy. Rearrangement of Equation 51 will yield the following equation with E_s as a positive square root function of γ since $0<E_s<m_e c^2$.

$$E_s = \frac{m_e c^2}{\sqrt{1 + \frac{Z^2\alpha^2}{\gamma^2}}} \text{ or } E_e = \frac{E_s}{m_e c^2} = \frac{1}{\sqrt{1 + \frac{Z^2\alpha^2}{\gamma^2}}} \tag{52}$$

After dividing Equation 49 through by $(2\beta)^2$ and substituting in γ, Equation 49 ends up in a similar form as for the classical Schrödinger differential radial wave equation but with the addition of the $Z^2\alpha^2$ term divided by ρ^2.

$$\frac{2}{\rho}\frac{dR}{d\rho} + \frac{d^2R}{d\rho^2} + \frac{\gamma}{\rho}R - \frac{1}{4}R + \frac{Z^2\alpha^2 - l(l+1)}{\rho^2}R = 0 \tag{53}$$

And again, the analytical solution of Equation 53 will be very similar to the classical Schrödinger differential radial wave equation (Walker et al., 2014) concerning radial function $R(\rho)$, but what will be different is the exponent s in the polynomial $F(\rho)$.

$$R(\rho) = R = e^{-\rho/2}F(\rho) = e^{-\rho/2}F \tag{54}$$

The negative exponential factor in Equation 54 is derived for large values of ρ where the expression in Equation 53 becomes the following approximation.

$$\frac{d^2R}{d\rho^2} - \frac{1}{4}R \approx 0 \left(\text{Analytical solution } R = e^{-\rho/2}.\right) \tag{55}$$

After taking the first and second derivative of Equation 54 with respect to ρ, substituting them into Equation 53, and dividing out $e^{-\rho/2}$

$$\frac{d^2F}{d\rho^2} + \left(\frac{2}{\rho} - 1\right)\frac{dF}{d\rho} + \left(\frac{\gamma - 1}{\rho}\right)F + \frac{Z^2\alpha^2 - l(l+1)}{\rho^2}F = 0 \tag{56}$$

If one multiplies Equation 56 with ρ and then subtract the right-hand term on both sides of this equation, one has the following result which is a nonhomogeneous associate Laguerre differential equation.

$$\rho\frac{d^2F}{d\rho^2} + (2 - \rho)\frac{dF}{d\rho} + (\gamma - 1)F = \frac{l(l+1) - Z^2\alpha^2}{\rho}F \tag{57}$$

The homogenous associate Laguerre differential equation is the following in terms of x and y.

$$x\frac{d^2y}{dx^2} + (\kappa + 1 - x)\frac{dy}{dx} + \eta y = 0 \text{ (Arfken, and Weber, 2005)} \tag{58}$$

In Equation 58, both κ and η are integers with the following analytical series solution and coefficients.

$$y = \sum a_k x^k \qquad a_1 = \frac{-\eta}{\kappa + 1}a_0 \qquad a_{k+1} = \frac{k - \eta}{(k+1)k + (\kappa + 1)(k+1)}a_k \tag{59}$$

Apparently, the series solution in Equation 59 terminates when $k=\eta$. Compared to Equation 59, in Equation 56 $F=y$, $\rho=x$, $\kappa=1$ and $\eta=\gamma-1$.

Therefore, the analytical solution to the function $F(\rho)$ is the following expansion series in powers of ρ, as for the classical Schrödinger differential radial wave equation (Walker et al., 2014), where a constant value s is added to the exponentials of ρ to match with the nonhomogeneous differential equation given in Equation 57.

$$F = \sum_{k=0}^{K} a_k \rho^{s+k} \qquad \frac{dF}{d\rho} = \sum_{k=0}^{K} (s+k) a_k \rho^{s+k-1} \qquad \frac{dF^2}{d\rho^2} = \sum_{k=0}^{K} (s+k)(s+k-1) a_k \rho^{s+k-2} \tag{60}$$

However, this time s will not be equal to angular momentum quantum number l, and $\eta{=}\gamma{-}1$ is a non-integer real number instead of an integer. If one performs the substitutions of the expressions in Equation 60 into Equation 57, one has the following result.

$$\sum_{k=0}^{K} (s+k)(s+k-1) a_k \rho^{s+k-1} + 2\sum_{k=0}^{K} (s+k) a_k \rho^{s+k-1} - \sum_{k=0}^{K} (s+k) a_k \rho^{s+k} + (\gamma-1)\sum_{k=0}^{K} a_k \rho^{s+k} = [l(l+1) - Z^2\alpha^2] \sum_{k=0}^{K} a_k \rho^{s+k-1} \tag{61}$$

Then separate out terms of $k{=}0$ for the two series on the left-hand side of Equation 61, and the same for the $k{=}0$ component of the series on the right-hand side of the equal sign.

$$[s(s-1) + 2s] a_0 \rho^{s-1} + \sum_{k=1}^{K} (s+k)(s+k-1) a_k \rho^{s+k-1} + 2\sum_{k=1}^{K} (s+k) a_k \rho^{s+k-1} - \sum_{k=0}^{K} (s+k) a_k \rho^{s+k} + (\gamma-1)\sum_{k=0}^{K} a_k \rho^{s+k} = [l(l+1) - Z^2\alpha^2] a_0 \rho^{s-1} + [l(l+1) - Z^2\alpha^2] \sum_{k=1}^{K} a_k \rho^{s+k-1} \tag{62}$$

Then reset the series on both sides of Equation 62 for terms ρ^{s+k-1} into ρ^{s+k} by addition of one so to have the initial value of $k{=}0$ instead of $k{=}1$, and collect like terms.

$$s(s+1) a_0 \rho^{s-1} + \sum_{k=0}^{K} [(s+k+1)(s+k) + 2(s+k+1)] a_{k+1} \rho^{s+k} - \sum_{k=0}^{K} (s+k) a_k \rho^{s+k} + (\gamma-1)\sum_{k=0}^{K} a_k \rho^{s+k} = [l(l+1) - Z^2\alpha^2] a_0 \rho^{s-1} + [l(l+1) - Z^2\alpha^2] \sum_{k=0}^{K} a_{k+1} \rho^{s+k} \tag{63}$$

In Equation 63 it is possible to evaluate s since a_0 cannot be equal to zero.

$$s(s+1) = l(l+1) - Z^2\alpha^2 \quad \text{or} \quad s^2 + s + [Z^2\alpha^2 - l(l+1)] = 0 \tag{64}$$

The quadratic formula below is used to evaluate s.

$$s = \frac{-1 \pm \sqrt{1^2 + 4[l(l+1) - Z^2\alpha^2]}}{2} = -\frac{1}{2} \pm \sqrt{\frac{1}{4} + l^2 + l - Z^2\alpha^2} = -\frac{1}{2} \pm \sqrt{\left(l + \frac{1}{2}\right)^2 - Z^2\alpha^2} \tag{65}$$

Next, the following part of Equation 63 is rearranged and set equal to zero so to be able to evaluate γ.

$$\sum_{k=0}^{K} \{(s+k+1)(s+k) + 2(s+k+1) + [Z^2\alpha^2 - l(l+1)]\} a_{k+1} \rho^{s+k} + \sum_{k=0}^{K} [(\gamma-1) - (s+k)] a_k \rho^{s+k} = 0 \tag{66}$$

Thus, one has the following relationship between coefficients a_k and a_{k+1} from Equation 66 above

$$a_{k+1} = \frac{(s+k) - (\gamma-1)}{(s+k+1)(s+k) + 2(s+k+1) + [Z^2\alpha^2 - l(l+1)]} a_k \tag{67}$$

And the series terminates when the numerator in Equation 67 is equal to zero. Hence, γ is the following function in Equation 68 below noting that addition instead of subtraction in the analytical solution given in Equation 65 is utilized, since theoretically a quantum number of any orbital must be positive and greater than zero in value.

$$\gamma = s + k + 1 = -\frac{1}{2} + \sqrt{\left(l+\frac{1}{2}\right)^2 - Z^2\alpha^2} + (n-l) = n - \left(l+\frac{1}{2}\right) + \sqrt{\left(l+\frac{1}{2}\right)^2 - Z^2\alpha^2} > 0 \tag{68}$$

The $k{+}1{=}n{-}l$, as in the classical Schrödinger differential wave equation (Walker et al., 2014), mandates that $l_{max}{=}n{-}1$. Angular momentum quantum number l is less than the principal quantum number n. Substituting addition in Equation 65 for s and Equation 68 for γ, Equation 67 becomes the next expression.

$$a_{k+1} = \frac{k+l+1-n}{2(k+1)\left[\sqrt{\left(l+\frac{1}{2}\right)^2 - Z^2\alpha^2}\right] + k^2 + 2k + 1} a_k \tag{69}$$

Another important fact is that values of γ for the $1s$ orbitals of all 118 elements on the current Periodic Table of Elements, beyond copper to element 118 (oganesson), are estimated to be greater than 1/2.

Two Problems of the Relativistic Schrödinger Differential Wave Equation for $l{=}0$ Quantum Levels

There are two problems with the relativistic version of the Schrödinger differential wave equation for quantum levels with angular momentum quantum number $l{=}0$. With regard to the first problem, the value E_e in units of the electron rest mass energy, calculated from the measured $1s$ ionization energy of Cu^{28+} (Table III) (Wikipedia: The Free Encyclopedia, 2025), is 0.9773612, greater than the theoretical value 0.9762209 evaluated by the analytical solution of the relativistic Schrödinger differential wave equation. Using Equation 68 to determine the value of γ for Cu^{28+} hydrogen-like cation containing 29 protons in the copper nucleus with the single electron in the $1s$ orbital

$$\gamma = n - \left(l+\frac{1}{2}\right) + \sqrt{\left(l+\frac{1}{2}\right)^2 - Z^2\alpha^2} = 1 - \left(0+\frac{1}{2}\right) + \sqrt{\left(0+\frac{1}{2}\right)^2 - 29^2\frac{1}{137.036^2}} = 0.9530073 \tag{70}$$

And using this value of γ from Equation 70 in Equation 52 yields the following theoretical E_e value for the $1s$ ionization energy in a Cu^{28+} hydrogen-like cation.

$$E_e = \frac{E_s}{m_e c^2} = \frac{1}{\sqrt{1+\frac{Z^2\alpha^2}{\gamma^2}}} = \frac{1}{\sqrt{1+\frac{29^2\left(\frac{1}{137.036}\right)^2}{0.9530073^2}}} = 0.9762209 \tag{71}$$

However, if one uses the measured $1s$ ionization energy IE for Cu^{28+} (Table III), experimental E_e is greater than the number calculated in Equation 71.

$$E_{e,Exp} = 1 - \frac{IE}{N_A}\frac{1}{m_e c^2} = 1 - \frac{1{,}116{,}105{,}000\ \text{Joules}}{6.022141\times10^{23}}\frac{1}{9.10938\times10^{-31}\text{kg}(299782458\ \text{m/s})^2} = 0.9773612 \tag{72}$$

Table III Measured Ionization Energies for the $1s$ Electron in Hydrogen and Hydrogen-Like Cations

Atomic Number	Element	Cation	Measured $1s$ Ionization Energy (kJ/mole)
1	Hydrogen	H	1,312.0
2	Helium	He^{+}	5,250.5
3	Lithium	Li^{2+}	11,815.0
4	Beryllium	Be^{3+}	21,006.6
5	Boron	B^{4+}	32,826.17
6	Carbon	C^{5+}	47,277.0
7	Nitrogen	N^{6+}	64,360.
8	Oxygen	O^{7+}	84,078.0
9	Fluorine	F^{8+}	106,434.3
10	Neon	Ne^{9+}	131,432
11	Sodium	Na^{10+}	159,076
12	Magnesium	Mg^{11+}	189,368
13	Aluminum	Al^{12+}	222,316
14	Silicon	Si^{13+}	257,923
15	Phosphorus	P^{14+}	296,195
16	Sulfur	S^{15+}	337,138
17	Chlorine	Cl^{16+}	380,760
18	Argon	Ar^{17+}	427,066
19	Potassium	K^{18+}	476,063
20	Calcium	Ca^{19+}	572,762
21	Scandium	Sc^{20+}	582,163
22	Titanium	Ti^{21+}	639,294
23	Vanadium	V^{22+}	699,144
24	Chromium	Cr^{23+}	761,733
25	Manganese	Mn^{24+}	827,067
26	Iron	Fe^{25+}	895,161
27	Cobalt	Co^{26+}	966,023
28	Nickel	Ni^{27+}	1,039,668
29	Copper	Cu^{28+}	1,116,105

In Equation 72, the numerical value of Avogadro's number N_A (Miessler et al., 2014) is in the denominator since ionization energies are normally given in units of kilojoules per mole. The calculated E_e in Equation 72 from measured data is greater than the result in Equation 71, showing that the theoretical value overestimates the actual ionization energy. Concerning the second problem, this appears in Equations 65 and 68 for the hydrogen-like cation Tm^{68+} when the angular momentum quantum number l=0. For the Tm^{68+} hydrogen-like cation, evaluation of s and γ using Equations 65 and 68 both yield a complex number.

$$\gamma = n - \left(0 + \frac{1}{2}\right) + \sqrt{\left(0 + \frac{1}{2}\right)^2 - 69^2 \frac{1}{137.036000^2}} = n - \frac{1}{2} + \sqrt{\frac{1}{4} - 69^2 \frac{1}{137.036000^2}} = n - \frac{1}{2} + i0.0594112 \quad (73)$$

To evaluate a numerical solution which matches experimental $1s$ ionization energy value for hydrogen-like cation Cu^{28+}, first compute γ_{Exp} from evaluated $E_{e,Exp}$ of Equation 72 after rearrangement of Equation 52 to separate out γ_{Exp}.

$$\gamma_{Exp} = E_{e,Exp} \frac{Z\alpha}{\sqrt{1 - E_{e,Exp}^2}} \tag{74}$$

Since there is no analytical solution that matches measurement, a numerical solution is necessary. As such, we first inserted the calculated value of γ_{Exp} from Equation 74 into Equation 53 and performed a numerical analysis of the radial differential wave equation using the finite-difference technique (LeVeque, 2017). This was performed by using Microsoft Excel (Microsoft, 2018) for the following expression:

$$\frac{2}{\rho}\frac{dR}{d\rho} + \frac{d^2R}{d\rho^2} + \frac{\gamma_{Exp}}{\rho}R - \frac{1}{4}R + \frac{Z^2\alpha^2 - l(l+1)}{\rho^2}R = 0 \tag{75}$$

After performing the next four steps, Equation 75 becomes the numerical expression in Equation 79 for the finite-difference technique used to perform a numerical integration.

In Step 1, use the following approximation in Equation 76 below for first and second derivatives with respect to ρ while using the calculated γ_{Exp} from experimentally measured ionization energy.

$$\frac{2}{\rho_{i+1}}\frac{R_{i+1} - R_i}{\Delta\rho} + \frac{\frac{R_{i+2} - R_{i+1}}{\Delta\rho} - \frac{R_{i+1} - R_i}{\Delta\rho}}{\Delta\rho} + \left[\frac{\gamma_{Exp}}{\rho_{i+1}} + \frac{Z^2\alpha^2 - l(l+1)}{\rho_{i+1}^2} - \frac{1}{4}\right]R_{i+1} = 0 \tag{76}$$

In Step 2, note that the approximate second derivative with respect to ρ is simplified to the ratio on the left-hand-side of Equation 77 given below.

$$\frac{R_{i+2} - 2R_{i+1} + R_i}{\Delta\rho^2} + \frac{2}{\rho_{i+1}}\left(\frac{R_{i+1} - R_i}{\Delta\rho}\right) + \left[\frac{\gamma_{Exp}}{\rho_{i+1}} + \frac{Z^2\alpha^2 - l(l+1)}{\rho_{i+1}^2} - \frac{1}{4}\right]R_{i+1} = 0 \tag{77}$$

For Step 3, collect all like terms in Equation 77 to arrive at the next expression.

$$\frac{R_{i+2}}{\Delta\rho^2} + \frac{R_i - 2R_{i+1}}{\Delta\rho^2} + \frac{2}{\rho_{i+1}}\left(\frac{R_{i+1} - R_i}{\Delta\rho}\right) + \left[\frac{\gamma_{Exp}}{\rho_{i+1}} + \frac{Z^2\alpha^2 - l(l+1)}{\rho_{i+1}^2} - \frac{1}{4}\right]R_{i+1} = 0 \tag{78}$$

Afterwards, finally in Step 4 separate out the newly calculated R_{i+2} value in Equation 79 as shown below.

$$R_{i+2} = 2R_{i+1} - R_i + \Delta\rho\frac{2}{\rho_{i+1}}(R_i - R_{i+1}) + \Delta\rho^2\left[\frac{1}{4} + \frac{l(l+1) - Z^2\alpha^2}{\rho_{i+1}^2} - \frac{\gamma_{Exp}}{\rho_{i+1}}\right]R_{i+1} \tag{79}$$

Then using the values of ρ_{i+1}, R_i, and R_{i+1} with $\Delta\rho$ value set equal to either +0.001 or −0.001, depending upon the direction in the ρ-axis taken, to calculate the new value of R_{i+2} in Equation 79.

For the 1s and other ns orbitals with angular momentum quantum number l=0, the following modification of Equation 79 was found to be necessary by adding constant σ-parameter to dimensionless ρ when using the experimental value of γ_{Exp} evaluated from measured $1s$ ionization energies of hydrogen-like cations.

$$R_{i+2} = 2R_{i+1} - R_i + \Delta\rho\frac{2}{\rho_{i+1}}(R_i - R_{i+1}) + \Delta\rho^2\left[\frac{1}{4} - \frac{Z^2\alpha^2}{(\rho_{i+1} + \sigma)^2} - \frac{\gamma_{Exp}}{(\rho_{i+1} + \sigma)}\right]R_{i+1} \tag{80}$$

Without this modification, the numerical plot of R as a function of ρ decreases in value within short distances from the atomic nucleus (Figure 1), resulting in a negative minimum value at the center

of the atomic nucleus rather than a positive maximum value. It is obvious that the small definite volume of the atomic nucleus, as well as that of the electron, is modeled by the insertion of a constant σ-parameter. This constant σ-parameter is set equal to an evaluated constant C equal to 3.71, such that σ is equal to 3.71 times an estimated nuclear radius (Table IV). A logarithmic plot of Figure 2 was utilized in estimating the value of the constant C where near the estimated copper nucleus radius the logarithmic plot becomes nonlinear and increases to a maximum value at the center of the atomic nucleus. In units of meters, the nuclear radius is estimated (Wong, 1998) as 1.2×10^{-15} times the atomic mass number A raised to the one-third power ($r_{nucl}=1.2\times10^{-15}A^{1/3}$ meter), but instead for copper, the atomic weight listed on the Periodic Table of Elements is used for estimating the radius of the copper nucleus due to two naturally occurring copper isotopes. Then, the calculation of $\sigma=C(2\beta\times r_{nucl})$ is employed to convert the value of σ-parameter from meters into the dimensionless ρ. The negative value of $\Delta\rho=-0.001$ is used instead of $+0.001$ since the maximum value of R is unknown at the center of the atomic nucleus. One can initially set R_1 to a very small value slightly greater than or slightly less than zero at $\rho_1\geq25.000$, initial value of ρ_1 dependent upon the ns orbital size, and then set the value of R_2 to a very small number slightly greater than or slightly less than R_1, depending upon the shape of the radial wave function, at $\rho_2=\rho_1+\Delta\rho$. The initial values of R_1 and R_2 are adjusted to have a normalized numerical plot of $R(\rho)$ and a continuous numerical solution for $F(\rho)$. Afterwards, finish off evaluation of the radial wave function R using Equation 80, rather than Equation 79, consistently up to $\rho_{i+2}=0$ at the center-of-mass of the atomic nucleus. Figure 2 displays the normalized numerical evaluation of the radial wave function for the $1s$ electron in the Cu^{28+} hydrogen-like cation using the measured ionization energy of the $1s$ orbital and the inclusion of the σ-parameter. The maximum value at the center of the atomic nucleus at $\rho=0$ is a positive number. With the inclusion of the σ-parameter, the differential expression in Equation 75 becomes a differential equation with no known analytical solution and only a numerical solution is possible using finite-difference technique with initial boundary conditions. Thus, measured data is required along with a numerical solution via the finite-difference technique. In addition, to obtain the smooth shape of the numerical integration at the center of the atomic nucleus ($\rho=0$), the value of the constant C is varied to determine the most appropriate value of the σ-parameter in Equation 80.

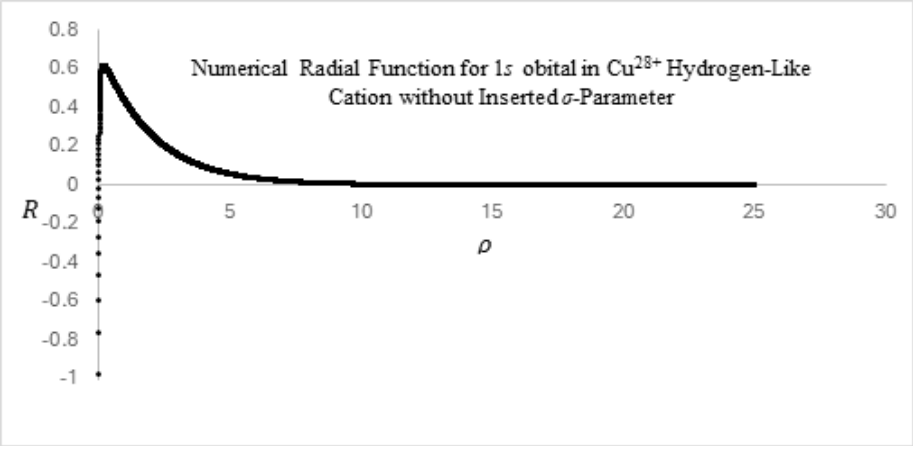

Figure 1 Normalized numerically calculated radial function R for the $1s$ orbital in the Cu^{28+} hydrogen-like cation with $\gamma_{Exp}=0.9775719$, factor $f_{exp}=0.489570$, and $E_{e,Exp}=0.9773612$. For the x-axis $r=0.912571\ \rho$ in units of picometers (10^{-12} meters).

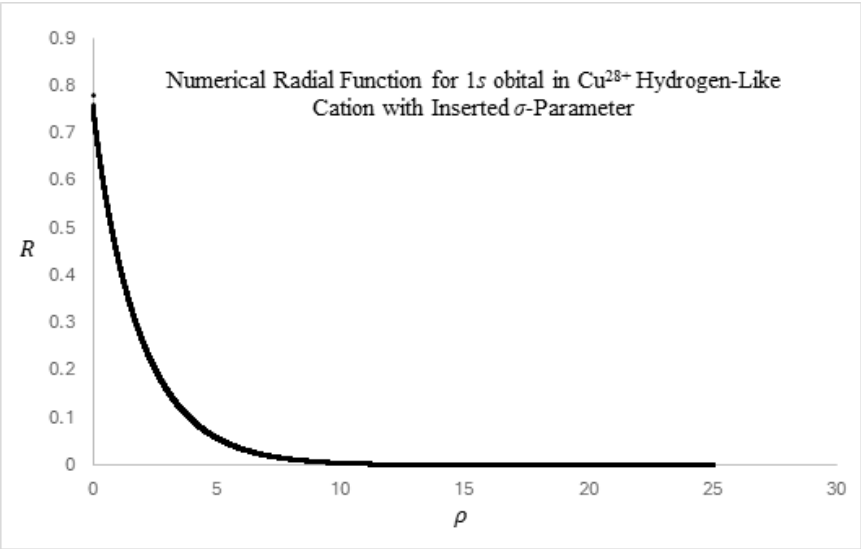

Figure 2 Normalized numerically calculated radial function R for the $1s$ orbital in the Cu^{28+} hydrogen-like cation with γ_{Exp}=0.9775719, factor f_{exp}=0.489570, and $E_{e,Exp}$=0.9773612. For the x-axis r=0.912571 ρ in units of picometers (10^{-12} meter) and σ=0.0195 in units of ρ.

Table IV Evaluated σ-Parameters for the Cu28+ Hydrogen-Like Cation in Unitless and Picometers

$\sigma = C2\beta \times r_{nucl} = C2\beta \times 1.2AW^{1/3} = C2\beta \times 1.2 \times 63.5^{1/3} = C2\beta \times 4.79$ femtometer (10^{-15} meter)
β given in units of 1/picometers and 1 picometer = 10^{-12} meter

Orbital	β (1/pm)	Constant C	r_{nucl} in unitless ρ	σ-Parameter in unitless ρ
$1s$	0.548	3.71	0.00525	0.0195
$2s$	0.276	3.71	0.00264	0.00979
$3s$	0.184	3.71	0.00176	0.00653
$4s$	0.138	3.71	0.00132	0.00490
$5s$	0.110	3.71	0.00105	0.00390
$6s$	0.0916	3.71	0.000877	0.00325
$7s$	0.0785	3.71	0.000752	0.00279

In addition, one can evaluate an experimental factor f_{exp} in Equation 81 below, by the calculated γ_{Exp} when using measured ionization energies of $1s$ electron in hydrogen-like cations for principal quantum number n=1 and angular momentum quantum number l=0.

$$\gamma_{Exp} = 1 - \left(0 + \frac{1}{2}\right) + \sqrt{\left(0 + \frac{1}{2}\right)^2 - f_{Exp} Z^2 \alpha^2} \tag{81}$$

Such that after separating out the factor f_{exp} in Equation 81, one has the following expression.

$$f_{Exp} = \frac{\gamma_{Exp} - \gamma_{Exp}^2}{Z^2\alpha^2} \tag{82}$$

If one assumes that the value of factor f_{exp} does not change with principal quantum number n, radial functions for larger values of the principal quantum number n with angular momentum quantum number l=0 can be determined numerically. However, it will again be necessary to insert the σ-parameter in Equation 80 to obtain continuous plots of both $R(\rho)$ and $F(\rho)$. Figure 3 displays the normalized numerical radial wave function of the $2s$ electron in the Cu^{28+} cation which has a higher energy value, and Table IV displays the evaluated σ-parameters for the $1s$ to $7s$ orbitals in both unitless parameter ρ and a constant value in femtometers (10^{-15} meters) for the estimated radius of a copper nucleus. For all the ns orbitals analyzed, the evaluated σ-parameters are displayed at three significant figures. In the numerical integration of Figure 3, the evaluated factor f_{exp} in Equation 82, from the measured ionization energy of the $1s$ hydrogen-like cation Cu^{28+}, is used again by insertion in Equation 83 below for principal quantum number n=2 and angular momentum quantum number l=0.

$$\gamma_{ns} = n - \left(0 + \frac{1}{2}\right) + \sqrt{\left(0 + \frac{1}{2}\right)^2 - f_{Exp}Z^2\alpha^2} \text{ and } E_s = \frac{m_e c^2}{\sqrt{1 + \frac{Z^2\alpha^2}{\gamma_{ns}^2}}} \tag{83}$$

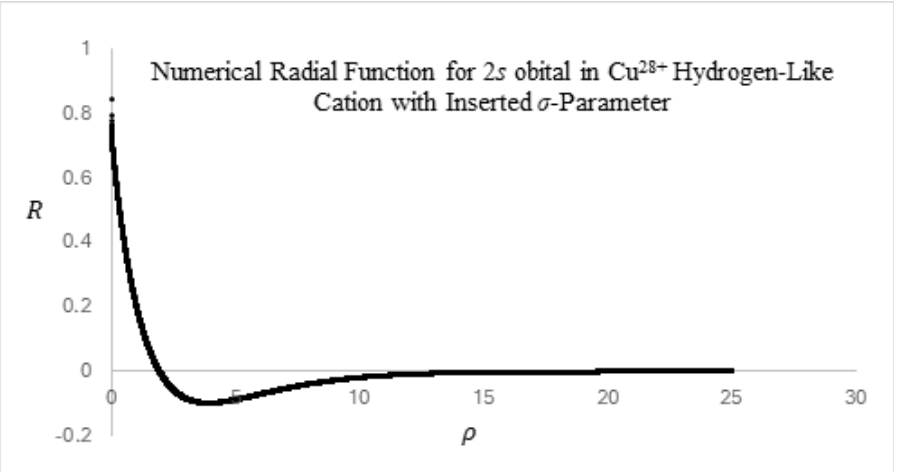

Figure 3 Normalized numerically calculated radial function R for the $2s$ orbital in the Cu^{28+} hydrogen-like cation using factor f_{exp}=0.489570 and γ_{ns}=1.977572, resulting in E_e=0.9943230>0.9773612. For the x-axis r=1.814588 ρ in units of picometers (10^{-12} meter) and σ=0.00979 in units of ρ.

This computed value of γ_{ns} is then used to calculate the energy level by Equation 52, and γ_{ns} is then inserted into Equation 80 to perform the numerical result with inclusion with the σ-parameter. Note that the radial wave function plot of the $2s$ electron in Figure 3 has a single node.

Theoretically, the ns electrons pass through the atomic nucleus in classical oscillations because there is zero angular momentum of the electron in an atomic orbital that has the angular momentum quantum number l=0. In classical physics (Walker et al., 2014), the electron inside the atomic nucleus will experience a Coulomb force matching that of the classical harmonic oscillator if the positive charge density of the atomic nucleus is constant, similar to an object falling through a linear hole through the center of a planet for the force of gravity. It is important to note that subatomic particles and the atomic nucleus as well are not point masses. Theoretically the electron, proton, and neutron are spherical in shape. The radius of the proton and neutron are estimated to be as small as 1 femtometer (10^{-15} meters). Since the electron has a rest mass value nearly 1,800 times less than that of a proton or neutron, the radius of the electron is around 10^{-17} meter assuming the electron has the same density as the proton or neutron. This may be the physical origin of the required σ-parameter for a numerical solution with lower ionization energy values as compared to the analytical solution of the relativistic Schrödinger differential wave equation.

Yet, it is important to note that the evaluated σ-parameter using experimental ionization energy is slightly more than twice the estimated radius of the nucleus or diameter. If one inserts the estimated radius of the atomic nucleus, the numerical value of the factor "f_{ns}" ends up lesser in value than the experimental value f_{Exp} and the calculated ionization energy will be larger in value than observed experimentally. Since the differential expression in Equation 75 with the addition of the σ-parameter in the denominator has no analytical solution and only a numerical one, it is necessary, therefore, to use experimental data in obtaining the most appropriate value of the σ-parameter. Again, due to the wave-particle duality of the electron and the atomic nucleus, this may help to explain why the σ-parameter is larger than the estimated diameter of the atomic nucleus.

.

The Relativistic Schrödinger Differential Wave Equation for l>0 Quantum Levels

When numerically displaying normalized radial wave functions for angular momentum quantum numbers greater than zero, l>0, the differential is $\Delta\rho$=+0.001, positive value since at ρ_1=0, R_1=0. Theoretically, electrons with angular momentum l>0 are exterior of the atomic nucleus due to having quantized value of angular momentum greater than zero. Initial value of R_2 at ρ_2=0.001 is set equal to a very small number slightly greater than zero, such that a normalized numerical plot for $R(\rho)$ is the result. When accomplishing a numerical plot for the radial wave function of angular momentum quantum number greater than zero l>0, a varied factor f_{nl} can be inserted into Equation 68

$$\gamma_{nl} = n - \left(l + \frac{1}{2}\right) + \sqrt{\left(l + \frac{1}{2}\right)^2 - f_{nl} Z^2 \alpha^2} \text{ and } E_s = \frac{m_e c^2}{\sqrt{1 + \frac{Z^2\alpha^2}{\gamma_{nl}^2}}} \tag{84}$$

This calculated value γ_{nl} can then be placed into Equation 79 instead of Equation 80 to conduct a numerical plot with no added σ-parameter (σ=0). The factor f_{nl} is varied until the numerical plot of R approaches zero at $\rho \geq 25.000$ without any divergences, along with the numerical plot of function $F(\rho)$ being continuous. Afterwards, the final value of γ_{nl} is determined by Equation 84 from the varied factor f_{nl}, and this final value γ_{nl} is used to calculate the energy level E_s by Equation 52. The factor

f_{nl} values observed are all slightly greater than one (Table V), showing that the analytical solution is appropriate for quantum states that have angular momentum quantum number l=1,2,3,... It is very likely that numerical error is the result of the factor f_{nl} being slightly greater than one. Yet, in the numerical analysis for l>0 orbitals, one can set factor f_{nl}=1 and vary the σ-parameter in Equation 80 instead to obtain similar results (Table V). This alternative version of numerical integration resulted in σ-parameter values less than the estimated nuclear radius or equal to zero. The requirement of inserting the parameter σ, for some of the orbitals with angular momentum quantum l>0, is again due to the small quantity of error in a numerical integration when using the finite-difference technique. The quantum energy E_s calculated from γ_{nl} values for factor f_{nl}=1 are nearly equal in value with ones for values of f_{nl} slightly greater than one (Table V).

Table V Evaluated f_{nl} Values with σ=0, Determined σ values for f_{nl}=1 for l>0 for Orbitals from $2p$ to $7p$ for Hydrogen-Like cation Cu^{28+}, and Calculated Energy Levels in Units of Electron Rest Mass Energy. Also, listed energy values do not include spin-orbit **S·L** coupling.

Orbital	f_{nl} ($\sigma = 0$)	Energy E_e	σ in unitless ρ ($f_{ln} = 1$)	Energy E_e
$2p$	1.005583	0.9943645	0.000122	0.9943650
$3p$	1.017	0.9974959	0.000245	0.9974963
$3d$	1.0056	0.9975063	0.0000875	0.9975064
$4p$	1.017	0.9985927	0.000236	0.9985929
$4d$	1.008	0.9985971	0.000131	0.9985971
$4f$	1.008	0.9985989	0.000131	0.9985989
$5p$	1.017	0.9991000	0.000252	0.9991001
$5d$	1.008	0.9991023	0.000000	0.9991023
$5f$	1.008	0.9991032	0.000105	0.9991032
$6p$	1.017	0.9993754	0.000000	0.9993755
$6d$	1.008	0.9993767	0.000000	0.9993767
$7p$	1.017	0.9995413	0.000000	0.9995414

Figure 4 displays the numerical plot of the $2p$ orbital using the analytical solution for f_{nl}=1 with the very small value of the σ-parameter equal to 0.000122 in dimensionless distance ρ with an atomic nucleus radius estimated to be 0.00263 in dimensionless distance ρ. Also, one of the energy values for the $2p$ quantum level, $2p_{3/2}$, is slightly higher in energy than the $2s$, but the other one, $2p_{1/2}$, is slightly less (Table VI), referred to as the Lamb shift (Lamb and Retherford, 1947), when taking spin-orbit **S·L** coupling into account between the electron and atomic nucleus. Thus, relativistic effects explain why quantum levels at the same principal quantum number n, but different angular quantum number l, have slightly different energy values. Larger values of the angular momentum quantum number l results in slightly higher energy if spin-orbit **S·L** coupling is not taken into consideration. In the classical Schrödinger differential wave equation (Walker et al., 2014), quantum levels with the same principal quantum number n and different angular momentum quantum number l are equal in energy and thus degenerate when not including spin-orbit **S·L** coupling.

Table VI Energy Levels: Relativistic Schrödinger and Dirac Differential Wave Equations, including Classical Schrödinger, for Cu^{28+} Cation which Incorporate Spin-Orbit **S·L** Coupling for Orbitals $1s$ to $4f$

Energy values are given in units of the rest mass energy of the electron, and the numerical solutions of the relativistic Schrödinger differential wave equation used for listed energy values with listed factor f_{nl}

Spin Level	Relativistic Schrödinger	Factor f_{Exp} and f_{nl}	Relativistic Dirac[1]	Classical Schrödinger[2]
$1s\ (j=0+\frac{1}{2})(l=0)$	0.9773612	0.489570	0.9773513	0.9776078
$2s\ (j=0+\frac{1}{2})(l=0)$	0.9943230	0.489570	0.9943217	0.9944020
$2p$ (No $\mathbf{S}\cdot\mathbf{L}$ coupling)$(l=1)$	0.9943650	1[3]		0.9944020
$2p_{1/2}\ (j=1-\frac{1}{2})(l=1)$	0.9943216	1	0.9943217	0.9943602
$2p_{3/2}\ (j=1+\frac{1}{2})(l=1)$	0.9943867	1	0.9943862	0.9944228
$3s\ (j=0+\frac{1}{2})(l=0)$	0.9974839	0.489570	0.9974835	0.9975120
$3p$ (No $\mathbf{S}\cdot\mathbf{L}$ coupling)$(l=1)$	0.9974963	1		0.9975120
$3p_{1/2}\ (j=1-\frac{1}{2})(l=1)$	0.9974834	1	0.9974835	0.9975058
$3p_{3/2}\ (j=1+\frac{1}{2})(l=1)$	0.9975028	1	0.9975026	0.9975151
$3d$ (No $\mathbf{S}\cdot\mathbf{L}$ coupling)$(l=2)$	0.9975064	1		0.9975120
$3d_{3/2}\ (j=2-\frac{1}{2})(l=2)$	0.9975026	1	0.9975026	0.9975083[2]
$3d_{5/2}\ (j=2+\frac{1}{2})(l=2)$	0.9975089	1	0.9975089	0.9975145
$4s\ (j=0+\frac{1}{2})\ (l=0)$	0.9985877	0.489570	0.9985875	0.9986005
$4p$ (No $\mathbf{S}\cdot\mathbf{L}$ coupling)$(l=1)$	0.9985929	1		0.9986005
$4p_{1/2}\ (j=1-\frac{1}{2})(l=1)$	0.9985875	1	0.9985875	0.9985953
$4p_{3/2}\ (j=1+\frac{1}{2})(l=1)$	0.9985956	1	0.9985956	0.9986031
$4d$ (No $\mathbf{S}\cdot\mathbf{L}$ coupling)$(l=2)$	0.9985971	1		0.9986005
$4d_{3/2}\ (j=2-\frac{1}{2})(l=2)$	0.9985956	1	0.9985956	0.9985989[2]
$4d_{5/2}\ (j=2+\frac{1}{2})(l=2)$	0.9985982	1	0.9985982	0.9986015
$4f$ (No $\mathbf{S}\cdot\mathbf{L}$ coupling)$(l=3)$	0.9985989	1		0.9986005
$4f_{5/2}\ (j=3-\frac{1}{2})(l=3)$	0.9985982	1	0.9985982	0.9985997[2]
$4f_{7/2}\ (j=3+\frac{1}{2})(l=3)$	0.9985995	1	0.9985995	0.9986010

[1]The Dirac relativistic differential wave equation involving 4×4 Puli spin matrices take **S·L** coupling into account, so there are no energy values for "No **S·L** coupling" in the solutions of the Dirac version.

[2]For the classical Schrodinger differential wave equation, there is a problem with inclusion of **S·L** coupling. The evaluated energy value of the $3d_{3/2}$ is less than for the $3s$, and the energy values of the $4d_{3/2}$ and $4f_{5/2}$ is less than that for the $4s$. This is in contradiction to what is observed experimentally.

[3]For angular momentum quantum number $l>0$, the analytical solution of the relativistic Schrödinger differential wave equation will not result in complex number for γ until the number of protons is greater than 205 for angular quantum number $l=1$, greater than 342 for quantum number $l=2$, and greater than 479 for quantum number $l=3$. Thus, one can assume that factor $f_{nl}=1$ unlike the situation for $l=0$ where it is necessary to evaluate the factor f_{Exp}.

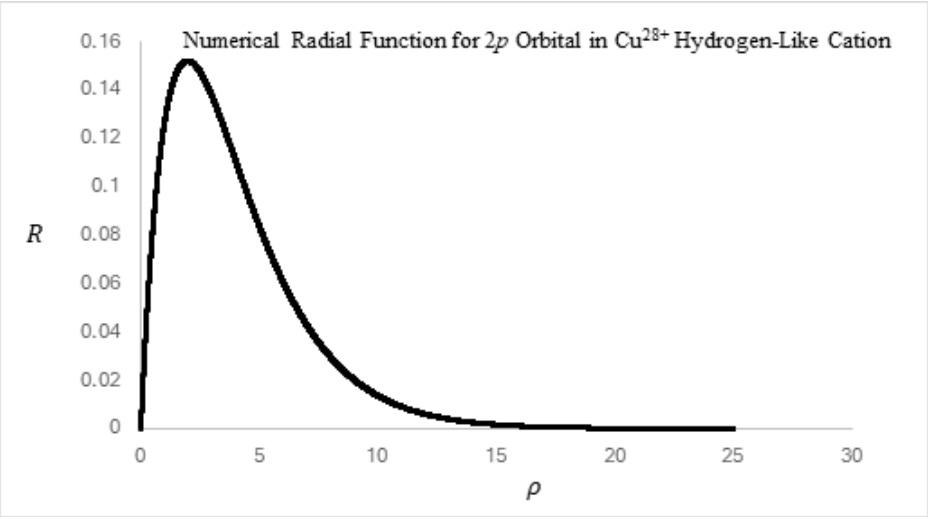

Figure 4 Normalized numerically calculated radial function R for the $2p$ orbital in the Cu^{28+} hydrogen-like cation using factor $f_{nl}=1$ and $\gamma_{nl}=1.984997$, resulting in $E_n=0.9943650>0.9943230$. For the x-axis $r=1.821324$ ρ in units of picometers (10^{-12} meter), and in units of ρ $\sigma=0.000122<r_{nucl}=0.00263$.

Since the analytical solutions for the relativistic Schrödinger equation are quite complex (Table VII), a normalized numerical solution is less tedious and nearly correct. The analytical solution involves gamma-functions of real, non-integer values $\Gamma(s+k)$ since s is equal to non-integer value by Equation 65, that result in irrational numbers evaluated numerically. The classical Schrödinger differential wave equation has gamma-functions of integers $l+k$, involving the angular momentum quantum number, such that $\Gamma(l+k)=(l+k-1)!$, and less complicated negative exponential in the radial wave function. Concerning quantum levels that have the angular momentum number $l=1$, the square root functions in Equations 65 and 68 will not involve negative numbers unless the number of protons is greater than 205.

$$\left(1+\frac{1}{2}\right)^2 - Z^2\alpha^2 = 0 \text{ or } Z = \frac{3/2}{\alpha} = \frac{3}{2} \times 137.036000 = 205.554 \tag{85}$$

With present day technology, element 118, oganesson, is the upper limit possible (Cook, 2010) for producing larger nuclei. From an engineering perspective, it may be impossible as well as physically impossible to produce a radioactive nucleus that has 206 protons due to the physics of the atomic nucleus. In addition, from extrapolation of the experimental data plotted in Figure 5, calculated using the measured data in Table III, one can estimate radial wave functions for hydrogen-like cations beyond copper up to element 118. From the extrapolation of data in Figure 5, element 118 as hydrogen-like cation Og^{117+} is estimated to have an $1s$ ionization energy $E_e=0.546868$ in units of the electron rest mass energy with $\gamma_{exp}=0.562458>1/2$ and factor $f_{exp}=0.331906$.

Table VII Coefficients as Functions of Atomic Number Z for the Analytical Solutions to the Relativistic Schrödinger Differential Wave Equation for $l > 0$ Series Expansion Exponents $k = 1$ to $k = 4$ for $\gamma > \frac{1}{2}$ so $a_{k+1} = \frac{k+l+1-n}{2(k+1)\left[\sqrt{\left(l+\frac{1}{2}\right)^2 - Z^2\alpha^2}\right] + k^2 + 2k + 1} a_k$

Value of k	
1	$a_1 = \frac{1+l-n}{2\sqrt{\left(l+\frac{1}{2}\right)^2 - Z^2\alpha^2}+1} a_0$
2	$a_2 = \left[\frac{2+l-n}{4\sqrt{\left(l+\frac{1}{2}\right)^2 - Z^2\alpha^2}+4}\right]\left[\frac{\mathbf{1+l-n}}{2\sqrt{\left(l+\frac{1}{2}\right)^2 - Z^2\alpha^2}+1}\right] a_0$
3	$a_3 = \left[\frac{3+l-n}{6\sqrt{\left(l+\frac{1}{2}\right)^2 - Z^2\alpha^2}+9}\right]\left[\frac{2+l-n}{4\sqrt{\left(l+\frac{1}{2}\right)^2 - Z^2\alpha^2}+4}\right]\left[\frac{\mathbf{1+l-n}}{2\sqrt{\left(l+\frac{1}{2}\right)^2 - Z^2\alpha^2}+1}\right] a_0$
4	$a_4 = \left[\frac{4+l-n}{8\sqrt{\left(l+\frac{1}{2}\right)^2 - Z^2\alpha^2}+16}\right]\left[\frac{3+l-n}{6\sqrt{\left(l+\frac{1}{2}\right)^2 - Z^2\alpha^2}+9}\right]\left[\frac{2+l-n}{4\sqrt{\left(l+\frac{1}{2}\right)^2 - Z^2\alpha^2}+4}\right]\left[\frac{\mathbf{1+l-n}}{2\sqrt{\left(l+\frac{1}{2}\right)^2 - Z^2\alpha^2}+1}\right] a_0$

Exponential Function and Exponential in Series for $0 < E_s < m_e c^2$

Exponential Function $e^{-\rho/2} = e^{\frac{-\sqrt{m_e^2c^2 - E_s^2}}{\hbar c} r}$

Exponential in Series $\rho^{s+k} = \rho^{\left[-\frac{1}{2}+\sqrt{\left(l+\frac{1}{2}\right)^2 - Z^2\alpha^2}\right]+k} = \left(\frac{2}{\hbar c}\sqrt{m_e^2c^2 - E_s^2}\, r\right)^{\left[-\frac{1}{2}+\sqrt{\left(l+\frac{1}{2}\right)^2 - Z^2\alpha^2}\right]+k}$

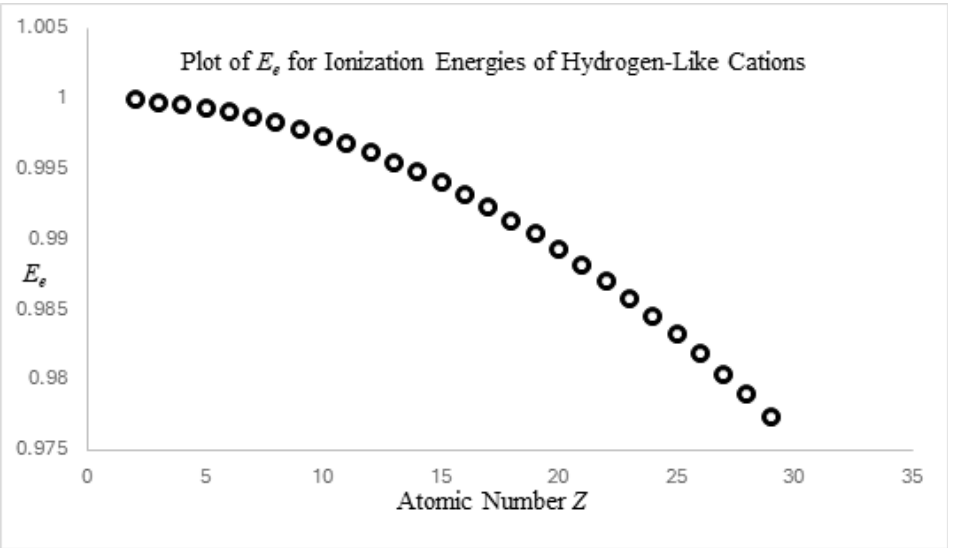

Figure 5 Plot of ionization energies E_e of hydrogen-like cations from He^+ to $Cu2^{8+}$ with respect to the rest mass energy of the electron $m_e c^2$. Black filled circles are from measured data and the white circles are from the following polynomial fit to the data.

$$E_e = 1 - (8.63884\times10^{-13}Z^5 + 3.23529\times10^{-10}Z^4 - 5.80965\times10^{-11}Z^3 + 2.66259\times10^{-5}Z^2 - 2.19743\times10^{-9}Z)$$

Spin-Orbit S·L Coupling for the Relativistic Schrödinger Differential Wave Equation

The orbiting electron in the atom experiences a magnetic field **B** from the positively charged atomic nucleus. Relative to the electron, the atomic nucleus is orbiting in the opposite direction producing this magnetic field. Thus, there is the following torque **τ** experienced by the electron which has the magnetic dipole $\boldsymbol{\mu}_s$ due to the intrinsic spin of the negatively charged electron.

$$\boldsymbol{\tau} = \boldsymbol{\mu}_s \times \mathbf{B} = \left(-\frac{g_s \mu_b}{\hbar}\right)\mathbf{S} \times \mathbf{B} \text{ (Walker et al., 2014)} \tag{86}$$

Concerning this torque in Equation 86, **S** is the angular momentum vector for the intrinsic spin of $1/2$ of the electron. Also, $\mu_b = \frac{q\hbar}{2m_e}$ in Equation 86 is the Bohr magnetron for the electron, and g_s=2 as determined by experimental results in the Stern-Gerlach experiment (Walker et al., 2014). The negative sign for the magnetic dipole $\boldsymbol{\mu}_s$ arises from the negative charge of the electron. Below in Equation 87, the mathematical expression of this magnetic field **B** is shown as derived by the Biot-Savart Law (Walker et al., 2014) since the tangential velocity is $-\mathbf{v}$ of the atomic nucleus relative to the electron tangential velocity **v** in the opposite direction.

$$\mathbf{B} = -\frac{\mu_0 Zq}{4\pi}\frac{\mathbf{v}\times\mathbf{r}}{r^3} = -\varepsilon_0\mu_0\left(\frac{1}{4\pi\varepsilon_0}\frac{Zq}{r^3}\right)\mathbf{v}\times\mathbf{r} = -\frac{1}{c^2}\left(\frac{1}{4\pi\varepsilon_0}\frac{Zq}{r^3}\right)\mathbf{v}\times\mathbf{r} \quad \text{Where } \varepsilon_0\mu_0 = \frac{1}{c^2} \tag{87}$$

And in Equation 87, μ_0 is the vacuum magnetic permeability which in MKS units is

$$\mu_0 = 4\pi\times10^{-7}\,\frac{\text{Newton}}{\text{Ampere}^2} = 4\pi\times10^{-7}\,\frac{\text{Newton}}{(\text{Coulomb/second})^2} \text{ (Tipler and Llewellyn, 2012)} \tag{88}$$

This results in the energy splitting ΔE, referred to as spin-orbit **S·L** coupling, in the following expression given in the vector dot product below after the substitution of Equation 87 for magnetic field **B**.

$$\Delta E = -\boldsymbol{\mu}_s\cdot\mathbf{B} = -\left(-\frac{g_s\mu_b}{\hbar}\right)\mathbf{S}\cdot\left[-\frac{1}{c^2}\left(\frac{1}{4\pi\varepsilon_0}\frac{Zq}{r^3}\right)\mathbf{v}\times\mathbf{r}\right] = -\frac{g_s\mu_b}{\hbar}\mathbf{S}\cdot\left[\frac{1}{c^2}\left(\frac{1}{4\pi\varepsilon_0}\frac{Zq}{r^3}\right)\mathbf{v}\times\mathbf{r}\right] \tag{89}$$

In the frame of reference of the atomic nucleus at rest, there is the Thomas precession (Walker et al, 2014) arising from the relativistic transformation of velocities, so the spin-orbit interaction in Equation 89 is multiplied by $1/2$.

$$\Delta E = -\frac{1}{2}\frac{g_s\mu_b}{\hbar}\mathbf{S}\cdot\left[\frac{1}{c^2}\left(\frac{1}{4\pi\varepsilon_0}\frac{Zq}{r^3}\right)\mathbf{v}\times\mathbf{r}\right] \tag{90}$$

Then multiply the right-hand side of Equation 90 with the charge ratio $\frac{q}{q}(=1)$ which will be useful for incorporating the unitless parameter α.

$$\Delta E = -\frac{1}{2}\frac{g_s\mu_b}{q\hbar c^2}\left(\frac{1}{4\pi\varepsilon_0}\frac{Zq^2}{r^3}\right)\mathbf{S}\cdot(\mathbf{v}\times\mathbf{r}) \tag{91}$$

Since the electron orbital angular momentum vector **L** being equal to $\mathbf{r}\times m_e\mathbf{v}$, such that $-\mathbf{L}=m_e\mathbf{v}\times\mathbf{r}$ because the cross product of two vectors anti-commute $(\mathbf{A}\times\mathbf{B})+(\mathbf{B}\times\mathbf{A})=\mathbf{0}$ (Wangness, 1986), Equation 91 becomes the following.

$$\Delta E = \frac{1}{2}\frac{g_s\mu_b}{q\hbar m_e c^2}\left(\frac{1}{4\pi\varepsilon_0}\frac{Zq^2}{r^3}\right)\mathbf{S}\cdot\mathbf{L} \tag{92}$$

Since experimentally g_s has been observed to be equal to 2 and the Bohr magneton μ_b of the electron is equal to $\mu_b = \frac{q\hbar}{2m_e}$ Equation 92 is the next expression.

$$\Delta E = \frac{1}{2m_e^2c^2}\left(\frac{1}{4\pi\varepsilon_0}\frac{Zq^2}{r^3}\right)\mathbf{S}\cdot\mathbf{L} \tag{93}$$

To determine what the vector dot product **S**·**L** is equal to, it is important to note that the total angular momentum **J** is equal to the sum of the **L** and **S** quantized angular momenta, **L** the orbital angular momentum vector and **S** the spin angular momentum vector of the electron.

$$\mathbf{J} = \mathbf{L} + \mathbf{S} \tag{94}$$

Performing the vector dot product **J**·**J** to obtain the following expression since vectors **L** and **S** are not orthogonal

$$\mathbf{J}\cdot\mathbf{J} = \mathbf{L}\cdot\mathbf{L} + \mathbf{S}\cdot\mathbf{S} + 2\mathbf{S}\cdot\mathbf{L} \tag{95}$$

This shows the following.

$$\mathbf{S}\cdot\mathbf{L} = \frac{\mathbf{J}\cdot\mathbf{J} - \mathbf{L}\cdot\mathbf{L} - \mathbf{S}\cdot\mathbf{S}}{2} = \frac{J^2 - L^2 - S^2}{2} \tag{96}$$

And since the magnitude of the dot products for each angular momentum vector **J**, **L**, and **S** with itself are the following expressions (Tipler and Llewellen, 2012),

$$\mathbf{J}\cdot\mathbf{J} = J^2 = j(j+1)\hbar^2 \qquad \mathbf{L}\cdot\mathbf{L} = L^2 = l(l+1)\hbar^2 \qquad \mathbf{S}\cdot\mathbf{S} = S^2 = s(s+1)\hbar^2 \tag{97}$$

Equation 93 becomes

$$\Delta E = \frac{\hbar^2}{4m_e^2c^2}\left(\frac{1}{4\pi\varepsilon_0}\frac{Zq^2}{r^3}\right)[j(j+1) - l(l+1) - s(s+1)] \tag{98}$$

Concerning Equation 98, for $j = l + \frac{1}{2}$, ΔE is

$$\Delta E = \frac{\hbar^2}{4m_e^2c^2}\left(\frac{1}{4\pi\varepsilon_0}\frac{Zq^2}{r^3}\right)\left[\left(l+\frac{1}{2}\right)\left(l+\frac{3}{2}\right) - l(l+1) - \frac{1}{2}\left(\frac{1}{2}+1\right)\right] = \frac{\hbar^2}{4m_e^2c^2}\left(\frac{1}{4\pi\varepsilon_0}\frac{Zq^2}{r^3}\right)l > 0 \tag{99}$$

And for $j = l - \frac{1}{2}$, ΔE equals the following equation representing a lower energy state for $l - \frac{1}{2}$

$$\Delta E = \frac{\hbar^2}{4m_e^2c^2}\left(\frac{1}{4\pi\varepsilon_0}\frac{Zq^2}{r^3}\right)\left[\left(l-\frac{1}{2}\right)\left(l+\frac{1}{2}\right) - l(l+1) - \frac{1}{2}\left(\frac{1}{2}+1\right)\right] = -\frac{\hbar^2}{4m_e^2c^2}\left(\frac{1}{4\pi\varepsilon_0}\frac{Zq^2}{r^3}\right)(l+1) < 0 \tag{100}$$

Now we have the expression in Equation 98 for the spin-orbit **S**·**L** coupling term that can be transformed in units of electron rest mass energy m_ec^2 as in Equations 52 for the quantum energy levels E_s of the relativisticSchrödinger differential wave equation. First, transform r into unitless ρ, since $r = \frac{\rho}{2\beta}$, by the following transformations of Equation 98 with substitution of $\alpha = \frac{q^2}{\hbar c 4\pi\varepsilon_0} = \frac{1}{137.036}$.

$$\Delta E = \frac{\hbar^3}{4m_e^2c}(2\beta)^3\frac{Z\alpha}{\rho^3}[j(j+1) - l(l+1) - s(s+1)] \tag{101}$$

$$\Delta E = \frac{2\hbar^3}{m_e^2c}\beta^3\frac{Z\alpha}{\rho^3}[j(j+1) - l(l+1) - s(s+1)] \tag{102}$$

Then substitute β^2 form Equation 48 into $\beta^3=(\beta^2)^{3/2}$

$$\Delta E = \frac{2\hbar^3}{m_e^2 c}\left(\frac{m_e^2c^4 - E_s^2}{\hbar^2c^2}\right)^{\frac{3}{2}}\frac{Z\alpha}{\rho^3}[j(j+1) - l(l+1) - s(s+1)] \tag{103}$$

One then substitutes Equation 52 for E_s and after performing some algebraic operations, Equation 103 becomes

$$\Delta E = m_e c^2 \frac{2Z\alpha}{\left(1+\frac{\gamma_{nl}^2}{Z^2\alpha^2}\right)^{\frac{3}{2}}}[j(j+1) - l(l+1) - s(s+1)]\frac{1}{\rho^3} \tag{104}$$

Then perform an integration, either numerically or use the analytical solutions for $l>0$ radial wave functions, to obtain the expectation value $\langle\frac{1}{\rho^3}\rangle$ evaluate the expectation value $\langle\Delta E\rangle$ of ΔE due to the wave characteristics of an electron in the atom.

$$\langle\frac{1}{\rho^3}\rangle = \int_0^\infty R(\rho)\frac{1}{\rho^3}R(\rho)\rho^2 d\rho \tag{105}$$

$$\langle\Delta E\rangle = m_e c^2 \frac{2Z\alpha}{\left(1+\frac{\gamma_{nl}^2}{Z^2\alpha^2}\right)^{\frac{3}{2}}}[j(j+1) - l(l+1) - s(s+1)]\langle\frac{1}{\rho^3}\rangle \tag{106}$$

$$\langle\Delta E_e\rangle = \frac{\langle\Delta E\rangle}{m_e c^2} = \frac{2Z\alpha}{\left(1+\frac{\gamma_{nl}^2}{Z^2\alpha^2}\right)^{\frac{3}{2}}}[j(j+1) - l(l+1) - s(s+1)]\langle\frac{1}{\rho^3}\rangle \tag{107}$$

Table VI displays the energy values including spin-orbit **S·L** coupling in the relativistic Schrödinger differential wave equations and that from the Dirac relativistic differential wave equation. Table VI also shows the experimentally observed Lamb shift (Lamb and Retherford, 1947) when using the relativistic Schrödinger differential wave equation with spin-orbit **S·L** coupling, such that the $2p_{1/2}$ orbital is slightly less in energy than the $2s$, and the same for the $3p_{1/2}$ and $3s$ orbitals as well as for the $4p_{1/2}$ and $4s$ orbitals. The Dirac relativistic differential wave equation yields these two orbitals in the n=2, n=3, and n=4 shells to be equal in energy.

The Dirac Relativistic Differential Wave Equation

In addition to the relativistic Schrödinger differential wave equation, Dirac developed a Hamiltonian for the relativistic effects of the electron in the hydrogen atom and hydrogen-like cations shown below.

$$\mathbf{H}\begin{bmatrix}\psi_a(r)\\ \psi_b(r)\end{bmatrix} = \begin{bmatrix} -\frac{1}{4\pi\varepsilon_0}\frac{Ze^2}{r} + m_e c^2 & -icp_r - c\frac{\hbar}{r} - \frac{c\hbar j'}{r} \\ icp_r + c\frac{\hbar}{r} - \frac{c\hbar j'}{r} & -\frac{1}{4\pi\varepsilon_0}\frac{Ze^2}{r} - m_e c^2 \end{bmatrix}\begin{bmatrix}\psi_a(r)\\ \psi_b(r)\end{bmatrix} = E\begin{bmatrix}\psi_a(r)\\ \psi_b(r)\end{bmatrix} \text{ (Dirac, 1930)} \tag{108}$$

Dirac based this upon the 2×2 matrix due to the intrinsic spin of $1/2$ in the electron. There are no spherical harmonics involving spherical polar coordinates θ and ϕ and in Equation 108, p_r and j' are the two following mathematic statements.

$$p_r = -i\hbar\frac{d}{dr} \qquad j' = j + \frac{1}{2} = \left(l \pm \frac{1}{2}\right) + \frac{1}{2} \tag{109}$$

In Equation 109, j is the sum or difference of the angular quantum number l and intrinsic spin quantum number $1/2$ for the electron in the atom. Instead of only one radial wave function, the Dirac relativistic differential wave equation has two due to the Hamiltonian being a 2×2 matrix based upon the Pauli spin matrixes of the electron intrinsic spin.

$$\psi_a(r) = \frac{1}{r}e^{-r/a}f(r) = \frac{1}{r}e^{-r/a}\sum_{k=0}^{K} f_k r^k \tag{110}$$

$$\psi_b(r) = \frac{1}{r}e^{-r/a}g(r) = \frac{1}{r}e^{-r/a}\sum_{k=0}^{K} g_k r^k \tag{111}$$

In Equations 110 and 111, a in both negative exponentials equals the following expression.

$$a = \sqrt{\left(\frac{\hbar c}{m_e c^2 - E_s}\right)\left(\frac{\hbar c}{m_e c^2 + E_s}\right)} \tag{112}$$

And the coefficients in both Equations 110 and 111 are different and have terminating series which yield the following equation for the sum energy levels E_s of the electron, which is the total mechanical energy E_m plus the rest mass energy $m_e c^2$ of the electron.

$$E_s = \frac{m_e c^2}{\sqrt{1 + \dfrac{Z^2\alpha^2}{\left[n - \left(j + \frac{1}{2}\right) + \sqrt{\left(j + \frac{1}{2}\right)^2 - Z^2\alpha^2}\right]^2}}} \tag{113}$$

It is important to note that Equation 117 will result in a complex number when the atomic number of a large nucleus has more than 137 protons for quantum number $j = \frac{1}{2}$. In comparison, Table VI displays the results by the Dirac's relativistic differential wave equation for the $1s$ to $4f$ orbitals in the hydrogen-like cation Cu^{28+} with that of the relativistic Schrödinger differential wave equations.

In addition, Table VI displays ionization energies of the hydrogen-like cation Cu^{28+} for the $1s$ to $4s$ orbitals calculated using the classical Schrödinger differential wave equation (Walker et al., 2014). However, in the classical Schrödinger differential wave equation, quantum levels with different angular momentum quantum number l are degenerate that have the same principal quantum number n when not taking spin-orbit **S·L** coupling into account. If one takes spin-orbit **S·L** coupling into account, the resulting energy values do not agree with experimental results since it is relativistic effects which cause the loss in degeneracy of the angular momentum quantum levels that have same principal quantum number n.

Conclusion

Results are reported in this paper which can match experimental ionization energies for hydrogen-like cations from numerical analyses of the relativistic Schrödinger differential wave equation if incorporating experimental ionization energies for the $1s$ electron. The likely reason why the theoretical relativistic Schrödinger differential wave equation and measurement of $1s$ ionization

energies of hydrogen-like cations differ in value is that the subatomic particles are not point masses as in the traditional treatment of wave-particle duality in quantum mechanics. For l=0 electron orbitals at any principal quantum number n, the analytical solutions for both the relativistic Schrödinger differential wave equation, assuming factor f_{ns}=1, and Dirac relativistic differential wave equation predict that the $R(\rho)$ function goes to infinity at the center of the atomic nucleus. This cannot be the real case since subatomic particles are not point masses but have very microscopic definite volumes. Both plots in Figures 2 and 3 have limited maximum values when the electron is at the center of the atomic nucleus.

This paper demonstrates the hyperfine anomalies seen in particularly large atoms which have different ionization energies. Interestingly, the experimental data generated with a numerical analysis in our work reveal the Lamb shift, which is not shown by the Dirac equation. For l=0, it is important to take into consideration that the nucleus is not a point mass and only a numerical solution with experimental data can be used to determine the shape of the orbital. While anomalies may seem irrelevant, they may explain some of the mysterious phenomena encountered in nature, such as the colors of copper and gold metals, the liquid state of mercury, and the malleability of lead. Perhaps there are other consequences of unknown anomalies in nature, which might even explain why some people see Bigfoot and others do not.

References

Arfken, George B., and Hans J. Weber. 2005. *Mathematical Methods for Physicists*. 6th Edition. Elsevier Academic Press, San Diego, CA.

Cook, Norman. 2010. *Models of the Atomic Nucleus: Unification Through a Lattice of Nucleons.* 2nd Edition. Springer-Verlag, New York.

Dirac, P.A.M. 1930. *The Principles of Quantum Mechanics*. Oxford University Press, Oxford, England.

Einstein, Albert. 1905a. Über einen die Erzeugung und Verwandlung des Lichtes betreffenden heuristischen Gesichtspunkt. Annalen der Physik 17:132-148.

Einstein, Albert. 1905b. Über die von der molekularkinetischen Theorie der Wärme geforderte Bewegung von in ruhenden Flüssigkeiten suspendierten Teilchen. Annalen der Physik 17:549-560. 21 Einstein, Albert. 1905c. Zur Elektrodynamik begetter Körper. Annalen der Physik 17:891-921.

Einstein, Albert. 1905d. Ist die Trägheit eines Körpers von seinem Energieinhalt abhängig? Annalen der Physik 18:639-641.

Eisberg, Robert, and Robert M. Resnick. 1986. *Quantum Physics of Atoms, Molecules, Solids, Nuclei and Particles*. 2nd Edition. John Wiley & Sons, Inc., Hoboken, NJ.

Kleppner, Daniel and Robert Kolenkow. 2014. *An Introduction to Mechanics*. 2nd Edition. Cambridge University Press, Cambridge, United Kingdom.

Lamb, Willis E. Robert C. Retherford. 1947. Fine Structure of the Hydrogen Atom by a Microwave Method. Physical Review. 72:241-243.

LeVeque, Randall J. 2007. *Finite-Difference Methods for Ordinary and Partial Differential Equations*. Society for Industrial and Applied Mathematics, Philadelphia, PA.

McNeill, James H., and J.E. Bidlack. 2018. Modifying the Redlich-Kwong-Soave equation of state. Proceedings of the Oklahoma Academy of Science. 98:127-138.

McNeill, James H., Robert A. Doti, and James E. Bidlack. 2021. Modern Perspectives on Einstein's General Theory of Relativity. Proceedings of the Oklahoma Academy of Science. 101:115-137.

Microsoft Corporation. 2018. Microsoft Excel. Retrieved from https://office.microsoft.com/excel. Accessed April 2025.

Miessler, Gary L., Paul A. Fischer, and Donald A. Tarr. 2014. *Inorganic Chemistry*. 5th Edition. Pearson, New York.

Tipler, Paul A. and Ralph A. Llewellyn. 2012. *Modern Physics*. 6th Edition. W. H. Freeman & Company, New York.

Walker, Jearl, Robert Halliday, and Robert Resnick. 2014. *Fundamentals of Physics*. 10th Edition. John Wiley & Sons, Inc., Hoboken, NJ.

Wangsness, Ronald K. 1986. *Electromagnetic Fields*. 1986. 2nd Edition. John Wiley & Sons, Inc., Hoboken, NJ.

Wikipedia: The Free Encyclopedia. 2025. Molar Ionization Energies of the Elements. https://en.wikipedia.org/wiki/Molar_ionization_energies_of_the_elements. Wikipedia Foundation. Accessed April 2025.

Wong, Samuel S. M. 1998. *Introductory Nuclear Physics*. 2nd Edition. John Wily & Sons, Inc., Hoboken, NJ. 22

ABSTRACTS OF THE 114TH OKLAHOMA ACADEMY OF SCIENCE TECHNICAL MEETING NOVEMBER 7, 2025 ORAL ROBERTS UNIVERSITY BIOLOGICAL SCIENCES CENTER TULSA, OK

(sorted by presenter's last name)

A PRECIPITATION-DRIVEN MICROBIAL SHIFT: BACTERIAL VS FUNGAL CORRELATES OF CARBON STORAGE IN OKLAHOMA FORESTS

Rustem Fatih Albayrak, Oklahoma State University - Stillwater

Outstanding Graduate Poster

Forest soils constitute the largest terrestrial carbon reservoir, yet their stability under changing precipitation regimes remains a critical uncertainty in climate projections. While belowground microbial communities regulate carbon cycling, how precipitation alters the relative importance of bacteria versus fungi as drivers of carbon storage is poorly understood. This study tests the hypothesis that precipitation regime determines whether bacterial or fungal communities are stronger predictors of total ecosystem carbon storage. We leverage Oklahoma's pronounced precipitation gradient (400-1200 mm/yr) across 50 forest plots representing major vegetation types. Bacterial (16S rRNA) and fungal (ITS2) communities are being characterized through amplicon sequencing, while carbon stocks are quantified through forest inventories and soil organic matter analysis. Using Structural Equation Modeling, we are testing how precipitation moderates relationships between microbial diversity and carbon storage. We predict a systematic shift from fungal-dominated carbon storage mechanisms in high-precipitation eastern forests to bacterial-dominated mechanisms in low-precipitation western woodlands. This research will provide crucial insights into climate-microbe-carbon interactions and inform climate-resilient forest management strategies tailored to Oklahoma's diverse precipitation regimes.

MICROBIAL DARK OXYGEN PRODUCTION IN FRESHWATER AQUIFERS

Samikshya Giri, Adrienne Jones, Anna Rockwood, Todd Halihan, Lauren Haygood, and Sabrina Beckmann, Oklahoma State University - Stillwater

Microbial dark-oxygen production has recently been observed in marine and groundwater environments, carried out by ammonium-oxidizing archaea (AOA). These archaea oxidize ammonium to nitrite to meet their energy needs and are abundant in environments with high, very low, or depleted oxygen levels. Recent studies have shown that the ammonium-oxidizer *Nitrosopumilus maritimus* can produce oxygen and dinitrogen in the dark (Kraft et al., Science, 2022). In this study, we examine the microbiology, hydrology, and geochemistry of both a contaminated groundwater site and a non-contaminated site within the Arbuckle-Simpson Aquifer. The contaminated site exhibits varying levels of contamination with chlorinated compounds. Electrical Resistivity Imaging (ERI) indicated low bioactivity within the contaminated groundwater plume, which aligned with total cell counts ranging from $1.1\times10^{1}6$ to $9.1\times10^{1}7$ cells/mL, similar to those in the non-contaminated control well ($3.7\times10^{1}7$ cells/mL). 16S rRNA sequencing and quantitative PCR (qPCR) targeting bacterial, archaeal, and dehalogenase genes revealed that dehalogenating bacteria belonging to the phyla Chloroflexi and Deltaproteobacteria are present at very low abundances, below 1% of the overall microbial community. They are likely mostly inactive due to high oxygen levels and the groundwater's redox potential. Surprisingly, we detected an aerobic or facultatively anaerobic microbial community comprising bacteria and archaea, predominantly ammonium-oxidizing archaea (AOA). The microbial communities were dominated by *Nitrosopumilus* and *Nitrososphaera*, with relative abundances of up to 65% and 21% of the community, respectively, consistent with high abundances of ammonium-oxidizing genes (amoA). At the non-contaminated groundwater site, seven bacterial and archaeal species capable of dark oxygen production were identified in the aquifer. The pathways for dark oxygen production are not yet fully understood. Our results suggest that these microbes could raise the aquifer's redox potential, resulting in implications for the development of new electrode-monitoring systems and overall aquifer assessment strategies.

DIVERGENCE IS SIK3 OF *DROSOPHILA* SPECIES

Jadie Brister[1], Lainy Lewis[1], Lindsey J. Long[1], and Laura Reed[2] , [1]Oklahoma Christian University; [2]Genomics Education Program-University of Alabama

Outstanding Undergraduate Paper in Biological Sciences (Zoology)

This study investigated the evolutionary divergence of two genes, Salt-inducible kinase 3 (Sik3) and rolled (rl), across five species of *Drosophila*, using *D. melanogaster* as the reference. Both genes are part of the insulin/TOR signaling pathway, which regulates growth and metabolism. We hypothesized that Sik3 would be more divergent due to its metabolic role and potentially fewer constraints on its function. Gene annotation was performed using tools provided by the Genomics Education Partnership to build gene models, analyze protein sequences, and examine genomic neighborhoods. While Sik3 had lower sequence divergence scores, rl is considered functionally more conserved, likely due to its central role in signal transduction and interaction with many other proteins. These results suggest that gene conservation is influenced not just by how much a gene's sequence changes, but also by how critical its role is in cellular networks.

134
FROM *FEROCACTUS* TO CORYPHATHA: THE COMPARATIVE ANATOMY OF EXTRAFLORAL NECTARIES IN THE TRIBE CACTEAE

Jackson Burkholder, Oklahoma State University - Stillwater

Extrafloral nectaries (EFNs) are specialized glands in plants that secrete an aqueous solution of sugars and amino acids. Unlike floral nectaries, which function primarily in pollination, EFNs are typically associated with plant defense, attracting invertebrates whose presence and activity can reduce herbivory. EFNs were first observed in the cactus family in 1837 and since the late 1890's it has been hypothesized that the EFNs of the tribe Cacteae represent highly modified secretory spines. Throughout the 20th century anatomical studies have been conducted on a small number of species, but the anatomy of these structures remains completely undocumented for many genera, and the comparative anatomy of EFNs across every genus in the tribe in which they occur has never been investigated. My study reaffirms the basic structure of these EFNs: a basal vascularized stalk filled with subnectary parenchyma topped with a broad secretory head of nectary parenchyma cells which secrete nectar through a ruptured cuticle. I provide additional evidence that they represent highly modified spines by proposing a classification system that shows a gradient of more spinelike characteristics to those that are more specialized for secretion. *Ferocactus*-type EFNs are the least specialized and have the most spine like characteristics, including their close association with the spines of areoles, loosely organized vascular tissue, and a secretory head that consists of fiber-like cells which elongate from an intercalary meristem. *Sclerocactus*-type EFNs are also associated with the spines of the areole but have a clavate secretory head devoid of fiber-like cells and a single ring of vascular tissue in the stalk. *Coryphantha*-type EFNs are the most specialized as they have a strongly capitate secrertory head without fiber-like cells, highly organized vascular tissue in a single ring of well-developed collateral bundles and are associated with the axillary extent of dimorphic areoles.

STEPS TO SUCCESS: HOW WELLNESS DRIVES FLOURISHING

Duoduo Cai, Emily Walz, Ella Howard, Kennedy Seggelke, Chloe Winkler, Myra Bloom, Scarlet Jost, Andrew Lang, Nancy Mankin, Philip Nelson, and Enrique Valderrama, Oral Roberts University

Outstanding Undergraduate Paper in Math, Computer Science, & Statistics

At Oral Roberts University, whole-person education is not just a value, it's a mission. Every student participates in a comprehensive health and physical activity program designed to nurture spirit, mind, and body. Over the past decade, our interdisciplinary undergraduate research group has investigated how wellness behaviors, especially physical activity, relate to academic performance, retention, and overall flourishing. Drawing on a large multi-year dataset, we find consistent evidence that students who maintain active, healthy lifestyles achieve higher GPAs and persist at greater rates, independent of background factors such as personality or socioeconomic status.

EVALUATING SOIL PHYSICAL PROPERTIES ON OKLAHOMA SOILS: THE ROLE OF BIOCHAR AMENDMENTS

MaKayla Friend, Jonathan Medellin, Nimalka Weerasuriya, and Benedicte Bachelot, Oklahoma State University - Stillwater

Outstanding Undergraduate Paper in Environmental Sciences

Promoting soil health and stimulating natural soil processes that have been depleted over time are the goal of current agriculture practices, including the use of organic amendments. Agricultural systems also heavily rely on the use of biocides, which could indirectly alter soil health. My aims of this study are (1) to evaluate the impacts of different biochar amendments on soil properties, and (2) to assess the possible interaction between biochar amendments and the use of biocides on soil health. The study was conducted at McPherson Prairie Preserve in the international BugNet experiment. The BugNet experiment consists in three blocks of 8 5x5m plots which have been receiving one of 8 biocide treatments for the last four years. In each subplot, two different feedstocks, spent brewer's grain and poultry litter, were converted to biochar and applied to two of the three quadrants. Bulk density, soil porosity, soil aggregate stability, soil respiration, root colonization, and infiltration rate will be assessed in all three quadrants. I will use statistical testing to analyze the effect of biochar and biocide (with their interaction) on soil physical properties using the experimental block as a random effect. We expect the biochar/no biocide treatments to increase infiltration rate, soil respiration, root colonization, soil stability, and porosity: and biochar/no biocide plots may decrease bulk and particle density. The biocide with biochar treatments may reduce some soil physical and biological properties. My work will provide insights into the benefits associated with the use of biochar for soil health and whether these benefits hold when using biocides. My study will therefore serve as a bridge between soil health and agriculture, which can lead to more restoration initiatives and funding to increase productivity in soils.

EFFECTS OF MAGNESIUM: PHOSPHORUS SUPPLY ON THE GROWTH OF PRIMARY PRODUCERS AND PRIMARY CONSUMERS IN FRESHWATER ECOSYSTEMS

Parna Ghosh, Justin Scott, and Puni Jeyasingh, Oklahoma State University - Stillwater

The availability and interactions of ~25 elements influence growth and production. Carbon (~50% of cellular dry mass), and nitrogen and phosphorus (building blocks of nucleic acids and proteins) are abundant intracellular elements. Phosphorus is present in ribosomal RNA (~50% cellular P), and in ATP, which are key molecules involved in protein synthesis and in energy transfer. Both in rRNA and ATP, magnesium (Mg) stabilizes the negative charge of phosphorus (P) and Mg:P ratio in these biomolecules is 1:2. Although Mg varies greatly in lakes from 100–8000 µg/L (nationally), and 3000–3700 µg/L across Oklahoma reservoirs, the role of Mg in eutrophication is poorly understood. We predicted that the largest impact of Mg on phosphorus use efficiency (PUE) in freshwater algae (Scenedesmus obliquus) and in their primary consumers (Daphnia), would align closest with the 1:2 Mg:P cellular requirement. We measured growth rate of Scenedesmus obliquus and Daphnia under a Mg:P supply concentration gradient (0.375–12 molar). For both producer and consumer, the highest growth rate was observed when Mg:P supply ratio was closer to 1:2 (1.5–4.5), indicating that biomass produced per unit of P assimilated is affected by the availability of Mg. Our results indicate that P loading in lakes is likely influenced by Mg availability and highlights the importance of understanding the impacts of Mg on PUE and productivity to effectively predict eutrophication of lakes with varying magnesium supplies.

136
MECHANISMS OF HEME IRON ACQUISITION IN *MYCOBACTERIUM TUBERCULOSIS*

Trevor Hensley, Taylor Menard, Emilyn Rainbolt, and Avishek Mitra, Oklahoma State University - Stillwater

Outstanding Undergraduate Poster

Mycobacterium tuberculosis (*Mtb*), a human lung pathogen, is completely dependent on acquiring iron from the host to survive and cause infections. Like most pathogens *Mtb* can acquire iron from host heme, which stores >75% of the host iron. However, the importance of Hm iron acquisition to *Mtb* virulence is unknown because we have a very limited understanding of *Mtb* HIA mechanisms. In principle, there are three main steps to Hm uptake in diderm bacteria like *Mtb*. As majority of host Hm is complexed with proteins like hemoglobin, the first step in bacterial Hm uptake invariably starts with extracting Hm from the host hemoprotein. After Hm is extracted, it is then transported across the outer membrane (OM) by a channel protein and then across the cytoplasmic membrane (CM) by another channel protein. The Mitra lab has made crucial discoveries in identifying potential components of this Hm uptake process in *Mtb*: 1) Deletion of rv0125 or rv0338c reduces growth of *Mtb* in the presence of hemoglobin. We hypothesize that Rv0125 and Rv0338c are somehow required to extract Hm from hemoglobin so that Hm can be used as an iron source. 2) Deletion of ppe60 reduces growth of *Mtb* in the presence of Hm. PPE60 is a predicted outer membrane protein and we hypothesize that it is required for Hm uptake in *Mtb*. The goals of this study are to determine how Rv0125, Rv0338c and PPE60 contribute to Hm iron acquisition in *Mtb*. Specifically: 1) We will clone these genes into an expression plasmid and then produce and purify these proteins from *E. coli*. 2) We will perform binding experiments using isothermal titration calorimetry to determine if these proteins bind Hm. 3) We will use *Mtb* mutant strains to determine if absence of the genes affects Hm uptake into *Mtb* cells.

DANDELION SEED EXTRACT EXHIBITS BROAD-SPECTRUM, DOSE-DEPENDENT CYTOTOXICITY ACROSS MULTIPLE CANCER CELL LINES

Christina Hendrickson, Oklahoma City University

Natural products such as *Taraxacum officinale* (dandelion) have gained attention for their potential anticancer properties. This study evaluated the cytotoxic effects of Dandelion Seed Extract (DSE) on five cancer cell lines, HeLa (cervical), A2780 (ovarian), Panc2 (pancreatic), 4T1 (murine breast), and HT1376 (bladder). Cells were treated with increasing concentrations of DSE (0–2 mg/mL) for 24 h, and viability was assessed using PrestoBlue HS assay. DSE significantly reduced viability in all tested cell lines in a dose-dependent manner. Two-way ANOVA revealed significant main effects of both DSE concentration ($p = 7.8 \times 10^{-75}$) and cell line ($p = 2.2 \times 10^{-19}$), as well as a significant interaction between the two factors ($p = 6.1 \times 10^{-9}$). Among all cell lines, 4T1 exhibited the greatest sensitivity, showing >50% viability reduction at 0.2 mg/mL. These findings demonstrate that DSE exerts broad-spectrum, dose-dependent cytotoxic effects, with differential sensitivity across cancer types. This study suggests DSE contains potent bioactive compounds that may warrant further mechanism and in vivo investigation as potential anticancer agent.

INVESTIGATING *E. COLI* MECHANISMS FOR POTENTIAL THERAPIES IN BLADDER CANCER

Shane Holmes, Alejandro Lopez, and Janaki Iyer, Northeastern State University

Outstanding Undergraduate Paper in Microbiology

Bladder cancer remains a major health challenge, with an estimated 1 in 28 men and 1 in 89 women diagnosed during their lifetime. In 2025, the American Cancer Society projects nearly 85,000 new cases and over 17,000 deaths from bladder cancer in the United States. There are many different treatments methods, including surgery, immunotherapy, radiotherapy, and chemotherapy; however, there is a rapid rise in tumors developing resistance. This highlights the need for alternative therapeutic strategies. We previously observed that bladder cancer cells exposed to uropathogenic *Escherichia coli* CFT073 (*E. coli* CFT) are severely damaged. To gain more insight on mechanistic aspects, we have focused on studying interactions between the bacteria and host cells. We transformed *E. coli* CFT073 with a plasmid encoding GFP that enabled fluorescence-based tracking of the bacteria. Since many uropathogenic *E. coli* are invasive, we hypothesize that this strain (*E. coli* CFT-GFP) will robustly interact with 5637 bladder cancer cells resulting in stress responses similar to those caused by the wild type. Flow cytometry and fluorescence microscopy showed bacterial cells interact with bladder cells and induce stress in a bacterial cell density dependent manner. These results support the idea that bacterial cell interactions cause cell stress in bladder cancer cells. Future studies will investigate whether disruption of interactions between 5637 bladder cancer cells and *E. coli* CFT can reduce the stress on bladder cancer cells. These findings will aid us in our long-term goal of identifying the factor that the bacteria synthesize to induce cell damage in bladder cells.

INVESTIGATING ACOUSTIC PROPERTIES OF OOBLECK

Chance Krueger, East Central University

Outstanding Undergraduate Paper in Physical Sciences

The non-Newtonian behavior of a cornstarch and water suspension (Oobleck) presents a unique challenge for acoustic characterization, as its viscosity and modulus change with applied shear stress. This study investigates the acoustic properties of Oobleck, specifically the speed of sound and attenuation coefficient, which are crucial for applications in fields such as sonification and biomechanics. Studies will be analyzed by exporting A-scan data to a computer and processed using Python software. Oobleck was prepared to a standard concentration and contained within a small container with a 38mm width. Acoustic measurements were performed using a 4 MHz transducer in a pulse-echo setup. The data were collected via the A-scan technique, which provides a single-dimensional view of the acoustic signal amplitude over time. The speed of sound was calculated from the known sample thickness and the measured time-of-flight between echoes, while the attenuation coefficient (α) was derived from the change in echo amplitude across the sample path. All measurements were performed under static, low-shear conditions. After collecting all data the information was analyzed using Python to complete tasks such as calculating attenuation coefficient, speed of sound, and running a linear regression model to find correlations between concentration and attenuation coefficients.Early analysis of the data indicates that the Oobleck exhibits a heavy increase in the attenuation coefficient that shows heavy correlation to concentration. The change in velocity of sound is minimal however still noticeable.

138
LABORATORY INVESTIGATION OF ENVIRONMENTAL EFFECTS ON COSMIC RAY CASCADES

Elena Gregg, Pavel Navitski, Wesley Klehm, Gabriel Pendell, Kolby Mostrom, Prem Thannickal, and John McLaughlin, Oral Roberts University

Outstanding Undergraduate Paper in Engineering Sciences

The Advanced Physics course at Oral Roberts University integrates authentic research experiences into undergraduate instruction to strengthen student understanding of experimental physics and scientific inquiry. A central component of this course is a student-led investigation of cosmic ray cascades, focusing on the detection and analysis of muons—massive elementary particles analogous to electrons, produced by high-energy interactions between cosmic rays and atmospheric molecules. This study represents the most recent phase of an ongoing research series conducted within the university laboratory. Earlier phases optimized detector configurations by calibrating steel plate thickness and mapping the angular distribution of muons under varied geometrical arrangements. Building on this foundation, the current phase investigates how environmental factors influence cascade formation and muon detection efficiency. Students employed an array of eleven steel plates inclined at 70° toward the northern horizon to record muon flux data across diverse atmospheric conditions. Measurements were systematically correlated with environmental parameters, including temperature, barometric pressure, and weather variability. Preliminary analysis indicates that elevated atmospheric temperatures are associated with reduced muon counts—consistent with higher meson decay altitudes—while lower pressure conditions appear to enhance muon transmission to ground level. The project provides a meaningful platform for undergraduate students to participate in hands-on particle physics research while contributing empirical data to the broader understanding of environmental modulation in cosmic ray cascades. This integration of experimental investigation with classroom instruction exemplifies the effectiveness of research-based learning in fostering scientific literacy, technical competence, and collaboration among emerging physicists.

A NOVEL APPROACH TO PRE-SERVICE TEACHER DEVELOPMENT: STEM CAMP INTERN

Robin Roberson, East Central University

East Central University is home to the I-DREAM grant (US Dept of Education) and the EdPASS-H2O grant (USEPA). I-DREAM's goals are to provide support to pre-service and in-service teachers to increase both the number entering the profession and the number retained in the profession. EdPASS-H2O's goals are similar, but for the water profession (increase those entering and retained), with the additional goal of increasing overall knowledge of water to produce better water consumers and advocates in the future. To support its goals, the EdPASS grant provides partial funding for the Human Water Cycle Academies which are offered through the OSRHE each summer. During summer 2025, I-DREAM provided a pre-service teacher intern for two of the Human Water Academies and followed this with a 3-week internship in which four pre-service teachers and one current Oklahoma middle school teacher developed and ran a 4-day STEM camp for 3rd-5th grade students at East Central University. This presentation will discuss what the interns gained from these experiences.

SURVEY OF THE ASSEMBLAGE OF DUNG BEETLES IN CIMARRON COUNTY, OKLAHOMA AND THE EFFICACY OF TWO DUNG TYPES AS BAIT

Byron Ross[1], Sue Fairbanks[2], Mary Liz Jameson[3], and George Wang[1], [1]East Central University; [2]Oklahoma State University; [3]Wichita State University

Outstanding Undergraduate Paper in Applied Ecology & Conservation

Dung beetles (Coleoptera: Scarabaeidae) provide important ecosystem services to agroecosystems, yet native dung beetle populations are declining faster than most other insects. Services provided by dung beetles include increased percolation and aeration of the soil, increased secondary seed dispersal, increased nutrient cycling, and pest control. Dung beetles can control pests such as the endoparasitic nematode *Haemonchus contortus*, an important parasite of pronghorn (*Antilocarpa americana*) transmitted by fecal material. Oklahoma's pronghorn population has also suffered declines in recent years, with a high fawn mortality rate. In this study, we sampled beetles in Cimarron County, Oklahoma to determine the species composition of the assemblage of dung beetles and their potential association with pronghorn in the Oklahoma panhandle area. We set up two transects of pitfall traps (n = 10 each) and baited them with either pronghorn dung or cattle dung. We recorded the arthropods collected in the traps for two days. We compared the abundance and species richness of beetles in our samples using negative binomial generalized linear models (NB-GLM). Pronghorn dung attracted significantly more beetle individuals ($z = 2.929$, $p = 0.0034$), but there was no difference in beetle species richness between the two types of bait ($z = 0.910$, $p = 0.363$). Our results suggest that dung beetles might be attracted more to the dung of native wildlife than domestic animals.

ABUNDANCE GRADIENT OF INVASIVE *BOTHRIOCHLOA ISCHAEMUM* IN A MIXED-GRASS PRAIRIE: VARYING IMPACTS ACROSS LEVELS OF ECOLOGICAL ORGANIZATION

Emani Rust, Caitlin Hodges, Xiangming Xiao, Heather McCarthy, and Lara Souza, University of Oklahoma

Outstanding Graduate Paper

Biological invasions are becoming more prevalent with the onset of climate change and anthropogenic development, threatening the ecological stability of terrestrial ecosystems by altering microhabitats and reducing native abundance and diversity. Grassland ecosystems are ubiquitous across space and time, providing several key ecological and economic services while also experiencing one of the greatest alterations to global changes, such as biological invasions. Here, we present results from a field experiment in a mixed-grass prairie that measured the impacts of a natural gradient of invasive *Bothriochloa ischaemum* on responses across levels of ecological organization. We found that increasing invader abundance was negatively associated with percent cover of a dominant native species, *Schizachyrium scoparium*. However, increasing invader abundance did not influence community structure (plot-level biomass and diversity) nor ecosystem function (soil respiration). These results suggest that *B. ischaemum* has competitive advantages over *S. scoparium* but is functionally redundant in mesic mixed-grass prairies. Furthermore, this study observed that the influence of biological invasions is not linear. Species-level responses may be the most sensitive to invasions, while community and ecosystem-level responses are more robust. By extension, species-level responses may be irrevocably altered by the time that responses in higher orders of ecological organization are detected.

HOOKLETS AND NEMATODES: FEATHER MICROSTRUCTURE AND EUCOLEUS DISPAR LESION SEVERITY IN SHARP-SHINNED HAWKS

Eden Ruth, Victoria Roper, Daniel Erikson, Briana Montgomery, Olivia Poplin, Jayna Vang, and Mark Peaden, Rogers State University

In recent years, banders in the Northeast have noted oral lesions in migrating Sharp-shinned Hawks, confirmed in New York (2016–2018) as Eucoleus dispar. Feather quality matters for flight, insulation, and waterproofing, yet links to parasite burden in raptors are largely unknown. We asked whether simple feather metrics track mouth-lesion severity so burden can be compared across seasons and sites when recaptures are rare. In fall 2023 at the Cedar Grove Ornithological Research Station (Glenbeulah, Wisconsin), banders scored oropharyngeal lesions (0–5) and collected two contour feathers per hawk (right pectoral tract and back). From a fixed imaging window (Leica; micrometer-calibrated) we counted barbules and hooklets (hamuli), recorded fault bars (narrow, paler bands from brief growth interruptions), and noted any longer thin zones in the vane. We then derived two metrics: a Feather Microstructure Index (FMI) (higher with more intact barbules/hamuli) and a Feather Quality Index (FQI) (feather mass per length). Body condition was estimated as mass relative to tarsus length within age–sex classes. The vane closes when hamuli on one barb's distal barbules catch the proximal barbules of the neighboring barb like Velcro hooks finding a loop. If barbules/hamuli are missing or misaligned, or if fault bars and thin zones occur, holes open in the vane. Air and water pass through those holes, increasing power needed to fly, lowering insulation and waterproofing, and increasing time spent preening—conditions linked to higher predation risk in songbirds. We related FMI and FQI to lesion score with linear mixed-effects models (age, sex, fat, crop, date as covariates), modeled fault-bar counts as counts, and tested body condition against FQI and lesion. Hypothesis: higher lesion scores are linked to lower FMI and FQI, greater faulting/thinning, and poorer condition. Small structures can scale to population-level effects; this work provides a simple, noninvasive signal of burden that banding stations.

ROLE OF THE TRANSCRIPTION FACTOR ZUR IN METAL HOMEOSTASIS IN *MYCOBACTERIUM TUBERCULOSIS*

Rashna Sharmeen Shama and Avishek Mitra, Oklahoma State University - Stillwater

Tuberculosis is caused by *Mycobacterium tuberculosis* (*Mtb*), a lung pathogen responsible for over 1.3 million deaths annually. To survive within the host, *Mtb* must tightly regulate metal homeostasis, particularly for essential metals such as iron and zinc. Under metal-replete conditions, metal acquisition genes are repressed, whereas in metal-restrictive environments, they are strongly induced. This balance is maintained by specialized transcriptional regulators that sense intracellular metal levels and modulate gene expression. Zur, a zinc-responsive transcription factor, is a key regulator of zinc homeostasis in *Mtb*. Recent evidence suggests that Zur also influences iron utilization, particularly heme (Hm). We found that deletion of zur impairs *Mtb*'s ability to use ferric iron across all ferric citrate concentrations. In the presence of Hm iron, the zur mutant shows a dose-dependent growth defect, with increasing heme concentrations exacerbating the phenotype, indicating that Zur fine-tunes iron acquisition under both ferric and heme iron conditions. Intracellular heme measurements revealed heme accumulation in the zur mutant, likely contributing to growth inhibition at higher heme concentrations. To define Zur's role in intracellular Hm levels, we will quantify mRNA levels of heme uptake and biosynthesis genes. Beyond metal regulation, Zur supports stress adaptation: zur deletion increases sensitivity to oxidative and membrane stress and disrupts biofilm formation. Biochemical characterization shows Zur functions as a homodimer, similar to other Fur-like regulators. UV–visible absorption spectroscopy confirms Zur-Hm interaction, suggesting Hm binding may modulate Zur's DNA-binding activity. Future work will examine how zinc homeostasis influences iron utilization in a Zur-dependent manner and assess Zur's role in virulence using macrophage infection models.

A PROBABLE NEW CARBONIFEROUS LAGERSTÄTTE IN NORTHEASTERN OKLAHOMA

Christen Shelton[1],[2], Kolby Dooling[3], Troy Rasbury[4], and Paul Northrup[4], [1]Rogers State University; [2]New Jersey State Museum; [3]Oklahoma State University; [4]Stony Brook University

A newly discovered fossil site in northeastern Oklahoma reveals exceptional preservation of Pennsylvanian-aged biota, comparable to the Buckhorn Asphalt Lagerstätte of the Arbuckle Mountains. The deposit, dated to approximately 310 million years ago, is embedded in hydrocarbon and uranium-rich sediments that may have helped facilitate the rare retention of original aragonite nacre layers in fossilized mollusks. These microstructural features, typically lost during diagenesis, can provide valuable insights into Paleozoic biomineralization and shell architecture. In addition to mineralized tissues, some phosphate nodules found at the site contain preserved soft tissue elements such as shark cartilage, skin, and brain endocasts, offering a rare anatomical perspective on Carboniferous life. Geochemical and sedimentological analyses are still on going. This discovery expands the known range of Late Carboniferous soft-tissue preservation and contributes significantly to our understanding of early molluscan evolution and taphonomic processes.

142
REGIONAL CLIMATE CHANGE BASED ON *SALIX NIGRA* HERBARIUM COLLECTION

Michael Sherwood, Seth Brecheen, Denna Bussinger, Dakota Cao, Caden Elizalde, Amy Howard, Emree Hutchens, Grace Scott-Lang, and Elissa Yardy (East Central University)

Outstanding Undergraduate Paper in Biological Sciences (Botany)

Climate change has brought about and is predicted to bring about environmental changes such as a global increase in CO2. A central theme in plant biology is how plants are likely to respond to these predicted changes. One way to assess what changes to expect is by looking at the past. Herbaria record past plant attributes and thus can be used to predict the future. If we assume that CO2 is changing at the regional scale, then plants may be responding both plastically and adaptively. For example, it may be that as CO2 increases, the number of leaf stomata for C3 plants declines. In the current study, *Salix nigra*, housed at the East Central University Herbarium, were evaluated. Dates ranged from 1940 to 1989 with locations from the central Oklahoma region; additional regional samples were collected October 2025. We analyze leaf stomata on both upper and lower epidermis and their ratio as a function of collection year. If plants alter the number of stomata on leaf surfaces to reduce water loss while maintaining carbon assimilation, then we predict that year and stomatal densities will be inversely related. Future work will endeavor to tease apart confounding effects such as temperature and water availability, also predicted to change according to current climate models.

BIOTHERAPEUTIC *CHRISTENSENELLA* SPP. FOR GUT MICROBIOTA MODULATION

Shiny Talukder and Crystal Johnson, Oklahoma State University - Center for Health Sciences

The gut microbiome constitutes of a complex community of bacteria, archaea, and viruses that helps maintain the balance between health and disease. Recently, *Christensenella* species have gained attention as potential “next-generation probiotics” because they are linked to maintaining a lean body type and supporting healthy metabolism. There are four species of Christensenellaceae that have been isolated so far and among them *Christensenella minuta* has been shown to help regulate energy balance by producing short-chain fatty acids (SCFAs) and breaking down carbohydrates, suggesting it could play a role in preventing obesity. Studies have also showed that it has a syntrophic relationship with the archaeon *Methanobrevibacter smithii*, likely through hydrogen gas exchange. In addition, *C. minuta* produces bile salt hydrolase (BSH) and SCFAs like propionate, which are important for gut and metabolic health. Other species such as *Christensenella tenuis* and *Christensenella intestinihominis* have been associated with lower cholesterol (LDL) and apolipoprotein levels, as well as lower body mass index (BMI). These effects may be linked to its influence on appetite-regulating hormones such as GLP-1 and PYY. In this research, we cultured four *Christensenella* spp. (*C. minuta*, *C. tenuis*, *C. intestinihominis* and *C. hongkongensis*) using anaerobic techniques to observe their general growth patterns. Understanding how these bacteria grow and interact with other organism and with each other is an important step toward using them as live biotherapeutic candidates in future animal studies. Our findings will help guide future research on how *Christensenella* species can be applied to improve human metabolic health

EXPOSURE TO 'ALTERNATIVE' FLAME RETARDANTS ALTERS RAT AORTIC SMOOTH MUSCLE CELL FUNCTION IN VITRO AND DECREASES HEART RATE IN OVO

Alex Webb, Melville Vaughan, Austin Aduddell, Matthew Roberts, and Christopher G. Goodchild, University of Central Oklahoma

Outstanding Undergraduate Paper in Biomedical Sciences

Flame retardants are routinely incorporated into common household items, including furniture, car seats, and crib mattresses, to enhance fire safety. In 2004, concerns regarding the toxicity of traditional flame retardants, such as polybrominated diphenyl ethers (PBDEs), led to their replacement with 'alternative' flame retardants. However, the potential toxicity of these alternatives remains largely unknown. A particular concern is the risk of maternal transfer to the developing embryo, as these flame retardants have been detected in breast milk and placental fluid of pregnant women. In utero exposure to alternative flame retardants may lead to congenital defects, especially if exposure occurs during early embryonic development, which involves sensitive processes. This study focused on the potential effects of two alternative flame retardants, Triphenyl phosphate (TPP) and Tris 2-chloroethyl phosphate (TCEP), on arterial wall development. We employed in vitro tests, including wound scrape migration assays and microscopy, to assess cell migration and proliferation. To better understand adverse outcomes on cardiac function, we conducted in ovo experiments with chicken embryos to examine the effects of TPP and TCEP on embryonic heart rate and organ mass. Our findings suggest that TPP and TCEP may inhibit aortic smooth muscle cell function, which could potentially impact proper heart development and function. These results underscore the importance of further investigation into the safety of alternative flame retardants in household products.

144
FUNGAL ESTROGENS: EXPLORING *PHALLUS IMPUDICUS* AS A NOVEL MODULATOR OF ESTROGEN RECEPTOR SIGNALING

Anna Wilson, Oral Roberts University

Outstanding Overall Undergraduate Paper

Outstanding Undergraduate Paper in Biochemistry & Molecular Biology

Estrogen receptors (ERs) play a fundamental role in women's health, regulating reproductive function, bone density, cardiovascular health, and neurological processes. While estradiol is the canonical ligand, structurally diverse natural compounds are increasingly recognized for their ability to mimic estrogenic activity. In this study, we investigated a novel mycoestrogen derived from the mushroom *Phallus impudicus* (colloquially known as the common stinkhorn) for its ability to activate ER signaling in T-47D breast cancer cells. To assess estrogenic potential, we compared the effects of the mycoestrogen to estradiol using cell viability assays and quantitative PCR analysis of ER-responsive gene expression. Treatment with the mycoestrogen elicited an upregulation of ER target genes, demonstrating functional receptor activation. These findings highlight the ability of fungal metabolites to influence human hormone receptor pathways, expanding our understanding of natural estrogen mimetics. Importantly, this work also seeks to address a persistent gap in women's health research. By characterizing naturally derived alternatives to synthetic estradiol—which is widely prescribed for contraceptive use and conditions such as endometriosis, PCOS, menopausal symptoms, osteoporosis, and hormone replacement therapy—our study opens the possibility of developing safer, more diverse treatment options. Our results position *Phallus impudicus*–derived compounds as promising new candidates for estrogen receptor modulation and as a step toward more inclusive research in women's health.

HOST-FEEDING BEHAVIOR OF MOSQUITOES IN CENTRAL OKLAHOMA

Maggie Wojan and Caio França, Southern Nazarene University

There is limited knowledge about the feeding habits of mosquito vectors of arboviruses in central Oklahoma. This study aimed to identify blood meal sources of mosquitoes collected in the Oklahoma City area to better understand potential transmission dynamics among vertebrate hosts. Blood meals from 152 mosquitoes across eight species and four genera were analyzed using PCR assays targeting the 12s rRNA gene. Amplificons 215-bp long successfully amplified from 73 individuals from which 65 were Sanger sequenced with raw reads visualized and trimmed in Geneious and taxonomically identified using the Basic Local Alignment Search Tool (BLAST). The results showed that Aedes' species fed primarily on mammals, including *Odocoileus hemionus* (white tail deer) and occasionally feeding on passerine birds (i.e. *Quiscalus quiscula*, common grackle). Meanwhile, the *Psorophora* genus showed species-dependent preferences as *Ps. ferox* preferred mammals like *Sylvilagus aquaticus* (swamp rabbit) and *Ps. columbiae* passerine birds. In contrast, *Culex* species, particularly *Cx. tarsalis* fed on a broader range of hosts, including *Sciurus niger* (fox squirrels), *Cardinalis cardinalis* (northern cardinal) and the common grackle. These findings suggest that while some mosquito species are primarily ornithophilic, others are generalists in their feeding behavior particularly *Cx. tarsalis*. These feeding behaviors support our understanding that some species can be infected by arboviruses yet are not competent vectors, while others like *Cx. tarsalis* and *Cx. pipiens* complex act as bridge vectors between birds and mammals. These findings can be useful to improve our understanding of enzootic transmission cycles of arboviruses in Oklahoma.

OKLAHOMA ACADEMY OF SCIENCE
2025 OFFICERS

President
Dr. Jerry Bowen
Rogers State University

President-Elect
Dr. Rachel Jones
University of Science and Arts of Oklahoma

Editor, *Proceedings*
Dr. Mostafa S. Elshahed
Oklahoma State University

Immediate Past President
Dr. Karen Williams
East Central University

Executive Director
Dr. Adam Ryburn
Oklahoma City University

Recording Secretary
Dr. Avi Mitra
Oklahoma State University

Section	Chair	Vice-Chair
A: *Biological Sciences*	Patrick McAnerney Cameron University	Dr. Zack Sanders University of Central Oklahoma
B: *Geology*	VACANT	Dr. Chris Shelton Rogers State University
C: *Physical Sciences*	Dr. Benjamin Tayo University of Central Oklahoma	Dr. Amanda Nichols Oklahoma Christian University
D: *Social Sciences*	Dr. Dustin Williams East Central Universit	VACANT
E: *Science Communication & Education*	Dr. Cheyenne Olson Northeastern State University	Dr. Karen Williams East Central University
F: *Geography*	VACANT	VACANT
G: *Applied Ecology & Conservation*	Dr. Renan Bosque Southwestern Oklahoma State Univ.	Dr. Daniel Gomes da Rocha Southern Nazarene Univ.
H: *Microbiology*	Dr. Avi Mitra Oklahoma State University	Dr. April Nesbitt East Central University
I: *Engineering Sciences*	Dr. Nesreen Alsbou University of Central Oklahoma	Dr. Gang Xu University of Central Oklahoma
J: *Biochemistry & Molecular Biology*	Dr. Subhas Das Oklahoma State University	Dr. Ashley Mattison Oklahoma State University
K: *Microscopy*	Dr. Hannah King Rogers State University	VACANT
L: *Mathematics, Computer Science & Statistics*	Dr. Andrew Wells East Central University	Dr. Michelle Lastrina East Central University
M: *Environmental Sciences*	Eric Howard East Central University	Dr. Charles Crittell East Central University
N: Biomedical Sciences	Dr. Alisha Howard East Central University	VACANT

Collegiate Academy of Science	*Director*	**Dr. Mark Peaden**, Rogers State University
Junior Academy	*Director*	**Dr. Hannah King**, Rogers State University
OAS Website	*Webmaster*	**Dr. Adam Ryburn**, Oklahoma City University

OKLAHOMA ACADEMY OF SCIENCE
STATEMENT OF REVENUES COLLECTED AND EXPENSES PAID
FOR THE YEAR ENDED DECEMBER 31, 2024

REVENUES COLLECTED:		
Membership Dues:		$1,375.00
Investment Income:		$9.01
Meetings:		$12,905.61
Registration – Fall Field Meeting	$4,126.08	
Registration – Technical Meeting	$8,779.53	
Donations		$65.00
POAS:		$6285.38
Woody Plants:		$0.00
Other Revenue:		$65.92
Total Revenue Collected		**$20,705.92**
EXPENSES PAID		
Stipends and Other Compensation:		$7,158.68
Stipends	$6,141.24	
Social Security & Medicare	$1,017.44	
Meeting Expenses:		$7204.77
Fall Field Meeting	$4,311.32	
Technical Meeting	$2,893.45	
POAS:		$5,320.50
Woody Plants:		$0.00
Dues/Meetings of NAAS/AJAS/AAAS:		$100.00
Other Expenditures:		$222.63
Total Expenses Paid:		**$20,006.58**
Revenues Collected Over Expenses Paid		**$699.34**

OKLAHOMA ACADEMY OF SCIENCE
STATEMENT OF ASSETS, LIABILITIES, AND FUND BALANCE
ARISING FROM CASH TRANSACTIONS
FOR THE YEAR ENDED DECEMBER 31, 2024

ASSETS

Cash:		$23,385.336
Checking Account	$20,581.84	
Endowment Savings Account	$2,803.52	
Investments:		$60,000
Certificate of Deposit	$60,000	
Total Assets:		**$83,385.09**

LIABILITIES AND FUND BALANCE

Liabilities:		$0.00
Fund balance:		
Beginning operation fund balance	$82,682.77	
Excess revenues collected over expenses	$699.34	
Total Funds:		**$83,382.11**

MEMBERSHIP APPLICATION
OKLAHOMA ACADEMY OF SCIENCE

Name_____ Affiliation_____
Last First Middle

Professional Address (if applicable)_____
Dept., Bldg., Office, etc. (if necessary for campus mail delivery)

_____
City State Zip

OR (not both)

Mailing Address (for home delivery)_____
Street, P.O. Box, Route, etc. City State Zip

Telephone_____E Mail_____

Please indicate whether this is a _____Renewal or _____New Membership. What year?
Note all annual memberships expire December 31 if you do not prepay for the following year.

Membership Type (check one):

____Life $600 _____Professional $30 ____Family $35 ____Undergraduate/Graduate Student $20

____$40 Library/Institute

Section Affiliations: Number up to three areas of interest. 1=first choice; 2=second choice; 3=third choice.

____A Biological Sciences	____E Science Education	____I Engineering Sciences	____M Environ. Sci.
____B Geology	____F Geography	____J Biochemistry/Biophysics	____N Biomedical Sci.
____C Physical Sciences	____G Fish and Wildlife	____K Microscopy	____Y Collegiate Acad.
____D Social Sciences	____H Microbiology	____L Mathematics/Computer Sci	____Z JuniorAcademy

Make checks payable to the **Oklahoma Academy of Science.**
Mail completed form and payment to: Dr. Adam Ryburn, Executive Director, Oklahoma Academy of Science, Oklahoma City University, Biology Department, 2501 N. Blackwelder Ave., Oklahoma City, OK 73106.
Or apply online
https://www.oklahomaacademyofscience.org/membership.html

Members, please photocopy this form and give that to a non member colleague or student.
Help strengthen OAS by recruitment!

DONATION FORM

Make tax deductible donations in memory or honor of a family member, friend, or colleague. All donated fund are placed as principle into the OAS Endowment Account and the interest generated funds the Academy's programs.

Donor_____
Name Mailing Address (Street or PO Box) City State Zip

Honoree_____
Amount

Editorial Policies and Practices

The *Proceedings of the Oklahoma Academy of Science* is published by the Oklahoma Academy of Science. Its editorial policies are established by the Editor and Associate Editors, under the general authority of the Publications Committee. The Editor is appointed by the Executive Committee of the Academy; Associate Editors are appointed by the Publications Committee in consultation with the Editor. The suitability for publication in the *Proceedings* of submitted manuscripts is judged by the Editor and the Associate Editors.

All manuscripts must be refereed critically. The *POAS* Editors have an obligation to the membership of the Academy and to the scientific community to insure, as far as possible, that the *Proceedings* is scientifically accurate. Expert refereeing is a tested, effective method by which the scientific community maintains a standard of excellence. In addition, expert refereeing frequently helps the author(s) to present the results in a clear, concise form that exceeds minimal standards.

The corresponding author is notified of the receipt of a manuscript, and the Editor sends the manuscript to at least two reviewers, anonymous to the author(s). After the initial review, the Editor either accepts the manuscript for publication, returns it to the author for clarification or revision, sends it to another referee for further review, or declines the manuscript.

A declined manuscript will have had at least two reviews, usually more. The Editors examine such manuscripts very carefully and take full responsibility. There are several grounds for declining a manuscript: the substance of the paper may not fall within the scope of the *Proceedings*; the work may not meet the standards that the *Proceedings* strives to maintain; the work may not be complete; the experimental evidence may not support the conclusion(s) that the author(s) would like to draw; the experimental approach may be equivocal; faulty design or technique may vitiate the results; or the manuscript may not make a sufficient contribution to the overall understanding of the system being studied, even though the quality of the experimental work is not in question.

A combination of these reasons is also possible grounds for declining to publish the MS. In most cases, the Editors rely on the judgment of the reviewers.

Reviewer's Responsibilities

We thank the reviewers who contribute so much to the quality of these *Proceedings*. They must remain anonymous to assure their freedom in making recommendations. The responsibilities or obligations of these reviewers are:

- Because science depends on peer-reviewed publications, every scientist has an obligation to do a fair share of reviewing.
- A reviewer who has a conflict of interest or a schedule that will not allow rapid completion of the review will quickly return the manuscript; otherwise, the review will be completed and returned promptly.
- A reviewer shall respect the intellectual independence of the author(s). The review shall be objective, based on scientific merit alone, without regard to race, religion, nationality, sex, seniority, or institutional affiliation of the author(s). However, the reviewer may take into account the relationship of a manuscript under consideration to others previously or concurrently offered by the same author(s).
- A reviewer should not evaluate a manuscript by a person with whom the reviewer has a personal or professional connection if the relationship could reasonably be perceived as influencing judgment of the manuscript.
- The manuscript is a confidential document. If the reviewer seeks an opinion or discusses the manuscript with another, those consultations shall be revealed to the Editor.
- Reviewers must not use or disclose unpublished information, arguments, or interpretations contained in a manuscript under consideration, or in press, without the written consent of the author.
- • Reviewers should explain and support their judgments and statements, so both the Editor and the author(s) may understand the basis of their comments.

Brief Instructions to Authors

The instructions to authors wishing to publish their research in the Proceedings of the Oklahoma Academy of Science are listed below. We ask the authors to recognize that the intent is not to establish a set of restrictive, arbitrary rules, but to provide a useful set of guidelines for authors, guidelines that, in most cases, are also binding on the Editors in their task of producing a sound and respected scientific journal.

A. Submission Process.

Manuscripts for the *Proceedings* should be submitted electronically via electronic mail (email) to:

poas@okstate.edu

Prospective authors should note carefully the policy statement "Policies of the *Proceedings*" on page ii. Complete instructions for manuscript formatting requirements, as well as a template for use may be found at:

https://ojs.library.okstate.edu/osu/index.php/OAS/submit

The Editors review the MS and carefully select other reviewers as described in "Editorial Policies and Practices" (see p. 167); all referee and editorial opinions are anonymous. Send a resubmitted and/ or revised manuscript and a point-by-point response to the reviewers'/Editor's comments.

All authors should approve all revisions (the corresponding author is responsible for insuring that all authors agree to the changes). A revised paper will retain its original date of receipt only if the revision is received by the Editor within two months after the date of the letter to the author(s).

B. Types of Manuscripts.

A manuscript may be a paper (report), review, note (communication), a technical comment, or a letter to the editor. All manuscripts should be submitted as a Microsoft Word document, 10-point Times New Roman font, single spaced, and include line numbers. Authors should carefully consider page size when producing manuscripts. The journal's page size is roughly 7 by 10 inches, portrait orientation, and does include margins.

Paper (a report; traditional research paper). A Paper may be of any length that is required to describe and to explain adequately the experimental observations.

Review. The Editor will usually solicit review articles, but will consider unsolicited ones. The prospective writer(s) of reviews should consult the Editor; in general, the Editor needs a synopsis of the area proposed for review and an outline of the paper before deciding. Re- views are typically peer- reviewed.

Note (Communication). The objective of a *Note* is to provide an effective form for communicating new results and ideas and/ or describing small but complete pieces of research. Thus, a *Note* is either a preliminary report or a complete account of a small investigation. *Notes* must not exceed four printed pages including text, figures, tables, and references. One journal page of standard text contains about 600 words; hence, there is space for presentation of considerable experimental detail. *Notes* are peer-reviewed.

Technical Comment. Technical comments (one journal page) may criticize material published in an earlier volume of *POAS* or may offer additional useful information. The author(s) of the original paper are asked for an opinion on the comment and, if the comment is published, are invited to reply in the same volume.

Letter to the Editor. Letters are selected for their pertinence to materials published in POAS or because they discuss problems of general interest to scientists and/or to Oklahomans. Letters pertaining to material published in *POAS* may correct

errors, provide support or agreements, or offer different points of view, clarifications, or additional information.

Abstract. You may submit an abstract of your presentation at the OAS Technical Meeting. For specific instructions, contact the Editor. Even though abstracts are not peer-reviewed, they must align with the policies and scope of the Proceedings. The quality or relevance of work may not be in question, but the printed material is still subject to scientific accuracy.

The same guidelines that apply to manuscripts and notes submitted for peer-review, also apply to abstracts submitted for print. Just as manuscripts and notes are subject to thorough testing, so are comments written in abstracts (supported by data). The *Proceedings* understands that all disciplines are in a search for a deeper understanding of the world some of which are through creative expression and personal interpretation. Science is a system by which one discovers and records physical phenomena, dealing with hypotheses that are testable. The domain of "science" while working within nature is restricted to the observable world. There are many valid and important questions to be answered but lie outside the realm of science.

C. Manuscript Organization.

1. General organization.

For papers (reports), the subsections should typically include the following: Abstract, Introduction, Experimental Procedures (or Methods), Results, Discussion, Acknowledgments (if any), and References. In the case of notes or short papers, you may combine some headings, for example, "Results and Discussion":

I. The title should be short, clear, and informative; it should not exceed 150 characters and spaces (three lines in the journal), and include the name of the organism, compound, process, system, enzyme, etc., that is the major object of the study.

II. Provide a running title of fewer than 60 characters and spaces.

III. Spell out either the first or second given name of each author. For example, Otis C. Dermer, instead of O.C. Dermer, or H. Olin Spivey, instead of H.O. Spivey.

IV. Every manuscript (including Notes) must begin with a brief Abstract (up to 200 words) that presents clearly the plan, procedure, and significant results of the investigation. The Abstract should be understandable alone and should provide a comprehensive overview of the entire research effort.

V. The Introduction should state the purpose of the investigation and the relationship with other work in the same field. It should not be an extensive review of literature, but provide appropriate literature to demonstrate the context of the research.

VI. The Experimental Procedures (or Methods) section should be brief, but adequate for repetition of the work by a qualified experimenter. References to previously published procedures can reduce the length of this section. Refer to the original description of a procedure and describe any modifications.

VII. You may present the Results in tables or figures or both, but note that it is sometimes simpler and clearer to state the observations and the appropriate experimental values directly in the text. Present a given set of results in only one form: in a table, or figure, or the text.

VIII. The Discussion section should interpret the Results and how these observations fit with the results of others. Sometimes thecombination of Results and Discussion can give a clearer, more compact presentation.

IX. Acknowledgments of financial support and other aid are to be included.

X. References are discussed below.

2. References

POAS uses the name-year system for citing references. Citations in the text, tables and figure legends include the surname of the author or authors of the cited document and the year of publication. The references are listed alphabetically by authors' surnames in the reference list found at the end of the text of the article. Below are given several examples of correct formats for citing journal articles, books, theses and web resources. For Additional information regarding the name-year system, consult the CBE Manual [*Scientific Style and Format: The CBE Manual for Authors, Editors, and Publishers, 6th edition*]. Abbreviate journal names according to the *International List of Periodical Title Word Abbreviations*.

If it is necessary to refer to a manuscript that has been accepted for publication elsewhere but is not yet published, use the format shown below, with the volume and page numbers absent, the (estimated) publication year included and followed by the words *in press* for papers publications and *forthcoming* for all other forms (CBE 30.68). If the materials are published before the manuscript with that reference is published in *POAS*, notify the Editor of the appropriate volume and page numbers and make the changes as you revise.

Responsibility for the accuracy of bibliographic references rests entirely with the author(s); confirm all references through comparison of the final draft of the manuscript with the original publications. We expect that the only changes in galley proof will be for typographical errors. Any mention of manuscript in preparation, unpublished experiments, and personal communication should be in parenthesis. Use of personal communication should be with written permission of the communicator and should be entered only in the text, not in the Reference list.

Examples of References in CBE Style and Format

Journal Articles

Miller LF, Chance CJ. 1954. Fishing in the tail waters of TVS dams. Prog Fish-Cult 16:3-9.

Ortenburger AI, Hubbs CL. 1927. A report on the fishes of Oklahoma, with descriptions of new genera and species. Proc Okla Acad Sci 6:123-141.

Books

Book with Authors:

Miller RJ, Robison HW. 1980. The fishes of Oklahoma. Stillwater (OK): Oklahoma State University Press. 246 p.

Book with Editors:

Gilman AG, Rall TW, Nies AS, Taylor P, editors. 1990. The pharmacological basis of theraputics. 8th ed. New York: Pergamon. 1811 p.

Book with Organization as Author:

International Union of Pure and Applied Chemistry, PhysicalChemistry Division. 1993. Quantities, units, and symbols in physical chemistry. 3rd. Oxford (UK): Blackwell Science. 166 p.

Chapter in Book with Editors:

Hamilton K, Combs DL, Randolph JC. 1985. Sportfishing changes related to hydro- power generation and non-generation in the tailwater of Keystone Reservoir, Oklahoma. In: Olsen FW,White RG, Hamre RH, editors. Proceedings of the symposium on small hydropower and fisheries. Bethesda (MD): American Fisheries Society. p 145-152.

Theses: Knapp MM. 1985. Effects of exploitation on crappie in a new reservoir [MSc thesis]. Stillwater (OK): Oklahoma State University. 84 p. Available from: OSU Library.

Internet: Oklahoma Climatological Survey. 2003. Climate of Oklahoma [online]. Available from: http://climate.ocs.ou.edu. (Accessed August 15, 2005).

D. Review Process.

The Editors review the MS and carefully select reviewers for all submitted manuscripts. All referee and editorial opinions are anonymous. A decision to accept, revise, or reject the manuscript is made by the editor after careful consideration of reviewers' comments and recommendations. If a "revise" decision is reached, the authors will be allowed to resubmit a revised version of the manuscript within a given time window. The authors are considered to address all reviewers' comments and concerns, or provide compelling reasons to explain why they chose not to do so. A point- by-point rebuttal letter is required with each revised manuscripts, which clearly indicates the
nature and locations of corrections within the revised manuscript. All authors should approve all revisions, with the corresponding author being responsible for insuring that all authors agree to the changes.

E. Page Charges

The OAS will publish accepted MSs with the implicit understanding that the author(s) will pay a charge per published page. Page charges are billed at the cost per page for the given issue: current rates of $90 per page for nonmembers of the Academy and $45 for members. All authors are expected to honor these page charges. Billing for page charges and receipt of payment are handled by the Business Manager, who is also the Executive Secretary and Treasurer for the
Academy.

Under exceptional circumstances, when no source of grant funds or other support exists, the author(s) may apply, at the time of submission, for a waiver of page charges.

F. Copyright Transfer

Before publication, authors must transfer copyright to the Oklahoma Academy of Science. All authors must sign, or the signing author must hold permission to sign for any coauthors. Copyright for papers reporting research by U.S. Government employees as part of their official duties will be transferred to the extent permitted by law.